NON-INVASIVE SPECTROSCOPIC SENSING OF ALCOHOL INTOXICATION

By

Szymon Paprocki

Supervisors: Prof. P.A. Kyriacou and Dr M. Qassem

PhD Thesis in Biomedical Engineering

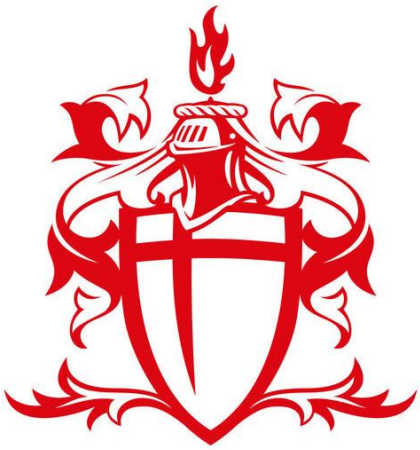

School of Science and Technology

City St. George's, University of London

Research Centre for Biomedical Engineering

City St. George's, University of London

This dissertation is submitted for the degree of
Doctor of Philosophy

January 2025

Dla wszystkich Tych co byli w pobliżu i dla Tych co nieco dalej……..

Declaration of own work

I declare that the work in this PhD thesis was carried out in accordance with the requirements of the University's Regulations and Code of Practice for Research Degree Programmes and that it has not been submitted for any other academic award. Except where indicated by specific reference in the text, the work is the candidate's own work. Work done in collaboration with, or with the assistance of others, is indicated as such. Any views expressed in the dissertation are those of the author.

Szymon Paprocki, January 2025

Abstract

The accurate detection and quantification of ethanol and acetic acid in biological systems remain a major challenge due to overlapping spectral signatures with water and other biomolecules. This thesis investigates the application of diffuse reflectance spectrophotometry in the short-wave infrared region, combined with bio-impedance analysis, to improve discrimination and quantification of ethanol and acetic acid in liquid and biological models. A comprehensive set of experiments was performed using water, human serum, artificial interstitial fluid, sheep blood, and intralipid as representative matrices, alongside gelatin phantoms and porcine skin to simulate tissue environments.

The optical analysis demonstrated strong predictive ability under controlled conditions. In water, polynomial regression achieved high determination coefficients with $R^2 = 0.884$ for ethanol and $R^2 = 0.979$ for acetic acid, with low errors (RMSE = 58.1 mg/dL and 1.49 mg/dL, respectively). In human serum, predictive accuracy remained robust ($R^2 = 0.871$ for ethanol, 0.898 for acetic acid), though errors increased due to protein interference. Artificial interstitial fluid showed greater variability, particularly for ethanol ($R^2 = 0.790$, RMSE = 78.3 mg/dL), while acetic acid maintained strong performance ($R^2 = 0.885$, RMSE = 3.5 mg/dL). In sheep blood, haemoglobin absorption and cellular scattering reduced predictive strength, with ethanol showing $R^2 = 0.729$ and acetic acid $R^2 = 0.793$. Intralipid, used as a scattering phantom, proved most challenging, with ethanol prediction deteriorating severely ($R^2 = 0.447$, RMSE = 123.5 mg/dL), while acetic acid retained moderate accuracy ($R^2 = 0.799$, RMSE = 4.6 mg/dL). Across all matrices, acetic acid consistently outperformed ethanol, reflecting the distinctiveness of its carbonyl absorption bands relative to overlapping O–H features.

Gelatin phantoms extended the investigation into tissue-analogue models with controlled scattering and absorption. Using partial least squares regression, ethanol achieved an R^2 of 0.967 with an RMSEP of 30.9 mg/dL, while acetic acid reached an R^2 of 0.950 with an RMSEP of 2.3 mg/dL. These results confirm that phantoms not only replicate tissue-like complexity but also support highly accurate prediction. Experiments on porcine skin further validated the approach in a true biological substrate, where both ethanol and acetic acid remained detectable with statistically significant correlations despite the increased scattering and heterogeneity of ex vivo tissue.

Complementary bio-impedance analysis was applied across all media and tissue models to characterise dielectric responses to ethanol and acetic acid. Principal component analysis revealed distinct clustering patterns associated with solute composition, confirming that impedance-based methods provide an orthogonal and supportive modality to optical measurements. The combined use of spectroscopy and bio-impedance improved separation of ethanol from acetic acid, highlighting the potential of integrated sensing platforms.

The results demonstrate that while diffuse reflectance spectroscopy alone achieves high accuracy in simple aqueous systems, predictive performance diminishes with increasing biological complexity. Nevertheless, statistically significant correlations were retained across all tested models, with acetic acid consistently yielding higher predictive fidelity. The integration of bio-impedance, gelatin phantoms, and porcine skin validation strengthened the robustness of the approach. Together, these findings provide a foundation for multimodal sensing technologies capable of quantifying ethanol and acetic acid in physiologically relevant environments, with implications for real-time intoxication monitoring and clinical diagnostics.

Contents

List of Figures

List of Tables

Nomenclature

aISF: Artificial Interstitial Fluid

AUD: Alcohol Use Disorder

BAC: Blood Alcohol Concentration

BrAC: Breath Alcohol Concentration

DUI: Driving Under the Influence

EBAC: Estimated Blood Alcohol Content

EtG: Ethyl Glucuronide

EtPA: Ethyl Phosphate

GABA: Gamma -aminobutyric acid

ISF: Interstitial Fluid

NIRS: Near-Infrared Spectroscopy

PLSR: Partial Least Squares Regression

PCA: Principal Component Analysis

SG Filter: Savitzky-Golay Filter

VOCs: Volatile Organic Compounds

NIR: Near-Infrared

SWIR: Short-Wave Infrared

RMSE: Root Mean Square Error

UV: Ultraviolet

DOS: Diffuse Optical Spectroscopy

BIS: Bioimpedance Spectroscopy

PPG: Photoplethysmography

THC: Tetrahydrocannabinol

FTIR: Fourier Transform Infrared Spectroscopy

TAC: Transdermal Alcohol Concentration

FFT: Fast Fourier Transform

VCSEL: Vertical-Cavity Surface-Emitting Laser

InGaAs: Indium Gallium Arsenide

Si Detector: Silicon Detector

PbS Detector: Lead Sulfide Detector

RMSEP: Root Mean Square Error of Prediction

ICF: Intracellular Fluid

ECF: Extracellular Fluid

TBW: Total Body Water

λ: Wavelength

ε: Molar Absorptivity

l: Path Length

c: Concentration

A: Absorbance

v: Vibrational Frequency

h: Planck's Constant

k: Force Constant

μ: Reduced Mass

T: Scores Matrix (for PCA)

P: Loadings Matrix

X: Spectral Data Matrix

Y: Response Matrix

S: Spectrum

B: Baseline Fit

θi: Angle of Incidence

θd: Angle of Diffraction

d: Grating Spacing

E: Energy of a Photon

f: Frequency

n: Diffraction Order

EV: Vibrational Energy

A(λ): Absorbance at a specific wavelength

ΔE: Change in Energy

Ohm (Ω): Unit of Electrical Resistance

log(Ohms): Logarithm of Electrical Resistance

vr: Vibrational Frequency (molecular)

vs: Symmetric Stretching

vas: Asymmetric Stretching

δ: Bending Modes (scissoring, rocking, wagging, twisting)

1. Introduction

Alcohol consumption has played an integral role in the fabric of societies throughout history, with references to fruit fermentation processes dating as far back as ancient Mesopotamia and present in civilisations such as Egypt, Greece, and Rome [1 - 4]. In those times, alcohol production was primarily a small-scale, domestic activity, which gradually evolved into the sophisticated vineyards and distillation processes we know today. In the modern era, alcohol is often associated with social events, celebrations, and spiritual rituals. However, excessive consumption can lead to severe consequences, most notably alcohol addiction, clinically referred to as Alcohol Use Disorder (AUD) [5]. Even the aforementioned ancient civilisations recognised the dangers of excessive drinking. Alcohol is linked to a range of severe health conditions, including various types of cancer and cardiovascular diseases [5 - 7]. Moreover, Driving Under the Influence (DUI) remains a critical societal issue, with over 200 fatalities attributed to drunk driving each year in the UK alone [8] and a staggering global estimate of 273,000 deaths annually [9]. Addressing DUI incidents is a pressing challenge in modern society. This presents a broader dilemma concerning the role of alcohol in contemporary life—where its cultural significance is weighed against its potential harm. As a result, the ability to accurately measure intoxication levels has become a highly sought-after objective, leading to the development of various devices and methods over time.

The prevailing methods to combat DUI are limited, with the most widespread being breath alcohol analysers that estimate Blood Alcohol Concentration (BrAC) by measuring alveolar ethanol content. While effective for roadside testing due to their portability, these devices have notable drawbacks, including the waste generated from single-use mouthpieces. Consequently, they are not widely adopted for personal monitoring, making them infrequent tools for individual use. Recent advances in optical technologies, particularly Near-Infrared Spectroscopy (NIRS), have shown promise in accurately measuring tissue alcohol content [10]. However, such technologies are primarily restricted to industrial settings—such as construction, manufacturing, and mining—where operating heavy machinery while intoxicated poses significant risks to human life and infrastructure.

The potential for personal intoxication monitoring systems holds great promise, enabling individuals to make more informed decisions about their drinking behaviour. Such systems could prevent overconsumption and reduce the occurrence of DUI (especially where local laws permit minimal levels of intoxication). This thesis will explore the current state of ethanol detection devices and techniques, discuss the mechanisms of ethanol metabolism and

intoxication, and propose research to develop a personal intoxication sensor system that considers not only the volume of ethanol in an individual's bloodstream, but also other analytes which correlate to regular consumption of alcohol. Additionally, the thesis will address the broader impact of alcohol, including the role of ethanol's specific metabolic by-products—acetic acid —which has been shown to influence intoxication, mainly by affecting the brain's reward system in experimental models [11].

1.1 Motivation and Research Question

The motivation driving this research stems from the urgent need to deepen our understanding of alcohol metabolism and develop comprehensive monitoring techniques through non-invasive methods. Conventional approaches to detecting alcohol and its metabolites in the human body often rely on invasive blood tests, which not only cause discomfort for the subject but also limit the practicality and frequency of such monitoring. Furthermore, the metabolic process of alcohol, which produces by-products like acetic acid, is crucial in understanding the physiological impact of alcohol consumption. Yet, current methods need to effectively track these metabolites alongside ethanol, providing an incomplete and fragmented view of alcohol's effects on the body. This research proposes an integrated approach using optical spectroscopy and bioimpedance measurements as a promising solution to these shortcomings. By enabling non-invasive, simultaneous detection of ethanol and acetic acid, this study seeks to enhance our capability to monitor and understand alcohol metabolism significantly, offering the potential for groundbreaking advancements in medical diagnostics, treatment of alcohol-related disorders, and broader public health initiatives.

The central research question guiding this investigation is: How can the integration of optical spectroscopy and bioimpedance measurements be optimised to accurately detect and quantify ethanol and its primary metabolite, acetic acid, in the human body? This question encompasses the challenge of navigating biological variability and external factors that may affect measurement precision. It also embodies the broader goal of developing a comprehensive, non-invasive monitoring system that provides real-time insights into alcohol metabolism. Achieving this requires characterising ethanol and acetic acid's spectral and impedance properties, refining analytical models to correlate these properties with concentration levels, and evaluating the system's effectiveness across various biological matrices. Through this inquiry, the research aims to make substantial contributions to biomedical engineering and public health, offering innovative and practical solutions for alcohol monitoring and studying metabolism.

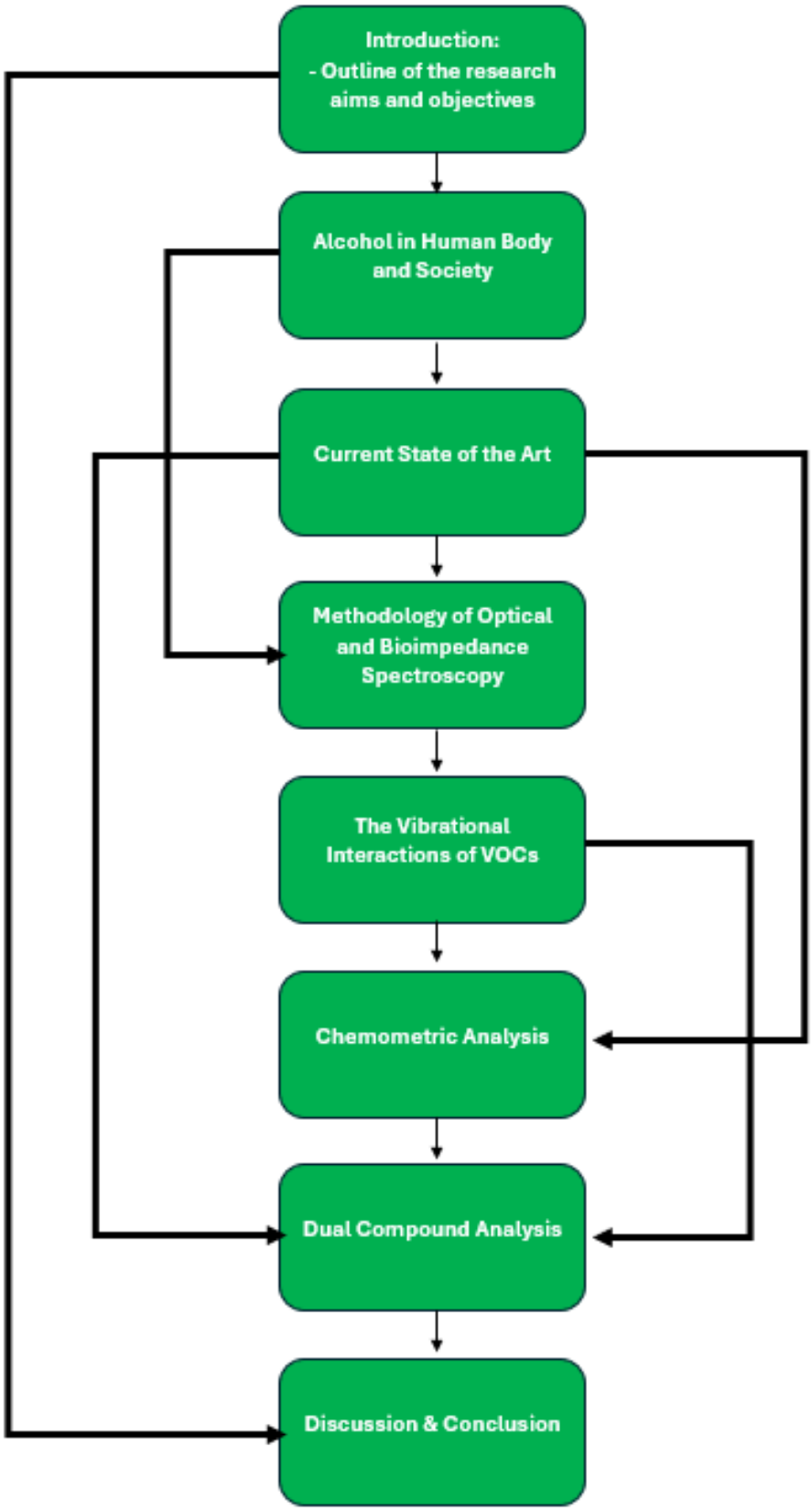

Figure 1.1Thesis Flow Diagram With Interconnected Sections

1.2 Aims and Objectives

Aim 1: Advance the understanding of alcohol metabolism using optical spectroscopy and bioimpedance measurements.

Objective 1.1: Characterise the spectral signatures of ethanol and acetic acid in various biological matrices.

Objective 1.2: Investigate the impedance properties of ethanol and acetic acid across various concentrations.

Objective 1.3: Analyse the correlation between spectroscopic and impedance measurements and metabolic pathways of ethanol.

Aim 2: Develop a novel framework for integrating spectroscopic and impedance data.

Objective 2.1: Design algorithms for synergistic spectroscopic and impedance data analysis.

Objective 2.2: Refine the framework to improve its accuracy and reliability in detecting ethanol and acetic acid.

Aim 3: Investigate the impact of biological variability on measurement accuracy.

Objective 3.1: Assess the effect of hydration levels and blood chemistry variations on detecting ethanol and acetic acid.

Objective 3.2: Study the influence of individual physiological differences on measurement outcomes.

Objective 3.3: Develop adjustment methodologies within the analytical models to account for biological variability.

Aim 4: Compile a comprehensive dataset for model development and validation.

Objective 4.1: Generate a detailed dataset of optical and impedance measurements across a spectrum of ethanol and acetic acid concentrations.

Objective 4.2: Analyse the dataset to identify patterns and correlations relevant to alcohol metabolism.

1.3 Contribution to the field

Development of a Non-Invasive Alcohol Monitoring Technique:

The thesis presents a novel, non-invasive technique for monitoring alcohol intoxication by integrating optical spectroscopy (NIRS and SWIR) and bioimpedance spectroscopy (BIS).

This integrated approach offers a more accurate and comprehensive method for detecting both ethanol and its metabolite, acetic acid, in biological tissues.

Characterization of Ethanol and Acetic Acid in Biological Matrices:

Detailed characterization of the spectral signatures and impedance properties of ethanol and acetic acid in various biological matrices, including human serum, artificial interstitial fluid (ISF), sheep blood, and porcine skin.

The findings provide valuable insights into how ethanol and acetic acid behave in different biological environments, particularly in the SWIR region.

Chemometric Analysis for Alcohol Detection:

Application of advanced chemometric techniques such as Partial Least Squares Regression (PLSR) and Principal Component Analysis (PCA) to correlate spectral data with ethanol and acetic acid concentrations.

This modelling framework enhances the predictability and precision of alcohol content measurements from spectral and impedance data.

Bioimpedance as a Complement to Spectroscopy:

Demonstration of the complementary role of bioimpedance spectroscopy in enhancing the sensitivity and specificity of alcohol detection, particularly in solid mediums such as porcine skin and gelatine phantoms.

Provides evidence that bioimpedance can improve the accuracy of ethanol and acetic acid detection beyond optical methods alone.

Novel Skin Replicative Phantom for Tissue Composition Investigations

The final contribution of this research is the development of a novel phantom capable of closely replicating skin tissue properties, allowing for a better understanding of the behaviour of volatile organic compounds in complex tissue matrices.

2 Alcohol in the Human Body and Society

In chemistry alcohol, also known as Ethanol, is a chemical from the family of organic compounds Alcohols. The OH function group characterises it at the end of the carbon chain. The chemical structure of ethanol is represented in Figure 2.1. Among its chemical properties, ethanol is a transparent liquid with a very pungent smell and is flammable.

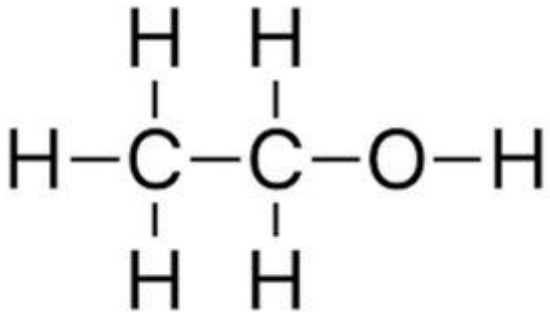

Figure 2.1: Chemical Structure of Ethanol

Ethanol is a naturally occurring compound, synthesised mainly by microbes such as yeast during the fermentation reaction [12]. During the fermentation reaction, sugars such as fructose and glucose are broken down and oxidised to form ethyl alcohol. This process is usually associated with producing alcoholic beverages such as beers or wines. Due to the presence of the OH group, ethanol has a more alkaline pH of 7.33, which also reduces its boiling point, compared to water, to 78.37 degrees Celsius. Besides fermentation, alcohol can also be manufactured by distillation, which separates ethanol from water mixtures through thermal separation due to the difference in boiling points between the two liquids. The distillation process is performed by fractional distillation in a distillation still. This process produces more pure ethanol mixtures for spirits, such as whiskey or vodka. It is vital to note that fermentation is still a key part of alcoholic beverage production, and fermentation is only the means of mixture purification. The following section will aim to outline the historical origin and significance of ethanol and how it evolved into the substance of abuse that it is today.

The earliest evidence for alcohol consumption dates back to 5,000 BC in Mesopotamia, modern-day Iran, by fermentation of cereal. During the same time, alcoholic beverages, mostly beer and cider, were consumed in China, Egypt, and later in Europe during the Bronze Age. The evidence for consuming those beverages was uncovered by the study of residue from remaining jars and ceramics, some dating consumption of fermented drinks between 9,000 – 7,000 BC in China [13]. The influence and recognition of alcohol as a product of regular consumption can be attributed to the purifying effects of ethanol, particularly the effects it has

on bacteria. Ethanol can be used as a disinfectant, and as water purification methods were limited at the time, alcoholic beverages proved to be a safer option than regular water. The extent can be seen in the worship of alcohol, particularly in the Greek methodology, depicting Dionysus as the god of wine [14]. Alcoholic beverages, such as wine, are also used in Christian celebrations. Numerous efforts have been made in the past to ban alcohol consumption, the most notable of which was the American Prohibition, which demonstrated the scale of society's dependency on alcohol [15].

Nowadays, the role of alcohol has evolved into an instrument used to ease social interactions and reduce social inhibition, and it is popularly consumed during celebratory events. As seen in Figure 2.2, alcohol consumption is a worldwide phenomenon, mainly prominent in Europe, Asia, North and South America and Australia. The discrepancies between these regions and North Africa, the Middle East and India could be attributed to cultural and religious differences. Average alcohol consumption per person across the whole world amounts to 6.4 litres of pure alcohol per year [16].

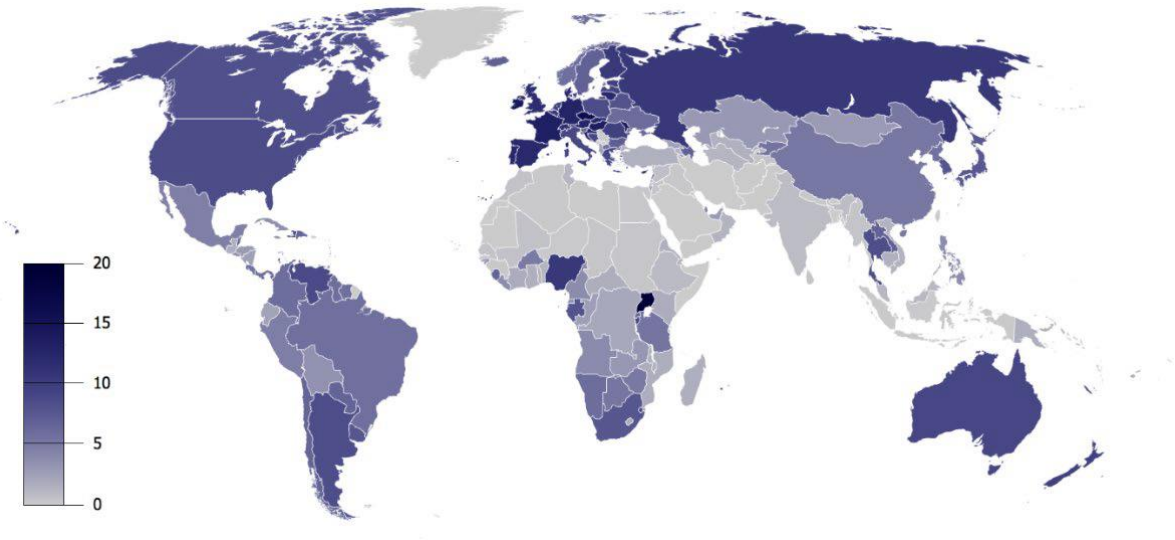

Figure 2.2: Worldwide alcohol consumption per capita in litters per year[16]

The worldwide alcohol beverage market is estimated to be worth around 1.5 trillion USD [17], with the UK market accounting for roughly 45 billion USD [18]. With such a large market cap, the alcohol industry is a very profitable business and, subsequently, a huge employer. Within the UK, there are 47,200 pubs and 2,274 breweries. The alcohol industry, therefore, is a significant component of the UK economy and should be regarded as a major staple of social life. Alcohol consumption has also been shown to grow steadily over the last decade, as reported by the Office for National Statistics (ONS) in 2014, as shown in Figure 2.3. However,

high consumption of alcohol contributes to an increase in antisocial behaviour, violence, and increased hospitalisations. All of these harm society and also carry a substantial cost.

Alcohol is a primary catalyst for violence and anti-social behaviour [19]. The incidence of these events can be directly correlated with the days on which alcohol is consumed at higher doses, particularly on the weekends and national holidays. These instances can be linked with destruction of property, physical violence, and crimes such as theft. However, the negative impact of alcohol intoxication is not only limited to the damage of physical objects but also to the consumer. Alcohol consumption can lead to altered judgement, making the consumer more prone to injury, and at higher levels of intoxication, the patient may experience loss of motor function and consciousness. In extreme cases where the body cannot no longer support the rate of alcohol metabolism, the acidity of the body increases, leading to alcohol poisoning, requiring medical assistance to remove excess alcohol from the stomach. In total, the cost of alcohol in British society due to alcohol has been estimated as £21 Billion, with some estimates putting this figure as high as £27 Billion [20]. This includes monetary losses due to criminal damage, NHS intervention and loss of productivity due to sickness and unemployment. Regardless of all of its flaws and problems caused by excessive consumption, alcohol remains the most popular intoxicant in the world. Reasoning for this continued consumption of a substance that seemingly only causes problems may be the influence of intoxication, mainly linked to the stimulated production of serotonin, a hormone associated with the reward system of the brain. Many people associate alcohol with relaxation and celebration; therefore, consumption of alcohol remains high across the world.

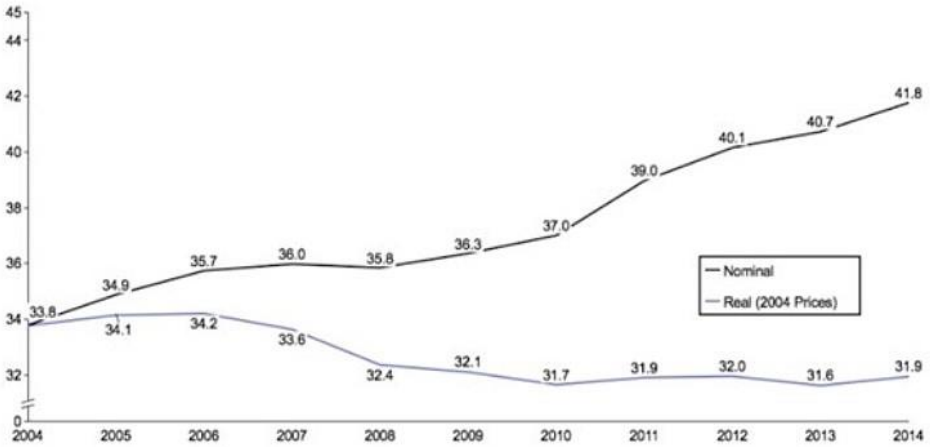

Figure 2.3: UK alcohol spending (£ billions)[21]

Some research in the field even suggests that minor to moderate doses of alcohol can be beneficial to health [22]. However, they are disputed in favour of other components in alcoholic beverages, which are the attributing factors for improved cardiovascular health, one of which is polyphenols found in red wine [23]. Alcohol consumption shows no signs of slowing down and is here to stay therefore, we must aim to find ways to prevent excessive alcohol consumption. To aid this aim, it is also vital to understand the toxicology of ethanol and hence explain its intoxicating effects.

2.1 Mechanism of Intoxication and Breakdown of Ethanol

Intoxication can be defined as loss of control over actions or behaviour changes under the influence of a drug. Intoxication due to ethanol can be divided into three main parts: initial take up, the peak, and the decay stage. This can be illustrated from the studies performed on human volunteers to investigate the changes of alcohol in their blood over time, as seen in Figure 2.4; the initial uptake of ethanol causes the blood alcohol concentration (BAC) to rise rapidly, reaching the peak intoxication at roughly 1 hour after the initial consumption. After the peak, BAC levels decay, reaching zero between six to eight hours after initial consumption. This, however, is also dependent upon the volume of ethanol consumed.

The standard unit of measurement of alcohol intoxication is not internationally agreed upon, with variations in the order of magnitude of measurement as well as the numerical systems used. In the medical literature, the consensus for the units of alcohol is to use BAC as representative of the volume of pure ethanol per 100 ml of blood, varying from 0 to 0.5, representing concentration levels between 0 and 500 mg/dL. For reference, the intoxication driving limit in the UK is 0.08 BAC, equivalent to 80 mg/dL.

Regarding the previously mentioned intoxication over time graph, the initial intake of ethanol is very rapid, reaching peak intoxication within one hour of consumption. This period is characteristic of euphoric behaviour, including laughter, social inhibition, and generally increased well-being due to the release of hormones such as serotonin. At the peak of intoxication, these effects begin to slowly fade away due to decreasing levels of ethanol in the body. The roll-off stage is associated with increased tiredness and depression [24].

The primary influence of ethanol intoxication originates in the central nervous system through the inhibition of Gamma-aminobutyric acid) GABA receptors. Alcohol molecules inhibit the active site of GABA receptors, resulting in reduced cognitive function and decreased special

awareness. Alcohol also contributes to the production of serotonin, resulting in a relaxed state of the consumer [25].

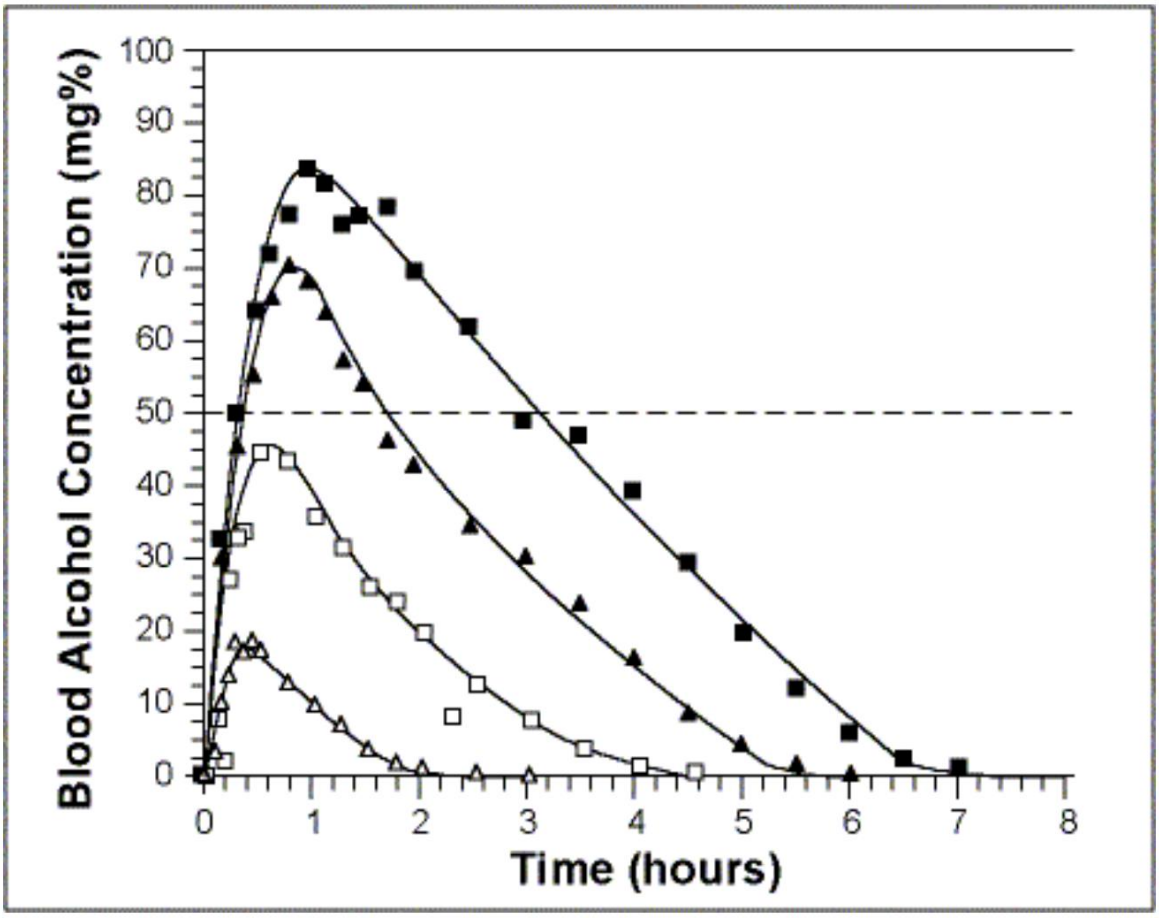

Figure 2.4: Blood alcohol concentration over time, comparing different levels of dosage [26]

These effects were off with time, depending on several factors, such as age, gender, and body weight. Several research articles also correlate gender as an aspect of the varied breakdown of ethanol, possibly explained by the lower resting metabolic rate in women [27]. Tolerance should also be a factor when considering the decay of ethanol in the blood, as it has been demonstrated that people with AUD can metabolise ethanol at a faster rate than occasional drinkers [28].

As seen from the Figure 2.4, the consumed volume of alcohol has an impact on the duration of the intoxication period, the peak of the intoxication, the gradient of increase and the rate of elimination. This example clearly illustrates that impact of intoxication can be categorised by the dosage. A regular sitting in a bar would expect the visitor to consume between 3 and 12 units, whilst the recommended limit for consumption is at 14 units per week. Further information about the dosage consumption impact is detailed in Table 2.1.

Table 1: Summary of Alcohol Dosage and Side Effects

Blood Alcohol Concentration (%)	Approximate Number of Drinks	Expected State
0.01 -0.03	1	Mild relaxation, slight warmth, subtle mood elevation. No significant impairment.
0.04 – 0.06	1-2	Relaxed, lowered inhibitions, mild euphoria, slight decline in judgment and coordination. Reaction time slows.
0.07 – 0.09	2-3	Impaired balance, reduced speech clarity, noticeable decline in motor skills. Legal intoxication threshold in many regions is **0.08%**.
0.10 – 0.12	3-4	Clear speech slurring, poor coordination, delayed reaction time, reduced self-control, exaggerated emotions.
0.13 – 0.15	4-6	Major motor impairment, blurred vision, poor balance, difficulty walking. Judgment severely impaired. Risk-taking increases.
0.16- 0.20	6-8	Severe impairment of motor control, blackouts may begin, nausea and vomiting common, confusion.
0.21 – 0.29	8-12	Stupor, possible blackouts, inability to stand or walk without help, severe confusion, risk of injury, loss of bladder control.
0.30-0.39	12 +	Severe central nervous system depression, possible unconsciousness, slow/irregular breathing, risk of death.
0.40 or more	Variable	Coma, respiratory arrest, **life-threatening alcohol poisoning**, high likelihood of death without immediate medical care

In the body, alcohol is subject to many chemical reactions, specifically those involved in its breakdown. A group of enzymes responsible for ethanol breakdown are known as alcohol dehydrogenase. These enzymes break down alcohol into acetaldehydes and, subsequently,

acetic acid. These waste products are dealt with in the body using various other enzymes. Specifically, the acetic acid is subject to the acid cycle for neutralisation. It is vital to highlight that high concentrations of these acids can lead to acidosis, a symptom of alcohol poisoning, requiring medical attention in severe cases.

Besides inhibiting GABA receptors and being broken down by enzymes, alcohol also influences the function of the cardiovascular and pulmonary systems. The impact of ethanol on the blood vessels primarily extends to the function of relaxation, achieved through vasodilation. It is vital to note that although alcohol relaxes the blood vessels, this is only seen in small doses of alcohol. This is also the contributing reason for the beneficial health impacts of alcohol. However, this is exclusively limited to small doses of alcohol. At higher levels of BAC, it begins to take a pressure operation, restricting the blood vessels [29]. This, once again, can be attributed to the acids produced through the metabolic breakdown of ethanol, although this effect's true origin is unclear.

2.2 Health Risks Associated with Alcohol Consumption

Alcohol is capable of affecting many systems in the body, resulting in an intoxicated state. As mentioned, these effects manifest in bodily organs such as the heart, lungs, liver, and brain. However, these effects are short-lived and fade away over time. On the other hand, long-term consumption of excessive amounts of alcohol can contribute to a multitude of diseases, spamming both the fields of physical and mental health.

Alcoholism, sometimes referred to as Alcohol Use Disorder (AUD), is a mental disease characterised by unregulated consumption of alcohol. The root causes of alcoholism are mostly unexplored in terms of explaining the susceptibility to developing an alcohol addiction [30]. Some research suggests that both genetic and environmental factors play a role in the development of alcoholism [31], [32]. Alcoholism is often characterised by large and frequent consumption of alcohol as well as by the attributing withdrawal symptoms, some of which include tachycardia, tremors, sweating, delirium, seizures, insomnia, and anxiety [33]. Several treatments exist to help recovering alcoholics [34], [35]. Regular and uncontrolled consumption of alcohol can lead to an alcohol dependency, which, if untreated, can become a gateway for the development of more severe health problems, some of which are fatal.

Cardiac health is significantly impacted by excessive and regular consumption of alcohol. The long-term effects of alcohol consumption include alcoholic cardiomyopathy (change of shape of the heart), high blood pressure, myocardial infarction (heart attack), arrhythmias (irregular

heart rhythm), fatal cardiac arrest and stroke [36]. The association between heavy alcohol use and cardiovascular disease (CVD) are unclear. The discussion around this topic focuses on alcohol's effect on the atherosclerotic process (hardening of blood vessels) in vessels and the toxic damage to the myocardium [37].

The liver, as the primary site of alcohol metabolism, experiences the most damage, much of which is mitigated by the regenerative properties of the liver [38]. However, even that is not enough to prevent the tissue damage caused by excessive and prolonged consumption of alcohol. Chronic and excessive alcohol consumption results in the formation of hepatic lesions on the liver, including steatosis (deposition of fat in hepatocytes), hepatitis (inflammatory type of liver injury), and fibrosis (tissue scarring) [39]. Continuous damage to the tissue of the liver and the formation of scar tissue contribute to and increase the risk of developing liver cancer, a very prominent disease amongst heavy alcohol users.

Alcoholism and heart and liver damage are only a few of many pathologies which can be attributed to excessive consumption of alcohol [40], [41]. Alcohol-related disease is a significant burden on the health system, especially in the UK, where the consumption of alcohol is embedded into culture and everyday life. Therefore, several safeguards have been implemented to limit the effects of the damage caused by alcohol consumption, both on the healthcare system and the society as a whole. The most prominent of these safeguards has been the development of technologies and techniques for quantifying ethanol levels in the blood to guide the intoxication level.

3 Current State of the Art in Intoxication Sensing

The literature review of ethanol intoxication sensors has yielded several results encompassing different aspects of alcohol intoxication ranging from behavioural, physiological, and chemical changes in the subject's body. The technologies and techniques were categorised into six main sections: pharmacokinetic estimates, breath sample testing, bodily fluids, physiological changes, transdermal, and optical spectroscopy. It is vital to note that many techniques and technologies overlap in this generic categorisation. The most obvious example is breath alcohol spectroscopy, which utilises both the features of breath alcohol devices and optical spectroscopy. More examples of these cases will be given in this chapter. The findings of the review and all the devices and techniques considered are summarised in Table 1.

Table 2: Summary of device and techniques for intoxication state assessment or proof of recent consumption, colour coded Type linked to Figure 3.6.

No.	*Device/Technique*	*Parameter*	*Type*	*Form Factor*
1	Nicloux Flask	Chemical reaction	Bodily fluid testing	Flask/blood extraction
2	Widmark Flask	Chemical reaction	Bodily fluid testing	Flask/blood extraction
3	EBAC Equation	Estimation based on physiological factors	Early estimation method	Equation
4	Photovoltaic Assay	Colour change based on oxidation level	Breath alcohol	Portable device
5	Intoxilyzer	Near-infrared spectroscopy	Breath alcohol	Benchtop device
6	Fuel-Cell Analyzer	Current generated by ethanol oxidation	Breath alcohol	Portable device
7	Semiconductor Breath Analyzer	Strip colour change	Breath alcohol	Portable device
8	Ignition Interlock Breath Analyzer	Alcohol oxidation reaction fuel cell	Breath alcohol	Portable device
9	Gas Chromatography	Evaporation and separation of components	Bodily fluid testing	Benchtop device
10	Headspace Gas Chromatography	Evaporation and separation of components	Bodily fluid testing	Benchtop device
11	Enzymatic Blood Testing	Strip colour change	Modern estimation method	Strip test
12	EtG Test	Strip colour change	Modern estimation method	Strip test
13	PPG Datum Line	Changes in PPG signal systolic and diastolic	Physiological factor analysis	PPG analysis/modern estimation method

No.	*Device/Technique*	*Parameter*	*Type*	*Form Factor*
14	Face Heat-Map Distribution	IR image analysis of the forehead and nose	Physiological factor analysis	IR in-vehicle cameras
15	Volvo SPA2 Platform	Head position	Physiological factor analysis	In-vehicle cameras
16	Bioimpedance Spectroscopy	Impedance across the body, legs, and arms	Transdermal sensor	Experimental device/benchtop
17	SCRAM CAM	Alcohol in sweat	Transdermal sensor	Wristband
18	GinerWrist TAS	Alcohol in sweat	Transdermal sensor	Wristband
19	BACtrack Skyn	Alcohol in sweat	Transdermal sensor	Wristband
20	Proof	Alcohol in sweat	Transdermal sensor	Wristband
21	Quantic Tally	Alcohol in sweat	Transdermal sensor	Wristband
22	Iontophoretic Biosensing System	Stimulated emittance of ethanol from the skin	Transdermal sensor	Tattoo sticker
23	Enzymatic Biosensors	Enzymatic redox reaction	Transdermal sensors	Transdermal sensors
24	Biosniffer	Inert gas and fluorescence	Transdermal sensors	Benchtop device
25	EtG Sensor	A by-product of ethanol metabolism	Transdermal sensor	Wristband
26	ISF Sensor	Extraction of ISF	Transdermal sensor	Wristband
27	ISF Microneedle Sensor	Sensing of ethanol in the ISF	Transdermal sensors	Skin-attachable patch
28	TTT1100	Spectroscopic measurement of tissue	Optical tissue spectroscopy	Benchtop
29	TTT2500	Spectroscopic measurement of tissue	Optical tissue spectroscopy	Benchtop
30	NIR Dynamic Spectrum	Spectroscopic measurement of tissue/physiological parameter	Optical tissue spectroscopy	Algorithm
31	Autoliv	Spectroscopic measurement of exhaled air	Optical breath spectroscopy	In-vehicle module
32	WD-DPTR	Spectroscopic measurement of tissue	Optical tissue spectroscopy	Benchtop device
33	Pulse Alcometry	Absorption of light at specific wavelengths and pulse variation	Optical tissue spectroscopy	PPG adaptation

No.	*Device/Technique*	*Parameter*	*Type*	*Form Factor*
34	THC and Alcohol Saliva Sensor	Saliva content reaction with electrodes	Bodily fluid testing	Ring
35	Breast-Milk Sensing	Strip colour change	Bodily fluid testing	Strip test
36	Rockley Photonics VitaSpex Pro	Spectroscopic measurement of tissue	Optical tissue spectroscopy	Wristband
37	Hair Analysis	Detection of EtG and EtPA	Modern estimation method	Laboratory test
38	Nail Analysis	Detection of EtG and EtPA	Modern estimation method	Laboratory test

3.1 Early Estimation Methods

The earliest methods of quantifying the level of alcohol in blood were introduced by Erik Widmark in 1918 [42] by a method based on Nicloux's oxidation separation [43], with an introduction of the S-shaped capillary tube for blood collection from the finger or the earlobe.

The ethanol content was measured by pouring the collected blood into a glass cup affixed to the neck of the flask. The ethanol would then separate from the blood by diffusion. The results of this experiment were reported as a mass concentration unit, giving rise to one of the first units of alcohol blood contents, the promise. The final level of ethanol was then determined by titration. An example of the apparatus used by Widmark is shown in Figure 3.1.

Later on, an equation introduced by Widmark and Tandberg in 1924 [44] aimed at estimating the levels of alcohol in the blood through analysis of the behaviour of ethanol as it was metabolised in the body. Their work proposed a mathematical formula to determine ethanol levels in a subject's blood based on the amount of ethanol consumed, body weight, alcohol elimination rate (β), distribution of water in the body (r) and time since the consumption began. This correlation is outlined by Equation 1. Notably, the values of constants β and r are subject to variation across individuals, most noticeably between sexes [45]. Those variations give rise to the error of the EBAC equation.

$$EBAC = \frac{A}{Wrt} - \beta T$$

Equation 1: Widmark estimation of blood alcohol concentration equation

This method of calculating the estimated level of BAC has been used extensively in forensic examinations and has contributed significantly to the field of ethanol toxicology [46]. Widmark and Tandberg also developed similar models for levels of methanol and acetone. [44].

For its time, the EBAC equation provided a quick and easy-to-use method for determining the blood's ethanol level. However, it has several shortcomings, mainly those associated with the values of β and r. Since these values vary considerably between individuals, the values used for generic applications of calculating EBAC often do not account for the natural variance between individuals. For that reason, Widmark developed variants of his equation to account for these natural variations between men and women, measuring the uncertainty of the result. As a result, the uncertainty of the EBAC is around ± 20 % [47]This high uncertainty results from assuming general values for β, r and other parameters in the EBAC equation.

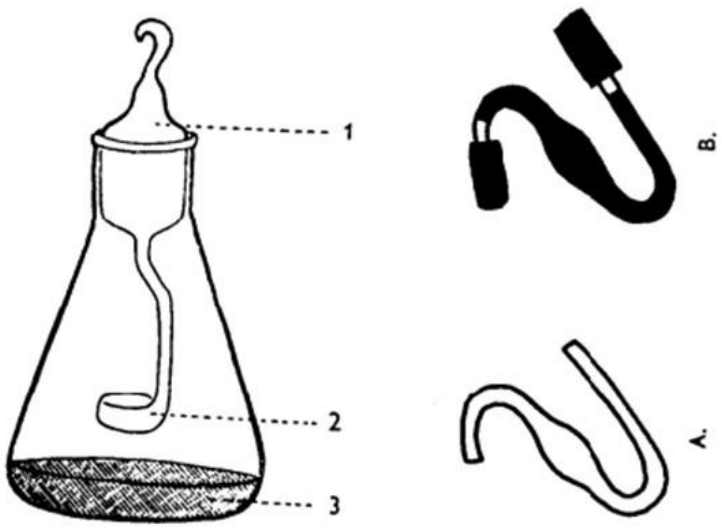

Figure 3.1: Widmark diffusion flask. 1: Ground glass stopper, 2: Blood cup, 3: Dichromate sulfuric acid oxidation reagent, A and B: S-shaped capillary tubes[46]

3.2 Breath Alcohol Devices

The earliest mentions relating BAC to Breath Alcohol Concentration (BrAC) date back to 1874, by Anstie [48], by observations that showed the presence of ethanol in the subject's breath after consumption of an alcoholic beverage. Later research in the field by Bogen in 1927 demonstrated a method of quantification of BrAC and using it to estimate BAC [49]. The first widely available commercial product for quantifying BAC, the Breathalyzer™ developed by Brokenstein [50]. Correlating the concentration of ethanol in the bloodstream to the amount of

ethanol exhaled was invented by measuring the chemical colour change as ethanol reacts with acid dichromate. The idea of using breath samples to estimate levels of ethanol in the bloodstream was implemented among law enforcement for the prevention of driving under the influence of alcohol incidents.

The scope of development of breath-alcohol devices is broad. It encompasses many areas of chemical analysis to determine the level of ethanol, subsequently giving rise to various devices measuring BrAC using numerous methods. Regardless of the variations in the devices used to measure subjects' BrAC, one feature remains unchanged: the calibration method. Most BrAC devices consider a calibrating ratio of 2,100:1 for the alveolar air and ethanol volume, such that 2,100 ml of alveolar air is equivalent to 1 ml of ethanol in a breath sample. [51]. This approximation is the major criticism of BrAC devices. Naturally, the above ratio can vary between individuals as much as between 1,448 and 3,818 [52]. The value of 2,100 has been taken as an average value for the alveolar lung volume and used in the calibration of BrAC devices. Depending on the country of use, the ratio used may vary. As a result, BrAC devices may give overestimates for individuals with larger lung capacities and underestimates for individuals with lower lung capacities.

BrAC devices may be divided into four main categories based on the ethanol detection principle they employ. *Photo-voltaic assay*: measuring the colour change of a liquid experiencing a redox reaction, usually from red/orange to green, when ethanol is detected. The degree of colour change is measured and translated into an output of BrAC level and converted into BAC. [50]. *Infrared spectroscopy* measures the spectral change of the breath sample by passing a beam of NIR radiation through the sample, with high specificity for ethanol. [53]. *Fuel cell BrAC devices*: measure the oxidation of ethanol into acetaldehyde on an electrode cell. The output of the current is measured across the cells, which is proportional to the level of oxidation and, in turn, the amount of ethanol in the breath sample [54]Fuel cell alcohol devices are much smaller and can be implemented in portable dimensions. This feature makes them the most popular type of BrAC device for roadside testing. [55]. *Semiconductor-based BrAC devices* operate on the change of conductance of the metal oxide layer in the presence of ethanol, which acts as a reducing agent [56]Semiconductor BrAC devices are still in the early stages of development. However, they present an opportunity to further minimise portable alcohol testing devices.

BrAC devices are generally convenient and practical for estimating BAC by considering an associated measure of BrAC. It is vital to note that BrAC devices are prone to erroneous readings and can only be used to calculate the level of ethanol in the subject's blood. Besides the error associated with the calibration of these devices, the environmental conditions under which the devices operate must also be considered, precisely the temperature, demonstrated by Legge [57]. Legge also cited that those measurement errors are not only impacted by the environmental factors during the test but also the equilibrium of the ethanol in the respiratory tract depending on the individual's breathing patterns. This was later confirmed by Jones [58], who showed that holding breath increases the concentration of expired ethanol by up to 18%, whilst hyperventilation can decrease it by up to 12 %. Therefore, for BrAC, system corrections have to be applied in numerous cases to achieve the most accurate results, many of which, suggested by Dubowski [59], should include a subtraction of 0.055 % from all results. As for the time being, BrAC devices are here to stay and still prove to be helpful as a deterrent for drunk driving as well as assisting in the serving of justice.

3.3 Bodily Fluid Testing

Among alcohol testing techniques, the bodily fluids of blood, urine, and saliva yield large variations, both in technique implementations and the results obtained by each method. Hence, each one finds its application in a different field of testing.

Bodily fluid testing concerns the measurement of ethanol concentration in the blood, urine and saliva. To determine the concentration of ethanol in the sample, the most common technique used is Gas Chromatography (GC) or Headspace GC, which measures the presence of exact levels of ethanol in a sample through separation of components in a gas state [60]. These tests can be performed on whole blood as well as plasma and serum, with highest possible accuracy [61]. However, it is not the only technique that can be used to determine the level of ethanol in a blood sample. Alternatives include oxidometric methods [62]; separation of ethanol from blood via diffusion, distillation or aeration and reacting ethanol with oxidising agents (dichromate or permanganate), where the residual agent determines the level of ethanol. Other techniques also include the use of enzymes [63], such methods utilise ADH and NADH to oxidise ethanol into acetaldehyde and by enzyme kinetics estimate the level of ethanol present in the sample.

It is key to note that blood samples must be handled with care and in many cases adhere to rigorous standards for storage. These include and are not limited to air-tight sealing of the tubes, mixing in additives such as anti-clotting agents and preservatives to prevent pathogen growth

[64]. All of which contribute to blood sampling testing to being an expensive and time consuming process, not suitable for personal intoxication monitoring.

Blood ethanol testing also comes with its own array of strengths and shortcomings, which determine its viability in ethanol testing. Since it is the most direct method of measuring ethanol levels the results obtained are considered totally true and representative, however one must consider the site of blood sample collection, since arterial blood has higher concentration of ethanol, however venous blood samples are easier to acquire [65]. Blood testing also requires a small sample size to obtain measurements, as little as 2.5 µl of plasma [66]. Blood sampling is an invasive procedure, which makes it difficult to be implemented in a standardised testing environment such as a roadside. Besides this, samples often must be sent off to external laboratories, due to the cost of equipment required for testing, more specifically the gas chromatograph. Therefore, blood ethanol testing has the most applications in forensics and research.

Besides blood testing, BAC levels can also be estimated from urine samples. This method comes with an entire range of short-comings, and it is not useful for accurate determination of ethanol levels in the subject's blood stream. The greatest error associated with urine ethanol testing comes from the behaviour of ethanol in the body, more specifically the changes in ethanol level during the absorption and elimination stages [28]. During this time the concentration of ethanol can change drastically. Therefore, urine samples, are more commonly used to determine the presence of ethanol in a sample, but not quantify the level of intoxication. This is because urine sampling represents the average exposure to ethanol during the collection of the urine in the bladder.

Urine ethanol testing techniques include those used for blood sample testing, such as gas chromatography. However, alternatives exist, such as the use of EtG tests [67], determining the level of ethanol in urine based on a colour change of a strip. Once again, this method cannot identify the level of intoxication due to ethanol, just estimate the level of exposure to ethanol in a specific time period. Regardless, urine testing can be used for monitoring subject's average exposure in order to alcohol to establish if they have a drinking problem. Urine samples may also be used to determine the presence of other intoxicants and performance enhancing drugs.

Besides the use of gas chromatography, urine samples may also be tested using head-space gas chromatography [68], due to its precision and the ability to distinguish aldehydes from ketones in urine. It is also key to note that urine sampling is subject to false positives, resulting from

sugar consumption which when fermented in the bladder turns into ethanol. Therefore, urine sampling finds most of its application in general alcohol exposure testing, such as monitoring of recovering alcoholics [69].

Lastly, the other bodily fluid that can be used to estimate BAC is saliva. Since ethanol is highly soluble in water, its level can be estimated from saliva samples, however, this technique also comes with many shortcomings. Like blood and urine sampling, the techniques used in measurement of saliva alcohol concentration (SAC) include gas chromatography and enzymatic oxidation of ethanol through alcohol dehydrogenase. SAC tests find the majority of their applications for testing trauma patients in emergency rooms [70]. In order to perform these tests, a volume of 2 mL of saliva is required, which may be difficult to obtain from patients who are highly intoxicated or have dry mucous membranes. Moreover, saliva testing can only capture a maximum intoxication level of 350 mg/dL, however due to its location site for the sample testing, the results are prone to false positives due to the residue of alcohol from consumption or from oral hygiene products. Saliva testing is more useful and more accurate than urine testing, but still far from the true level of ethanol given by the blood sample testing.

Bodily fluid testing has not been limited to chemical colour changes and analytical measurements of mixture composition. Recently developed by Mishra et al [71] a saliva testing ring is capable of establish the presence of alcohol and delta-9-tetrahydrocannabinol. The integrated sensors are in the centre of the ring. The system operates on the principle of electrochemical interaction between the electrodes and the substances of interest. The sensor element consists of four electrodes: two working electrodes - carbon modified with 1 % MWCNT and carbon/Persian-blue. The other two electrodes are the references Ag/Cl and carbon counter. The electrode pairs are responsible for sensing THC and ethanol respectively. The alcohol detection is established by the oxidation reaction between the ethanol molecules and the Persian-blue electrode. The generated current is then used to establish the quantity of ethanol in saliva. The sensor is still in early development and requires in-vivo testing. Currently the sensors are capable of distinguishing between levels of alcohol saliva in the ranges between 0 and 0.062 %. An implementation of alcohol sensing into wearable devices is mostly dominated by transdermal sensors, with few consumer-oriented products employing saliva for intoxication sensing. The above article illustrates the development in the chemical sensing techniques is prominent and has taken advantage of the electronic system and minimisation potentials, allowing for the entire device to fit inside a ring. The ring also contains a Bluetooth module for wireless data transfer.

Bodily fluid testing is an area of ethanol testing that produces mostly mixed results, depending on the fluid used. By far, the most accurate method of ethanol intoxication is blood testing, which is considered the gold standard of ethanol testing. On the other hand, urine provides a good enough indication of the consumption habits of alcohol, and saliva is a reasonable estimate of BAC with a correlation between 0.879 and 0.957 when tested against serum alcohol level [72]. Yet, it is still lower than those of BrAC devices. In conclusion, bodily fluid tests for saliva and urine still have a long way from being used as a reliable and accurate form of measuring ethanol intoxication levels.

3.4 Intoxication Estimation Algorithms

Besides considering the level of alcohol in breath, blood, urine and saliva, ethanol intoxication also manifests itself as a change of physiological parameters and behaviour. More recent developments in machine learning and image analysis have allowed for techniques to estimate the level of intoxication based on changes associated with typical symptoms of alcohol intoxication. Such changes found for this review concern changes to PPG signal, body temperature, eye position, etc. These methods provide a new outlook into measuring alcohol intoxication by not only considering the level of ethanol in the bloodstream but also the degree to which a person is affected, giving rise to the true definition of intoxication as changes in behaviour, regardless of the amount of alcohol ingested.

One emerging field of quantifying alcohol intoxication through physiological means is the analysis of the Photoplethysmography (PPG) signal, more specifically, the diastolic and systolic patterns of a PPG signal, as shown by Chen [73]; their proposed system is capable of determining alcohol intoxication shown to have an accuracy of 85.71% in a study of 84 subjects. Their algorithm considers the relationship between the systolic and diastolic portions of the PPG signal and joins them with a "Datum Line". This line acts as the principal component of the correlation with alcohol intoxication. These datum lines are then stored as a data set for the supervised machine-learning algorithm (SVM) classification, although different techniques can also be used. The algorithm works by comparing small changes in the PPG signal between sober and intoxicated data sets and decides the possible intoxication of an individual. It has been shown that a regular pattern in the PPG signal occurs when an individual ingests alcohol and even shows a threshold after which the change in heart rate behaviour changes significantly. As is the nature of all machine-learning algorithms, the greater the training set data, the better the outcomes; therefore, future implementation of this methodology has significant potential to change the landscape of alcohol testing whilst also outlining a

fundamental physiological change that occurs due to alcohol intake. It is also possible that the low accuracy figure is not attributed to the error of the SVM classification but rather the tolerance and individual circumstances of each subject. Therefore, this method should be examined with a much larger number of participants. Another criticism of this work would come from validating the results from the PPG algorithm, as per the use of BrAC device, which, as mentioned in the previous section (Breath Alcohol Devices), are notoriously associated with numerous sources of interference. The results should be validated using whole blood samples analysed with gas chromatography to determine the feasibility of this method for BAC estimation.

The development in the field of PPG analysis for intoxication levels has even been examined in comparison to ECG by Wang et al. [74]. Their study compared the operation and performance of support vector machine (SVM) trained for recognition of intoxication based on the features extracted from each of the respective signals. The findings of their work relate to the fact that both ECG and PPG produce identical classification performance. This has, in turn, motivated their work in developing an algorithm that could be applied to wearable sensors due to its fast computation time, supported by the fact that the action of the cardiac muscle is affected by the presence of alcohol in the blood. In conclusion, their model performed with the highest accuracy of 88%. Currently, the system can distinguish between sober and intoxicated levels (BrAC > 0.15 mg/L). It is vital to note that the system's calibration was performed with a breath alcohol device, associating their errors with the system. Ultimately, the system aims to be implemented in an existing PPG intelligent wearable platform.

PPG signal analysis for detecting intoxication has already been implemented into a "Smart-Steering" system developed by Rachakonda et al. [75]The system incorporates several sensors, including temperature, respiration rate, heart rate, and blood pressure. The combination of these sensors establishes the condition of intoxication based on changes in all of those parameters. Overall, the system claims to be 93% accurate in detecting intoxication. The system is intended to be implemented as an add-on device to a steering system and communicate wirelessly to the car dashboard or any smart device.

PPG signal analysis offers a convenient way of establishing if an individual is intoxicated. These algorithms can be implemented into well-established PPG data acquisition platforms, especially wearable smart devices—however, the criticism of these methods for established lies with the measurement itself. Without an extensive enough calibration set or special

conditions implemented into the algorithms, individuals with irregular heart action could fall victim to false positives if this system were to be more broadly implemented. Association of changes in the operation of the cardiac muscle can be of excellent guidance for the degree of intoxication influence ethanol has on an individual. These can vary based on the regularity of consumption and tolerance.

The effects of alcohol intoxication are not strictly limited to the changes in the behaviour of the heart but also of other parts of the body. Recent research conducted by Kubieck et al [76] suggest a link between the facial temperature distribution and the alcohol intoxication level. By adopting a multi-regional segmentation procedure to analyse symmetries of facial regions such as the nose and the forehead through IR imaging, temperature changes on the individual's face are tracked. Their hypothesis stated an expected reduction in the coldest area on the nose and the hottest intensity on the forehead to expand, hinting at a general increase in temperature of the facial region, supported by the vessel dilation after alcohol consumption. [77].

Their work concluded that multiregional segmentation can distinguish changes in the nose and the forehead temperature associated with alcohol consumption. Their results showed a noticeable shift in thermal region in each of the facial areas investigated, suggesting a link between facial temperature distribution and gradual alcohol intake, particularly useful for continuous monitoring and prevention of DUI. It is important to note that it is only an early stage of method development, only pointing at areas of consideration for IR image intoxication measure, and further work on the classification of intoxication level is required.

Large automobile manufacturers such as Volvo are also implementing similar efforts in passive driver monitoring [78], proposing a system of in-vehicle cameras pointed at the driver's faces to establish whether they are intoxicated or experiencing a distraction. The system proposed by Volvo operates on the principle of analysing the facial expression of the driver and the direction they are looking towards, including the time they spend looking away from the road. The system operates by splitting into three stages, Support: a gentle reminder for the driver to keep their eyes on the road; an Emergency State: a warning message to the driver that they are at high risk of an accident; and an Emergency Stop: the vehicle changes from manual operation to in-built control to pull over and stop the car at the nearest appropriate place and alerting local authorities about the incident. Volvo implemented this system into their vehicles in 2020 with the launch of their new platform, SPA2.

Such implementation of image analysis can potentially reduce the number of incidents caused by drunk drivers. However, it is susceptible to possible exploits such as the covering of the cameras or false negatives from individuals with higher-than-average tolerance to alcohol intoxication. [79].

Additionally, the influence of ethanol consumption impacts the impedance of the skin, as demonstrated by Chaplik et al. [80] In their pilot study, the impedance of the skin was measured between two groups of participants consuming water and ethanol. Their findings showed that the strongest correlation between consumption of ethanol and body impedance was apparent for measurements between the hand and leg. Their investigation also considered hand-to-hand impedance measurement, showing no significant change in body impedance. Although moderate results with correlation coefficients r ranging between 0.22 and 0.39, when considering the relative and initial impedance values, a correlation of 0.47 was reported. Bioimpedance was measured through BIS and ICG thoracic measurements, determining the current path in the body, and evaluated by computing extracellular and intracellular resistances.

Bioimpedance measurement of the skin provides a unique application for estimating ethanol intoxication, as bioimpedance can be measured with capacitive and induction sensors. [81][82], such they can be implemented into everyday objects, for example, chairs or even textiles [83]. However, as shown above, the correlation between alcohol consumption and body impedance is only significant between the extremities of the body parts (hand and leg). With changes to the bioimpedance of the skin, one must consider the origin of such changes and find attributing factors. As ethanol is metabolised in the body, the excretion of its by-products through the skin is a phenomenon that may be linked to changes in skin bioimpedance.

3.5 Transdermal Sensors

Besides considering testing the behavioural and physiological changes that occur as a result of alcohol intoxication, the metabolic rate of ethanol can also be used as an indicator of the level of intoxication experienced by an individual. A series of sensory devices have been developed over the last two decades to allow monitoring of the rate of expulsion of ethanol through the skin by measuring the contents of the sweat through wearable or standalone devices. Wearable devices have received much attention over recent decades, with several review papers published covering different devices available on the market and those in laboratory testing. The findings of these papers were included in this section, and other techniques for transdermal alcohol intoxication measurement were added.

The review by Swift et al [84] from 1992 considered the state of contemporary methods for transdermal alcohol monitoring and evaluating their reliability and potential future implementations. Their review focused on the operation of a device developed by Giner Inc. that measured the current generated by an electrochemical cell when exposed to ethanol from sweat. The operation of the Giner Inc. device showed promising results, with a correlation of $r = 0.94$ ($p > 0.001$) for a variety of doses, showing that early implementation of transdermal alcohol sensors has been successful in determining the quantity of alcohol in the blood.

The review of wearable devices for Alcohol Use Disorder by Davis-Martin et al [85] in 2021, outlined the most noticeable devices on the market, including SCRAM CAM, GinerWristTAS, BACtrack Skyn, Proof, Quantic Tally, Iontophoretic-biosensing system [86], AlcoWear, Sensor-equipped smart shoes, AlcoGait, and DrinkTRAC. The review categorised the wearable transdermal alcohol sensors into three categories: *Alcohol Specific Biosensors*, such as SRCAM and Giner WristTAS, used for monitoring the excreted alcohol from the surface of the skin through electrochemical techniques; *Physical Activity Biosensors*, AlcoWear and AlcoGait to monitor physical activity of an individual using gyroscopes and accelerometers, paired with a smartphone; and *Emotion Focused Biosensors*, such as Empatica E4, used by Leonard et al [87], who investigated its feasibility for use on subjects with a history of alcohol abuse.

Within the selection of the listed devices, one strictly distinctive device is the Iontophoretic-biosensing system. [86]. It is unlike the traditional methods of measuring BAC transdermally through sweat by a process of measuring the current generated by an oxidation reaction, correlated with the concentration of ethanol being released through the skin; this is primarily a passive process taking measurement over long periods and presenting the user with data outlining their overall intoxication curve. In the case of the Iontophoretic-biosensing system, the measurement is taken in a short time, providing a snapshot of the level of intoxication. The operation of the system is outlined in Figure 3.2. The Iontophoretic-biosensing system operates on the principle of induced sweat by pilocarpine delivery via iontophoresis -electrical stimulation of tissue to generate sweat. Ethanol in the induced sweat is then measured amperometrically with alcohol-oxidase enzyme and Prussian Blue electrode transducer. The system also interfaces with a smartphone device for continuously monitoring ethanol levels in the sweat on a flexible printed, electronic circuit. Although limited in in-vivo testing, the results showed a correlation of 0.99 between the level of current measured by the system and the BAC

level. Further testing is required to verify the operation of this system and its applicability for continuous alcohol measurement in the future.

It is key to note that the review considered many works, including those concerning the level of alcohol in tissue, but also those focusing on the physical and mental influences of alcohol use to control (AUD). However, The review is limited to electrochemical wearable devices for measuring intoxication levels. This review considered two alternative techniques for measuring tissue alcohol concentration (TAC), using Enzymatic Biosensors and Bio-sniffers.

Developed by Lansdorp et al [88] An enzymatic Alcohol Biosensor utilises the enzyme Alcohol Oxidase (AOx) and a screen-printed Prussian Blue (PB) electrochemical sensor as a transducer. Due to the denaturing of enzymes over time, the device operates one of the prisms of replaceable cartridges. The device was tested on individuals and showed a strong relationship between the BAC level and the current generated from the enzymatic biosensor. This particular method of acquiring the level of TAC is helpful for continuous and long-term monitoring of subjects over a period of time, especially for alcohol toxicology research. Currently, the device has a US patent and is undergoing further development.

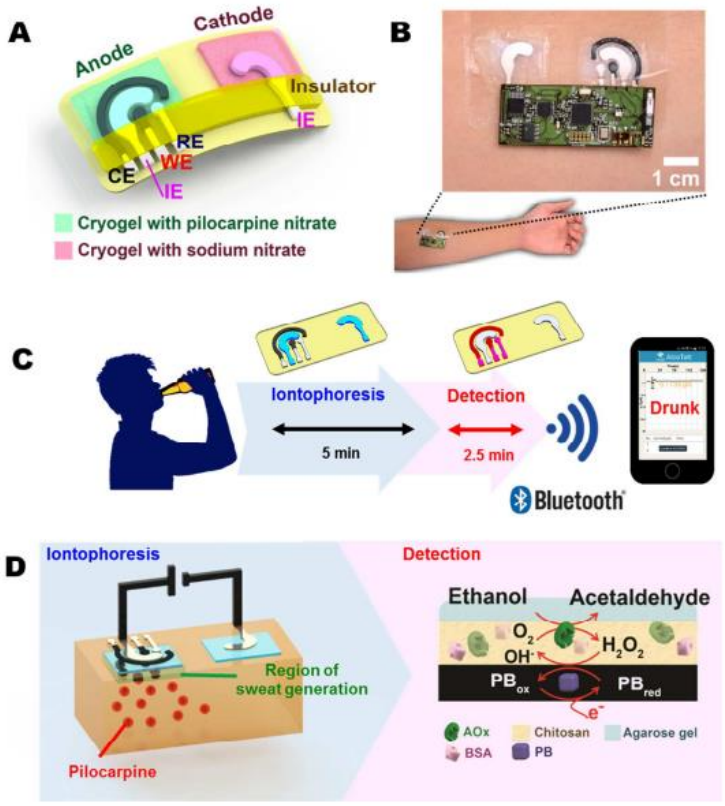

Figure 3.2: Iontophoretic-biosensing system developed by Kim et al[86]

Development in transdermal sensors is not exclusively limited to wearable devices but also to standalone devices. A Biosniffer device developed by Arakawa et al [89] Based on the enzymatic reaction of alcohol dehydrogenase (ADH) targeting ethanol released through the skin as a gas. The device operates on the principle of pumping a carrier gas, mixing with the gas released through the skin, and passing through to the bio sniffer system to detect and measure ethanol concentration through fluorescence detection. Their findings concluded that gas chemistry analysis with fluorescence is a feasible way of accurately measuring the concentration of ethanol in the blood and also to investigate the metabolic rate of ethanol as well as other blood gases.

Developed by Selvam et al [90] a wearable biochemical sensor moving away from the traditional measurement of intoxication by not measuring the ethanol concentration in the skin, but rather considers the amount of Ethyl glucuronide (EtG) as a metabolite of ethanol [91]. The device operates on a principle of electrochemical sensing using gold and zinc-oxide electrodes. As EtG is a metabolite of ethanol produced by the liver, the detection of EtG from an individual's tissue can be used to examine relapsing drinkers or confirm abstinence. As EtG stays in the body for up to 3 days, the device can also take snap-shot measurements of the EtG concentration in the tissue, giving it a broad application area.

When using electrochemical sensors to measure ethanol metabolites, much attention must be given to the metabolite's natural occurrence and any possible interference from associated by-products. Regardless of these interferences, the sensor presented in this paper achieved a linear relationship between the amount of EtG measured and the impedance of the electrodes, as $r^2 = 0.97$.

Conclusively, the field of active wearable sensors is expanding. However, a distinction has to be made regarding the nature of the measurement. The developed sensors cannot quantify the level of intoxication but only indicate the presence of one of the metabolites of ethanol, not a subject's BAC.

Alternative methods for measuring alcohol levels in the tissue are not limited to analysing the sweat components but can also be more active in their operation. Venugopal et al [92] presented an example of this with a development of an interstitial fluid (ISF) sensor for alcohol monitoring. The ISF is extracted by using vacuum pressure from micropores on the stratum corneum layer of the skin. The pores on the skin are created via near-infrared laser focused on a black dye on the skin. This method is essentially painless. The findings of this paper state

that alcohol can be detected in ISF within 15 minutes of consumption and shows a linear relationship with the concentration of ethanol in the concentration range 0-0.2% with a resolution of 0.01% through biomedical transducers. In addition, this system is interfaced with a wireless health monitoring system linked to a Wide Area Network (WAN) for continuous patient monitoring. Their findings also report that the illumination system is only viable for three days. A prototype of this system is shown in Figure 3.

Their reviews concerning the current state of transdermal technology for the measurement of alcohol intoxication include those by Fairbairn et al [93], categorising the use of transdermal sensor into four fields of application for the new-generation transdermal sensors: Prevention, Intervention, Medical and Motor vehicle Research. A systematic review by van Egmond et al [94], evaluating the operation of transdermal devices in the field of clinical study.

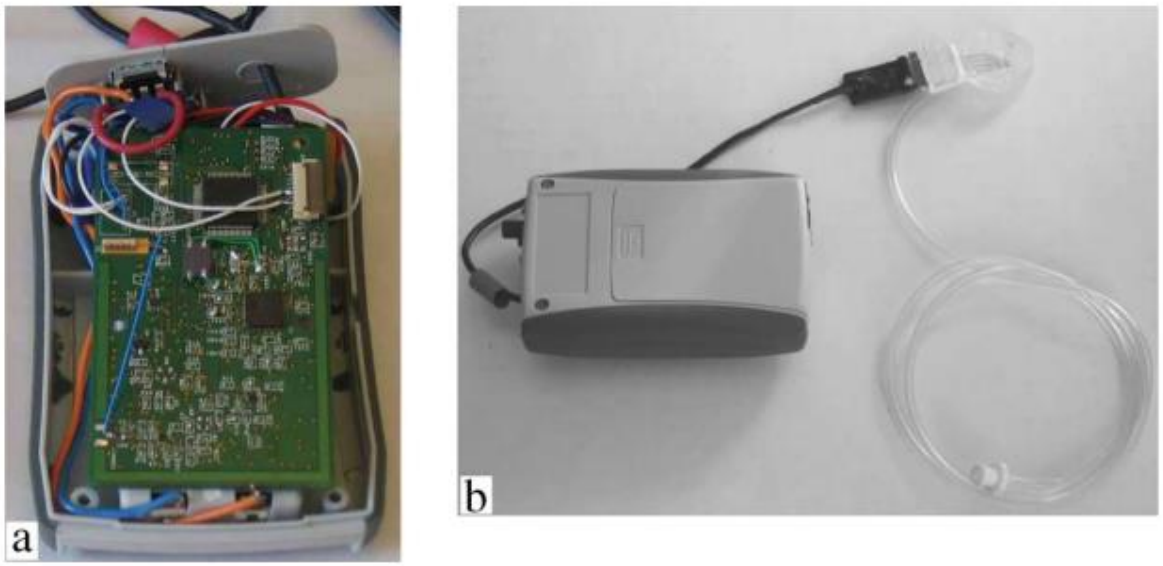

Figure 3.3:ISF alcohol sensor prototype (a: The electronic circuit use for control of the system and responsible for the measurement of ISF. b: The fully assembled system with an ISF extraction tube.

In conclusion, transdermal sensors have been at the forefront of innovation in the field of non-invasive alcohol intoxication sensing, strongly supported by the number of review papers already published on this particular topic. Transdermal sensors provide a unique outlook on the measurement of alcohol intoxication by their incorporation into wearable systems linked with smartphones, increasing both the number of sensors available to measure intoxication and the computing power for processing all the data points gathered from those sensors. However, both electrochemical sensors and enzymatic biosensors suffer from the wear of materials over time, impacting the operation of the sensors and increasing the error in the measurements they gather. This is partially mitigated by the enzymatic biosensors, which incorporate a replaceable cartridge; however, this increases the engagement of the user and introduces the possibility of

human error. The next generation of alcohol sensing devices should aim to move away from using systems that are directly exposed to a chemical process and instead focus on more passive forms of measurement, such as light spectroscopy.

3.6 Optical Spectroscopy

The transdermal sensors described in the above section focus on the sensor's ability to capture the release of ethanol or ethanol-related compounds to estimate the BAC. These methods, however, are susceptible to the variance between individuals, both in the metabolic rate of ethanol elimination and in the variance of the individual's physiology, such as the rate of sweat release. Optical spectroscopy aims to eliminate the bias caused by individuals' ability to excrete sweat by not considering the release of gases and liquids by the skin tissue but rather investigating the state of the tissue itself. It has been shown that optical spectroscopy can be applied to measure the concentration of an analyte to a high precision, both in transmission and diffuse reflectance modes. [95]. This is supported by numerous publications related to blood oxygenation and blood glucose level monitoring. [93]– [95].

Consequently, the field of optical spectroscopy has grown to investigate the tissue spectroscopy changes associated with alcohol consumption. BAC is not estimated by metabolic rates of ethanol and sweat release but instead directly measured from tissue through analysis of the detected light intensities, spectra shifts, or time delays.

Since ethanol is highly miscible in water and its presence in tissue can be detected in the dermal layer of the skin, consisting of roughly 65 to 70% water, the probability of finding ethanol in the tissue post-consumption is likely. Most of the problems associated with optical spectroscopy of biological analytes focus on the selectivity (differentiate between compounds in a mixture) and the specificity (assessment of a particular compound in a mixture) of the device/model implemented.

This review focuses on a particular optical technique, of using near-infrared spectroscopy (NIRS) - to detect the presence of ethanol. Besides NIRS, other optical techniques will also be evaluated.

The most notable devices for measuring TAC are the TruTouch AlcoSense devices, including TT1100 and TT2500, which are the first and second devices developed respectively. These devices use NIR absorption spectra to measure the skin tissue. Based on the Michaelson interferometer Fourier Transform IR (FTIR), operating in the wavelength range between 1.25 and 2.50 μm, capturing the 1st overtones and combination bonds of C-H and O-H bonds, which

are specific to the structure of ethanol, but not exclusive [99]. In the later version of the device (TT2500), an InGaAs detector was used to record the reflected signal. Both the devices utilised diffuse reflectance mode, with TT1100 sampling from a whole hand and TT2500 sampling from a finger only.

In the US patent for TT2500 [100] The system outlined is divided into four main sections: The Illumination/Modulation System, consisting of VCSEL electronics, VCSEL light sources, and homogenisers; the Sampling Subsystem, made from an optical probe and homogeniser; the Data Acquisition Subsystem, made of the lens and the detector crystal; and the Computing Subsystem consisting of elements such as data processing, display, memory, and communications. TT2500 has two iterations, MARK I & MARK II and MARK III, a standalone device for testing individuals and a system to be implemented into a vehicle's ignition system. MARK I & II devices have been implemented in testing heavy machinery users to ensure safe operation. The MARK III version of the device is still undergoing trials for implementation in-vehicle testing. The results obtained from TT2500 clinical trials showed a high correlation between the BAC and TAC in the case of the measuring site being the finger. The results achieved when measuring the forearm were less reliable. This could be attributed to the thickness of the skin at the forearm and the abundance of blood capillaries in the finger. The authors also considered the difference in probe design as an attributing factor to the difference between measurement sites. The research regarding the analytical side of the operation of these devices was conducted by TruTouch Technologies [101], [102], [103], [104]. The devices TT1100 and TT2500 are shown in Figures 3.4 and 3.5, respectively.

Proposed by Wen-fei et al [105], a non-invasive measurement of BAC based on NIR dynamic spectrum. The beat of the human heart causes the expanding and shrinking of blood vessels, by using a set of dynamic spectra and extracting the fundamental frequencies using FFT, the data was compared to the original dynamic spectra (sober) and the dynamic spectra of a test subject who had imbibed a quantity of ethanol and used to estimate the BAC based on the changes in the fundamental frequencies. The results show a strong correlation between the change in frequency of the signal and the intoxication state, with an error as low as 0.6%, averaging out at 3.26%. Conclusively, their work proved that it is possible to accurately measure the BAC level for an individual through partial least square (PLS) analysis of dynamic spectrum.

Besides measuring the tissue directly, a sensor developed by Autoliv [106]passively measure the contents of ethanol in the driver's breath. The operation mechanism can detect the location of the exhaled ethanol by measuring the concentration of CO2 exhaled by the means of NIRS. This technique is to be implemented into a vehicle where each passenger can be monitored passively throughout the duration of a car ride. This implementation, however shares many of the same shortcomings and sources of error as any other traditional BrAC devices. [59].

Figure 3.4: TruTouch Technologies TTT1100 Guardian

Figure 3.5: TruTouch Technologies TTT2500 AlcoSense

Alternatively, to NIRS techniques, a method developed by Guo et al [107], uses wavelength-modulated differential photo-thermal radiometry (WM-DPTR) to estimate BAC in the mid-infrared range. The WM-DPTR method is based on the modulation of laser beams, which are out-of-phase with respect to each other, where one of the wavelengths is the peak absorption and the other is the baseline for the analyte, in this case, ethanol. Their study found that WM-DPTR can be used to estimate the level of BAC at a resolution of 5mg/dL with a detection limit of 10 mg/dL. Similar to other optical spectroscopy devices, this particular technique is aimed to be implemented into the vehicle operating system as a direct preventative factor against DUI. The report also found the optimal peaks for ethanol detection in MIR as 9.56 and 9.77 μm to avoid interference with glucose, which occupies similar frequency bands as ethanol.

Alongside the developments in the broad field of spectroscopy, a suggested system by Yamakoshi et al. [69] approaches the detection of ethanol the same way as measuring oxygen saturation with pulse oximetry. Pulse Alcometry, named “integrated sphere finger-photoplethysmography”,. The technique is based on the principle of optical density, removing the baseline over the measured wavelengths using second derivatives (1150,1185, and 1220

nm). A regression model was then implemented with the measured optical density at each wavelength to predict BAC. The developed technique has been relatively successful, achieving a correlation between 0.773 and 0.846. Their system had a varied error between 0.134 and 0.333 mg/dl. The system utilises transmission FPPG combined with an integrated sphere element. An enhancement of scattered light collection justified the use of the integrated sphere. However, as noted in their original work, this method still requires more research and investigation. The authors specifically mention their work's limitations, the size of the sphere, placement of the finger, comparison with reflectance FPPG, and influences of skin colour. Conclusively, this technique has plenty of potential for the measurement of blood constituents, such as ethanol. However, considerations of application feasibility remain questionable, due to the small sample size of the pilot study.

Different from transdermal sensors, optical spectroscopy sensors have received less interest than electrochemical or enzymatic sensors, with only a few published works and even fewer devices available on the market. This raises questions regarding the current state and future of in-vivo alcohol sensing technology. As far as this review is concerned, no optical spectroscopy wearable devices have been developed for measuring ethanol intoxication, presenting a unique gap for future research and development.

3.7 Gaps in the Knowledge

The field of measuring ethanol blood concentration encompasses a wide variety of techniques, including pharmaceutical, electrochemical, enzymatic and optical, and considering changes to the physiological signals, i.e., PPG and dynamic NIR spectroscopy, to establish patterns associated with alcohol intoxication. Much attention is given to the application of BAC testing for the prevention of DUI incidents, especially shown by the BrAC and NIRS devices. [10]. Since vehicle incidents are a common occurrence for drivers under the influence of any drugs, it is evident that integration of an "Intoxication Sensor" into car ignition systems would assist in combating this reckless behaviour.

Electrochemical and enzymatic sensors are the most diverse innovations in the field, with a wide range of techniques, both for signal acquisition and data processing. The results of the review literature also indicate their foremost application in long-term monitoring of individuals either in law enforcement for individuals who have a history of alcohol-related crimes or in alcohol intoxication-related studies, where it is not feasible to take blood or breath samples from an individual regularly. Transdermal sensors are also handy in cases where a subject's cooperation is not possible, such as when gaining a breath or blood sample is impossible.

However, as previously discussed, those sensors are only as good as the pharmacokinetic model on which they are based, and any variance from the model will increase the measurement error. Transdermal sensors also present a unique opportunity to introduce personal alcohol testing using wearable technology. The instrumentation required for electrochemical/enzymatic ethanol testing can be miniaturised. However, using chemical/enzymatic sensors presents a unique shortcoming regarding the operating life of such sensors. Since they depend on either enzymatic reaction rate or deposition of by-products on electrodes, the wear experienced by these components will impact their operation over more extended periods of time. This can only be resolved by regularly replacing the sensing component of the device, increasing the cost to the consumer and labour manufacturing overheads.

A cheaper alternative to wearable electrochemical/enzymatic devices is the strip tests available for bodily fluid testing. These are inexpensive and simple to use, however are by no means an accurate method of measurement of BAC levels, but rather just indicators about the presence of alcohol in a specific period. Although bodily fluid alcohol testing is far more advanced in the forensic field of study [108], by means of instruments such as gas chromatography, which is considered the gold standard for BAC testing. This method, however, is expensive and requires trained staff and, in some cases, an additional instrument, a mass spectrometer, which is naturally very large and unportable.

A narrow field of measuring physiological changes in the body included systems such as the one implemented by Volvo to monitor facial expression and gaze for accident prevention and the measurement of changes in IR imaging of the subject's face, which indicated what changes occur in human behaviour when they are under the influence. Such systems carry a unique advantage, as they are passively measuring the effects of intoxication and even being able to act when the effects of intoxication put lives at risk. However, as with any of the devices and techniques reviewed in this paper, there are shortcomings. Implementing such a system in the next generation of cars would be no easy task, requiring a lot of capital investment. The system must also be fault-proof, such that a person who "looks" tiered or intoxicated is not recognised as a false positive. It is also crucial to remember that these systems do not measure the level of ethanol in a subject by any means, only considering changes in the face position or surface skin temperature. Therefore the accurate estimation of BAC by these methods is unreliable and highly dependent on the data collected for calibration or the training of the model. However, the innovation of the automotive industry to limit the number of incidents caused by DUI is to be applauded. Yet, the application of a correct method is also a question worthy of exploring.

This has subsequently increased in the interest of monitoring the intoxication of drivers in the car by devices such as the one developed by Autoliv to measure the exhaled air ethanol content and trace the origin of the ethanol through a CO2 sensor, a method similar to BrAC devices. This technique, unlike the one suggested by Volvo or the thermal imaging comparison, measures the presence of ethanol. But as for any BrAC device the conversion rate of 2100:1 for the BAC estimation combined with all the uncertainties of breath measurement itself demean the accuracy of these devices. Moreover, the question should also be raised about the practicality of measuring BrAC passively in a closed car, with multiple subjects, not necessarily the driver can be intoxicated but one of the passengers can possibly exhale ethanol and set off a false positive.

Therefore, a more feasible application of BrAC devices where a subject has to blow into a tube, and the breath sample can be analysed without any interference from other passengers in the vehicle. The accuracy of the BrAC devices, has been proven to be effective at estimating BAC of a subject to a relatively high accuracy, yet not specific enough as compared to gas chromatography. BrAC devices, also depend highly on the cooperation of the subject, and the results of a BrAC test can be manipulated by controlled ventilation before the test is undertaken. However, as a deterrent factor for DUI, breath alcohol devices help to prevent many accidents every year, but only at one point in time. Implementations of BrAC devices exist, where they are linked to the ingestion system and require a driver to blow into a BrAC device before the vehicle can be engaged [109]. This however is not person specific and can be tricked by a breath sample of a sober individual who is not the driver.

In order for any of the physiological devices/techniques to find an appropriate implementation would need to link the system to an alcohol sensor, to justify the changes in the physiological factor that is measured. Therefore, any of these implementations have to be combined with a sensor for ethanol level, either the tissue or breath. However, physiological changes devices and techniques are useful at pointing out the outlining the changes that may be associated with ethanol consumption. Therefore, these sensors would find a far more applicable implementation in determining the physical state of individual to assess whether they are physically impaired by ethanol, as the variance in ethanol metabolism and tolerance is high. These devices would be more appropriate in determining the physical impact of alcohol intoxication, to determine the state of the person, rather than trying to establish an estimate of BAC, which would reach a bottleneck for subjects consuming high doses of alcohol.

Ultimately all techniques reviewed show that the effects of ethanol intoxication can be attributed to many changes in physiological behaviours, yet the results they obtain for some of the techniques are mostly insignificant or are not feasible for everyday applications. These reasons may include, the time required for measurements or the principle of measurement which may be faculty by not considering other compounds which originate or increase from their normal concentration during an intoxication period. In the case of devices which measure physiological changes, the measurement is only noted as a change of a physiological factor, which may not be an exclusive change for ethanol intoxication. These types of devices and techniques are most likely not going to find any application for real life intoxication testing, due to the fact that the knowledge of intoxication is given in all of them, and they are not well-adapted for recognition of false positives, such as tiredness or use of medication with similar effects as ethanol. However, one must also consider the fact that none of the devices and techniques reviewed in this paper, considered the use of neural networks or any other deep learning algorithms for classification of data, A system which would encompass all three of these fields would be the new competitor in the field of ethanol intoxication testing.

The review of literature for ethanol testing identified several different techniques for measuring and estimating the BAC level through numerous means, including metabolic rate estimation, breath sample analysis, physiological changes, transdermal sensors, and optical spectroscopy. The most accurate way to measure the concentration of alcohol in blood is through gas chromatography. Regardless, many of the techniques outlined in this chapter showed a lot of promise and impressive results for the methods they use to estimate BAC. As shown by the vast majority of the reviewed literature, the main focus of alcohol intoxication sensing is related to the incidents caused by DUI, preventing their occurrence. Large branch of alcohol intoxication sensor focuses on the transdermal techniques, analysing the presence of ethanol or ethanol related compounds in sweat. The devices are compact and many of them implement a wearable application as a smart sensor linked to a smartphone. The problem associated with these devices, is the question of their reliability after regular use, due to the use of deteriorating components which may give inaccurate readings, if not maintained appropriately.

Although the field of alcohol intoxication is broad, it still hasn't been established as a social habit to measure personal intoxication during a consumption episode. This mostly arises from the impracticality of the handheld devices, or the above outlined shortcomings of electrochemical/enzymatic biosensors. This review can therefore conclude that the field of alcohol intoxication measurement has not yet been introduced into the consumer domain, but

also the current technology, still hasn't implemented a system for using NIRS as a smart wearable device as a possible area for further innovation in this field. In addition, the measure of intoxication is not strictly limited to the amount of ethanol in the bloodstream but also, dependant on individual's tolerance to the intoxicating effects of ethanol. Such impacts can be observed in variations such as changes in PPG morphology or face heat signatures Therefore, a combination of measurements from both the concentration of ethanol in the blood and the changes in physiological signals, may be a better indicator as to the state of an individual, a device attempting this should consider individual factors such as weight, gender, and the metabolic rate of ethanol breakdown as outlined by Widmark.

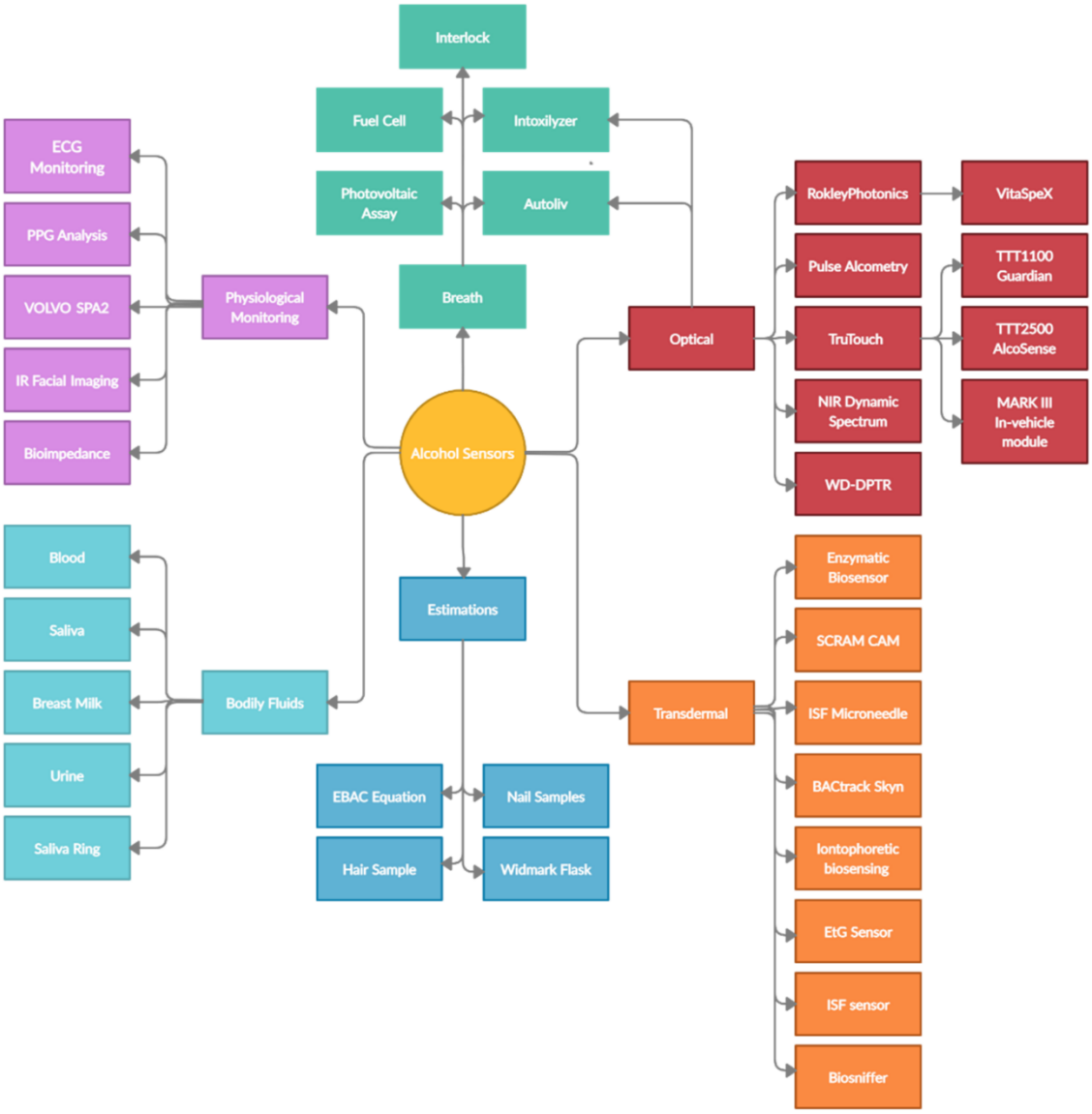

Figure 3.6: Map of alcohol devices and techniques

The field of alcohol, its health impacts, and sensing is broad. Studies on the influences of alcohol intoxication are still largely unexplored. So far, the most effective metric of alcohol intoxication is the measure of blood alcohol concentration (BAC). The justification for this metric lies with the influence of ethanol on GABA receptors, resulting in symptoms of intoxication. Although the metabolism of ethanol in the body has been studied in great detail [27], [28], it was until recently that an interest has developed in the effects of acetic acid on the reward system of the brain in mice [11]. Data obtained by Chap et al suggests neural activation caused by the presence of acetic acid, both in separation and combined with ethanol. Perhaps it is about time we rethink the idea of intoxication due to ethanol to include its metabolites. This in turn could serve as an explanation for tolerance levels amongst individuals who consume large amounts of alcohol exhibit high tolerance to its influence. Alcoholics have higher levels of acetic acid compared to non-drinkers [110].

Consideration for the influence of acetic acid and the nature of its increase in the body has been missed by researchers in the field of intoxication sensing, especially in the case of TruTouch Technologies and their devices TTT1100 and TTT2500, the latter being the most recent alliteration. TruTouch Technologies' progress in the field of non-invasive spectroscopic sensing of ethanol, being the first and only commercially available device on the market. This is due to the high precision and accuracy of their system, results of which are shown in Figure 3.7 for the finger measurements and Figure 3.8 for the forearm measurements. Graphs on the left illustrate all data point collected, whilst graphs on the right show measurement after one hour from consumption.

Their data showed a very strong correlation between the true value of alcohol in the blood and the finger measurement, reaching a correlation as high as 0.96. However, the results from the measurement of the forearm don't resemble the same strong correlation as do the finger measurements. Only reaching a maximum of 0.88 correlation. The authors attribute the differences between the measurement of the finger and forearm to two key factors: the forearm probe design, and the difference in the thickness of the skin. However, this may not be the case.

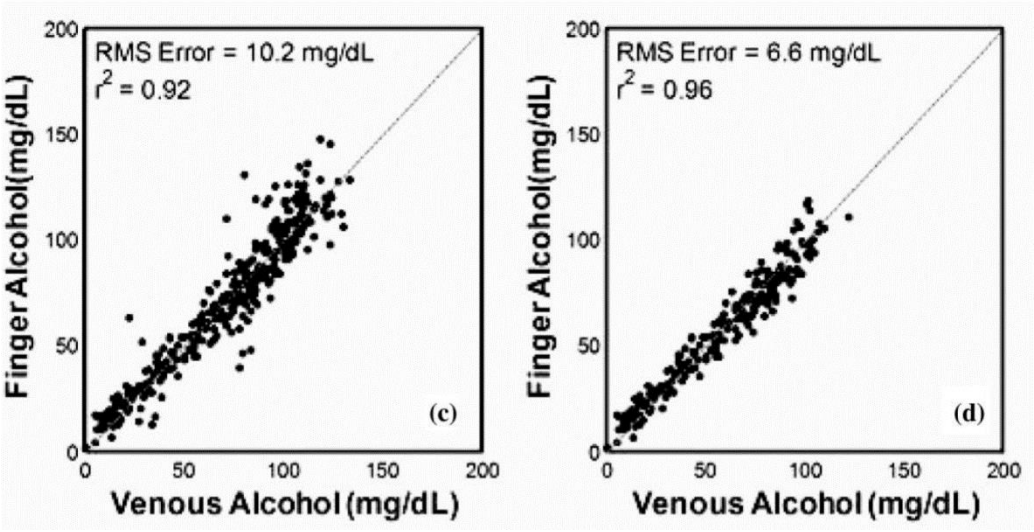

Figure 3.7: TruTouch Finger vs Blood Ethanol Levels[10]

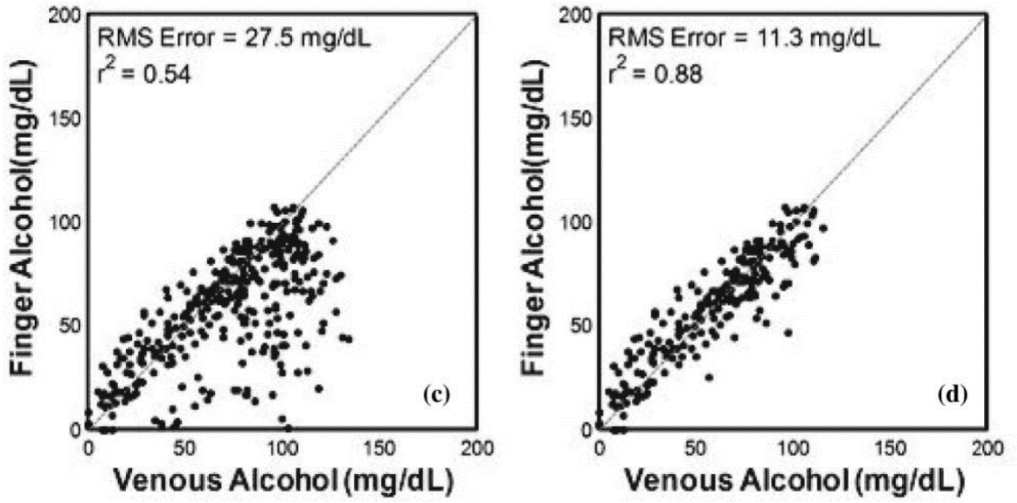

Figure 3.7: TruTouch Forearm vs Blood Ethanol Levels[10]

Graphs on the left illustrate all data point collected, whilst graphs on the right show measurement after one hour from consumption.

If the differences between these two sets of results were to be due to the thickness of the skin and the probe design, this difference would have been roughly the same for both sets of data. After the removal of the data from the first hour, the difference in correlation between the finger and the forearm is 0.08, whilst the same comparison for all the data points for both measurement yields a difference of 0.38, much greater than that the previous comparison.

However, the most astonishing comparison arises from consideration of the forearm data only. After the removal of the data points from the first hour, the correlation improved by 0.34. This difference and its origins are unaccounted for. It may, however, be explained by the presence of acetic acid.

The publication in question does not contain the data from the first hour of the trial. In order to establish whether and how significantly the measurements are impacted, that data was extracted by means of image subtraction using MATLAB. The results from the first hour of the TruTouch trial can be seen in Figure 3.9.

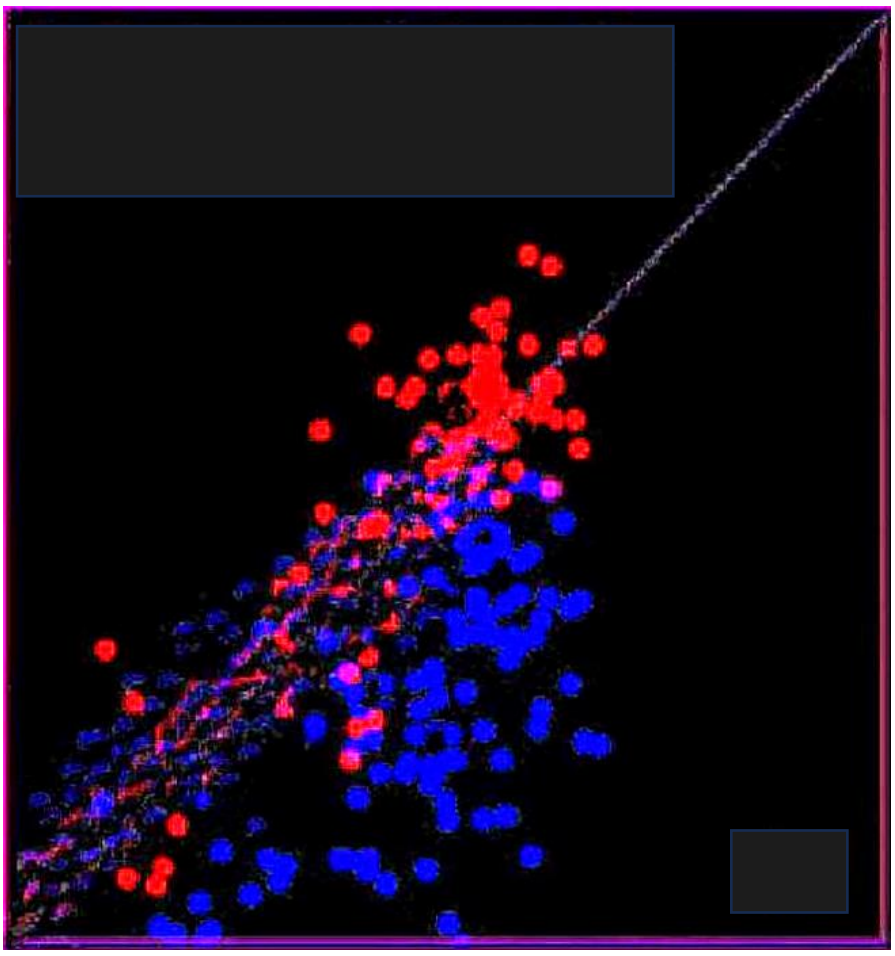

Figure 3.8: TruTouch data from the absorption phase, finger = red, forearm = blue

Figure 3.8 clearly illustrates that the system developed by TruTouch Technologies performs very poorly during the first hour of intoxication period. This is especially true in the case of forearm measurements (blue). The finger measurements (red), also fall further away from the line of best fit, yet still resemble the general patters of the correlation. The same cannot be stated for the measurements of the forearm.

This in turn possess another question about the influence of acetic acid on spectroscopic measurements of ethanol in-vivo: Why does the correlation improve massively for the forearm after the removal of data points from the first hour, whilst the finger data improvement is only

minimal in comparison? The only feasible explanation for this difference would be to assume that muscle tissue of the forearm “retains” the acetic acid, such that the concentration of it in the finger capillaries is much smaller than that of the arterial blood. Hence the difference in measurement. The retention effect may be due to the structure of the muscle and its ability to metabolise acids, for example lactate. If this hypothesis proves to be true, the measurements of ethanol in-vivo can be achieved given the calibration model includes the influences of acetic acid.

As shown in Chapters 4 and 5, ethanol and acetic acid occupy the same regions of spectra that make them distinctive from water, and as acetic acid and acetaldehyde are both metabolites of ethanol, their concentration increases with an increase in alcohol consumption. Therefore, to consider the changes in concentration of three compounds they all must be included in the calibration model of the system, as models implemented without it yield low accuracy results.

3.8 Conclusion

This review of the literature on ethanol testing identified several different techniques for measuring and estimating the BAC level through numerous means, including metabolic rate estimation, breath sample analysis, physiological changes, transdermal sensors and optical spectroscopy. Although many of these techniques claim to accurately and precisely measure the BAC levels, they are far from the accuracy achieved by gas chromatography–mass spectrometry. Regardless, many of the techniques outlined in this paper showed promising and impressive results for the methods they use to estimate BAC. As shown by most of the reviewed literature, the main focus of alcohol intoxication sensing is related to incidents caused by DUI ad preventing their occurrence. A large branch of alcohol intoxication sensors focuses on transdermal techniques, analysing the presence of ethanol or ethanol-related compounds in sweat. These devices are compact and many of them implement a wearable application, such as a smart sensor linked to a smartphone. The problem associated with these devices is the question of their reliability after regular use, due to the use of deteriorating components that may give inaccurate readings if not maintained appropriately.

Although the field of alcohol intoxication is broad, it still has not been established as a social habit to measure personal intoxication during a consumption episode. This mostly arises from the impracticality of the handheld devices, or the above outlined shortcomings of electrochemical/enzymatic biosensors. This review thus concludes that the field of alcohol intoxication measurement has not yet been introduced into the consumer domain, and current technology still has not implemented a system for using NIRS as a smart wearable device as a

possible area for further innovation in this field. In addition, the measure of intoxication is not strictly limited to the amount of ethanol in the bloodstream but is also dependent on individual's tolerance to the intoxicating effects of ethanol. Such impacts can be observed in variations such as changes in PPG morphology or face heat signatures Therefore, a combination of measurements from both the concentration of ethanol in the blood and the changes in physiological signals may be a better indicator as to the state of an individual. A device attempting this should consider individual such factors as weight, sex, and the metabolic rate of ethanol breakdown, as outlined by Widmark. By also considering recent interest in the role of other metabolites of ethanol, namely acetaldehyde and acetic acid, it is possible that the next generation of intoxication sensors will increase the number of factors. As the field of intoxication is vast and ethanol intoxication remains an intensively studied research area, so do the methods and tests used for measuring and quantifying intoxication.

Current alcohol intoxication measurement methods, ranging from breath analysis and metabolic estimation to transdermal sensing and optical spectroscopy, remain limited in accuracy compared to gas chromatography–mass spectrometry. While transdermal and wearable devices show promise, their reliability deteriorates with prolonged use, and no practical or socially adopted system exists for continuous self-monitoring of intoxication during consumption episodes. Furthermore, most approaches focus solely on ethanol concentration, neglecting individual variability in tolerance and physiological responses. There is also little integration of multimodal sensing (e.g., combining BAC with physiological signals such as PPG changes or thermal imaging) and insufficient exploration of ethanol metabolites like acetaldehyde and acetic acid as additional markers. Thus, the research gap lies in the development of robust, multimodal, and metabolite-inclusive systems that can provide reliable, personalized intoxication monitoring.

4 Methodology of Optical and Bioimpedance Spectroscopy

The accurate detection and quantification of ethanol in biological matrices, particularly for real-time, non-invasive applications, is a challenge that continues to drive innovation in the field of intoxication sensing. Traditional methods such as breath analysis and blood tests have inherent limitations, primarily due to their invasiveness, dependence on biological variability, and lack of continuous monitoring capabilities. In response, this chapter explores the potential of two promising non-invasive techniques: optical spectroscopy and bioimpedance spectroscopy. By leveraging the strengths of each technique, this research aims to provide a comprehensive framework for the detection of ethanol and its key metabolite, acetic acid, within human tissue.

Spectrophotometry, a widely utilized method in biochemical and biomedical applications, offers the ability to measure specific absorption patterns of molecules like ethanol within various biological matrices. This method, particularly effective in the near-infrared (NIR) and short-wave infrared (SWIR) regions, allows for the identification of key vibrational modes associated with ethanol. When paired with bioimpedance spectroscopy, which measures the electrical properties of tissues in response to applied current, the combined approach provides an innovative, multi-modal solution. Bioimpedance adds a complementary dimension by detecting the physiological changes related to ethanol metabolism, particularly the shifts in tissue conductivity that occur as a result of ethanol and acetic acid interaction within the body.

In this chapter, the focus will be on detailing the technical aspects and procedural methodology behind these two techniques. First, we will describe the principles of spectrophotometry and its applicability to ethanol detection, followed by an in-depth discussion of bioimpedance spectroscopy. The chapter will then provide a comprehensive review of the types of samples used for validation, including liquid and biological matrices, such as human serum, animal blood, and intralipid solutions. Additionally, we will highlight how these techniques are applied in tandem to enhance the accuracy and reliability of ethanol and acetic acid detection in real-world conditions.

This methodological chapter serves as the foundation for the experimental work discussed in subsequent sections, where the integration of these techniques is examined in greater detail. The ultimate goal of this research is to refine the use of optical and bioimpedance spectroscopy for dual-compound quantification, opening new avenues for non-invasive alcohol intoxication monitoring.

4.1 Spectrophotometry

Spectrophotometry is the study of light and matter interactions, particularly concerned with the effects of interactions with solids on light and its characteristics, namely intensity and wavelength. The following section will outline the rationale for using spectrophotometry in the SWIR region for investigating ethanol and acetic acid interactions. The section will also include mathematical tools used to treat and analyse the obtain spectral data.

Some of the earlier works of the 19th century focused heavily on understanding the inert nature of light and its interactions. One of the most famous relations established in that time was the correlation between the energy of the photon and its wavelength, linked by Plank's constant. This equation went on to form the basis of modern photonics and spectroscopy. This correlation is given by the Equation 2.

$$E = hf$$

Equation 2: Energy of a photon

As the range of wavelengths of light varies, so does its energy, along the electromagnetic spectrum, which in itself is divided into smaller regions denoting their energy levels. Figure x, illustrates this division below. Some of the most notable regions of the spectrum include the visible range between 380 and 700 nm, with photon energy ranging between 150,00 to 300,000 Joules (J). Yet the more important region for this investigation is the NIR region of the spectrum and specifically a particular section of it the SWIR. This particular type of vibrational spectroscopy only allows for the promotion of electron in the sample to lowest excited vibrational states. The advantage of using SWIR spectroscopy is its ability to clearly portray functional groups of the samples, which in turn can be used to assess the concentration of a particular species in the mixture.

The SWIR region encompasses a range between 1100 and 2500 nm. This particular study however will only be looking into the vibrational effects between 1,200 and 2,400 nm for the liquid samples, and between 1000 and 2400 nm for the solid samples. Optical windows are regions of the spectrum where there is a reduced water absorbance, they are denoted with Roman numerals. Within that range, optical windows can be found in the following ranges :1100 – 1350 nm (II), 1600 – 1870 nm (III), and 2100 to 2400 (IV). These regions are illustrated on Figure 4.1. In each of the optical windows there is clear reduction in absorbance of the water, and a significantly higher absorbance for both ethanol and acetic acid, with many of the functional group elements clearly showing. This feature of the spectrum gives a unique

insight into the contents of mixtures and potentially tissue. A major drawback exists when dealing with SWIR, which is the fact that they are high susceptible to scattering. This means that the further up we travel the wavelength in the region, the amount of light returning can be significantly lower than what was originally emitted. This drawback becomes especially important when dealing with reflectance spectroscopy of solid samples, a subject that will be discussed in Chapter 7.

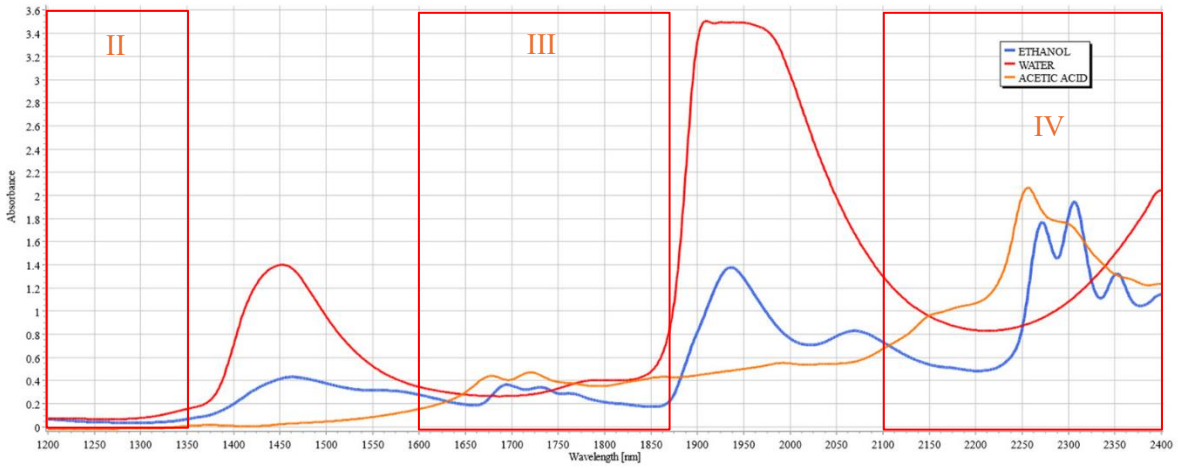

Figure 4.1: Spectra of water (red), acetic acid (yellow) and ethanol (blue), including the optical windows regions (red rectangles)

4.1.1 Vibrational Spectroscopy and Absorbance Bands

Vibrational spectroscopy, particularly in the Near-Infrared (NIR) region, is a powerful tool for analysing the molecular structure and dynamics of compounds like ethanol and its metabolites. The NIR region (700-2500 nm) is characterized by the presence of overtones and combination bands, primarily arising from the fundamental vibrational modes of molecules. These spectral features provide valuable information about the chemical environment and molecular interactions within complex biological samples.

In the NIR region, radiation of a specific frequency can excite a molecule from one vibrational state to a higher energy state if the energy of the incident photons matches the energy difference between these states. This process is described by Equation 3 below, where ΔE is the energy difference between vibrational states, h is Planck's constant and v_r the vibrational frequency of the molecule.

$$\Delta E = h v_r$$

Equation 3: Change in energy equation for molecule excitation

When the energy of the incident NIR light corresponds to the energy required to transition between these states, selective absorption occurs. The resulting absorption spectrum is a fingerprint unique to each molecule, reflecting its vibrational modes, bond strengths, and interactions with its environment.

The vibrational modes in molecules can be broadly categorized as stretching and bending movements of the bonds. In the case of ethanol, these vibrations primarily involve the O-H and C-H bonds. The stretching vibrations (changes in bond length) and bending vibrations (changes in bond angle) are represented by the following fundamental modes:

- Symmetric Stretching (v_s): Both O-H and C-H bonds extend or contract uniformly.
- Asymmetric Stretching (v_{as}): One bond lengthens while another shortens.
- Bending Modes (δ): Changes in bond angles, which can occur in-plane (scissoring and rocking) or out-of-plane (wagging and twisting).

In the NIR region, these fundamental modes give rise to overtones and combination bands. Overtones are multiples of the fundamental frequency, while combination bands result from simultaneous excitation of two or more fundamental vibrations. These spectral features are particularly prominent in the NIR due to the anharmonic nature of molecular vibrations[111].

Overtones and Combination Bands in NIR Spectroscopy

In the NIR region, the vibrational overtones and combination bands of functional groups such as C-H, O-H, and C=O are particularly important. These spectral features provide information about the molecular environment and are influenced by factors such as hydrogen bonding and molecular conformation.

Overtones occur when a molecule transitions between multiple vibrational states, such as from v = 0 to v= 2 (first overtone) or v=0 to v=3 (second overtone). The energy of an overtone transition is *approximately n x v*, but due to anharmonicity, the observed frequency is slightly lower.

Combination bands arise when two or more vibrational modes are excited simultaneously. For example, the combination of O-H stretching and bending modes in ethanol leads to complex spectral patterns in the NIR region, making it possible to distinguish between different functional groups and molecular configurations.

Functional Group Absorption in the NIR Region

The NIR region is highly sensitive to the vibrational modes of functional groups involving hydrogen atoms, such as C-H, O-H, and N-H bonds. The absorption bands for these groups are influenced by the anharmonicity of their vibrations and the interactions between different vibrational modes. Table 4.1 summarizes the approximate wavelengths for common functional groups and their overtone or combination band assignments in the NIR spectral region:

These characteristic bands allow for the identification of ethanol and its metabolites. The sensitivity of NIR spectroscopy to these functional groups makes it an ideal tool for non-invasive alcohol detection.

Table 3: Band assignment in the SWIR region

Wavelength (nm)	*Functional Group*	*Assignment*	*Notes*
1140-1150	C-H	Second overtone	Slightly lower range, weaker band
1200-1300	C-H	Second overtone	Most common for C-H overtones
1400-1450	O-H	First overtone	Strong absorption (water, alcohols)
1440-1480	C-H	Combinational band	Seen in hydrocarbons
1700-1900	O-H	Combinational band	Typical for water and alcohols
1920-1950	O-H/HOH	Combinational band	Often observed in water
1900-2000	C=O	Second overtone	Weaker band, seen in carbonyl compounds
2070	O-H	Combinational band	Common for water and hydroxyl groups
2300-2340	C-H	Stretch/Deformation combination	Hydrocarbons (CH_3,CH_2)

4.1.2 Ethanol and Acetic Acid Interactions

The interaction between ethanol and acetic acid in aqueous environments reveals a complex interplay of molecular behaviours that influence spectroscopic measurements, particularly in the short-wave infrared (SWIR) range. Ethanol and acetic acid share structural similarities, such as the presence of hydroxyl (-OH) groups and carbon chains, which play a critical role in their interactions. These shared atomic features lead to overlapping vibrational modes in SWIR spectroscopy, resulting in distinctive absorbance patterns when the two compounds coexist in a medium. Their mutual influence is particularly evident in regions where molecular interactions between their functional groups affect the surrounding medium's optical properties.

In water, the presence of ethanol and acetic acid alters the spectral profile significantly. Water's inherent absorbance is dominated by its O-H bonds, but the addition of these compounds introduces new interaction dynamics. The vibrational modes of ethanol's hydroxyl group and acetic acid's carboxyl group influence each other and the surrounding water molecules. These interactions create regions of spectral activity where the combined absorbance differs from that of the individual compounds. The extent of this spectral modification depends on the relative concentrations of ethanol and acetic acid, with higher concentrations amplifying these effects. The overlapping vibrational modes from their similar atomic structures create challenges in isolating their individual contributions to the overall absorbance. This is clearly seen from observations to the skeletal structure of ethanol and acetic acid molecules, as seen from Figure 4.2 below.

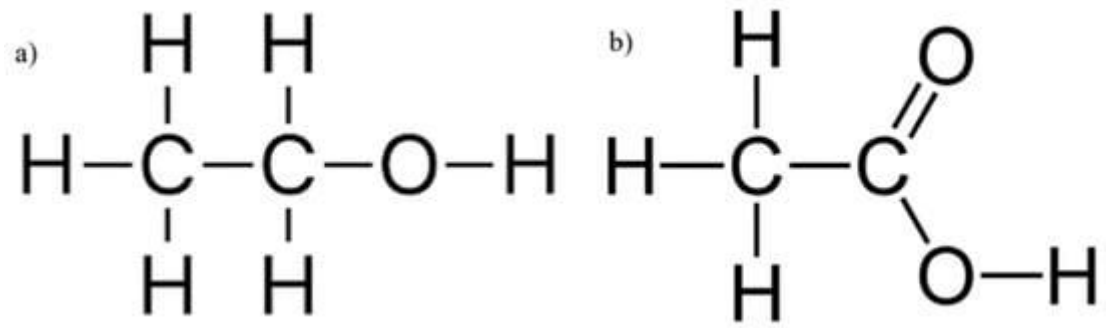

Figure 4.2: Skeletal structure of molecules of ethanol(a) and acetic acid(b)

Ethanol and acetic acid also affect SWIR measurements due to the molecular similarities in their carbon chain structures and the presence of polar bonds. Their interactions result in changes to the overall hydrogen bonding network in the mixture, which is detectable in specific regions of the SWIR spectrum. These regions exhibit variations in absorbance intensity and

profile, stemming from the altered vibrational modes of the molecules. For example, the interplay between ethanol's hydroxyl group and acetic acid's carbonyl group generates complex absorbance features that are distinct from those seen in their isolated forms.

The overlapping spectral behaviour of ethanol and acetic acid underscores the challenges in SWIR analysis when both compounds are present. Their shared atomic features lead to combinational absorbance bands that may obscure or enhance specific spectral regions. These regions are characterized by significant changes in the vibrational modes of functional groups, such as C-H, O-H, and C=O bonds, which influence the light absorption patterns. This in turn in clearly visible from the spectral signatures within spectral optical windows. The combined effect creates a need for careful spectral interpretation to differentiate the contributions of each compound, particularly in applications requiring precise quantification using the appropriate type of instrumentation.

4.1.3 Instrumentation

This study utilized the Lambda 1050 spectrophotometer from Perkin Elmer, designed specifically for high-resolution measurements in the Near-Infrared (NIR) spectrum. This section details the principles of operation, components, and mathematical background relevant to the instrument's function and data acquisition. As seen from Figure 4.3

Figure 4.3: Perkin Elmer Lambda 1050 Spectrophotometer

The Lambda 1050 employs two light sources: a deuterium lamp for the UV range (175-400 nm) and a tungsten-halogen lamp for the visible and NIR ranges (400-3300 nm). This dual-

lamp system provides consistent illumination across the spectrum, minimizing variations in intensity that could affect the accuracy of measurements.

The spectrophotometer uses a double monochromator system for precise wavelength selection. A monochromator separates light into its constituent wavelengths using a diffraction grating. The wavelength selection process can be understood through the diffraction equation below, where n is the diffraction order, λ is the wavelength of light, d is the grating spacing, θi is the angle of incidence, and θd is the angle of diffraction. Adjusting the angles of incidence and diffraction allows the selection of a specific wavelength from the broad-spectrum light source, ensuring high spectral purity and resolution.

$$n\lambda = d(\sin\theta_i + \sin\theta_d)$$

Equation 5: Diffraction equation

4.1.4 Sample Compartment and Holders

The Lambda 1050's sample compartment accommodates various sample types, including liquids, solids, and semi-solids. For liquid samples, the Beer-Lambert Law is employed to relate the absorbance of light to the concentration of the absorbing species. The law is expressed as shown in Equation 6, where A is the absorbance, ε is the molar absorptivity, l is the path length and c is the concentration of the analyte. This relationship allows for the quantitative determination of the concentration of a sample based on its absorbance.

$$A = \varepsilon lc$$

Equation 6: Beer Lambert Law

The Lambda 1050 features a three-detector system that covers a wide spectral range: Silicon (Si) Detector: Effective from 175 nm to 1100 nm, providing sensitivity in the UV and visible regions. Lead Sulfide (PbS) Detector: Operates from 1100 nm to 2500 nm, ideal for lower energy transitions in the NIR. Indium Gallium Arsenide (InGaAs) Detector: Covers 800 nm to 2500 nm, offering low noise and high sensitivity in the NIR region.

The choice of detector impacts the quality and sensitivity of the measurements. The InGaAs detector, for example, is preferred for its low thermal noise and high performance in the NIR region, making it suitable for detecting subtle spectral features in biological samples.

Calibration is essential for accurate spectrophotometric measurements. The instrument is typically calibrated using reference standards with known absorbance properties. This process involves adjusting the instrument to ensure that the measured absorbance matches the expected

values for the standards. A typical calibration correction equation used is as shown below in Equation 8, where $A_{measured}$ is the absorbance of the sample and A_{blank} is the absorbance of a blank sample (without the analyte). This correction accounts for any baseline shifts or instrumental noise.

$$A_{corrected} = A_{measured} - A_{blank}$$

Equation 9: Reference measurement

The vibrational frequencies of a diatomic molecule can be modelled using Hooke's Law and the principles of classical mechanics. The vibrational frequency of a molecule is given by Equation 9, where k is the force constant of the bond and μ is the reduced mass of the system calculated by Equation 10, with m_1 and m_2 being the masses of the two atoms in a diatomic molecule.

$$v = \frac{1}{2\pi}\sqrt{\frac{k}{\mu}}$$

Equation 9: Vibrational frequencies

$$\mu = \frac{m_1 m_2}{m_1 + m_2}$$

Equation 10: Reduced mass

The energy of these vibrational modes can be calculated using the quantum mechanical model for a harmonic oscillator, where E_V is the vibrational energy, h is Planck's constant, and v is the vibrational frequency. These equations provide the theoretical framework for understanding the vibrational spectra obtained from the Lambda 1050.

$$E_v = \left(v + \frac{1}{2}\right)hv$$

Equation 11: Vibrational energy for harmonic oscillations

4.2.2 Acquisition and Processing

Data was collected using Perkin Elmer's UVWinLab software, which offers tools for real-time monitoring and analysis. Post-acquisition, data was processed in MATLAB for more advanced analysis, including Principal Component Analysis (PCA) and Partial Least Squares (PLS) regression.

Baseline correction was performed to eliminate instrumental noise. A polynomial fit was used to approximate the baseline, which was then subtracted from the original spectrum, where $S_{corrected}$ is the corrected spectrum, $S_{measured}$ is the raw spectrum and B is the baseline fit.

$$S_{corrected}(\lambda) = S_{measured}(\lambda) - B(\lambda)$$

Equation 12: Baseline Correction

Smoothing techniques, such as the Savitzky-Golay filter, were applied to reduce noise without distorting spectral features. The Savitzky-Golay filter works by fitting a polynomial to a moving window of the spectral data and replacing each data point with the value of the polynomial at the centre of the window. In the case of the dealing with analysis of ethanol and acetic acid, the optimal window size and order of the SG filter was determined to be of order 3 and window size 25. This particular combination of parameters preserved the distinctive characteristics of each f the analytes without blending their absorbance bands and losing spectral resolution.

Principal Component Analysis (PCA)

PCA was used to reduce the dimensionality of the spectral data and identify key features. The spectral data matrix X was decomposed into scores and loadings, where T is the scores matrix, P is the loadings matrix and E is the residual matrix.

$$X = TP^T + E$$

Equation 13: PCA reduction in dimensionality

The first few principal components (columns of T) capture the most variance in the data, allowing for simplified visualization and analysis.

Partial Least Squares (PLS) Regression

PLS regression was used to correlate the spectral data with known concentrations of analytes. The PLS model relates the predictor matrix X (spectral data) to the response matrix Y(concentrations) as Equation 14 where T and U are the score matrices for X and Y, P and Q are the loading matrices for X and Y, E and F are the residual matrices, B is the regression coefficient matrix and H is the error matrix. The PLS algorithm minimizes the sum of squared residuals in both X and Y, providing a robust model for predicting analyte concentrations from spectral data.

$$X = TP^T + E$$

$$Y = UQ^T + F$$

$$T = UB + H$$

Equations 14 - 16: PLS algorithm for minimisation of sum of square residuals

Polynomial Curve Fitting

In this study, polynomial curve fitting was employed to model the relationship between the concentration of ethanol and acetic acid and their absorbance values at selected wavelengths. This method provided a way to capture the non-linear relationships between absorbance and concentration, offering a more flexible approach than simple linear regression. Polynomial fitting is particularly effective when the relationship between these variables cannot be described adequately by a straight line, allowing for a more precise prediction of concentration from absorbance data.

The mathematical basis of polynomial curve fitting involves fitting a polynomial equation to data points that represent the absorbance at a specific wavelength and the corresponding concentration of the compound. The degree of the polynomial is chosen based on the complexity of the relationship. For example, a quadratic or cubic polynomial can be applied when non-linear trends in the data are apparent. The general form of the polynomial equation used in this analysis can be expressed as:

$$A_\lambda = a_0 + a_1 C + a_2 C^2 + \cdots + a_n C^n$$

Equation 17: General equation of a polynomial for analysis

In this equation, A_λ represents the absorbance at a particular wavelength λ, while C denotes the concentration of either ethanol or acetic acid. The coefficients a_0, a_1 are determined through the fitting process, which seeks to minimize the error between the predicted and observed values. The degree of the polynomial, denoted by n, is adjusted based on the nature of the data. The fitting process relies on the least squares method to minimize the sum of squared residuals, thereby optimizing the polynomial coefficients. An example of the polynomial curve fitting operation is illustrated in Figure 4.3.

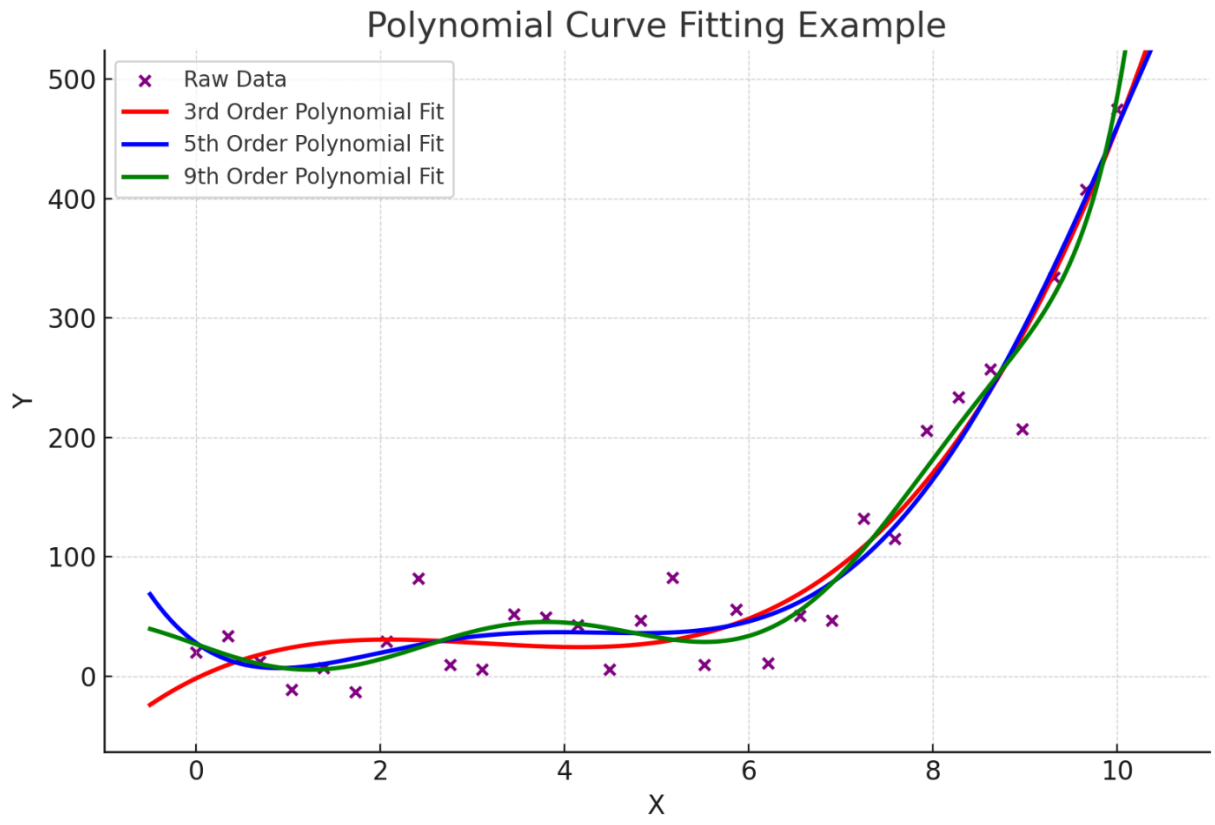

Figure 4.4: Polynomial Curve Fitting example

Relevant wavelengths were selected based on prior correlation analysis or knowledge of the molecular properties of ethanol and acetic acid to implement polynomial curve fitting. Wavelengths that showed strong sensitivity to changes in concentration were prioritized for fitting. Once selected, the polynomial curve was fitted to the concentration-absorbance data at each wavelength. Depending on the degree of the polynomial, the curve could capture not only the direct relationship between absorbance and concentration but also more complex behaviours, such as quadratic or cubic trends.

This allows the model to account for both linear and non-linear effects, providing a more accurate representation of the relationship between absorbance and concentration, particularly in cases where the data shows curved patterns.

The quality of the polynomial fit was evaluated using standard statistical metrics such as the coefficient of determination and the root mean square error (RMSE). These metrics were crucial in assessing how well the fitted polynomial explained the variance in the data. A higher coefficient of determination value, closer to 1, indicated a better fit, while a lower RMSE indicated a minimal error in the predictions. This approach proved advantageous for predicting ethanol and acetic acid concentrations at specific wavelengths, where the relationship between

concentration and absorbance is often non-linear due to molecular interactions or the optical properties of the matrix in which the compounds were dissolved.

The flexibility of polynomial curve fitting lies in its ability to capture these complex, non-linear relationships, making it an ideal method for analyzing spectrophotometric data where the absorbance changes with varying concentrations of analytes. By selecting the appropriate polynomial degree for each wavelength, the method provided improved accuracy in predicting the concentrations of ethanol and acetic acid from their absorbance spectra. This method was particularly useful when working with heterogeneous media, where light scattering and absorption can introduce non-linear effects that simpler models would fail to capture.

In summary, polynomial curve fitting was an essential analytical tool in this study, enabling the detection of ethanol and acetic acid concentrations with greater precision than would be possible with linear models. By accounting for non-linear relationships between absorbance and concentration, this method enhanced the ability to interpret spectrophotometric data, particularly in complex biological or synthetic matrices. Through careful selection of wavelengths and fitting of polynomial models, this approach allowed for more accurate and reliable quantification of these compounds, contributing significantly to the overall analytical framework of the research.

4.2 Bioimpedance Spectroscopy

Bioimpedance spectroscopy (BIS) is a non-invasive technique used to measure the electrical properties of biological tissues. It involves applying a small, painless electrical current through the body and measuring the resistance (impedance) to this current. The impedance is affected by the volume and composition of the body's fluids and tissues, making BIS a useful tool for analyzing body composition and fluid status.

BIS measures impedance at multiple frequencies ranging from low (around 3 kHz) to high (up to 1000 kHz). This multi-frequency approach allows for a detailed assessment of different fluid compartments within the body: Extracellular Fluid (ECF): Measured at low frequencies because the current does not penetrate the cell membrane, providing information on the fluid outside the cells. Intracellular Fluid (ICF): Measured at higher frequencies as the current can pass through cell membranes, providing data on fluid within the cells. Total Body Water (TBW): Calculated using impedance measurements at both low and high frequencies, providing a complete picture of body water content.

BIS has numerous applications in clinical and research settings, including: Monitoring Fluid Balance: Particularly useful in managing conditions like heart failure, kidney disease, and lymphedema, where accurate fluid monitoring is crucial. Body Composition Analysis: Used to assess muscle mass, fat mass, and hydration status, which can be helpful in sports science, nutrition, and sarcopenia research.

Unlike traditional bioimpedance analysis (BIA) methods that use a limited number of frequencies, BIS provides a more accurate and detailed breakdown of fluid compartments. This is because it can measure impedance across a wide range of frequencies, allowing it to differentiate between intracellular and extracellular fluids more effectively.

While BIS is a powerful tool, it does have some limitations. Factors such as extreme obesity or cachexia can affect BIS measurements. Accurate BIS measurements require high-quality equipment and precise protocols to ensure reliable results. Overall, BIS is a versatile and valuable tool for non-invasive body composition and fluid status assessment, with broad applications in both clinical and research environments.

In this study, a custom-made bioimpedance measurement box module was employed to determine the impedance of solid samples. This device is specifically designed to measure the impedance of heterogeneous solid samples using a probe connected to an oscilloscope. The impedance measurements were conducted across a frequency range of 1 kHz to 10 kHz.

Custom Bioimpedance Measurement Box module was equipped with a built-in signal generator to produce the required frequency range. It featured an integrated amplifier and filter circuits to ensure accurate signal generation and minimize noise interference.

A specialized probe was used to interface with the solid samples. The probe consisted of two electrodes placed at a fixed distance to ensure consistent measurement conditions across all samples. The probe was designed to penetrate or make contact with the surface of the sample, providing reliable and repeatable impedance measurements.

An oscilloscope was connected to the probe to capture the voltage and current signals. The impedance of the sample was calculated by analyzing the phase shift and amplitude ratio between the input voltage and the output current.The oscilloscope was configured to operate in a range that captured the entire spectrum of interest, allowing for detailed frequency-dependent impedance characterization.

All solid samples were prepared in a standardized manner to ensure uniformity. The samples were stored at room temperature (24 °C) and kept consistent in terms of size and shape to eliminate any variables that could affect the impedance readings. Each sample was connected to the probe, and measurements were taken at discrete frequencies within the 1 kHz to 10 kHz range at 1 kHz intervals. The frequency response of each sample was recorded and analysed to understand the material properties, such as resistance and reactance. The impedance values at various frequencies were used to model the electrical behaviour of the solid samples, aiding in the interpretation of their material characteristics.

The use of a custom-made bioimpedance measurement box allowed for a high degree of control over the experimental conditions, which was essential for the accurate characterization of solid samples. The probe and oscilloscope setup enabled precise measurement of small impedance changes, making it possible to detect subtle variations in the electrical properties of the samples across different frequencies.

This methodology was particularly suitable for the study as it provided reliable data on the dielectric properties of the solid media used, which could then be correlated with their chemical and structural characteristics. The circuit diagram for the impedance module is shown in Figure 4.4.

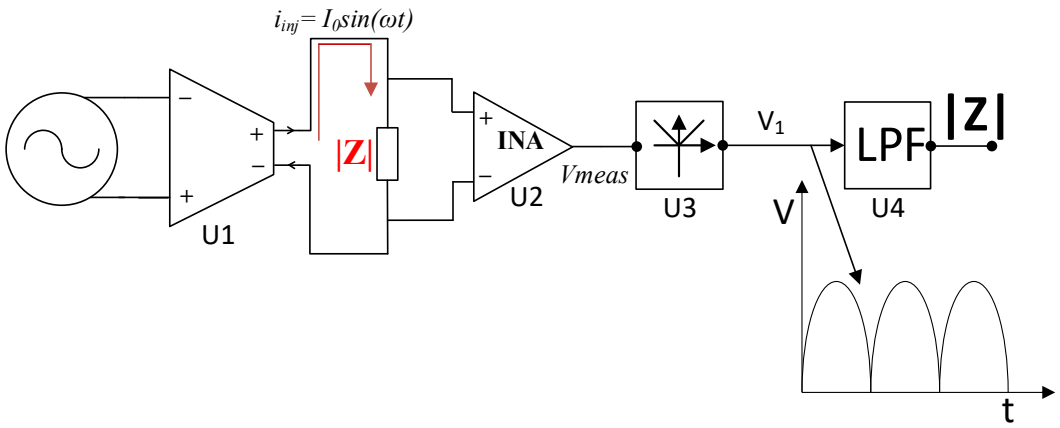

Figure 4.5: Circuit Diagram of the Impedance Measuring Module

Rationale for the combined measurement methodology

The detection of ethanol and acetic acid in biological matrices presents a significant analytical challenge due to the spectral overlap of their vibrational modes with those of water and other endogenous biomolecules. Optical spectroscopy, particularly in the near-infrared (NIR) and short-wave infrared (SWIR) regions, provides valuable information about the absorption

features of these analytes. However, optical signals are often confounded by the high background absorption and scattering properties of tissue or complex fluids, making it difficult to resolve low concentrations with precision. Despite the ability of optical techniques to identify specific wavelength regions sensitive to ethanol or acetic acid, relying solely on spectroscopy risks limited sensitivity and poor specificity when deployed in physiologically relevant environments.

Bioimpedance spectroscopy (BIS) offers a complementary approach that is sensitive to changes in ionic content, permittivity, and conductivity of the medium, properties which are altered by the presence of ethanol and acetic acid. Unlike optical methods, BIS does not rely on chromophoric or vibrational signatures but instead probes how molecular composition affects the dielectric landscape of the sample. Ethanol, as a small polar molecule, reduces solution permittivity, while acetic acid, with its dissociation into acetate ions, modulates both ionic strength and conductivity. These mechanisms allow bioimpedance to capture changes that are orthogonal to the absorption-based information gained through optical spectroscopy, thereby addressing some of the blind spots inherent to either method used in isolation.

The combination of optical and bioimpedance spectroscopy thus provides a multimodal sensing framework that exploits the complementary strengths of both modalities. Optical spectroscopy ensures analyte-specific detection based on molecular absorption features, while bioimpedance spectroscopy improves robustness against confounding spectral background and enhances sensitivity to concentration-dependent changes in the chemical environment. By fusing both data streams, a more reliable discrimination between ethanol and acetic acid can be achieved, particularly in complex biological systems where overlapping optical signatures are common. Moreover, multimodal measurements open the possibility of applying multivariate analysis techniques, such as polynomial regression or PLSR, to integrate independent features and enhance predictive accuracy.

From a translational perspective, the justification for combining these modalities also lies in the potential for miniaturization and portability. Optical components and bioimpedance electrodes can be co-integrated into compact probes, enabling real-time, non-destructive monitoring of ethanol and acetic acid in tissue phantoms, biofluids, or in vivo systems. Such hybrid devices would address the current research gap by moving beyond single-modality limitations, paving the way toward clinically relevant and consumer-ready solutions that can monitor alcohol metabolism and its by-products more accurately and holistically.

4.3 Samples

In this study, a total of 36 samples were prepared for each type of media, each with varying concentrations of ethanol and acetic acid. The goal was to create a comprehensive dataset that would allow for the analysis of different chemical interactions and their impact on the spectral properties of various biological and synthetic media.

Baseline Sample (Sample 0): This sample contained no ethanol or acetic acid and served as a reference point for all measurements.

Ethanol-Only Samples (Samples 1-5): These samples contained only ethanol at concentrations ranging from 100 to 500 mg/dL in increments of 100 mg/dL.

Acetic Acid-Only Samples (Samples 6, 12, 18, 24, 30): Each of these samples contained only acetic acid, with the concentration corresponding to the sample number (e.g., Sample 6 contained 6 mg/dL of acetic acid, Sample 12 contained 12 mg/dL, and so on).

Mixed Samples (Remaining Samples): The remaining samples were mixtures of ethanol and acetic acid at various concentrations, combining the characteristics of the individual components.

For each of the mediums used, a separate set of the above was prepared to ensure that the ethanol and acetic acid concentrations were considered across various matrices to establish which one of them yields the best results. Table 3 below illustrates the sample concentrations across all samples along with their number. Figure 4.5 illustrates this sample arrangement, all the fluid samples were prepared using the exact same technique. To minimise the impact of stratified error arising from running get e samples in the order of their numbering, the order in which the samples were processed was randomised, by generating a random number between 0 and 35, once drawn the sample number would be removed from the draw pool. This process was done for all media used in this study.

The samples were tested across various biological and synthetic media, each chosen for its specific relevance to physiological and experimental conditions. The media used in this study included:

Water served as a simple, clear medium for establishing baseline spectroscopic characteristics of ethanol and acetic acid without the interference of complex biological components. It is essential for understanding the fundamental interactions and absorption features of the analytes.

Table 4: Sample mapping table, the column represents the ethanol concentrations, and the row represents the acetic acid concentrations

Concentration in mg/dl	*0*	*6*	*12*	*18*	*24*	*30*
0	*0*	*6*	*12*	*18*	*24*	*30*
100	*1*	*7*	*13*	*19*	*25*	*31*
200	*2*	*8*	*14*	*20*	*26*	*32*
300	*3*	*9*	*15*	*21*	*27*	*33*
400	*4*	*10*	*16*	*22*	*28*	*34*
500	*5*	*11*	*17*	*23*	*29*	*35*

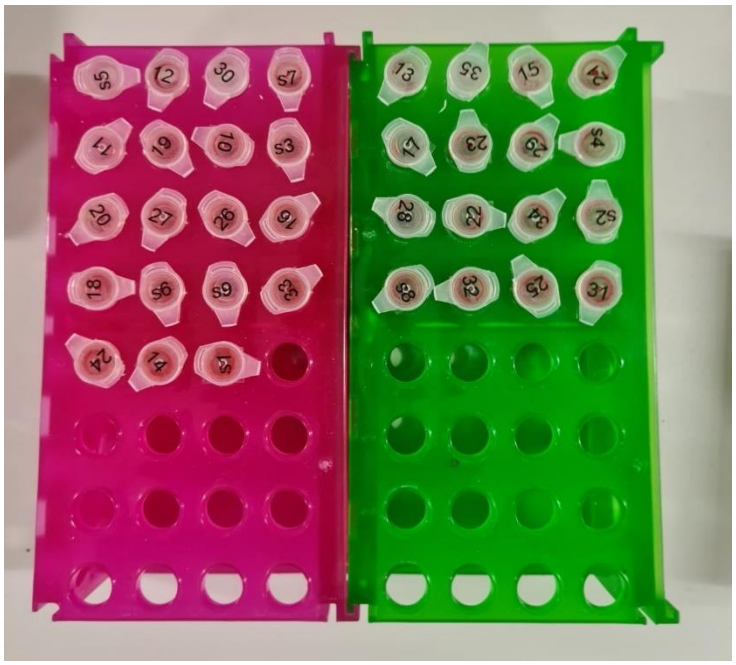

Figure 4.6: Sample arrangement used in the study (sheep blood example)

Human Serum was used to mimic the behaviour of ethanol and acetic acid in a biological fluid representative of human physiology. This medium is crucial for studies related to clinical diagnostics and understanding how these compounds behave in blood-like environments.

Sheep blood was selected as a substitute for human blood due to its similar optical properties and availability. It provides a realistic model for investigating the interaction of ethanol and acetic acid in a whole blood environment, which is important for forensic and clinical toxicology studies.

Artificial ISF was included to simulate the extracellular environment in tissues, particularly for applications related to transdermal and subcutaneous measurements. It allows for the exploration of how ethanol and acetic acid diffuse and interact in a matrix that resembles the fluid found between cells.

Intralipid, a lipid emulsion, was used to model the scattering properties of tissue. This medium helps to understand how light interacts with samples that have high scattering, providing insights into in vivo applications such as non-invasive sensing and imaging. The samples for this medium were prepared by first diluting the intralipid until it reached 5% from the original 20%. The samples were prepared by adding the desired volume of ethanol and acetic acid, constant volume of intralipid, and appropriate dilution of water, in order to maintain a 2% dilution per sample. This was done replicate the optical properties of skin [112]

Porcine skin was chosen as a surrogate for human skin due to its similar structural and optical properties. It was used to study the penetration and absorption of ethanol and acetic acid through a skin barrier, which is relevant for topical and transdermal delivery studies.

Gelatine Artificial ISF and Intralipid Molds: These composite media were designed to simulate the mechanical and optical properties of soft tissues. The inclusion of gelatine provides a matrix that closely resembles the elasticity and refractive properties of tissues, while ISF and Intralipid contribute to the biochemical and optical characteristics. These moulds are particularly useful for calibration and validation of optical devices intended for tissue studies. Similarly to the intralipid the concentration f intralipid across all of the phantoms was 2% by volume.

Each of these media provided unique insights into the interactions of ethanol and acetic acid under different physiological and experimental conditions. By analysing the spectral data across these diverse matrices, it was possible to develop a robust understanding of the behaviour of these compounds in various environments, thereby enhancing the applicability of the findings to real-world scenarios.

5 The Vibrational Interactions of Volatile Organic Compounds (VOCs) in Conditions Imitating Intoxication States Using Short Wave Infrared (SWIR) Spectroscopy

Volatile organic compounds (VOCs), including ethanol and its metabolic by-products, play a pivotal role in understanding the complex biochemical dynamics that occur during alcohol intoxication. Short Wave Infrared (SWIR) spectroscopy, with its capacity to detect molecular vibrations through absorption in the 1,200-2,400 nm range, offers an advanced approach to characterizing these interactions. This chapter explores the application of SWIR spectroscopy to study the vibrational behaviours of ethanol and acetic acid in conditions simulating various stages of intoxication.

In alcohol intoxication sensing, precise detection of ethanol is crucial, but equally important is the ability to identify and quantify its metabolites, such as acetic acid, which significantly impact the body's physiological state. SWIR spectroscopy is well-suited for this purpose due to its sensitivity to the C-H, O-H, and C=O vibrational modes, which are characteristic of ethanol, acetic acid, and other VOCs. These spectral bands offer the opportunity to distinguish between ethanol and its by-products even in complex biological matrices.

This chapter delves into the specific spectroscopic properties of VOCs under conditions designed to mimic intoxication. The focus is placed on identifying the key absorbance bands of ethanol and acetic acid, analysing their overlap, and exploring the potential of discrete wavelength analysis for enhanced specificity. A detailed assessment of the spectral morphology of these compounds under various concentration levels will also be conducted, particularly considering the impact of acetic acid on ethanol detection accuracy.

Through a combination of experimental data and chemometric analysis, this chapter will provide insight into how VOC interactions affect spectral patterns and how SWIR spectroscopy can be optimized for real-world applications in intoxication monitoring. By simulating different physiological states, this work aims to refine spectroscopic techniques for higher accuracy in ethanol quantification, providing a robust foundation for the development of non-invasive intoxication sensing technologies.

5.1 Absorbance Band Overlap

To accurately analyse the vibrational interactions of ethanol and acetic acid, it is essential to understand how their absorbance bands behave individually and in mixtures. Figure 5.1 presents the SWIR absorbance spectra of ethanol, acetic acid, and water in isolation. These

spectra serve as a baseline for understanding the interactions when these compounds are present in various biological and synthetic mediums.

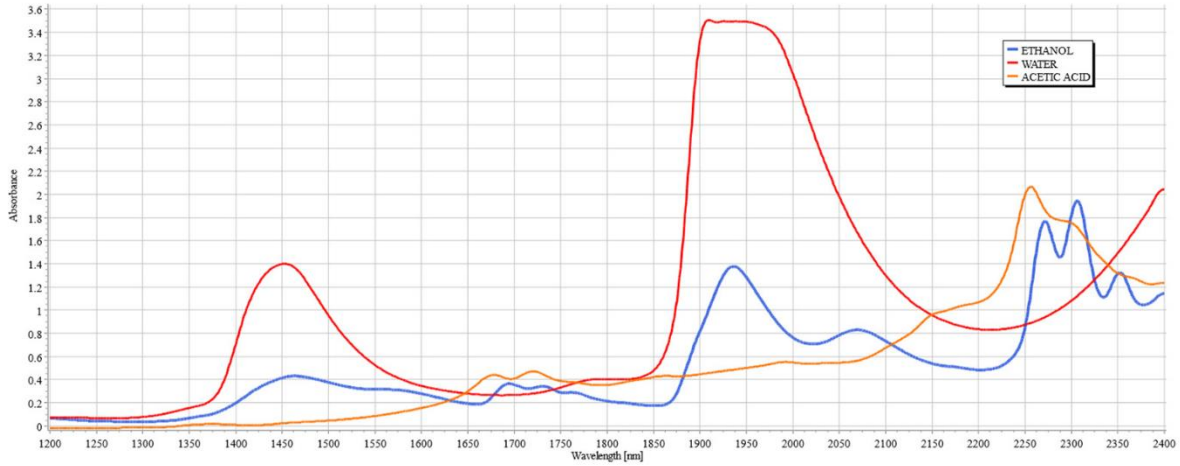

Figure 5.1: Spectra of Water, Ethnaol and Acetic Acid Between 1200 and 2400 nm

The vibrational interactions of ethanol and acetic acid were analysed using their SWIR absorbance spectra, as shown in Figure 5.1. This figure illustrates the isolated absorbance spectra of ethanol, acetic acid, and water, providing a baseline for understanding the spectral behaviour of these compounds. The distinct absorbance bands observed in the spectra were critical for identifying and differentiating these substances, both individually and in various mixtures.

Ethanol displayed significant absorbance peaks in the SWIR region, particularly around 1400-1500 nm and 1700-1800 nm. The first peak corresponded to the first overtone of the O-H stretching vibration, while the latter was associated with a combination of C-H stretching and bending modes. These key bands served as primary indicators for ethanol detection in both isolated samples and mixtures. Additionally, minor features around the 2200-2300 nm range were identified, attributed to C-H bending modes, providing supplementary information for ethanol characterization.

Acetic acid exhibited a strong absorbance band in the 1700-1800 nm range, predominantly due to C=O stretching vibrations. This band overlapped with the ethanol O-H stretch region, complicating the spectral analysis in mixed samples. Acetic acid also showed notable absorbance features between 2000-2200 nm, linked to a combination of C-H and C=O stretching modes. These secondary bands, although less intense, were crucial in differentiating acetic acid from ethanol, particularly in mixed samples with varying concentrations.

The presence of water, a common component in many biological and synthetic samples, introduced additional complexity to the spectral analysis due to its dominant absorbance bands. Water showed strong absorption around 1400-1450 nm and 1900-1950 nm, corresponding to O-H stretching vibrations. These bands could obscure the spectral features of both ethanol and acetic acid, especially when water was present in high concentrations. Therefore, it was necessary to carefully examine the overlapping regions and utilize advanced analytical techniques to accurately differentiate these substances in complex samples.

The spectral characteristics observed in Figure 5.1 served as a foundational reference for evaluating the behaviour of ethanol and acetic acid in various biological and synthetic matrices. These baseline spectra were essential for identifying deviations and interactions when these compounds were present together, or in mixtures with other components. A detailed analysis of the average spectra from different mediums, compared to these baseline spectra, provided insights into the vibrational interactions and absorbance band behaviours of ethanol and acetic acid.

To further investigate the influence of different mediums on the absorbance patterns, the baseline absorbance of all samples was removed, and the average absorbance for each medium was calculated. Figure 5.2 presents the average absorbance spectra for each medium, highlighting the impact of different biological and synthetic environments on the detection of ethanol and acetic acid.

The data presented in Figure 5.2 demonstrates that each medium exhibits a distinct spectral response. For example, water, being the most transparent in this range, shows minimal absorbance, while more complex biological mediums such as human serum and sheep blood display significant variations. These differences are critical for understanding the specific interactions between VOCs and their surrounding matrix, which is essential for accurate quantification in real-world applications.

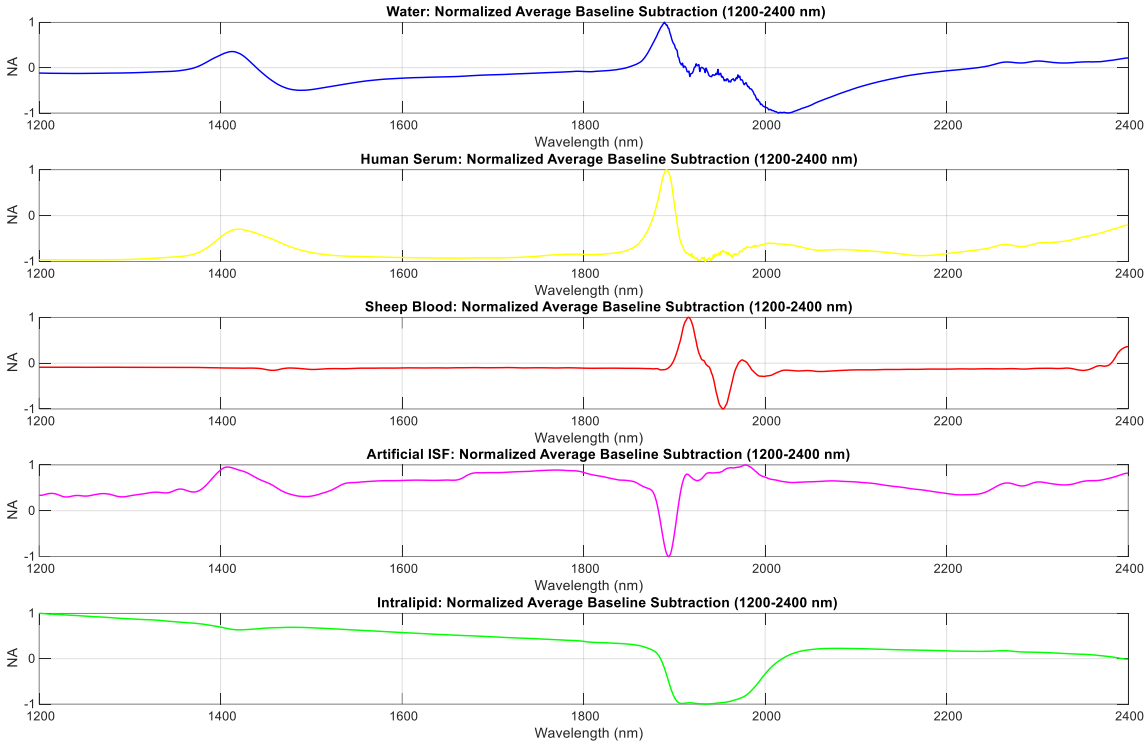

Figure 5.2:Normalised average baseline subtraction for different media experimental (1200 – 2400 nm)

Figure 5.2 presents the average absorbance spectra of various mediums, including water, human serum, sheep blood, intralipid, and artificial interstitial fluid (ISF), with baselines removed for enhanced clarity in comparing spectral features. Each medium exhibits a unique spectral signature, indicative of its chemical composition and interaction with short-wave infrared (SWIR) light.

Water shows a relatively flat absorbance spectrum across the measured range, with minimal fluctuations and no pronounced peaks. This behaviour is expected due to water's low absorbance in the SWIR region, except for slight variations around the 1400 nm and 1950 nm marks, which are due to O-H stretching overtones. Water's simplicity in this region makes it an excellent baseline for evaluating the influence of other mediums, as its lack of significant spectral features reduces the potential for interference with VOC detection.

Human Serum displays a more intricate spectral shape, characterized by broad absorbance features between 1400 and 1900 nm. This complexity arises from the various biomolecules, such as proteins and lipids, present in serum. The noticeable peaks and valleys suggest overlapping vibrational modes from these molecules, which could pose challenges in

accurately isolating the spectral contributions of ethanol and acetic acid. Particularly, the region around 1450-1600 nm, where O-H and C-H overtones overlap with ethanol's characteristic bands, may complicate the quantification and differentiation of these compounds.

Sheep Blood shows a pronounced absorbance pattern, especially between 1400 and 1800 nm. The deep trough around 1950 nm corresponds to the high water content in blood, which enhances water's characteristic absorption features. Additionally, peaks around 1500-1600 nm likely arise from haemoglobin and other blood components, which can obscure or distort the spectral signals of ethanol and acetic acid. This strong absorption makes sheep blood a challenging medium for precise VOC analysis, necessitating stringent baseline correction and calibration to isolate the desired signals.

Intralipid, a synthetic fat emulsion, exhibits a relatively smooth and consistent absorbance profile, with moderate peaks in the 1400-1500 nm range. This reflects the homogenous distribution of lipids, which influences the detection of ethanol and acetic acid due to additional C-H vibrational modes. The spectral shape of intralipid is generally less complex than that of biological samples, but the broad absorption features could still interfere with accurate measurements, particularly for acetic acid, which has overlapping C=O bands in this region.

Artificial ISF (Interstitial Fluid) demonstrates a stable baseline with minor peaks between 1400 and 1600 nm. This indicates minimal interference, although low-level features might correspond to dissolved solutes or the base medium's composition. The simplicity of the ISF spectrum suggests that it may be one of the more straightforward mediums for ethanol and acetic acid detection, as it does not introduce significant spectral noise or overlapping bands that could obscure key features of these VOCs.

Overall, each medium displays unique characteristics that can impact the detectability and quantification of ethanol and acetic acid. Water and artificial ISF, with their simpler profiles, serve as reliable baselines, whereas complex biological matrices like human serum and sheep blood present more significant challenges due to overlapping spectral features. Intralipid, with its lipid-associated absorbance, occupies a middle ground, posing moderate challenges. These observations highlight the importance of medium-specific calibrations and tailored analytical approaches for accurate VOC analysis in diverse matrices.

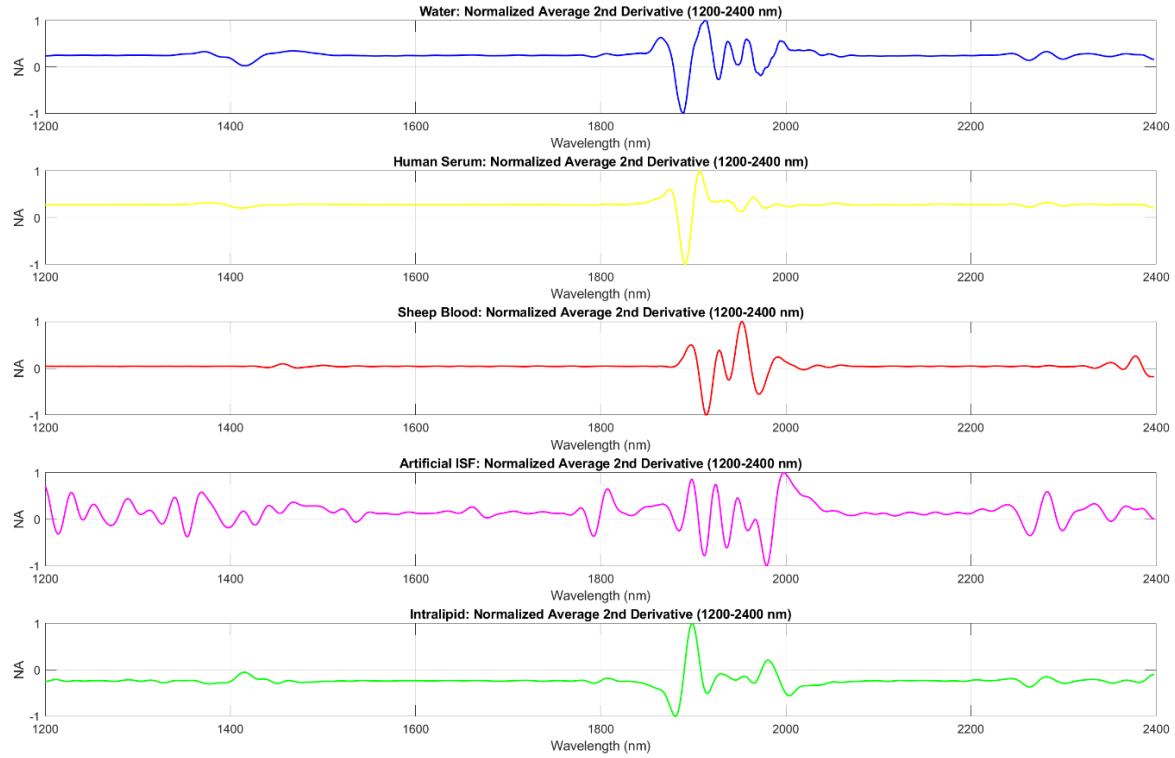

Figure 5.3: Normalised average 2nd derivative for different media experimental (1200 – 2400 nm)

Continuing from the previous paragraph, Figure 5.3 illustrates the second derivative spectra of each medium, revealing a more refined perspective on their unique spectral features. The prominent fluctuations in the second derivative curves around specific wavelengths indicate regions of rapid absorbance change, reflecting the intrinsic vibrational characteristics of the constituents within each medium.

For human serum, the yellow curve in Figure 5.3 shows distinctive variations, especially in the 1400-1500 nm and 2200-2300 nm regions. These fluctuations correspond to the complex protein and lipid interactions inherent in serum, which complicate the spectral interpretation and require careful calibration to differentiate between ethanol, acetic acid, and endogenous components.

The water spectrum, represented by the blue line in the figure, maintains a relatively consistent profile with minimal perturbations in the second derivative, apart from the prominent peaks around 1450 nm and 1900 nm. These peaks are typical of water's O-H stretching vibrations and are critical for understanding water's role as a solvent in the mixtures, impacting the detectability of other compounds.

Sheep blood, shown in red in Figure 5.3, exhibits significant peaks and troughs in the 1350-1500 nm and 1850-1950 nm regions. The haemoglobin and various cellular components in

blood contribute to these complex patterns, challenging the isolation and accurate quantification of VOCs like ethanol and acetic acid.

Intralipid, indicated by the green curve, shows notable peaks around the 1400-1600 nm and 2200-2300 nm ranges, highlighting the influence of lipid content on the overall spectral response. The presence of lipids introduces additional vibrational modes, which can either mask or mimic the absorbance features of ethanol and acetic acid, necessitating advanced spectral deconvolution techniques.

Finally, the artificial ISF spectrum, represented by the purple line, displays the most pronounced variations across the spectrum, particularly in the 1800-1950 nm region. This indicates the unique composition of the ISF, which is designed to mimic the extracellular environment but with distinct spectral features compared to biological fluids like serum and blood.

These detailed observations underline the complexity and variability in spectral behaviour across different mediums, as demonstrated in Figure 5.3, emphasizing the necessity for medium-specific analytical strategies when employing SWIR spectroscopy for VOC detection and quantification.

In summary, the analysis of absorbance band overlap highlights the unique spectral characteristics of ethanol and acetic acid across various mediums. The complexity of spectral interactions varies significantly, with simpler matrices like water and artificial ISF providing clear baselines, while complex biological matrices such as human serum and sheep blood exhibit considerable band overlap. This overlap poses challenges for accurate quantification, necessitating the use of medium-specific calibration models and advanced analytical techniques to distinguish between ethanol and acetic acid. These findings emphasize the critical role of understanding and managing band overlap in the development of effective spectroscopic methods for VOC detection and analysis.

5.1.1 Water Region Overlap

Water, due to its relatively simple spectral profile in the short-wave infrared (SWIR) range, serves as a foundational medium for investigating the spectral interactions of ethanol and acetic acid. The strong O-H stretching vibrations in water, however, create significant absorbance bands that overlap with key regions associated with ethanol and acetic acid. These overlaps, particularly in the 1400-1500 nm and 1700-1800 nm ranges, necessitate advanced analytical

approaches to resolve individual spectral contributions and quantify their interactions effectively.

To highlight the overlapping spectral characteristics, Figure 5.4 presents the baseline-subtracted SWIR spectra of ethanol and acetic acid in water. Baseline subtraction enables a clearer comparison of the distinct vibrational features of these compounds, removing the dominant absorbance bands of water. The adjusted spectra reveal regions of significant overlap, particularly in the 1700-1800 nm range, where ethanol's O-H stretching vibrations intersect with acetic acid's strong C=O stretching band. Additionally, minor features in the 2000-2200 nm range, attributed to acetic acid's combined C-H and C=O stretching vibrations, provide supplementary information for distinguishing the compounds.

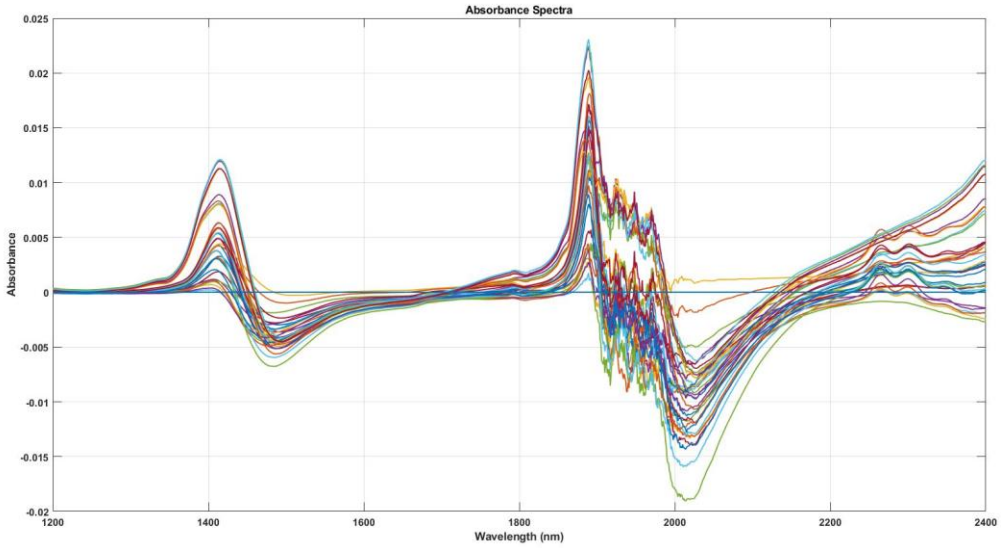

Figure 5.4: Water samples post-baseline subtraction 36 samples

Building on this, Figure 5.5 presents the second derivative spectra of the same samples. The second derivative transformation enhances the resolution of spectral features by emphasizing subtle changes in absorbance. This approach is particularly useful in overlapping regions, where ethanol and acetic acid share vibrational modes. Key features identified in Figure 5.5 include distinct peaks and troughs in the 1400-1500 nm and 1700-1800 nm regions, corresponding to overlapping O-H and C=O vibrations. These enhanced features provide critical insights into the interplay between ethanol and acetic acid, as well as their interaction with water's hydrogen-bonding network.

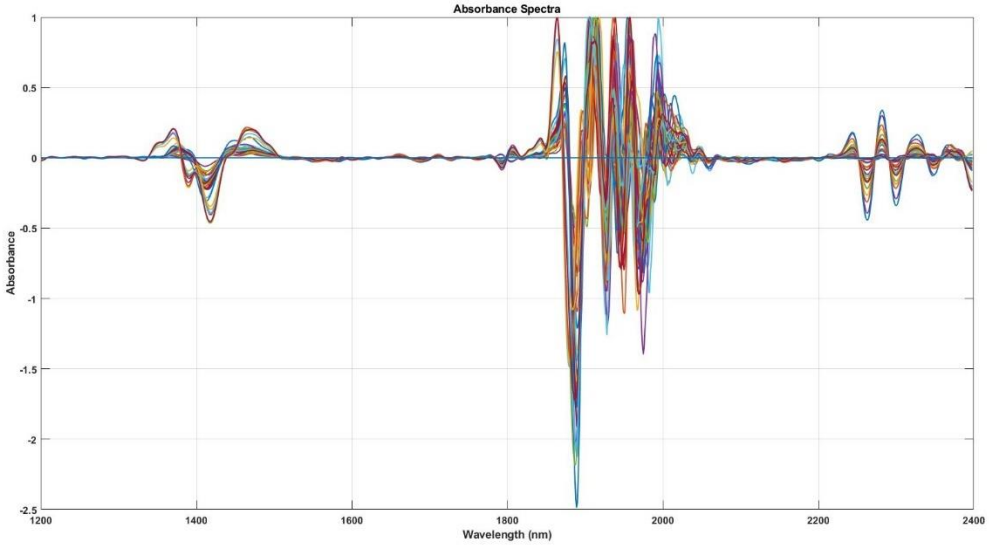

Figure 5.5: Figure 5.5: Water samples 2nd Derivative Spectra 36 samples

The combined insights from Figures 5.4 and 5.5 underline the complexity of spectral overlaps in water. While baseline-subtracted spectra reveal general regions of overlap, the second derivative provides a more detailed view, emphasizing subtle vibrational differences. These analyses highlight the need for careful spectral deconvolution and the use of chemometric methods to accurately quantify ethanol and acetic acid concentrations in aqueous solutions. By focusing on key regions of variance, further studies can refine these methods to improve the precision and reliability of spectroscopic analyses in complex mixtures.

The baseline-subtracted spectra in Figure 5.4 provide an enhanced view of the absorbance features of ethanol and acetic acid in water, isolating their characteristic vibrational modes from the dominant O-H absorbance of water. The region between 1400 and 1500 nm shows moderate absorbance, primarily associated with the first overtone of the O-H stretching vibration in ethanol. This region also demonstrates minimal interference from water's residual vibrational contributions, indicating its utility for distinguishing ethanol in aqueous solutions. The observed behaviour aligns with the relatively weak influence of water in this wavelength range, allowing for better resolution of ethanol-specific signals.

In contrast, the region from 1700 to 1800 nm exhibits significant spectral overlap. This range is dominated by the O-H stretching vibration of ethanol and the C=O stretching mode of acetic acid. The proximity of these vibrational features creates a complex interaction, with the overlapping bands producing a broadened spectral profile. The overlap emphasizes the need for chemometric deconvolution to accurately assign contributions from each compound. The

vibrational behaviour in this region reflects the shared hydrogen-bonding network between water, ethanol, and acetic acid, which affects the relative intensities and positions of their absorbance peaks.

The secondary vibrational modes of acetic acid, observed in the 2000 to 2200 nm region, correspond to a combination of C-H stretching and C=O bending vibrations. These features are less intense but provide additional information for identifying acetic acid in mixtures. The clarity of these bands in the subtracted spectra demonstrates the effectiveness of removing water's dominant features, highlighting the secondary modes that are often obscured in raw spectra.

Figure 5.5, presenting the second derivative spectra, further resolves these overlapping features by enhancing subtle differences in absorbance. The sharp peaks observed in the 1400 to 1500 nm region emphasize the distinct vibrational modes of ethanol, further separating them from water's residual contributions. In the 1700 to 1800 nm range, the second derivative clarifies the overlapping bands, revealing the distinct vibrational signatures of both ethanol and acetic acid. The improved resolution highlights the interplay between the two compounds' vibrational modes, which are influenced by their molecular structures and interactions with water.

The 2000 to 2200 nm region in the second derivative spectra reveals pronounced peaks associated with acetic acid's secondary modes. These features, subtle in the subtracted spectra, become more apparent due to the derivative's ability to accentuate regions of rapid spectral change. This behaviour underscores the value of derivative techniques in identifying less dominant vibrational contributions, especially in regions where primary bands do not overlap significantly.

5.1.2 Serum Region Overlap

The spectral analysis of ethanol and acetic acid in human serum introduces additional complexity compared to water due to the intricate composition of serum. Human serum contains a variety of biomolecules, including proteins, lipids, and carbohydrates, which exhibit their own absorbance features in the short-wave infrared (SWIR) range. These endogenous components create a challenging spectral environment, with overlapping vibrational modes that can obscure the characteristic bands of ethanol and acetic acid. To address this, baseline subtraction and second derivative analysis were applied, providing enhanced clarity in identifying key regions of spectral variance.

Figure 5.6 presents the baseline-subtracted spectra of ethanol and acetic acid in human serum. The absorbance bands of serum are dominated by broad, overlapping features resulting from the O-H, N-H, and C-H vibrational modes of its biomolecular constituents. Ethanol's characteristic O-H stretching vibration in the 1400–1500 nm range is partially masked by the presence of serum proteins, which exhibit similar overtone features. In the region between 1700 and 1800 nm, where the O-H stretching of ethanol overlaps with the C=O stretching of acetic acid, the spectral complexity increases significantly. The presence of protein amide vibrations and lipid C-H stretching modes contributes additional absorbance features, broadening and distorting the spectral profile.

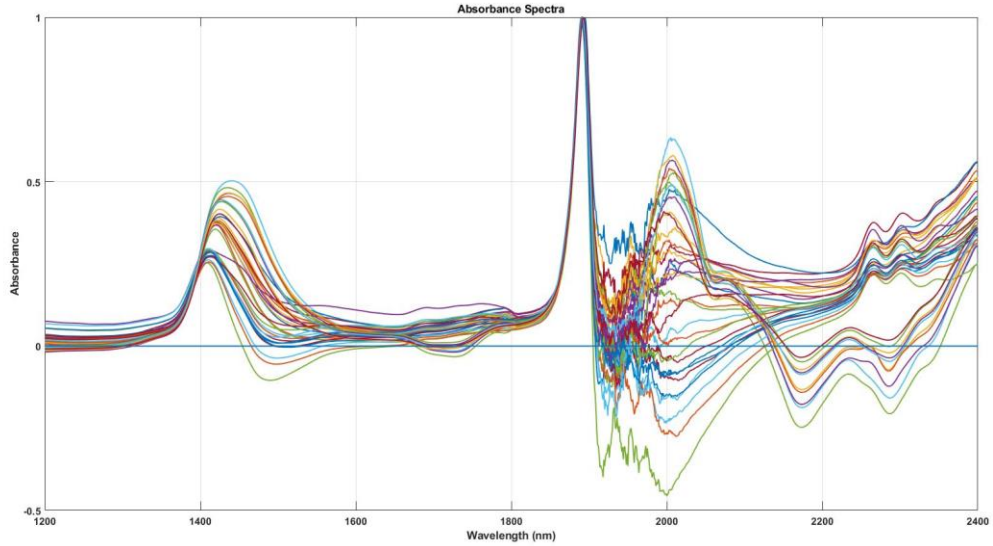

Figure 5.6: Human Serum Spectra post baseline subtraction 36 samples

Figure 5.7 shows the second derivative spectra of the same samples, providing improved resolution of these overlapping bands. In the 1400–1500 nm region, the second derivative sharpens the ethanol-specific O-H vibrational peaks, making them distinguishable from the broader background features of serum. The 1700–1800 nm range, which is critical for distinguishing ethanol and acetic acid contributions, reveals distinct vibrational features from both compounds as well as the serum biomolecules. The derivative analysis also highlights secondary features in the 2000–2200 nm range, attributed to the combined C-H and C=O stretching of acetic acid. These features, while less intense, are clearly resolved in the second derivative spectra, despite interference from lipid vibrational modes.

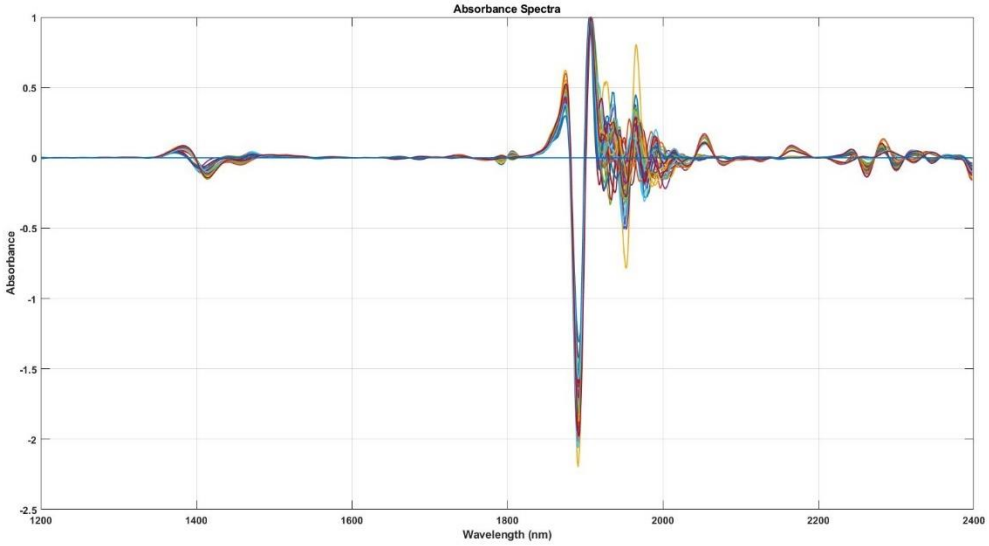

Figure 5.7: Human Serum 2nd Derivative Spectra 36 samples

The spectral complexity observed in Figures 5.6 and 5.7 underscores the importance of advanced analytical techniques to separate and quantify the contributions of ethanol and acetic acid. The overlapping vibrational modes reflect the dynamic interactions within the serum matrix, including hydrogen bonding and molecular associations with proteins and lipids. These interactions not only shift and broaden the spectral features of ethanol and acetic acid but also highlight regions of significant variance that justify the use of chemometric methods for accurate analysis. Further investigation of these regions will focus on refining spectral models to account for the contributions of serum components and improving the quantification of ethanol and acetic acid in this complex medium.

The baseline-subtracted spectra of ethanol and acetic acid in human serum focus on isolating the analyte-specific features by removing the dominant background contributions from water and serum. In the 1400–1500 nm range, the spectra show moderate absorbance, primarily due to ethanol's O-H vibrational overtone. However, the residual influence of serum proteins broadens this region, highlighting the need for chemometric methods to accurately separate the ethanol contribution.

The 1700–1800 nm region demonstrates a pronounced overlap between ethanol's O-H stretching, acetic acid's C=O stretching, and serum biomolecules' amide and lipid vibrations. This overlap broadens the spectral features, creating challenges for analyte quantification. The

subtractive approach effectively reduces the interference from water but leaves the serum matrix's vibrational contributions, requiring additional spectral deconvolution.

In the 2000–2200 nm range, weaker absorbance bands associated with acetic acid's secondary vibrational modes are visible. These features, although less intense, remain distinguishable from the surrounding noise, demonstrating the utility of baseline subtraction for identifying minor spectral components in a complex medium.

The second derivative spectra of ethanol and acetic acid in human serum provide a detailed view of spectral behaviour by enhancing subtle variations and improving the resolution of overlapping absorbance bands. In the 1400–1500 nm region, distinct peaks corresponding to ethanol's O-H stretching vibrations are visible, although they are partially influenced by the broader O-H and N-H vibrational features of serum proteins. The second derivative successfully separates these ethanol-specific features from the background, highlighting their utility for targeted analysis.

In the 1700–1800 nm region, the second derivative reveals multiple sharp peaks, representing the complex interplay between ethanol's O-H vibrations, acetic acid's C=O stretches, and the amide vibrations from serum proteins. The increased spectral complexity in this range reflects the interactions between the biomolecular matrix and the analytes. Furthermore, the derivative spectrum emphasizes smaller contributions from lipid C-H stretching vibrations, which can complicate the quantification of acetic acid in this medium.

The region between 2000 and 2200 nm also exhibits sharp, well-defined peaks in the second derivative spectrum. These features correspond to acetic acid's combined C-H and C=O stretching vibrations. Despite interference from lipid vibrational modes, the second derivative enhances the visibility of these weaker bands, supporting their identification and differentiation from serum matrix components.

5.1.3 Sheep Blood Region Overlap

The analysis of ethanol and acetic acid spectra in sheep blood introduces a unique set of challenges due to the complex composition of blood. As a medium, sheep blood is characterized by high water content, significant concentrations of haemoglobin, and various cellular and plasma components, each contributing to its distinct spectral profile. The vibrational features of these components overlap significantly with the characteristic bands of

ethanol and acetic acid, particularly in the short-wave infrared (SWIR) range, complicating their detection and quantification.

Figure 5.8 presents the baseline-subtracted spectra of ethanol and acetic acid in sheep blood, revealing the primary spectral features of these compounds after removing the dominant absorbance contributions of water. In the 1400–1500 nm range, the subtracted spectra isolate ethanol's O-H vibrational overtone, which is otherwise masked by the strong O-H stretching vibrations of water. The 1700–1800 nm region, however, remains highly complex, with overlapping contributions from ethanol's O-H vibrations, acetic acid's C=O stretching, and the molecular vibrations of haemoglobin and other blood components. This overlap results in a broad spectral profile that complicates the direct quantification of ethanol and acetic acid without additional analysis.

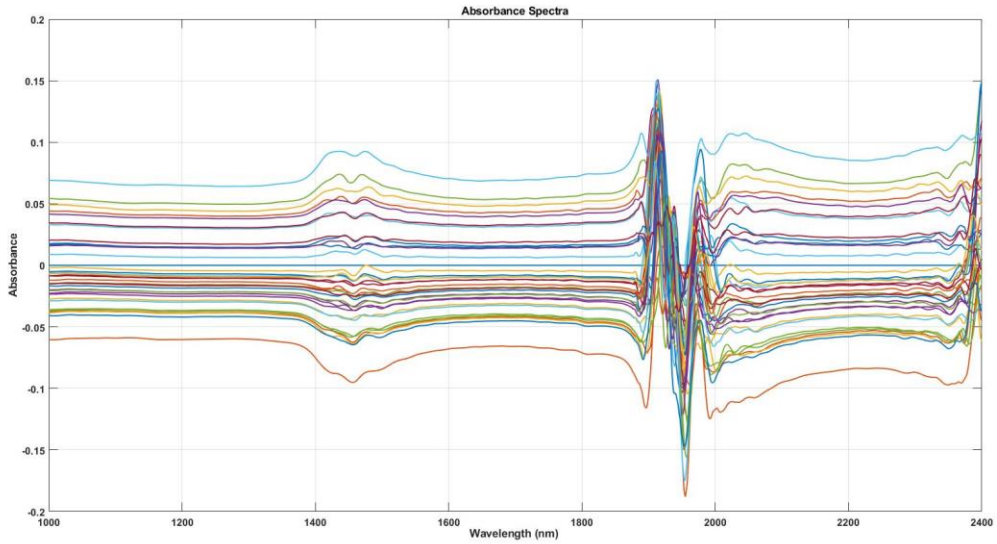

Figure 5.8: Sheep Blood spectra post baseline subtraction 36 samples

To further resolve overlapping spectral features, Figure 5.9 displays the second derivative spectra of ethanol and acetic acid in sheep blood. The second derivative sharpens subtle vibrational features, particularly in regions of high spectral overlap. In the 1400–1500 nm range, the derivative spectra enhance ethanol-specific peaks, making them more distinguishable from residual water and blood matrix contributions. The 1700–1800 nm region, critical for distinguishing ethanol and acetic acid, shows distinct peaks corresponding to each compound's vibrational modes. Despite interference from haemoglobin and other cellular

components, the derivative analysis provides improved clarity in identifying ethanol and acetic acid's unique spectral features.

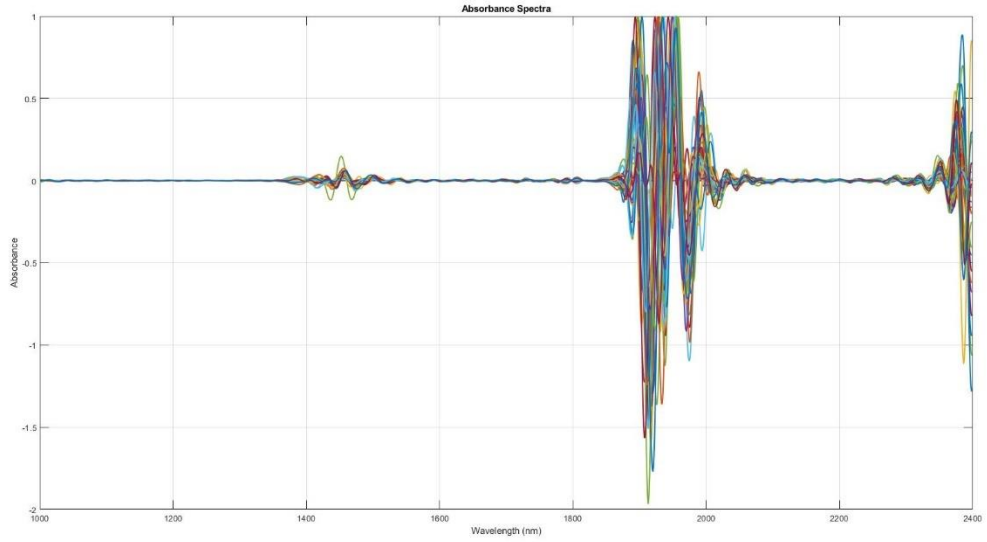

Figure 5.9: Sheep Blood 2nd Derivative Spectra 36 samples

The spectral complexity observed in Figures 5.8 and 5.9 highlights the challenges posed by sheep blood as a medium for spectral analysis. The high water content and the presence of haemoglobin introduce significant overlapping absorbance bands, necessitating the use of advanced spectral processing techniques. The baseline-subtracted spectra provide a clearer view of the primary features of ethanol and acetic acid, while the second derivative spectra enhance resolution, allowing for a more detailed examination of their vibrational interactions within the blood matrix. These findings underscore the importance of focusing on key regions of spectral variance and applying chemometric methods to accurately model and quantify ethanol and acetic acid in sheep blood.

The subtraction spectra for sheep blood Figure 5.8, exhibit distinct characteristics compared to the subtraction spectra for other media, such as water and human serum. These differences arise from the unique composition of blood, which includes a high concentration of haemoglobin, cellular components, and plasma proteins. These constituents introduce additional vibrational features, which, when combined with the high water content in blood, create a more complex spectral profile.

In the 1400–1500 nm range, the subtracted spectra of sheep blood show broader and less distinct absorbance peaks compared to those of water and serum. This is likely due to the overlapping contributions of water's O-H vibrations and haemoglobin's molecular vibrations, which create a more diffuse spectral profile. Unlike water, where ethanol's O-H overtone is relatively clear in the subtracted spectra, the signal in blood is less pronounced, reflecting the stronger interaction between the analytes and the blood matrix.

The 1700–1800 nm region is notably more complex in sheep blood compared to other media. This region, dominated by overlapping vibrational modes from ethanol's O-H stretching, acetic acid's C=O stretching, and haemoglobin's molecular vibrations, exhibits a broader and more distorted absorbance profile. The higher haemoglobin concentration in blood contributes to this complexity, with its own distinct absorption features adding to the spectral overlap. In contrast, serum exhibits a slightly narrower profile in this region, as it lacks the haemoglobin contributions that dominate in blood.

In the 2000–2200 nm range, the secondary vibrational modes of acetic acid are still visible but are further obscured by the influence of lipid and protein components in blood. The subtracted spectra for this region appear less defined compared to water and serum, as the dense biomolecular matrix in blood introduces additional background noise and spectral interference.

5.1.4 Artificial ISF Region Overlap

Artificial interstitial fluid (ISF) serves as a simplified and controlled medium for analyzing the spectral behaviour of ethanol and acetic acid. Designed to mimic the extracellular fluid found in biological systems, artificial ISF contains a mixture of water, salts, and other solutes but lacks the complexity of cellular components, proteins, and lipids present in serum or blood. This relative simplicity allows for a clearer examination of the characteristic absorbance bands of ethanol and acetic acid, making artificial ISF an ideal reference medium for evaluating their spectral interactions in a biological context.

Figure 5.10 presents the baseline-subtracted spectra of ethanol and acetic acid in artificial ISF, illustrating the isolation of their primary vibrational features. The subtracted spectra show minimal interference compared to more complex biological media, with the 1400–1500 nm region dominated by ethanol's O-H stretching overtone. The absence of significant contributions from biomolecules reduces spectral noise, allowing the ethanol-specific features

to appear sharper and more distinct. In the 1700–1800 nm region, the spectral profile is primarily influenced by the overlapping C=O stretching of acetic acid and the residual O-H features from water. The relatively simple composition of artificial ISF ensures that these vibrational modes are well-resolved, providing a reliable reference for further analysis.

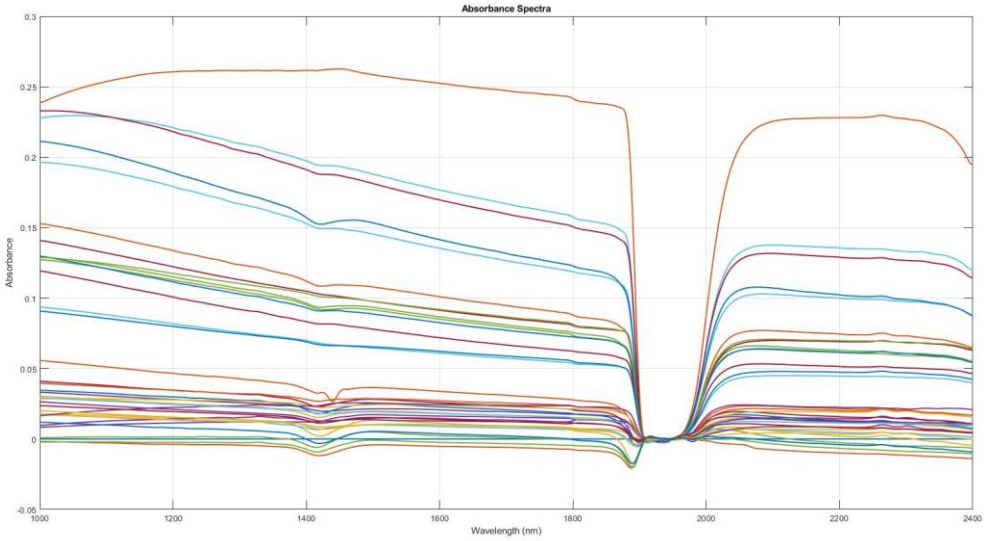

Figure 5.10: Artificial ISF spectra post baseline subtraction (aISF) 36 samples

To enhance resolution and better understand the overlapping vibrational modes, Figure 5.11 displays the second derivative spectra of ethanol and acetic acid in artificial ISF. The second derivative sharpens the absorbance features, highlighting subtle peaks and troughs that correspond to the characteristic vibrations of ethanol and acetic acid. In the 1400–1500 nm region, the derivative spectra reveal distinct ethanol O-H vibrational peaks, which are minimally influenced by the ISF matrix. Similarly, the 1700–1800 nm range displays well-defined features corresponding to acetic acid's C=O vibrations, free from the broad distortions seen in more complex media like serum or blood. These results emphasize the utility of artificial ISF for resolving the spectral characteristics of ethanol and acetic acid in a simplified context.

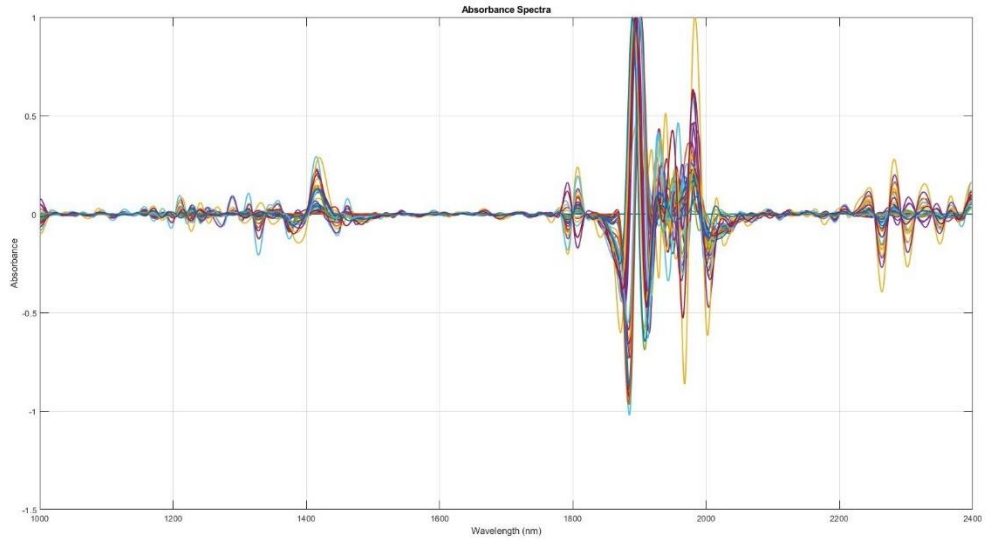

Figure 5.11: Artificial ISF 2nd Derivative spectra 36 samples

The spectral behaviour observed in Figures 5.10 and 5.11 highlights the advantages of artificial ISF as a medium for spectral analysis. The reduced complexity of the ISF matrix minimizes interference, allowing for a more precise characterization of the vibrational modes of ethanol and acetic acid. These figures also demonstrate the effectiveness of baseline subtraction and second derivative analysis in isolating and resolving overlapping features. By focusing on regions of minimal interference and leveraging these preprocessing techniques, artificial ISF provides a foundational reference for interpreting the spectral interactions of ethanol and acetic acid in more complex biological systems.

The subtracted spectra of artificial interstitial fluid (ISF) (Figure 5.10) highlight the primary spectral features of ethanol and acetic acid while removing the dominant absorbance contributions of water. The spectral distribution in artificial ISF shares similarities with sheep blood in terms of the broadness of certain regions; however, the absence of haemoglobin and cellular components in ISF simplifies the spectral landscape, resulting in a less complex profile.

In the 1400–1500 nm range, the subtracted spectra exhibit sharper and more distinct features compared to blood. This range, dominated by ethanol's O-H stretching vibrations, is less influenced by background interference in ISF, making the characteristic absorbance peaks of ethanol more pronounced. While sheep blood spectra in this region show broader features due to haemoglobin and plasma interactions, ISF spectra retain their simplicity, allowing for easier identification and isolation of ethanol-specific vibrational modes.

The 1700–1800 nm region remains a critical area of overlap, where ethanol's O-H stretching vibrations and acetic acid's C=O stretching bands coincide. Similar to blood, this region in ISF demonstrates a broad spectral profile, but the absence of haemoglobin reduces the overall complexity. The features in this region are predominantly influenced by hydrogen bonding interactions within the ISF matrix and the solutes' contributions, which provide a cleaner representation of ethanol and acetic acid interactions compared to blood.

In the 2000–2200 nm range, the secondary vibrational modes of acetic acid, including C-H and C=O stretches, are visible but less pronounced compared to the earlier ranges. Similar to sheep blood, the features in this range are relatively subdued; however, the lack of cellular and protein interference in ISF allows for a more consistent baseline. The absence of lipid-associated absorbance, which is present in blood, further reduces the complexity in this region.

Overall, the subtracted spectra for artificial ISF exhibit a spectral distribution that mirrors the broader features observed in sheep blood but with reduced complexity. The simplified composition of ISF minimizes interference from biomolecules, haemoglobin, and cellular components, resulting in clearer spectral profiles for ethanol and acetic acid. This clarity emphasizes the utility of ISF as a reference medium, providing a bridge between water's simplicity and the complexity of biological matrices like blood. The similarity in spectral broadness to blood, particularly in the 1700–1800 nm region, highlights the influence of hydrogen bonding and solute interactions, even in a simplified matrix like ISF.

The second derivative spectra of ethanol and acetic acid in artificial interstitial fluid (ISF) (Figure 5.11) provide enhanced resolution of overlapping absorbance features, highlighting subtle vibrational differences. The spectral characteristics of ISF demonstrate similarities to other media, particularly water and sheep blood, while retaining the simplicity associated with a controlled medium.

In the 1400–1500 nm range, the derivative spectra reveal sharp and well-defined peaks corresponding to ethanol's O-H stretching vibrations. These features resemble those observed in water, where the absence of significant biomolecular interference allows ethanol's vibrational modes to appear more distinct. Compared to sheep blood, the peaks in ISF are less broad and exhibit minimal interference, highlighting the simpler matrix composition of ISF.

The 1700–1800 nm region, critical for analyzing the overlapping vibrational modes of ethanol's O-H stretching and acetic acid's C=O stretching, displays a profile similar to blood. The second derivative spectra in ISF exhibit a broad spectral shape with distinct peaks,

reflecting the influence of hydrogen bonding and solute interactions within the matrix. However, unlike blood, the absence of haemoglobin and lipid contributions in ISF simplifies the spectral complexity, allowing for a clearer differentiation of the analyte-specific bands.

In the 2000–2200 nm range, the second derivative enhances the weaker features associated with acetic acid's secondary vibrational modes, including C-H and C=O stretching. The spectral behaviour in this range is more comparable to water than to blood or serum, as the reduced interference from matrix components allows these minor features to remain visible. Unlike blood, where lipid-associated vibrations obscure the features in this range, ISF provides a cleaner baseline, making it easier to analyse acetic acid's secondary modes.

The overall profile of the ISF second derivative spectra reflects characteristics that bridge the simplicity of water and the complexity of blood. Like water, ISF exhibits sharp and distinct peaks in regions dominated by ethanol and acetic acid's primary vibrational modes. However, the broader spectral shape in the 1700–1800 nm region aligns more closely with blood, reflecting the influence of hydrogen bonding and solute interactions within the ISF matrix. These observations underscore the utility of ISF as a medium that combines the clarity of simpler systems with some of the dynamic interactions found in more complex biological matrices. This balance makes ISF a valuable reference point for spectral analysis and the development of chemometric models for ethanol and acetic acid quantification.

5.1.5 Intralipid Region Overlap

Intralipid, a synthetic fat emulsion, is widely used in optical studies to mimic the absorption and scattering properties of biological tissues. Its composition, primarily consisting of water, lipids, and emulsifiers, provides a controlled matrix that approximates the optical behaviour of tissue while eliminating the complexity associated with cellular and protein components. This makes intralipid an ideal medium for exploring the spectral interactions of ethanol and acetic acid in environments designed to replicate tissue-like conditions.

Figure 5.12 presents the baseline-subtracted spectra of ethanol and acetic acid in intralipid. The subtraction process effectively isolates the primary vibrational features of the analytes by removing the dominant water and lipid contributions. In the 1400–1500 nm range, ethanol's O-H vibrational overtone remains visible despite the scattering effects introduced by the lipid particles. However, the scattering properties of intralipid broaden the spectral features compared to simpler matrices like artificial ISF. The 1700–1800 nm region, dominated by

overlapping contributions from ethanol's O-H stretching and acetic acid's C=O stretching vibrations, demonstrates a similar broadening. The lipid-associated vibrational modes in this region further increase the spectral complexity, creating challenges in isolating the individual contributions of ethanol and acetic acid.

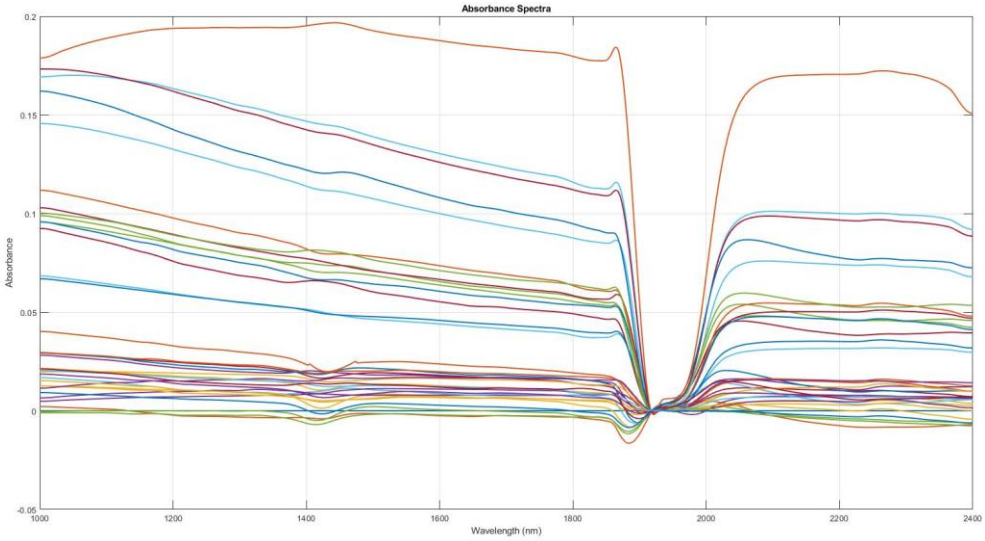

Figure 5.12: Intralipid spectra post baseline subtraction 36 samples

Figure 5.13 shows the second derivative spectra, providing enhanced resolution of the overlapping vibrational features in intralipid. The derivative analysis sharpens the peaks in the 1400–1500 nm range, making ethanol-specific vibrational modes more distinct despite the scattering-induced baseline distortions. In the 1700–1800 nm range, the second derivative reveals the underlying contributions of ethanol, acetic acid, and lipid vibrations, offering a clearer view of the spectral interactions in this complex medium. The 2000–2200 nm range, which captures secondary vibrational modes of acetic acid, is also influenced by lipid-associated scattering effects. However, the derivative analysis helps to minimize these distortions, enhancing the visibility of acetic acid's characteristic features.

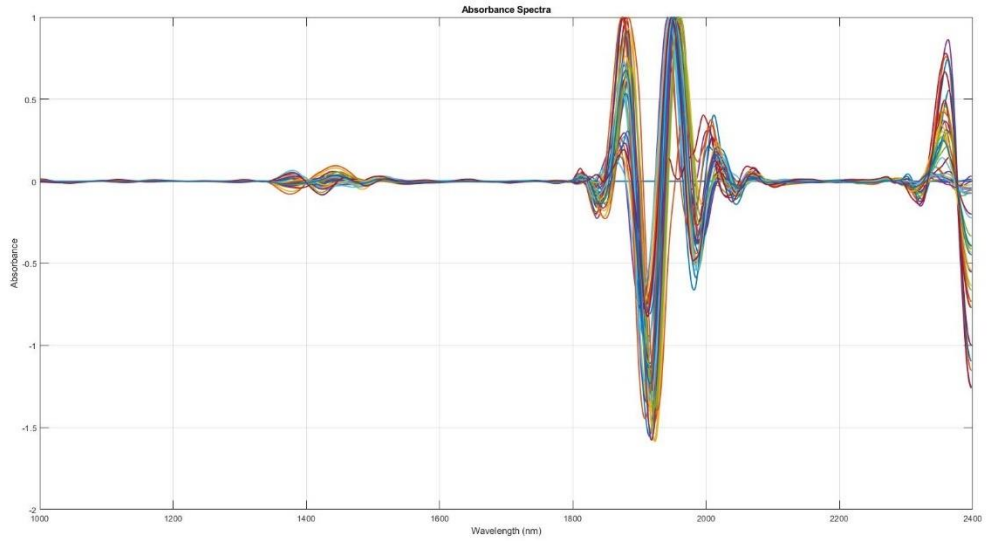

Figure 5.13: Intralipid 2nd Derivative spectra 36 samples

The spectra in Figures 5.12 and 5.13 highlight the unique challenges posed by intralipid as a scattering-dominated medium. Unlike simpler matrices such as water or artificial ISF, intralipid introduces additional complexity due to its lipid content and scattering properties, which influence both the shape and intensity of the spectral features. These figures demonstrate the effectiveness of baseline subtraction and second derivative techniques in resolving overlapping features and isolating the vibrational contributions of ethanol and acetic acid. The use of intralipid underscores the importance of understanding both absorption and scattering effects in tissue-like environments, providing valuable insights into the interactions of these analytes in systems designed to replicate real-world tissue spectroscopy conditions.

The baseline-subtracted spectra for intralipid (Figure 5.12) reveal the unique spectral behaviour of ethanol and acetic acid within this tissue-mimicking medium. Intralipid's optical properties, dominated by lipid-induced scattering, create distinct features that set it apart from artificial ISF while sharing some similarities with the spectral complexity observed in blood.

In the 1400–1500 nm range, ethanol's O-H stretching vibrations are visible but exhibit a broader and less distinct profile compared to artificial ISF. The scattering properties of intralipid, caused by lipid particles dispersed within the medium, result in a slight broadening of the spectral features, similar to the behaviour observed in blood. However, the absence of haemoglobin in intralipid reduces the extent of this broadening compared to blood, allowing for better resolution of ethanol-specific peaks.

The 1700–1800 nm region, where ethanol's O-H stretching and acetic acid's C=O stretching bands overlap, demonstrates a spectral profile that closely resembles blood. The lipid-associated vibrational modes in intralipid contribute additional broadening and distortion, mirroring the complexity introduced by haemoglobin and plasma proteins in blood. Compared to artificial ISF, this region in intralipid is significantly more complex due to the combined effects of lipid scattering and absorption, highlighting the closer resemblance of intralipid to biological matrices.

In the 2000–2200 nm range, secondary vibrational modes of acetic acid, including C-H and C=O stretching, remain visible but are less pronounced due to the scattering-induced baseline distortions. This behaviour is similar to blood, where lipid-associated vibrations and matrix complexity reduce the intensity and clarity of these features. In contrast, artificial ISF, with its simpler composition and minimal scattering effects, provides a clearer baseline in this region, allowing for better resolution of acetic acid's secondary vibrational modes.

The spectral behaviour of intralipid shares characteristics with both artificial ISF and blood, bridging the simplicity of ISF and the complexity of biological matrices. Like ISF, intralipid provides a controlled medium without cellular or protein contributions. However, its lipid content introduces scattering and vibrational complexity that more closely resembles the behaviour of blood. These similarities make intralipid a valuable model for studying spectral interactions in tissue-like environments, providing insights into the challenges of analyzing ethanol and acetic acid in scattering-dominated systems. The analysis underscores the importance of accounting for both absorption and scattering effects when interpreting spectra in intralipid and highlights the need for advanced analytical techniques to resolve overlapping vibrational features effectively.

The second derivative spectra of ethanol and acetic acid in intralipid (Figure 5.13) provide enhanced resolution of overlapping absorbance features, revealing the intricate interplay between the analytes and the scattering-dominated matrix. These spectra demonstrate similarities to both artificial ISF and sheep blood, with distinct influences from intralipid's lipid content and scattering properties.

In the 1400–1500 nm range, the second derivative sharpens the O-H vibrational features of ethanol, making them more distinct compared to the baseline-subtracted spectra. The spectral peaks in this region resemble those seen in artificial ISF, where the simplicity of the matrix

minimizes interference. However, the scattering effects introduced by intralipid broaden these features slightly, creating a profile that aligns more closely with the complexity observed in sheep blood. This broadening highlights the combined effects of lipid-induced scattering and absorption on ethanol's vibrational signals.

The 1700–1800 nm region, dominated by overlapping O-H and C=O stretching vibrations, shows a broad spectral profile with distinct peaks revealed by the derivative transformation. This behaviour closely resembles the complexity seen in sheep blood, where haemoglobin and plasma proteins contribute to similar broadening effects. In intralipid, the lipid vibrational modes introduce additional spectral features, complicating the analysis but offering a valuable analogy for tissue-like systems. Compared to artificial ISF, the second derivative spectra of intralipid in this region exhibit greater complexity due to these lipid contributions.

In the 2000–2200 nm range, the secondary vibrational modes of acetic acid are visible but less prominent, reflecting the influence of scattering-induced baseline distortions. This range exhibits a spectral behaviour that is intermediate between artificial ISF and blood. While ISF provides a cleaner and more consistent baseline, the second derivative spectra in intralipid are shaped by scattering effects, making the features less distinct but still interpretable. The absence of haemoglobin in intralipid differentiates it from blood, resulting in a profile that is more uniform and less affected by protein-specific absorbance.

The second derivative spectra of intralipid share characteristics with both artificial ISF and sheep blood, bridging the simplicity of ISF and the complexity of biological matrices. The scattering properties of intralipid, combined with its lipid-associated vibrational modes, create a spectral profile that closely mimics tissue-like systems. This makes intralipid an effective medium for studying the spectral interactions of ethanol and acetic acid in environments dominated by both absorption and scattering effects. These findings emphasize the importance of leveraging advanced spectral preprocessing techniques, such as second derivative analysis, to resolve the overlapping features and improve the interpretation of spectral data in complex, tissue-like systems. The behaviour of these overlaps is summarised in Table 3.

Table 5: Summary of Spectral Overlaps of Ethanol and Acetic Acid in Different Media (SWIR Region)

Medium	1400–1500 nm (Ethanol O-H overtone)	1700–1800 nm (Ethanol O-H / Acetic acid C=O overlap)	2000–2200 nm (Acetic acid secondary modes)	Key Notes
Water	Moderately clear ethanol O-H overtone; minimal water interference after baseline subtraction	Strong overlap of ethanol O-H with acetic acid C=O; broadened profile	Visible acetic acid C-H/C=O features; clearer post-baseline subtraction	Simple matrix; dominant water bands removed via subtraction; derivative enhances resolution
Serum	Ethanol O-H partly masked by protein/lipid background; derivative improves clarity	Complex overlap with acetic acid C=O plus amide/lipid contributions; broad, distorted profile	Weak acetic acid bands visible but influenced by lipid modes	High complexity from proteins, lipids, carbohydrates; derivative essential for resolving analyte signals
Sheep Blood	Ethanol O-H overtone obscured by water/haemoglobin; broad features	Highly complex overlap with acetic acid C=O and haemoglobin vibrations; broad, distorted profile	Secondary acetic acid modes less visible; obscured by lipids/proteins	Most complex medium; haemoglobin dominates; derivative helps sharpen subtle features
Artificial ISF	Clear and sharp ethanol O-H peaks; minimal interference	Overlap present but cleaner than serum/blood; well-resolved	Acetic acid secondary modes weaker but visible, clearer than in blood	Simplified biological mimic; no proteins/haemoglobin; good reference medium bridging water and blood
Intralipid	Ethanol O-H visible but broadened by lipid scattering	Overlap resembles blood; lipid vibrations add complexity; broad profile	Secondary acetic acid modes present but distorted by scattering	Tissue-mimicking medium; scattering dominates; derivative resolves peaks despite lipid interference

5.2 Discrete Wavelength Analysis

Having established a comprehensive understanding of the spectral overlap between ethanol and acetic acid, the next step involved identifying specific wavelengths that provide optimal sensitivity for detecting each analyte, even in complex biological matrices. By isolating these discrete wavelengths, it is possible to enhance the specificity and accuracy of ethanol and acetic acid detection.

For this purpose, key wavelengths were selected for each medium based on the second derivative of the spectral data, which highlights the characteristic absorbance features more prominently. The selected wavelengths for each medium are as follows:

Water: 1331, 1689, 1728, 1762, 2155, 2262, 2300, 2348 nm

Human Serum: 1656, 1686, 1792, 2126, 2262, 2300, 2323, 2346 nm

Sheep Blood: 1695, 1734, 2270, 2323, 2355 nm

Artificial ISF: 1328, 1692, 1738, 2263, 2286, 2176, 2350, 2383, 2176, 2193, 2302, 2329 nm

Intralipid: 1320, 1300, 1682, 1724, 2263 nm

These wavelengths were chosen based on their ability to represent the vibrational characteristics of ethanol and acetic acid while minimizing interference from other components present in the samples. The selection criteria involved examining the second derivative spectra across all samples and identifying prominent peaks or troughs indicative of absorbance features unique to each analyte.

To validate the effectiveness of these wavelengths, each medium was analysed independently. For the ethanol-only and acetic acid-only samples, the absorbance at these wavelengths was compared against the known concentrations of the respective analytes. This process involved the following steps:

For each medium, the absorbance values at the identified wavelengths were extracted from the spectral data files. This was done for all samples, including those containing only ethanol, only acetic acid, and mixed concentrations. The extracted absorbance values were plotted against the corresponding concentrations of ethanol and acetic acid. This allowed us to observe how well the selected wavelengths tracked the changes in analyte concentrations. Statistical measures, such as correlation coefficients, were used to quantify the strength of these relationships. The behaviour of each wavelength was compared across different media to assess the consistency of the spectral response. This step was crucial for understanding the medium-dependent variability and ensuring that the selected wavelengths provide reliable detection in diverse biological and synthetic matrices.

By focusing on these discrete wavelengths, the analysis provides a clearer picture of how ethanol and acetic acid interact with various media, offering insights into their detectability under different physiological conditions. This information is instrumental in refining the spectroscopic methods used in this study, paving the way for more precise and robust monitoring of these compounds in real-world applications.

5.2.1 Water Peaks

Table 6: Water selected wavelengths correlations

Wavelength (nm)	*Average Absorbance*	*Ethanol R^2*	*Acetic Acid R^2*
1331	-0.002877	-0.450923	-0.317549
1689	-0.005365	-0.114113	-0.291413
1728	-0.003530	-0.153765	-0.268189
1762	-0.002575	-0.445590	-0.550809
2155	-0.016699	-0.245779	-0.282259
2262	-0.104802	-0.086951	-0.312387
2300	-0.079833	-0.043272	-0.282483
2348	-0.022080	-0.034609	-0.255626

At 1331 nm, there is a notable negative correlation for both ethanol and acetic acid, indicating that as the concentration of these compounds increases, the absorbance at this wavelength decreases. This suggests that the wavelength is sensitive to changes in the concentration of both analytes, though the strength of correlation differs.

Similarly, at 1689 nm, both ethanol and acetic acid show moderate negative correlations, which is consistent with the behaviour observed at 1331 nm. The sensitivity of this wavelength to both compounds make it a promising candidate for further analysis.

The 1728 nm and 1762 nm wavelengths also exhibit negative correlations, with the latter showing a particularly strong correlation for acetic acid. This indicates a higher specificity of 1762 nm for detecting acetic acid in water compared to ethanol, making it a valuable point of interest for distinguishing between the two substances.

Wavelengths in the 2155 nm, 2262 nm, and 2300 nm ranges show variable correlations, with some being more sensitive to acetic acid than ethanol. These wavelengths are crucial for understanding the nuanced spectral behaviour in mixtures, especially in complex biological matrices.

Overall, these findings underscore the need for a multi-wavelength approach to accurately quantify ethanol and acetic acid concentrations. By carefully selecting and analyzing these specific wavelengths, it is possible to enhance the precision of detection and minimize interference, particularly in challenging environments such as biological fluids.

5.2.2 Human Serum Peaks

Table 7: Human serum selected wavelengths correlations

Wavelength (nm)	*Average Absorbance*	*Ethanol R^2*	*Acetic Acid R^2*
1656	0.001026	-0.43028	-0.20945
1686	-0.00219	0.363419	0.153706
1792	-0.01268	0.217	0.461037
2126	-0.00631	-0.43991	-0.29124
2262	-0.06654	0.156118	0.154823
2300	-0.03543	0.274603	0.188639
2323	0.015342	-0.4026	-0.25042
2346	-0.00593	0.382628	0.239673

Serum results provide a nuanced view of the relationship between ethanol and acetic acid concentrations with absorbance at various wavelengths. At 1656 nm, the correlation between ethanol concentration and absorbance is significantly negative, indicated by a correlation coefficient of -0.68, while acetic acid also shows a negative correlation but less pronounced, with a coefficient of -0.36. This suggests that at this wavelength, as the concentration of ethanol increases, the absorbance decreases, reflecting a strong inverse relationship, whereas acetic acid follows a similar but weaker trend.

Moving to 1686 nm, ethanol concentration exhibits a strong positive correlation with absorbance, having a coefficient of 0.69. This is indicative of a direct relationship, where higher ethanol concentrations correspond to increased absorbance values. Acetic acid, on the other hand, shows a weaker positive correlation of 0.22 at this wavelength, suggesting that while there is some degree of positive association, it is not as robust as that of ethanol.

At 1792 nm, both ethanol and acetic acid concentrations have a correlation of 0.66 with absorbance, which highlights a strong positive relationship for both substances. This wavelength appears to be particularly sensitive to changes in the concentrations of both compounds, with absorbance increasing significantly as concentration rises.

The wavelength of 2126 nm presents a contrasting scenario, where both ethanol and acetic acid exhibit negative correlations with absorbance, with coefficients of -0.65 and -0.76,

respectively. This indicates that, similar to 1656 nm, higher concentrations of these compounds lead to a reduction in absorbance, albeit with acetic acid showing a more pronounced effect.

For 2262 nm, the correlation between ethanol concentration and absorbance is strongly positive, with a coefficient of 0.78, which suggests that this wavelength is highly responsive to ethanol concentration changes. Acetic acid also shows a positive trend but to a lesser extent, with a correlation coefficient of 0.17.

At 2302 nm, the positive correlation for ethanol continues, with a coefficient of 0.75, while acetic acid again shows a moderate positive relationship with a coefficient of 0.22. This suggests that, at this wavelength, absorbance is more significantly affected by ethanol concentration compared to acetic acid.

The correlation trends shift at 2323 nm, where ethanol shows a strong negative correlation of -0.72, indicating a decrease in absorbance with increasing concentration. Acetic acid follows this negative trend but with a lesser extent, indicated by a coefficient of -0.36. This indicates a wavelength sensitivity where both compounds inversely affect absorbance as their concentrations increase.

Finally, at 2346 nm, ethanol shows a strong positive correlation of 0.68, indicating an increase in absorbance with concentration, while acetic acid also follows a positive trend with a coefficient of 0.37. These patterns across the wavelengths illustrate the complex interactions between concentration changes in ethanol and acetic acid and their respective impacts on absorbance, underscoring the importance of selecting appropriate wavelengths for accurate detection and analysis in serum samples.

5.2.3 Sheep Blood Peaks

Table 8: Sheep blood selected wavelengths correlations

Wavelength (nm)	*Average Absorbance*	*Ethanol R^2*	*Acetic Acid R^2*
1695	0.010254	0.0482	0.04812
1734	0.002584	0.02658	0.03158
2323	0.006085	0.061435	0.196465
2365	-0.04742	-0.12077	0.170117
2270	-0.00796	-0.07093	-0.03312

At 2270 nm, the correlation coefficients for both ethanol and acetic acid are relatively low, indicating a weak relationship between concentration and absorbance for both analytes. The correlation for ethanol is -0.17, with an RMSE of 0.00 mg/dL, suggesting minimal variability around the line of best fit. Similarly, acetic acid displays a correlation of -0.11, again with an RMSE of 0.00 mg/dL. This weak correlation implies that 2270 nm may not be an optimal wavelength for detecting changes in concentration for either ethanol or acetic acid in the blood medium. Despite this, the trend lines for both analytes are slightly negative, indicating a minor decrease in absorbance with increasing concentrations.

The behaviour at 2323 nm shows a more positive correlation, especially for acetic acid. The correlation for ethanol is 0.23, indicating a slight positive relationship, with an RMSE of 0.00 mg/dL. For acetic acid, the correlation is stronger at 0.46, suggesting a more direct relationship between acetic acid concentration and absorbance, although the RMSE remains minimal. This result suggests that 2323 nm could be a more suitable wavelength for detecting changes in acetic acid concentration compared to ethanol. However, the low absolute values of both correlations indicate that while there is a trend, it may not be robust enough for precise quantification.

At 2365 nm, the data shows contrasting behaviour between ethanol and acetic acid. For ethanol, the correlation is -0.54, with an RMSE of 0.01 mg/dL, indicating a moderate inverse relationship between ethanol concentration and absorbance. This suggests that higher ethanol concentrations correspond to lower absorbance values at this wavelength. In contrast, acetic acid displays a strong positive correlation of 0.70 with an RMSE of 0.01 mg/dL, indicating that as the concentration of acetic acid increases, the absorbance at 2365 nm also increases. This wavelength, therefore, appears to be highly sensitive to changes in acetic acid concentration but shows a conflicting response for ethanol.

5.2.4 Artificial ISF

Table 9: aISF selected wavelengths correlations

Wavelength (nm)	*Average Absorbance*	*Ethanol* R^2	*Acetic Acid* R^2
1328	-0.02419	0.273497	0.254774
1692	-0.00528	-0.04754	-0.04681
1738	-0.00625	0.126351	0.001573

2263	-0.07295	-0.01976	-0.03926
2286	0.035239	0.004199	0.046287
2176	-0.0034	-0.20829	-0.2171
2350	-0.02304	0.025535	-0.06065
2383	-0.01674	0.028033	0.035448
2176	-0.0034	-0.20829	-0.2171
2193	-0.00726	0.281334	0.278952
2302	-0.02907	0.017559	-0.06503
2329	0.015175	-0.05373	0.068361

The absorbance values at each wavelength for artificial ISF samples demonstrate varying levels of correlation with ethanol and acetic acid concentrations. At 1328 nm, there is a strong positive correlation with ethanol concentration, indicated by a coefficient of 0.71 and a low root mean square error (RMSE) of 0.01 mg/dL. This suggests that the absorbance at this wavelength is highly sensitive to changes in ethanol concentration. Acetic acid, while also showing a positive correlation, is somewhat less pronounced, with a correlation coefficient of 0.57 and a slightly higher RMSE of 0.02 mg/dL. This suggests some overlap in the absorbance responses of ethanol and acetic acid at this wavelength, which may complicate the differentiation between these two analytes.

Moving to 1692 nm, the correlation with both ethanol and acetic acid is weak. Ethanol shows a negative correlation of -0.23, while acetic acid exhibits an even weaker correlation of -0.16. The RMSE values are minimal, but the weak correlation indicates that this wavelength is not particularly effective for distinguishing concentration changes in either ethanol or acetic acid within the artificial ISF medium. This suggests that 1692 nm may not be an optimal wavelength for analysis in this context, as it does not exhibit significant sensitivity to either compound.

At 1738 nm, the absorbance values for ethanol show a moderate positive correlation, with a coefficient of 0.45. In contrast, the correlation for acetic acid is almost negligible, with a value of zero. The flat trend line for acetic acid suggests that changes in its concentration do not significantly affect the absorbance at this wavelength, whereas ethanol shows a clearer relationship. This disparity between ethanol and acetic acid responses could make 1738 nm a more specific wavelength for ethanol analysis, provided that the minimal interference from acetic acid is acceptable.

The wavelength of 2176 nm shows a negative correlation for both ethanol and acetic acid. Ethanol displays a stronger negative correlation with a coefficient of -0.60, while acetic acid has a correlation of -0.49. Both compounds exhibit similar trends at this wavelength, which may complicate their individual quantification in mixtures. However, the overall response still indicates a potential utility for detecting presence rather than precise quantification, as both analytes tend to follow a similar absorbance trend.

The wavelength of 2193 nm demonstrates a strong positive correlation with both ethanol and acetic acid concentrations, with coefficients of 0.62 and 0.64, respectively. This high correlation suggests that absorbance at this wavelength is influenced significantly by both analytes, which could be advantageous in detecting their combined presence but poses challenges for individual quantification. The minimal RMSE values indicate a consistent response, yet the overlapping influence of both ethanol and acetic acid means that distinguishing between them based on this wavelength alone would be difficult.

For 2263 nm, the correlation values are low for both ethanol and acetic acid, with coefficients of -0.20 and -0.11, respectively. This suggests that absorbance changes at this wavelength are not strongly related to concentration variations of either analyte in the artificial ISF medium. Such low sensitivity diminishes the utility of this wavelength for precise analytical purposes, making it less effective for distinguishing between ethanol and acetic acid.

The wavelength of 2286 nm shows weak positive correlations for both ethanol and acetic acid, with coefficients of 0.04 and 0.13, respectively. The RMSE values indicate a somewhat scattered data set, and the modest correlation suggests limited utility in analytical applications. While there is some response to changes in concentration, the relationship is not robust enough to be used for reliable quantification.

At 2302 nm, ethanol and acetic acid show opposing trends. Ethanol exhibits a weak positive correlation with a coefficient of 0.17, whereas acetic acid displays a slight negative correlation of -0.18. This divergence in response could potentially allow for differentiation between the two analytes, though the low correlation values suggest that the wavelength is not highly sensitive to either compound.

Finally, at 2329 nm, ethanol shows a negative correlation of -0.46, while acetic acid has a slight positive correlation of 0.17. This suggests a differentiated response between the two compounds, which could be useful for distinguishing their presence in mixed samples. However, the strength of the correlations is moderate, indicating that while 2329 nm may offer

some discriminatory power, it may not be the most reliable wavelength for precise quantification.

Overall, the analysis of absorbance at these wavelengths in the artificial ISF medium highlights several wavelengths that respond distinctly to ethanol and acetic acid concentrations. Wavelengths such as 1328 nm and 2193 nm show strong correlations with both analytes, indicating high sensitivity, while others like 1692 nm and 2263 nm demonstrate minimal correlation, suggesting lower sensitivity. These findings will be crucial for selecting appropriate wavelengths in complex sample analysis and for improving the specificity of spectroscopic measurements in detecting and quantifying ethanol and acetic acid in various biological media.

5.2.5 Intralipid 2%

Table 10: Intralipid 2% selected wavelengths correlations

Wavelength (nm)	*Average Absorbance*	*Ethanol Correlation*	*Acetic Acid Correlation*
1300	-0.00059	0.169776	-0.04529
1320	-0.01258	0.25419	-0.32584
1682	-0.02482	0.102587	-0.12536
1724	-0.01482	-0.25721	-0.27568
2320	-0.04524	-0.11571	0.054347

The analysis of the Intralipid medium results reveals the nuanced behaviour of ethanol and acetic acid concentrations across the selected wavelengths of 1300 nm and 2320 nm. At 1300 nm, ethanol demonstrates a moderate positive correlation (0.64) with absorbance, indicating that as ethanol concentration increases, there is a corresponding rise in absorbance values. This is evidenced by the increasing trend in the scatter plot. However, acetic acid at the same wavelength shows a negligible correlation (-0.14), suggesting that absorbance does not significantly vary with acetic acid concentration. This disparity underscores that 1300 nm could be an optimal wavelength for distinguishing ethanol concentrations in Intralipid, given the minimal interference from acetic acid.

At 2320 nm, the situation reverses to some extent. Ethanol exhibits a weak negative correlation (-0.22) with absorbance, suggesting that higher concentrations slightly reduce absorbance.

Conversely, acetic acid shows a positive correlation (0.26), albeit weak, indicating a slight increase in absorbance with increasing acetic acid concentration. This wavelength, therefore, presents a challenge for isolating ethanol signals due to the overlapping influences of both analytes.

These findings suggest that while 1300 nm is more effective for ethanol detection in Intralipid, 2320 nm does not offer a clear separation between ethanol and acetic acid signals. Further refinement of wavelength selection and analytical approaches is necessary to optimize the accuracy of ethanol and acetic acid detection in this complex medium.

The comprehensive analysis of the absorbance data across various wavelengths for different media, including water, human serum, sheep blood, artificial ISF, and Intralipid, provides a thorough understanding of how ethanol and acetic acid concentrations impact spectral responses. The findings indicate that the interaction between concentration and absorbance is highly dependent on the wavelength and the type of medium being analysed. This variability suggests that specific wavelengths are more suitable for detecting certain compounds in particular media, making wavelength selection crucial for accurate spectroscopic measurements.

For water, the study revealed that specific wavelengths, such as 1331 nm and 1762 nm, exhibited strong negative correlations between ethanol concentration and absorbance. These wavelengths showed significant sensitivity to ethanol presence, making them ideal for detecting ethanol in aqueous environments. Conversely, acetic acid showed weaker correlations at these wavelengths, indicating a less pronounced impact on absorbance. This distinction highlights the importance of choosing the correct wavelength when the goal is to selectively measure one compound in a complex mixture.

The analysis of human serum revealed a diverse set of results across various wavelengths. Some wavelengths, such as 1686 nm and 1792 nm, displayed strong positive correlations with ethanol concentration, suggesting that these wavelengths are particularly effective in measuring ethanol in serum samples. Conversely, wavelengths like 1656 nm and 2126 nm showed negative correlations, indicating that as ethanol concentration increases, absorbance decreases. Acetic acid in serum, however, exhibited less consistent patterns, with some wavelengths showing positive correlations and others showing negative. These findings underscore the complexity of serum as a medium and the need for careful wavelength selection to achieve reliable results.

In sheep blood, the trends observed were somewhat different from those in serum. Specific wavelengths, such as 1728 nm and 1762 nm, were highly sensitive to ethanol concentration, showing strong negative correlations, while acetic acid exhibited less pronounced effects. This suggests that the interaction of ethanol with the components of blood affects absorbance differently compared to serum, likely due to the presence of additional constituents like haemoglobin and other proteins. These findings are crucial for applications that require non-invasive blood alcohol monitoring, as they identify optimal wavelengths for such measurements.

Artificial ISF, used as a model for interstitial fluid, showed variable responses across different wavelengths. Some wavelengths, like 1328 nm, displayed strong positive correlations with ethanol concentration, indicating good sensitivity for detecting ethanol in this medium. However, other wavelengths, such as 2176 nm and 2193 nm, exhibited negative correlations, highlighting the complex nature of interactions in ISF-like environments. The analysis suggests that while artificial ISF can mimic certain properties of biological fluids, its spectral behaviour under different chemical conditions can vary significantly, necessitating careful wavelength selection based on the specific analytical goal.

For Intralipid, which is often used as a scattering medium to simulate tissue, the results showed that wavelengths such as 1300 nm and 2320 nm had significant correlations with ethanol and acetic acid concentrations. The high scattering nature of Intralipid poses challenges for absorbance measurements, but these identified wavelengths provide a pathway for improving sensitivity and accuracy in spectroscopic applications involving similar media. These findings are valuable for the development of non-invasive monitoring devices, particularly those that operate in complex scattering environments like human tissue.

Overall, the study emphasizes that each medium—be it water, serum, blood, ISF, or Intralipid—has unique spectral characteristics that influence how ethanol and acetic acid concentrations affect absorbance at various wavelengths. The variability in correlations across wavelengths and media suggests that a one-size-fits-all approach is not feasible for spectroscopic measurements. Instead, tailored wavelength selection is necessary to optimize sensitivity and specificity for each medium and compound of interest.

In conclusion, this comprehensive analysis provides a foundation for future work in spectroscopic detection and monitoring of ethanol and acetic acid in different biological and model media. By identifying key wavelengths that correlate strongly with concentration

changes, the study offers valuable insights for developing more accurate and reliable non-invasive diagnostic tools and measurement systems. The findings highlight the need for further investigation into the interaction mechanisms between chemical species and different media, which will be essential for advancing spectroscopic techniques in clinical and research settings.

5.3 Assessment of Acetic Acid's Impact on Spectral Morphology

The presence of acetic acid introduces specific vibrational modes primarily associated with the C=O stretching and O-H bending of the carboxylic group. These vibrational modes significantly influence the overall spectral morphology by superimposing additional features onto the spectrum of ethanol, which is dominated by C-H stretching and O-H stretching vibrations. Understanding these contributions is crucial for accurately interpreting the spectral data and identifying the unique fingerprints of each compound.

The selection of peaks and regions of interest is guided by the known vibrational characteristics of acetic acid and ethanol. For instance, the C=O stretching vibration of acetic acid typically appears around 1700-1750 nm, while the O-H bending occurs in the region of 1200-1400 nm. Ethanol, on the other hand, exhibits prominent peaks due to O-H stretching around 3300 nm and C-H stretching between 2850-2970 nm. When acetic acid is present, these distinct vibrational modes can cause shifts or broadening in the corresponding ethanol peaks due to hydrogen bonding interactions or changes in the molecular environment. This results in modified spectral shapes that can be used to discern the relative contributions of each compound in a sample.

By examining the correlations established in the previous section, we can estimate the levels of ethanol and acetic acid based on their spectral contributions. For example, strong positive or negative correlations between specific wavelengths and compound concentrations suggest that changes in absorbance at these wavelengths can be directly linked to the presence of acetic acid or ethanol. These correlations can serve as a basis for developing predictive models to quantify each compound's concentration. However, in this section, we will focus more on the qualitative assessment of how these correlations reflect the spectral morphology rather than quantitative chemometric analysis, which will be addressed in Chapter 6.

The impact of acetic acid on the spectral shape of ethanol can be visualized through the comparison of spectra with varying acetic acid concentrations. At certain wavelengths, the presence of acetic acid may cause the ethanol peaks to become less pronounced or to shift in

position. This is particularly evident in the O-H stretching region, where the overlap of the vibrational modes of both compounds can lead to complex spectral patterns. Similarly, in the C-H stretching region, the introduction of acetic acid can alter the baseline and peak intensities, reflecting the molecular interactions occurring in the sample.

In regions where ethanol and acetic acid have overlapping spectral features, such as around 1650-1750 and 2150-2350 it becomes challenging to distinguish between the contributions of each compound. Here, the detailed analysis of peak shapes and their variations with changing concentrations becomes essential. The characteristic shoulders, peak broadening, or flattening observed in these regions can be attributed to the combined vibrational effects of both ethanol and acetic acid. This morphological change provides a spectral signature that can be used to infer the relative amounts of each compound present.

While the correlations derived earlier offer a preliminary indication of the relationship between spectral changes and concentration levels, a more detailed spectral interpretation is required to connect these observations to specific molecular vibrations. For instance, a decrease in absorbance at a wavelength associated with C=O stretching could suggest a reduction in acetic acid concentration, while changes in the C-H stretching region might indicate fluctuations in ethanol levels. Such interpretations need to be supported by the theoretical understanding of vibrational spectroscopy, considering the potential interactions between the molecules.

In summary, this section will provide a qualitative assessment of how acetic acid modifies the spectral morphology of ethanol. By focusing on the specific vibrational bonds involved, we will highlight the regions of interest where these effects are most pronounced. The correlations established previously will aid in interpreting these morphological changes, paving the way for more rigorous quantitative analysis in subsequent chapters. This approach allows us to build a comprehensive picture of how acetic acid influences the spectral characteristics of ethanol, contributing to a deeper understanding of the chemical dynamics in mixed sample.

5.3.1 Water

Water represents the simplest and most controlled matrix in which to evaluate the predictive performance of the polynomial regression model for ethanol and acetic acid. As a polar solvent with well-characterised absorption features in the near-infrared region, it provides a useful baseline against which more complex biological media can be assessed. The characteristic

overtone and combination bands of O–H stretching dominate the water spectrum, particularly in regions around 1450 nm and 1940 nm, creating strong absorption features that are highly sensitive to perturbations by solutes. The introduction of ethanol and acetic acid into this environment results in specific molecular interactions, most notably hydrogen bonding, that alter both the intensity and the shape of the absorption bands. The ability of the predictive model to disentangle these contributions is best visualised in the scatter plots presented in Figure 5.14 and the Bland–Altman analysis provided in Figure 5.15.

In Figure 5.14, the predicted concentrations of ethanol and acetic acid are plotted against the actual reference concentrations derived from sample preparation. For ethanol, the regression demonstrates a high degree of alignment with the line of identity, indicating that the polynomial model is capable of capturing the concentration dependence with reasonable accuracy. The coefficient of determination for ethanol is 0.884, showing that nearly 88 percent of the variation in ethanol concentration can be explained by the model. The root mean square error of 58.1 mg/dL highlights the presence of residual discrepancies, yet these errors remain relatively modest when considered across the entire concentration range, which extends from zero to over 500 mg/dL. Importantly, the distribution of points shows only minor scatter at low and mid concentrations, with deviations becoming more noticeable at higher levels. This suggests that nonlinear interactions between ethanol and the water matrix, such as changes in hydrogen bonding density and clustering at elevated concentrations, introduce complexities that are not fully captured by the polynomial fitting approach.

The performance for acetic acid, also shown in Figure 5.14, is even more striking. The R^2 value of 0.979 indicates that the regression explains almost the entirety of the variance in acetic acid concentration across the tested samples. This exceptionally strong correlation is accompanied by a very low root mean square error of 1.49 mg/dL, confirming that the predicted values deviate only minimally from the actual concentrations. The tight clustering of points along the line of identity illustrates the model's robustness in resolving acetic acid contributions in an aqueous environment. The superior performance relative to ethanol may be attributed to the unique vibrational features of the carboxylic group in acetic acid, specifically the C=O stretching band, which contributes distinct absorption patterns that are less obscured by the dominant O–H bands of water. Furthermore, the smaller concentration range over which acetic acid was tested—up to around 25 mg/dL—reduces the likelihood of nonlinear deviations that often complicate ethanol predictions at higher levels.

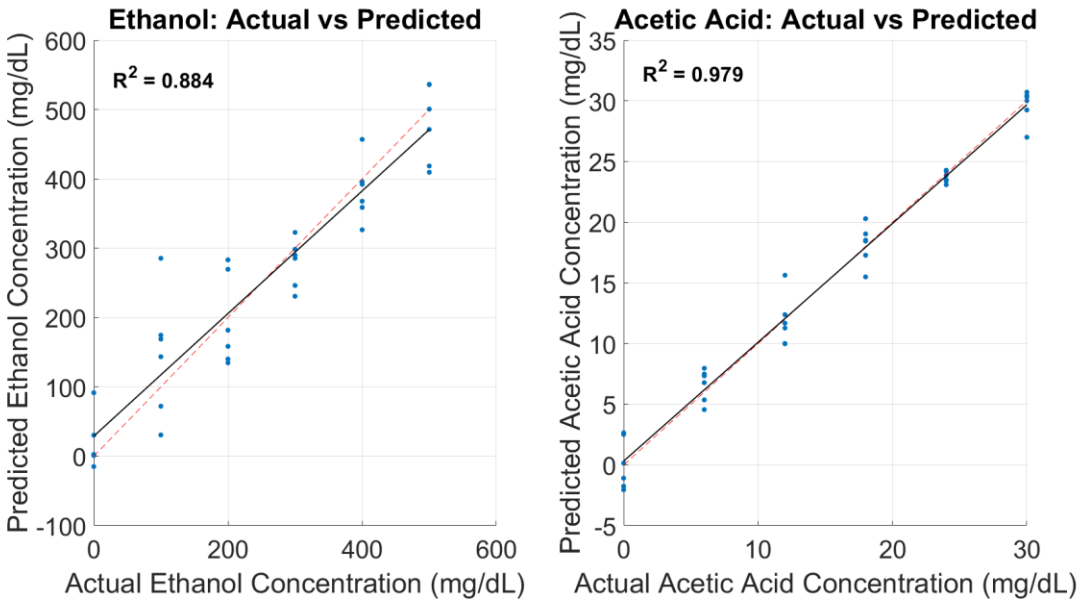

Figure 5.14:Polynomial curve fitting for water wavelengths

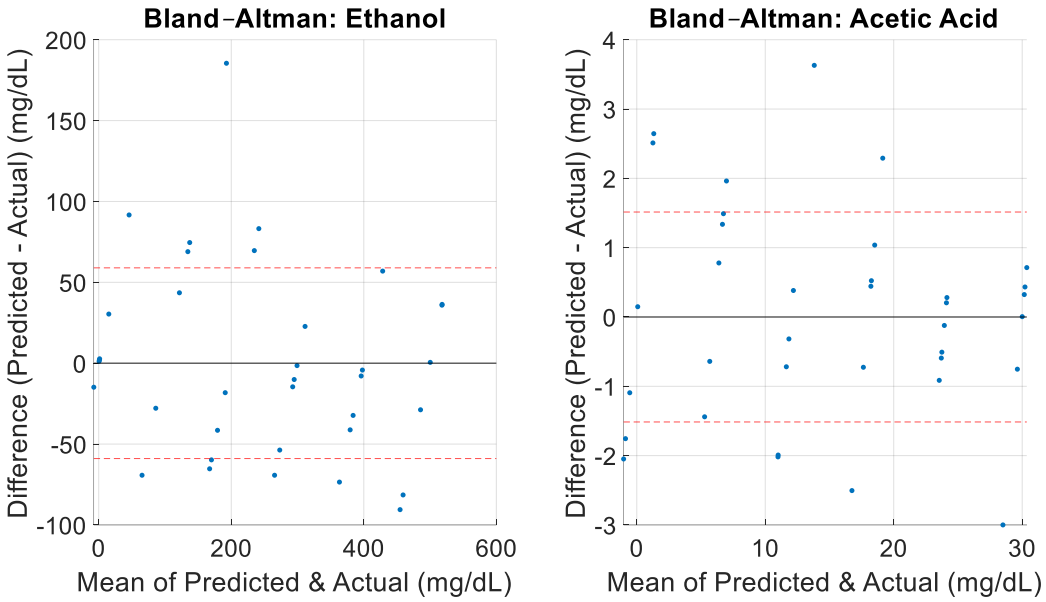

Figure 5.15: Bald-Altman Analysis of the Polynomial Curve Fitting

The high degree of statistical significance for both compounds strengthens these observations. For ethanol, the p-value associated with the regression is 7.45×10^{-10}, while for acetic acid it is below 2.2×10^{-16}, values that indicate that the observed correlations are not attributable to random chance. In practical terms, these results confirm that the selected wavelengths provide reliable markers for the presence of both ethanol and acetic acid in water, and that the

polynomial regression framework is capable of exploiting these features to achieve accurate predictions.

Further insight into the predictive accuracy is gained from the Bland–Altman analysis presented in Figure 5.15. This plot compares the mean of predicted and actual concentrations with their corresponding differences, allowing for a visualisation of bias and agreement across the concentration range. For ethanol, the Bland–Altman plot demonstrates a relatively narrow spread of differences around the zero-bias line, though with a discernible trend toward greater deviations at higher concentrations. This observation aligns with the scatter seen in the regression plot and confirms that while the model is well calibrated for low to moderate ethanol levels, its performance diminishes somewhat at the upper range. Such behaviour can be attributed to the nonlinear clustering phenomena described earlier, as well as possible saturation effects in the absorption features.

For acetic acid, the Bland–Altman analysis reveals exceptionally tight limits of agreement. The differences between predicted and actual concentrations are minimal across the full tested range, and there is no obvious systematic bias. This indicates that the polynomial model not only predicts acetic acid concentrations accurately but also does so consistently across all samples. The stability of these predictions suggests that the absorption features exploited by the model are both specific and resilient to potential confounding effects from the water matrix.

Together, Figures 5.14 and 5.15 demonstrate that water serves as an optimal environment for predictive spectroscopic analysis of ethanol and acetic acid. The simplicity of the medium allows the regression to leverage distinct vibrational features with minimal interference, resulting in high R^2 values and low error metrics. The comparative performance of the two compounds highlights the importance of spectral distinctiveness: while ethanol predictions are strong, they are still challenged by the extensive overlap between ethanol and water absorption features in the O–H stretching region. Acetic acid, by contrast, benefits from the additional spectral signature of the carbonyl group, which enhances separability and reduces predictive error.

These findings have significant implications for the broader study. By establishing that the model performs exceptionally well in water, the results provide a benchmark against which to evaluate subsequent analyses in more complex matrices such as serum, artificial interstitial fluid, and blood. The water data confirm that the polynomial fitting approach is fundamentally sound and capable of producing highly reliable predictions when spectral interference is

minimal. At the same time, the limitations observed at higher ethanol concentrations foreshadow the challenges that will arise in biological systems, where nonlinear interactions and overlapping spectral features are expected to be even more pronounced.

In summary, the water results establish two critical points. First, they validate the predictive capacity of the polynomial regression approach under ideal conditions, demonstrating that both ethanol and acetic acid can be quantified with high precision. Second, they reveal the mechanisms by which prediction error emerges, particularly at elevated ethanol concentrations, thereby setting expectations for the performance in more complex biological matrices. The combination of strong scatter plot alignment and reassuring Bland–Altman agreement provides a clear and convincing case that water is the most straightforward and reliable matrix for spectroscopic prediction, and that the model is well suited for baseline calibration in this environment.

5.3.2 Human Serum

Human serum introduces a significantly greater degree of complexity compared to water and thus represents a more challenging matrix for predicting ethanol and acetic acid concentrations. The serum environment is not a simple aqueous solution but a heterogeneous medium containing proteins, lipids, electrolytes, and metabolites, all of which contribute their own absorption signatures in the near-infrared range. These additional absorptive and scattering features introduce potential confounding effects that can obscure the relatively subtle signals of ethanol and acetic acid. Consequently, evaluating the performance of the polynomial regression model in serum is crucial for determining its robustness in biological matrices more representative of physiological conditions.

The predictive performance of the model in serum is illustrated in Figure 5.16, where scatter plots of predicted versus actual concentrations are presented for both ethanol and acetic acid. The ethanol scatter plot demonstrates a strong overall linear trend, with an R^2 of 0.871. This indicates that the model accounts for nearly 87 percent of the variance in ethanol concentration across the dataset. The root mean square error of 61.5 mg/dL, while modestly higher than that observed in water, remains within a range that indicates reliable predictive capacity for most practical purposes. The spread of data points shows tighter clustering at low to mid ethanol concentrations, with greater divergence emerging at the upper end of the scale. This suggests that at higher concentrations, interactions between ethanol and serum proteins, such as albumin and globulins, may alter the spectral profile in ways that diminish predictive precision.

Conformational changes induced by ethanol binding to proteins are well documented and can cause subtle but significant alterations in baseline absorbance that the polynomial regression model is not fully equipped to accommodate.

For acetic acid, the results in Figure 5.16 are similarly encouraging but reveal greater scatter compared to water. The R^2 value of 0.898 reflects a robust correlation between predicted and actual concentrations, and the root mean square error of 3.3 mg/dL is low enough to indicate that predictions remain highly reliable across the tested range, which extends up to approximately 30 mg/dL. However, unlike in water where points were tightly aligned to the line of identity, the serum scatter plot shows noticeable deviations, particularly in mid-concentration ranges. This pattern suggests that acetic acid interacts with serum components in ways that complicate straightforward spectral interpretation. The carboxylic group of acetic acid is capable of forming hydrogen bonds with protein side chains and interacting with amino acid residues, effects that can broaden absorption bands and reduce the specificity of spectral markers.

The statistical significance of these predictions underscores their reliability despite the increased variability. Ethanol yielded a p-value of 1.95×10^{-9}, while acetic acid produced an even stronger p-value of 2.33×10^{-10}, confirming that the observed correlations are not the result of random variation. These outcomes provide confidence that, while serum introduces additional noise, the model is still able to capture meaningful concentration-dependent relationships.

Further clarity is provided by the Bland–Altman analysis shown in Figure 5.17. For ethanol, the Bland–Altman plot reveals a central clustering of differences close to zero bias, but with wider limits of agreement than observed in water. The deviations increase at higher concentrations, confirming that predictive errors become more pronounced as ethanol levels rise. Importantly, while the variance increases, there is no evidence of a strong systematic bias across the dataset; instead, the error appears to be random, reflecting the heterogeneous nature of the serum environment.

For acetic acid, the Bland–Altman plot demonstrates narrower limits of agreement than ethanol but still wider than in water. The differences remain small across most of the concentration range, although isolated deviations suggest that the model occasionally over- or underestimates concentrations depending on local spectral interferences. This variability likely stems from

overlapping absorption bands contributed by proteins and lipids, which are absent in the water matrix but unavoidable in serum.

Taken together, Figures 5.16 and 5.17 highlight both the strengths and limitations of serum as a predictive medium. On one hand, the regression results show that both ethanol and acetic acid can be estimated with strong accuracy and statistical confidence, indicating that the fundamental approach is valid in biologically relevant fluids. On the other hand, the increased scatter and wider limits of agreement demonstrate the extent to which biological complexity can erode predictive precision. Compared with water, where acetic acid prediction was almost perfect, serum introduces additional variability that necessitates recalibration and potentially more advanced chemometric approaches.

The comparison between ethanol and acetic acid performance in serum is also revealing. While ethanol achieves a high R^2 value, its higher RMSE indicates that absolute predictive errors are larger, which is consistent with the broader concentration range tested. Acetic acid, by contrast, maintains a low RMSE despite modest scatter, reflecting the narrower concentration range and more distinct spectral features of its functional groups. However, because both analytes interact with serum proteins, their signals are partially masked by the complex background, limiting the capacity of polynomial regression alone to fully resolve their contributions.

From a methodological perspective, the serum results underscore the importance of medium-specific calibration. Models trained and optimised in water cannot be expected to transfer directly to serum without loss of performance. The reduced precision observed here suggests that larger training datasets, expanded wavelength coverage, and advanced analytical techniques such as partial least squares regression or machine learning may be required to compensate for overlapping signals. Furthermore, the introduction of spectral preprocessing methods—such as baseline correction, scatter normalisation, or derivative spectroscopy—may improve the separability of ethanol and acetic acid signals in the serum environment.

In summary, the human serum results provide a valuable intermediate step between the idealised water matrix and the highly complex environments of interstitial fluid and blood. The predictive performance remains strong, as demonstrated by high R^2 values and low RMSEs, but with clear signs of variability and reduced precision compared to water. The scatter plots in Figure 5.16 and the Bland–Altman analysis in Figure 5.17 both confirm that serum introduces biological noise that cannot be ignored. These findings reinforce the need for more

sophisticated modelling when working in physiologically realistic media but also demonstrate that the underlying approach remains valid, offering a promising pathway for eventual clinical translation.

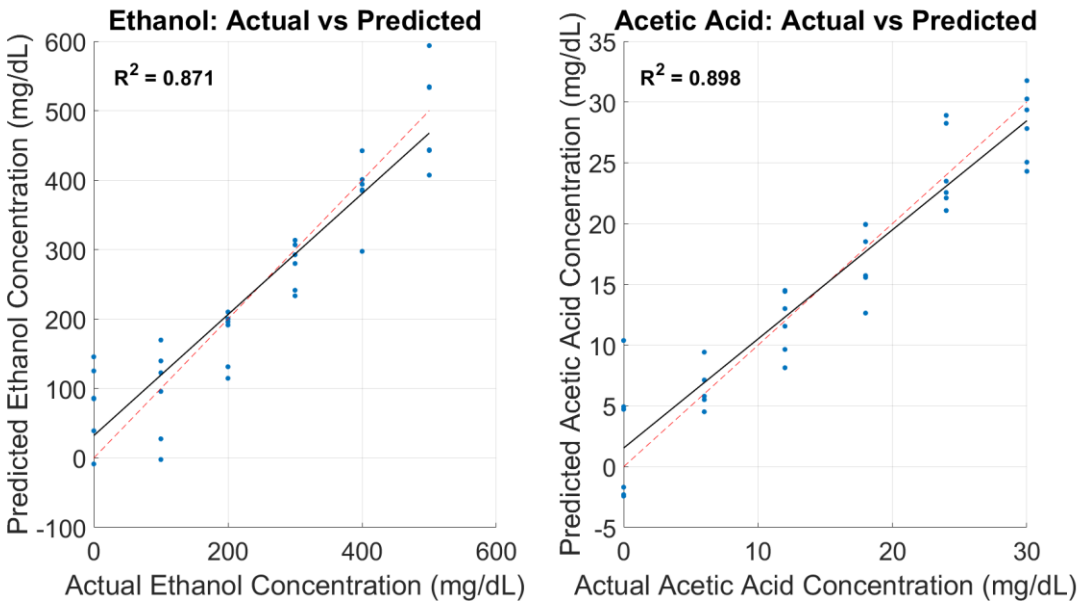

Figure 5.16: Polynomial curve fitting for human serum wavelengths

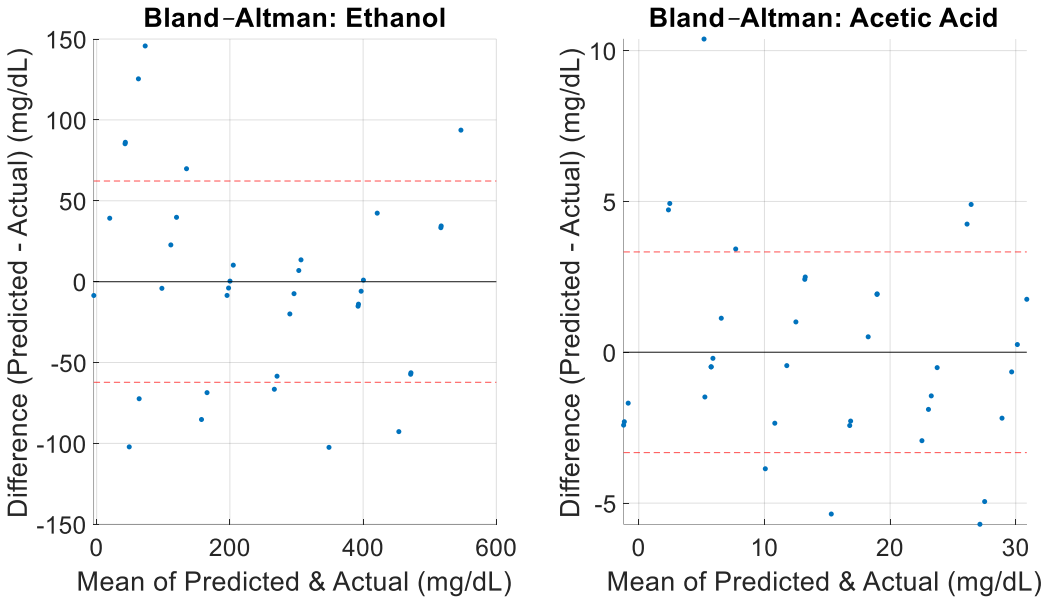

Figure 5.17: Bland – Altman Analysis for Human Serum

5.3.3 Artificial ISF

Artificial interstitial fluid represents a synthetic but biologically inspired medium designed to replicate the ionic composition and solute balance of true interstitial fluid. Unlike water, which

provides a relatively clean optical environment, or serum, which introduces protein and lipid interferences, artificial ISF occupies an intermediate position: it contains salts, glucose, and other solutes that contribute to optical absorption and scattering, but lacks the full molecular complexity of whole biological fluids. This controlled complexity makes ISF an important test system for evaluating whether the polynomial regression model can extend beyond aqueous calibration conditions and still capture the concentration-dependent behaviour of ethanol and acetic acid.

The predictive performance of the model in ISF is summarised in the scatter plots presented in Figure 5.18. For ethanol, the relationship between predicted and actual concentrations remains positive and linear, but the degree of correlation is reduced compared to both water and serum. The coefficient of determination is 0.790, indicating that the model explains approximately 79 percent of the variance. The root mean square error, however, rises to 78.3 mg/dL, reflecting a notable increase in predictive error relative to both water (58.1 mg/dL) and serum (61.5 mg/dL). This increase is also visible in the scatter plot, where the clustering of data points is less tight, and deviations from the line of identity become apparent, particularly at higher concentrations. At these levels, the model shows a tendency to underestimate ethanol, producing values consistently lower than the reference concentrations. This systematic deviation suggests that the spectral regions used for prediction are influenced by overlapping absorptions from solutes in the ISF matrix, which obscure the ethanol-specific vibrational signatures.

For acetic acid, the predictive performance is somewhat stronger, though still reduced compared to water and serum. The R^2 value of 0.885 indicates a robust correlation, but the root mean square error of 3.5 mg/dL is slightly higher than that achieved in serum (3.3 mg/dL) and substantially higher than in water (1.49 mg/dL). The scatter plot shows that while many points remain close to the line of identity, there is a broader spread across the range, particularly at lower concentrations. Here, the model exhibits a tendency to overestimate acetic acid, producing predicted concentrations higher than the actual values. This pattern may result from the difficulty of disentangling the carboxylic acid vibrational features from the absorptions of other solutes present in ISF, which likely interfere in the same spectral regions.

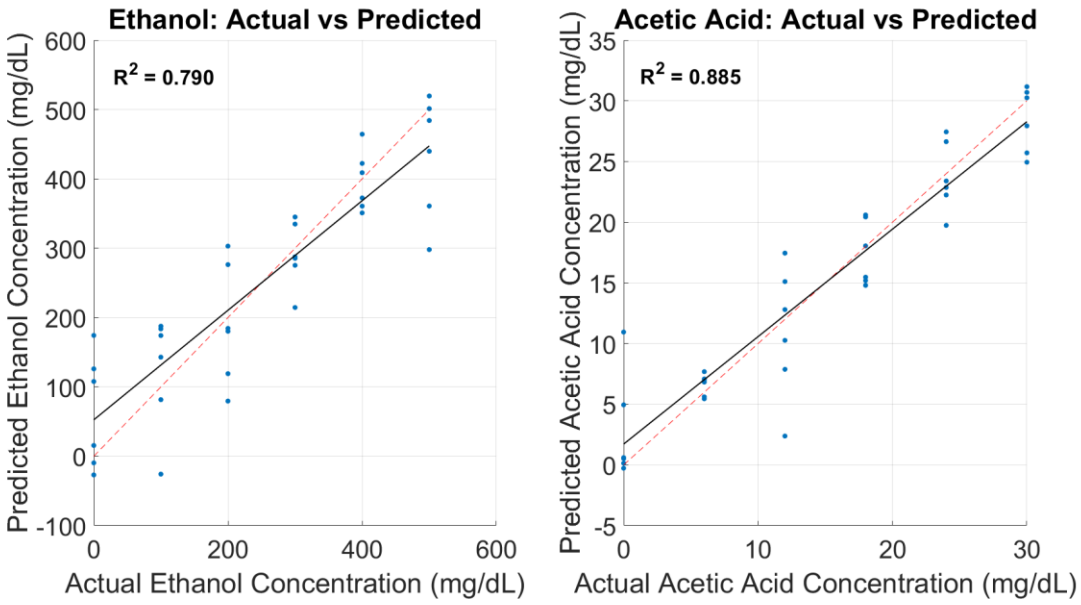

Figure 5.18: Polynomial curve fitting for aISF wavelengths

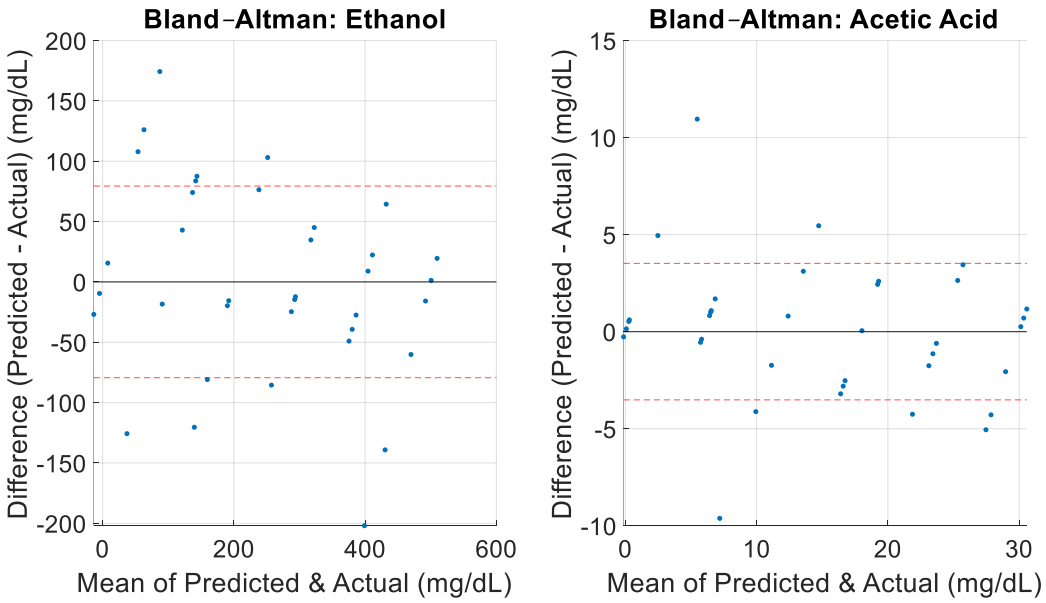

Figure 5.19: Bland Altman Analysis for aISF

The statistical robustness of these predictions is confirmed by the p-values. Ethanol yields a significance of 1.64×10^{-7}, while acetic acid achieves 6.89×10^{-10}, both of which indicate that the correlations are highly unlikely to arise by chance. Despite the reduced precision compared to simpler media, the statistical evidence demonstrates that the polynomial regression framework continues to capture meaningful relationships even in the more complex ISF matrix.

The Bland–Altman analysis in Figure 5.19 provides further insight into the reliability and limitations of the predictions. For ethanol, the Bland–Altman plot reveals wider limits of agreement than were seen in either water or serum, with deviations increasing markedly at

higher concentrations. The negative bias observed at the upper end confirms the underestimation noted in the scatter plot, suggesting a systematic limitation of the polynomial model when applied to ethanol in ISF. The increased variance across the dataset underscores the extent to which background solutes interfere with ethanol prediction.

For acetic acid, the Bland–Altman plot shows narrower differences overall, but the pattern of overestimation at lower concentrations is clearly visible. This introduces a concentration-dependent bias that was not evident in water or serum, where predictions were more evenly distributed. The consistency of this bias indicates that the spectral regions most informative for acetic acid overlap with ISF solute absorptions in ways that skew the regression, highlighting a limitation of the model that would need to be addressed through recalibration or alternative chemometric strategies.

Comparing the ISF results to those in water and serum highlights important trends. In water, both ethanol and acetic acid predictions achieved high accuracy, with acetic acid in particular showing near-perfect regression. In serum, performance declined somewhat due to the presence of proteins, but predictions remained strong, particularly for acetic acid. In ISF, however, ethanol predictions degrade substantially, with both reduced correlation and increased error, while acetic acid predictions remain moderately robust but show systematic bias. This suggests that ISF poses greater challenges for ethanol than for acetic acid, likely because ethanol's weaker vibrational signatures are more easily obscured by the overlapping absorptions of salts and glucose.

From a methodological standpoint, the ISF results reveal the limits of applying a polynomial regression approach directly across different media. While the model retains statistical significance, the increased scatter, wider error margins, and systematic biases point to the need for more sophisticated approaches. Potential strategies include spectral preprocessing to correct for background interference, expansion of the wavelength set to include regions less affected by ISF solutes, or the use of multivariate chemometric techniques such as partial least squares regression that can better manage correlated variables.

In summary, the artificial ISF results demonstrate both the adaptability and the fragility of the polynomial regression model in complex but controlled biological analogues. Ethanol predictions suffer from underestimation at higher concentrations and a general reduction in precision, while acetic acid predictions remain strong but exhibit systematic overestimation at lower levels. Figures 5.18 and 5.19 together confirm that while ISF can support predictive

modelling, the complexity of the medium introduces biases that cannot be ignored. These findings establish ISF as an important intermediate step toward biological realism, showing where polynomial regression begins to falter and highlighting the adjustments needed for reliable application in vivo.

5.3.4 Sheep Blood

Sheep blood provides one of the most complex and biologically relevant test environments used in this investigation. Unlike artificial ISF, which reproduces some aspects of extracellular chemistry but lacks cellular and protein complexity, blood contains a dense mixture of red and white blood cells, plasma proteins, electrolytes, lipids, and metabolic by-products. The strong optical absorption of haemoglobin in particular dominates near-infrared spectra and introduces overlapping features that can obscure the comparatively subtle vibrational signals of ethanol and acetic acid. As such, sheep blood represents a stringent test of the robustness of the polynomial regression model and provides valuable insights into the limits of spectroscopic quantification in highly heterogeneous biological matrices.

The regression results for ethanol and acetic acid in blood are displayed in Figure 5.20. For ethanol, the scatter plot shows a weaker alignment to the line of identity compared with previous media. The coefficient of determination is 0.729, meaning that just over 72 percent of the variance in ethanol concentration is explained by the model. This represents a decline in performance relative to water, serum, and even artificial ISF. The root mean square error of 88.9 mg/dL is the second-highest observed across all tested media, exceeded only by intralipid, indicating a substantial level of predictive error. The distribution of points shows clustering between 200 and 300 mg/dL, suggesting that within this range the model is not effectively distinguishing concentration changes. At higher and lower levels, deviations from the line of identity become even more pronounced, confirming that ethanol prediction in blood is compromised by strong spectral interference from haemoglobin and other cellular components.

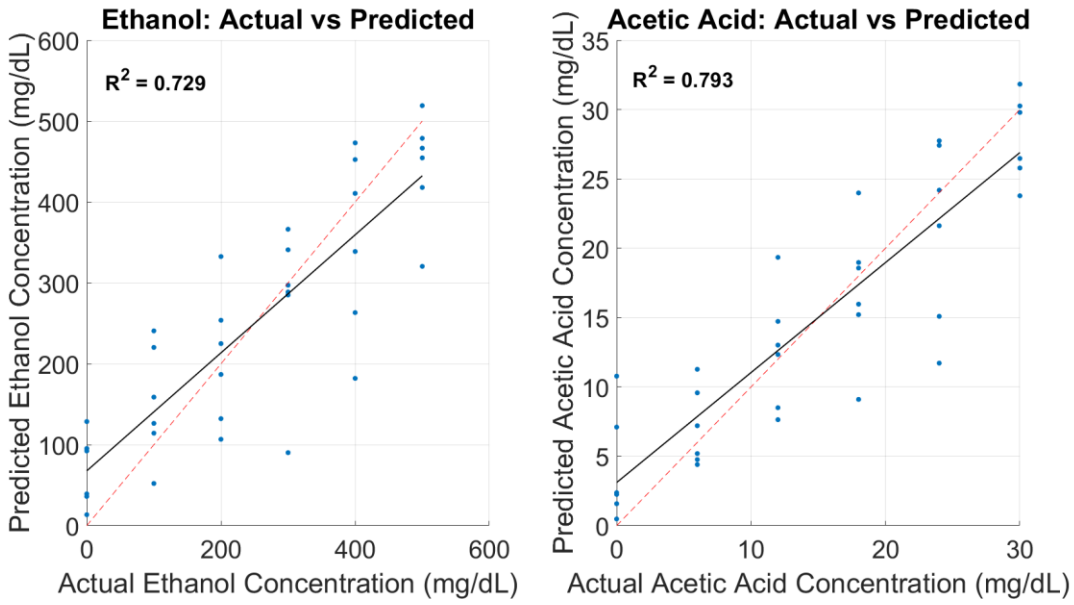

Figure 5.20: Polynomial curve fitting for sheep blood wavelengths

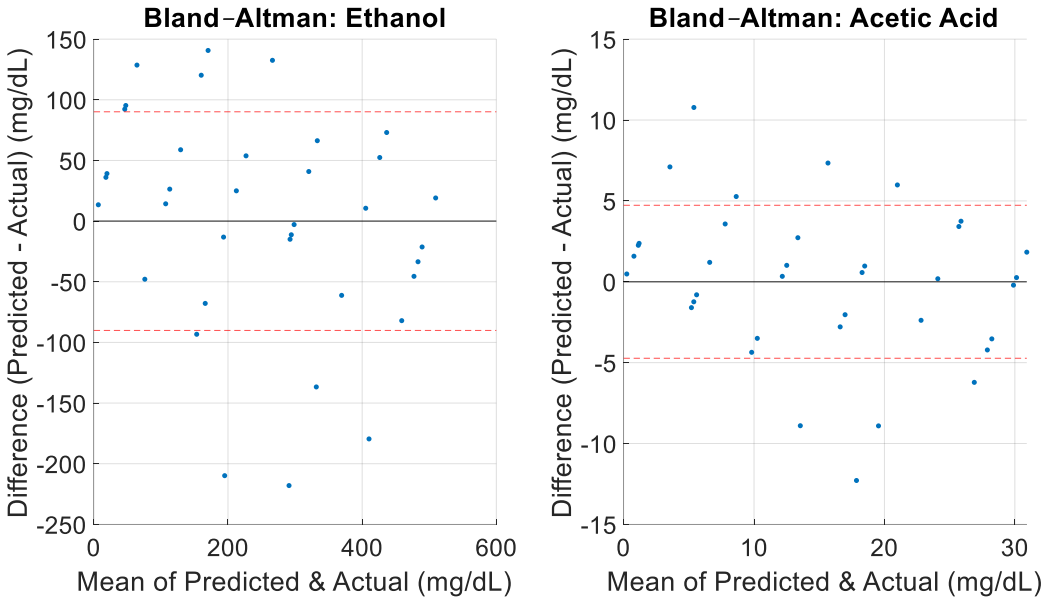

Figure 5.21: Bland Altman Analysis for Sheep Blood

For acetic acid, the scatter plot in Figure 5.20 reveals a somewhat stronger regression but with evident variability. The R^2 value of 0.793 indicates that almost 80 percent of the variance is explained, which is robust in statistical terms, yet the root mean square error of 4.7 mg/dL reflects a decline in predictive precision compared with both serum and ISF. The scatter of points reveals that predictions tend to plateau at around 15 mg/dL, with the model underestimating concentrations at higher levels and overestimating at the lower end. This nonlinearity is indicative of spectral overlap between the vibrational modes of acetic acid and

haemoglobin, which absorbs strongly in similar regions. As a result, the regression appears to fit certain ranges well but fails to generalise consistently across the full spectrum of concentrations.

The statistical robustness of these correlations is confirmed by the p-values. Ethanol in sheep blood yields a significance level of 1.68×10^{-6}, while acetic acid achieves 1.44×10^{-7}. Although these values confirm that the observed correlations are not due to random chance, they do not mitigate the substantial predictive errors reflected in the RMSE values and scatter distribution.

The limitations of the regression approach in blood are further illustrated by the Bland–Altman analysis shown in Figure 5.21. For ethanol, the Bland–Altman plot demonstrates a wide spread of differences between predicted and actual concentrations, with limits of agreement significantly broader than those observed in water, serum, or ISF. The deviations show no consistent bias but instead reflect random scatter, underscoring the difficulty of reliably quantifying ethanol in the presence of strong haemoglobin absorption. Importantly, this scatter is not uniform across the concentration range: the mid-range clustering seen in the scatter plot is mirrored here by a concentration band where deviations fluctuate unpredictably, further undermining confidence in the model.

For acetic acid, the Bland–Altman analysis also reveals variability, though with a somewhat tighter distribution than ethanol. The plot highlights the plateauing effect noted in the scatter results, where predicted concentrations fail to increase proportionally at higher levels. This introduces a systematic underestimation that broadens the limits of agreement and reduces predictive fidelity. The overlap between acetic acid absorption bands and haemoglobin is the most likely cause, compounded by background absorptions from plasma proteins that contribute additional noise.

Taken together, Figures 5.20 and 5.21 demonstrate that blood presents the most formidable challenge to the polynomial regression model apart from intralipid. While statistically significant correlations are achieved for both ethanol and acetic acid, the predictive precision is limited by high error values and wide variability. The dominance of haemoglobin absorption creates spectral environments in which the distinct vibrational modes of the analytes are effectively masked. Moreover, the presence of scattering from cellular components introduces further distortions, reducing the reliability of simple regression-based approaches.

The comparison with earlier media underscores these challenges. In water, ethanol and acetic acid predictions were strong, with acetic acid approaching near-perfect regression. In serum,

performance declined modestly but remained reliable, reflecting the influence of proteins. ISF introduced additional complexity, with ethanol suffering more than acetic acid. In blood, however, both compounds are significantly compromised, with ethanol particularly affected due to its weaker vibrational signatures and greater spectral overlap with haemoglobin. Acetic acid retains moderate predictive strength but suffers from nonlinearity that undermines its quantitative utility.

From a methodological perspective, these findings highlight the need for advanced strategies when dealing with blood as a medium. Polynomial regression, while effective in simpler matrices, struggles to capture the nonlinear interactions and overlapping spectral features in blood. More powerful multivariate techniques such as partial least squares regression, support vector machines, or even deep learning approaches may be required to achieve reliable predictions. Additionally, spectral preprocessing to isolate haemoglobin contributions or to normalise scattering effects could help reduce interference. Without such refinements, predictive modelling in blood risks producing results that are statistically significant yet practically unreliable due to their high error margins.

In summary, sheep blood results underscore the inherent difficulty of spectroscopic quantification in complex biological fluids. Ethanol predictions suffer from high error, reduced correlation, and clustering effects, while acetic acid predictions demonstrate systematic biases that reduce their reliability. The scatter plots in Figure 5.20 and the Bland–Altman analysis in Figure 5.21 confirm that while correlations can be established, their predictive value is limited. These findings reveal both the challenges and the opportunities of working in blood: they expose the inadequacy of simple regression models in such environments while pointing the way toward more sophisticated methods capable of managing the complexities of real biological systems.

5.3.5 Intralipid

Intralipid represents the most challenging of the test media considered in this investigation. As an emulsion of lipids suspended in water, it is widely used as a tissue-mimicking phantom in biomedical optics because it closely replicates the scattering properties of adipose-rich biological tissues. Unlike the relatively clean absorption spectra of water or the structured but soluble interference of serum and ISF, intralipid introduces a fundamentally different type of optical complexity: light scattering. The suspended lipid droplets act as strong scatterers of

near-infrared light, altering the effective path length, redistributing photon trajectories, and reducing the clarity with which analyte-specific absorption features can be distinguished. These scattering effects compound the absorption signals of ethanol and acetic acid, producing spectra that are noisy, distorted, and difficult to interpret through simple regression approaches. As a result, intralipid provides an essential test of the resilience of the polynomial regression model under conditions where scattering dominates over pure absorption.

The predictive outcomes in intralipid are shown in Figure 5.22. For ethanol, the regression plot demonstrates a substantial degradation in predictive performance compared with all other media. The coefficient of determination falls to 0.447, meaning that less than half of the variance in ethanol concentration can be explained by the model. The root mean square error of 123.5 mg/dL is the highest of any medium, indicating that the predictions diverge significantly from the actual concentrations. The scatter plot shows that predicted ethanol values cluster disproportionately in the mid-range, leading to consistent overestimation at low concentrations and underestimation at high concentrations. This curvature away from the line of identity illustrates the inability of the polynomial regression to capture the nonlinear effects introduced by strong scattering. Instead of preserving proportionality across the concentration range, the regression appears to compress predictions toward the centre, diminishing its quantitative value.

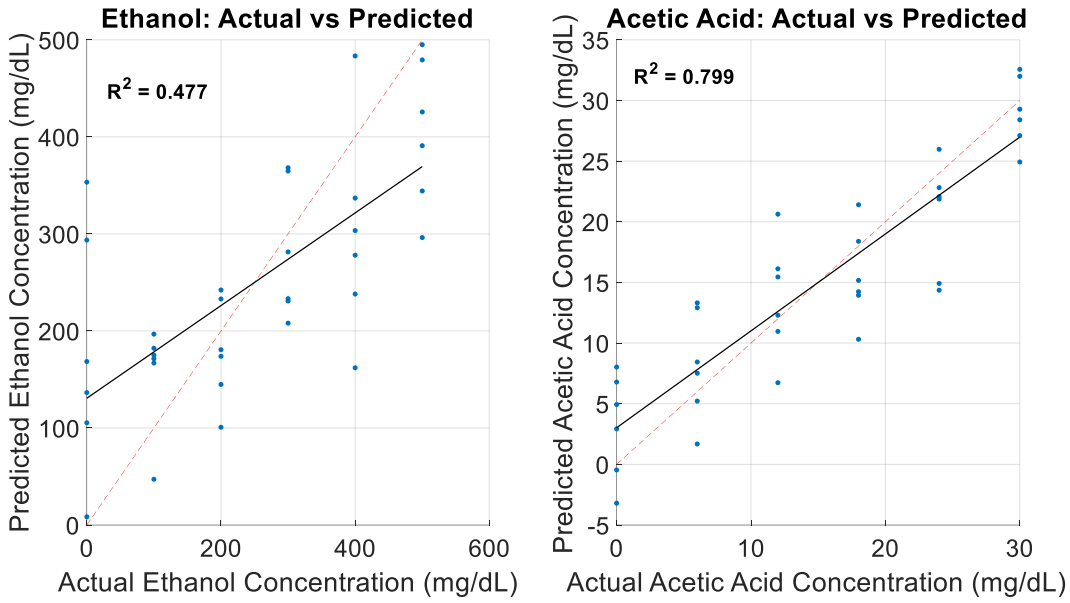

Figure 5.22: Polynomial curve fitting for intralipid wavelengths

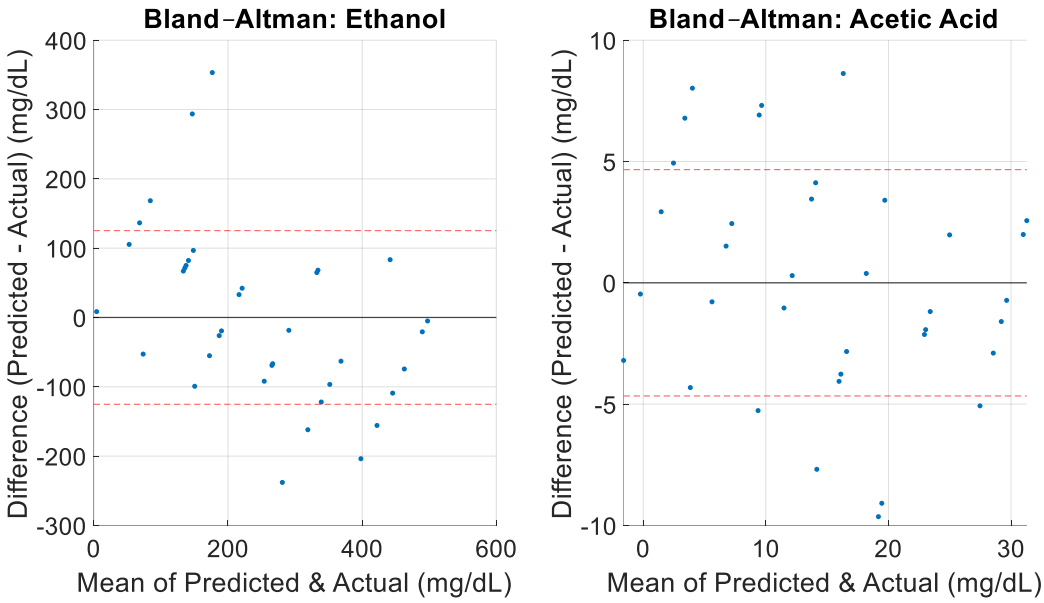

Figure 5.23: Bland Altman Analysis for Intralipid

For acetic acid, the regression results are somewhat stronger but still impaired compared to simpler matrices. The R^2 value of 0.799 indicates that nearly 80 percent of the variance can still be explained by the model, yet the root mean square error rises to 4.6 mg/dL, which is markedly higher than in water or serum and even greater than in ISF. The scatter plot reveals that predicted acetic acid concentrations cluster within a narrow band, showing less sensitivity to actual concentration changes across the full range. This indicates that the model struggles to differentiate between low and high concentrations, flattening predictions and reducing their discriminatory capacity. The spectral basis for this behaviour is likely the differential interaction of acetic acid with lipid droplets. As a hydrophilic molecule, acetic acid does not partition into the lipid phase, but its vibrational signatures are nonetheless masked by the distortive scattering effects introduced by the lipid environment, particularly in regions where light absorption and scattering overlap.

The statistical significance of both sets of predictions is maintained, though less compelling than in other media. Ethanol yields a p-value of 1.27×10^{-3}, while acetic acid achieves 1.10×10^{-7}. Both values indicate that the observed correlations are unlikely to be due to random chance, but the relatively higher p-value for ethanol, combined with its very low R^2, underscores that the statistical significance does not equate to practical predictive reliability.

The Bland–Altman analysis in Figure 5.23 provides a clearer illustration of these limitations. For ethanol, the Bland–Altman plot demonstrates very wide limits of agreement, with deviations that span a large proportion of the tested concentration range. The pattern of bias

mirrors the scatter plot findings: ethanol concentrations are consistently overestimated at the lower end and underestimated at the higher end, with the mid-range clustering representing the point of closest alignment. This systematic distortion reflects the nonlinearity induced by scattering, which the polynomial regression cannot account for.

For acetic acid, the Bland–Altman plot shows narrower limits of agreement than ethanol but still wider than those observed in water, serum, or ISF. The differences remain relatively stable across most of the concentration range, but there is a tendency for the model to compress predictions toward the mean, resulting in reduced responsiveness to actual concentration changes. While this bias is less dramatic than that seen for ethanol, it nonetheless limits the quantitative precision of acetic acid predictions in intralipid.

Taken together, Figures 5.22 and 5.23 confirm that intralipid represents the most problematic medium for polynomial regression modelling. The scattering properties of the emulsion dominate the spectral signal, obscuring analyte-specific vibrational modes and introducing nonlinear distortions that simple regression cannot resolve. Ethanol, which already faces challenges in separating its O–H vibrational features from water background signals, is particularly compromised, producing the weakest regression performance of all tested conditions. Acetic acid retains somewhat stronger predictive capacity due to the distinctiveness of its carbonyl stretch, but even here the flattening of predictions reduces practical accuracy.

Comparisons with the other media highlight the specific challenges posed by scattering. In water, ethanol and acetic acid predictions were highly reliable, with acetic acid in particular showing near-perfect regression. Serum and ISF introduced biochemical complexity that reduced performance but still allowed for statistically robust predictions. Blood, dominated by haemoglobin absorption, impaired both analytes but still produced stronger ethanol predictions than intralipid. It is only in intralipid that ethanol prediction performance collapses almost entirely, demonstrating that scattering is a more intractable obstacle than absorption interference when using simple polynomial regression.

These findings carry significant methodological implications. First, they demonstrate that scattering-rich environments cannot be reliably modelled using polynomial regression of raw spectral features. Corrective preprocessing steps such as multiplicative scatter correction, standard normal variate normalisation, or derivative spectroscopy are essential to mitigate scattering effects before regression. Second, they suggest that more sophisticated chemometric methods, such as partial least squares regression or nonlinear machine learning approaches,

may be required to adequately capture the nonlinearities introduced by scattering. Finally, they highlight the importance of validating models in scattering phantoms like intralipid before attempting translation to tissue, since scattering is a dominant feature of in vivo optical environments.

In summary, intralipid results expose the limitations of the polynomial regression model in scattering-dominated systems. Ethanol predictions suffer from extremely poor correlation and high error, while acetic acid predictions, though statistically significant, are flattened and less discriminative. The scatter plots in Figure 5.22 and the Bland–Altman analysis in Figure 5.23 both confirm that while correlations exist, their predictive utility is compromised by systematic biases. These findings reinforce that scattering correction and advanced modelling are indispensable for extending spectroscopic quantification into lipid-rich biological contexts, and they position intralipid as a critical testbed for refining methods before clinical application.

All the results have been compiled into table 11 together with their associated statistical significance.

Table 11: Summary of Polynomial Curve Fitting Results

Medium	***Compound***	***R^2***	***RMSE (mg/dL)***	***p-value***
Water	Ethanol	0.884	58.1	7.45×10^{-10}
	Acetic Acid	0.979	1.49	2.2×10^{-16}
Human Serum	Ethanol	0.871	61.5	1.95×10^{-9}
	Acetic Acid	0.898	3.3	2.33×10^{-10}
Artificial ISF	Ethanol	0.790	78.3	1.64×10^{-7}
	Acetic Acid	0.885	3.5	6.89×10^{-10}
Intralipid	Ethanol	0.447	123.5	1.27×10^{-3}
	Acetic Acid	0.799	4.6	1.10×10^{-7}
Sheep Blood	Ethanol	0.729	88.9	1.68×10^{-6}
	Acetic Acid	0.793	4.7	1.44×10^{-7}

6 Chemometric Analysis of Ethanol and Acetic Acid

The accurate quantification of ethanol and its metabolites, such as acetic acid, in biological systems is essential for developing reliable intoxication sensing technologies. While spectroscopic techniques provide a wealth of data regarding molecular absorption characteristics, their full potential can only be realized through advanced data processing and analysis. This chapter focuses on the chemometric analysis of ethanol and acetic acid in various liquid samples, utilizing methods such as PLS regression and PCA to extract meaningful insights from the spectroscopic data.

The complexity of biological systems, where multiple compounds can interfere with ethanol and acetic acid detection, necessitates the application of chemometric techniques. These methods allow for the deconvolution of overlapping spectral features and improve the accuracy of concentration estimates, even in the presence of background noise. By applying these statistical tools, this chapter aims to enhance the precision of ethanol and acetic acid quantification across a range of biological matrices, including water, artificial interstitial fluid (aISF), intralipid solutions, animal blood, and human serum.

This chapter will begin with an overview of chemometric techniques, explaining their relevance to spectroscopic data analysis. Following this, the experimental setup used to collect SWIR spectroscopic data from liquid samples will be outlined, with a particular focus on ethanol-acetic acid interactions. The core of the chapter will detail the application of PLS and PCA to assess the spectral data, providing insights into the concentration levels of the compounds in question. Finally, the results of the chemometric analysis will be discussed in the context of improving non-invasive alcohol sensing technologies, setting the stage for further research into multi-compound quantification in biological systems.

6.1 Water

The study of spectral data is crucial for understanding the behaviour and interactions of chemical analytes in various mediums. In this chapter, we employ PCA and PLSR to investigate the complex relationships between ethanol and acetic acid within a water matrix. Unlike univariate approaches, multivariate techniques such as PCA and PLSR allow us to analyse the spectral data holistically, capturing the interdependencies between different variables and thus providing a more robust predictive model. By leveraging these techniques, we aim to evaluate the efficacy of these multivariate models in predicting the concentrations of ethanol and acetic acid based on spectral data. The chapter also compares the results from

these advanced methods to the traditional univariate analyses conducted in Chapter 5, showcasing the advantages of multivariate approaches in handling complex datasets.

The spectral data for this study was obtained from aqueous solutions containing varying concentrations of ethanol and acetic acid. The data was normalized to minimize the influence of baseline shifts and intensity variations across samples. We selected three optical windows, 1200–1350 nm, 1600–1870 nm, and 2100–2400 nm, for analysis based on their relevance to the characteristic absorption bands of ethanol and acetic acid. These windows encompass the C-H stretching and overtone regions, which are particularly sensitive to the presence of ethanol and acetic acid.

The pre-processed spectral data was used to perform PCA, which reduces the dimensionality of the dataset while preserving the variance that is most informative. The PCA model generated principal components that were then used to visualize the clustering of different sample groups, such as ethanol-only, acetic acid-only, and mixtures of both. Additionally, PLSR models were constructed to predict the concentrations of ethanol and acetic acid from the spectral data. This approach allowed us to quantify the effectiveness of the spectral features in distinguishing between the two analytes.

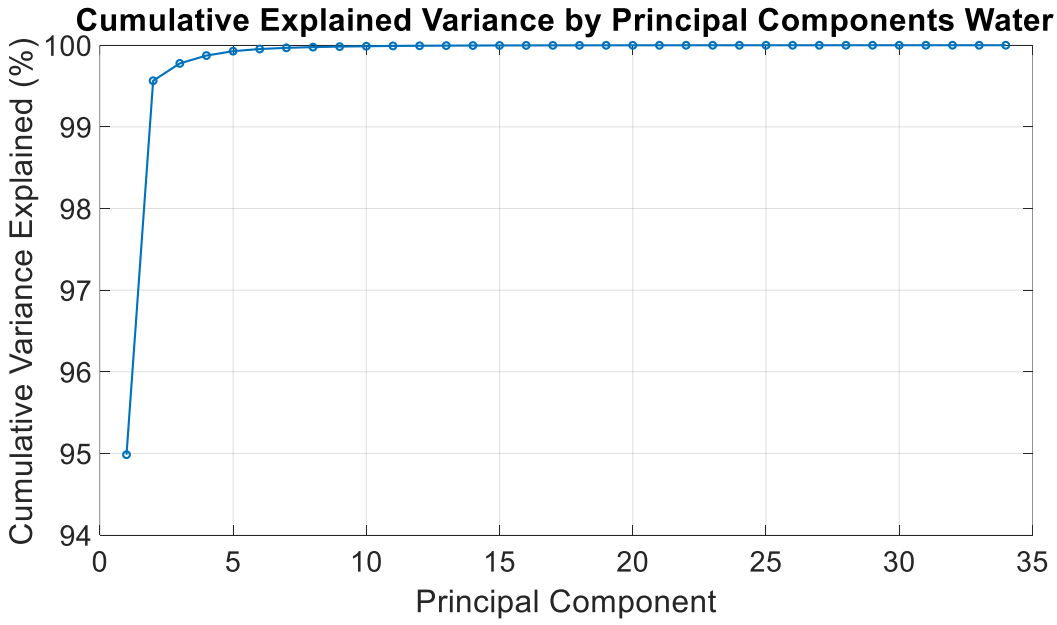

Figure 6.1: Water PLS cumulative variance explained

Figure 6.1 shows the explained variance by principal components for the water spectral data. The first three principal components account for over 99% of the variance in the data, with the

first component alone explaining approximately 95%. This indicates that most of the variability in the dataset can be captured by a few principal components, making PCA an effective tool for dimensionality reduction in this context. The cumulative variance plot further illustrates that adding more than three principal components provides negligible additional explanatory power.

The PCA score plot in Figure 6.2 highlights the separation between different sample groups. Ethanol-only samples, represented in green, are distinctly separated from acetic acid-only samples, shown in red. Mixtures of ethanol and acetic acid, represented in blue, form a cluster that overlaps partially with both pure components, indicating spectral features characteristic of both analytes. The zero-sample, depicted in black, remains distinct from other groups, demonstrating that the PCA model can effectively differentiate between samples with and without the analytes. The 3D PCA plot Figure 6.3 provides a more nuanced view of the clustering, revealing subtle variations that are not apparent in the 2D plot.

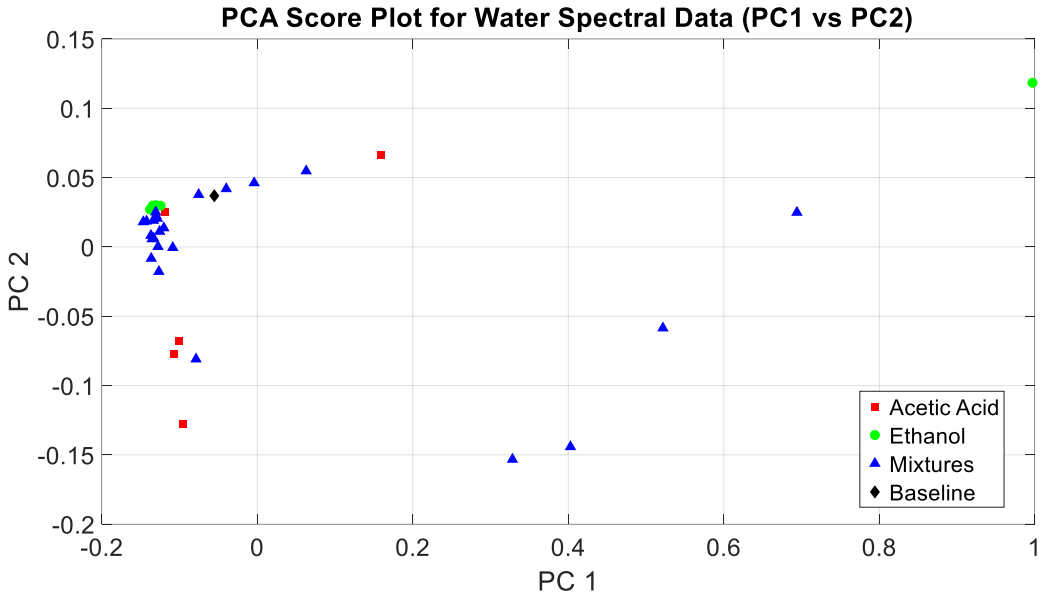

Figure 6.2: PCA Scores for water spectral data

PLSR was performed to model the relationship between the spectral data and the concentrations of ethanol and acetic acid. The R^2 values for the PLSR models were 0.88898 for ethanol and 0.81041 for acetic acid, as shown in the summary table (Table 1). These high R^2 values indicate that the models explain 89% and 81% of the variance in ethanol and acetic acid concentrations, respectively. The Root Mean Square Error of Prediction (RMSEP) values were 56.903 mg/dL

for ethanol and 4.4617 mg/dL for acetic acid, indicating good predictive performance for both analytes.

Figures 6.4 show the predicted versus actual concentrations for ethanol and acetic acid, respectively. The diagonal red line represents perfect agreement between the predicted and actual values. Most data points for ethanol fall close to this line, indicating accurate predictions across a wide concentration range. However, some deviation is observed at higher concentrations, suggesting potential model limitations when extrapolating beyond the calibration range. For acetic acid, the predictions are similarly accurate, although the spread of points is slightly broader compared to ethanol, reflecting the lower R^2 value.

The multivariate models developed using PCA and PLSR outperform the univariate models discussed in Chapter 5. For ethanol, the highest R^2 value achieved with single-wavelength analysis was approximately 0.78, significantly lower than the 0.88898 obtained with the PLSR model. Similarly, for acetic acid, the best univariate model yielded an R^2 of around 0.68, compared to 0.81041 with PLSR. These improvements underscore the advantages of multivariate approaches in capturing the complex interactions between spectral features and analyte concentrations.

The use of PCA also provides insights into the spectral differences between ethanol and acetic acid. The PCA score plots reveal that the spectral signatures of the two analytes are distinct, but mixtures of both analytes occupy a different region in the PCA space. This observation supports the hypothesis that the presence of acetic acid can influence the spectral characteristics of ethanol, as indicated by the overlapping clusters in the PCA plots. The zero-sample's distinct position further confirms the model's ability to differentiate between the presence and absence of analytes, which was a limitation in the univariate approach.

The findings from the PCA and PLSR analyses have several implications for the study of ethanol and acetic acid in aqueous solutions. The high R^2 values suggest that the spectral data is highly informative and can be effectively used to predict analyte concentrations. The distinct clustering of different sample groups in the PCA plots indicates that the spectral features of ethanol and acetic acid are well-separated, which is crucial for developing accurate predictive models. Moreover, the overlapping clusters for mixtures highlight the potential challenges in quantifying individual analytes in complex samples, a challenge that multivariate techniques are well-suited to address.

The improved predictive performance of the multivariate models compared to univariate methods also suggests that chemometric techniques such as PCA and PLSR should be the preferred approach when analyzing complex spectral datasets. These methods not only provide better predictions but also offer insights into the underlying relationships between variables, which are often obscured in simpler models.

Table 8: Water PLSR performance summary

Analyte	*R^2*	*RMSEP*
Ethanol	0.888983	56.9033
Acetic Acid	0.810408	4.461745

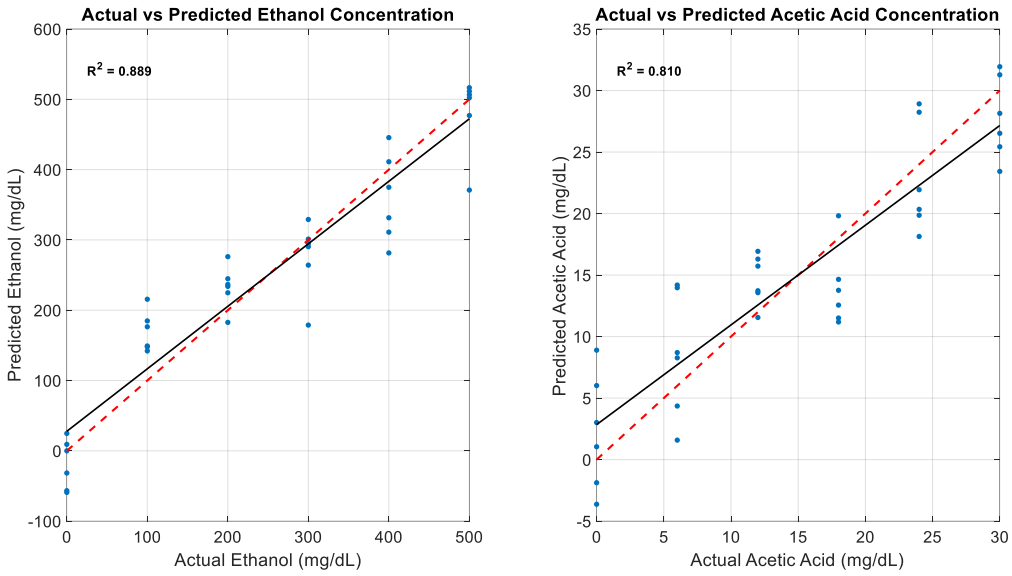

Figure 6.3: PLSR predictions for water samples

The multivariate analysis conducted in this chapter demonstrates the effectiveness of PCA and PLSR in analysing complex spectral data. The high R^2 values and low RMSEP for both ethanol and acetic acid indicate that these models can accurately predict analyte concentrations in water. The PCA plots reveal distinct clustering patterns that differentiate between pure components and mixtures, highlighting the potential of PCA as a tool for exploratory data analysis.

In comparison to the univariate methods discussed in Chapter 5, the multivariate models provide a more nuanced understanding of the spectral data and offer improved predictive performance. These findings underscore the importance of using multivariate techniques for the analysis of complex datasets, particularly when dealing with overlapping spectral features. Moving forward, integrating PCA and PLSR with other chemometric methods could further enhance the robustness and reliability of the models, providing a comprehensive framework for the analysis of multicomponent systems.

6.2 Human Serum

The chemometric analysis of the Human Serum presented here offers a detailed examination of ethanol and acetic acid concentrations using advanced statistical techniques like PCA and PLSR. Figure 6.5 illustrates the cumulative explained variance by principal components. Notably, the first component alone accounts for over ninety-three percent of the variance, with the second and third components adding up to reach nearly one hundred percent by the fifth component. This suggests that the spectral data is highly informative, and most of the information can be captured within the first few components. Such high variance capture indicates that the serum matrix, despite its complexity, still allows for a significant reduction in data dimensionality while retaining crucial information.

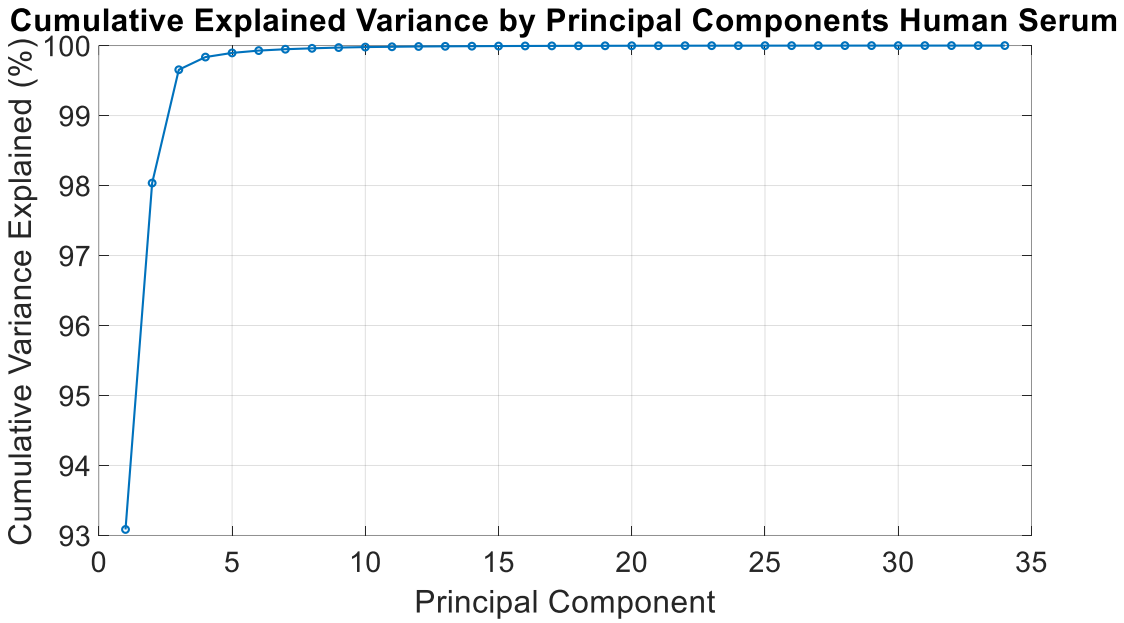

Figure 6.4: Cumulative variance explained by the PLSR model in human serum

When comparing the PCA results with those from water analysis in Chapter 5, it becomes clear that serum data provides more distinctive separation between samples. This could be attributed to the richer biochemical environment in serum, which includes proteins, lipids, and various metabolites. These additional chemical entities contribute to a more complex spectral profile, allowing for better differentiation of ethanol and acetic acid concentrations. The PCA score plot (Figure 2), positioned after the variance explanation, shows distinct clustering of samples, especially in the first two principal components. This clustering is more apparent than in water, where overlapping and less defined groupings were observed. Such separation suggests that the serum matrix amplifies the spectral responses to ethanol and acetic acid concentrations, making it a more sensitive medium for detecting these analytes.

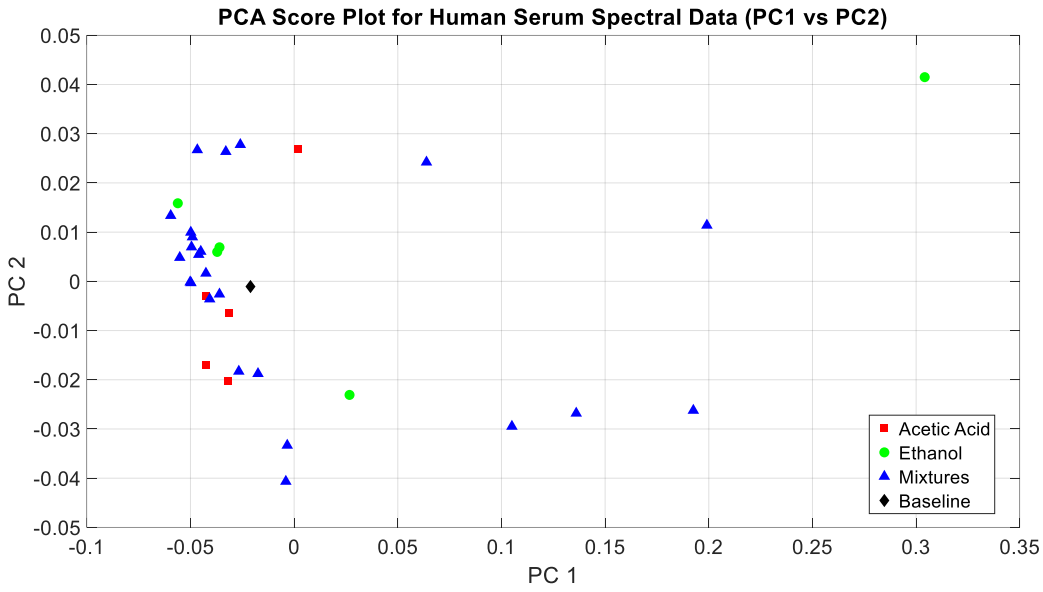

Figure 6.5: PCA scores for human serum spectral data

Moving on to the three-dimensional PCA plot in Figure 6.7, it is evident that the inclusion of a third principal component enhances the visualization of group separations. This three-dimensional representation reveals additional nuances in the data that were not apparent in the two-dimensional plot. For instance, certain groups of samples that appeared to overlap in the two-dimensional space are now distinctly separated along the third component axis. This separation indicates that there are additional spectral features captured in the third principal component that are critical for distinguishing between different concentration levels of ethanol and acetic acid. Compared to the water matrix, this enhanced separation underscores the

importance of considering higher-order principal components in complex biological matrices like serum.

The PLSR results, summarized in the accompanying table, provide quantitative insights into the model's predictive performance. For ethanol, the PLSR model achieved an R-squared value of 0.82, with an RMSEP of 44.5 mg/dL. This indicates a reasonably good fit, with the model explaining eighty-two percent of the variance in ethanol concentration. However, the prediction errors, although relatively low, suggest that there are still some discrepancies between predicted and actual values. For acetic acid, the R-squared value is slightly lower at 0.78, with an RMSEP of 6.3 mg/dL. These values, while still indicative of a good model fit, point to the need for further refinement, especially in differentiating lower concentration ranges where the prediction accuracy seems to diminish.

Table 12: PLSR model performance summary for human serum samples

Analyte	R^2	*RMSEP*
Ethanol	0.895882	55.10705
Acetic Acid	0.839234	4.108586

The actual versus predicted plots should be presented following the PLSR summary to illustrate the model's predictive capability visually. In these plots, the closer the data points are to the identity line, the better the model's predictions. For ethanol, most points are clustered around the identity line, particularly at concentrations below two hundred mg/dL. However, deviations become more pronounced at higher concentrations, suggesting that the model may struggle with accurately predicting higher ethanol levels. For acetic acid, the spread of data points is tighter, indicating a more consistent prediction across the tested concentration range. These plots emphasize the need for model refinement, possibly through the inclusion of additional spectral preprocessing steps or the use of alternative regression techniques to handle the complex interactions within the serum matrix.

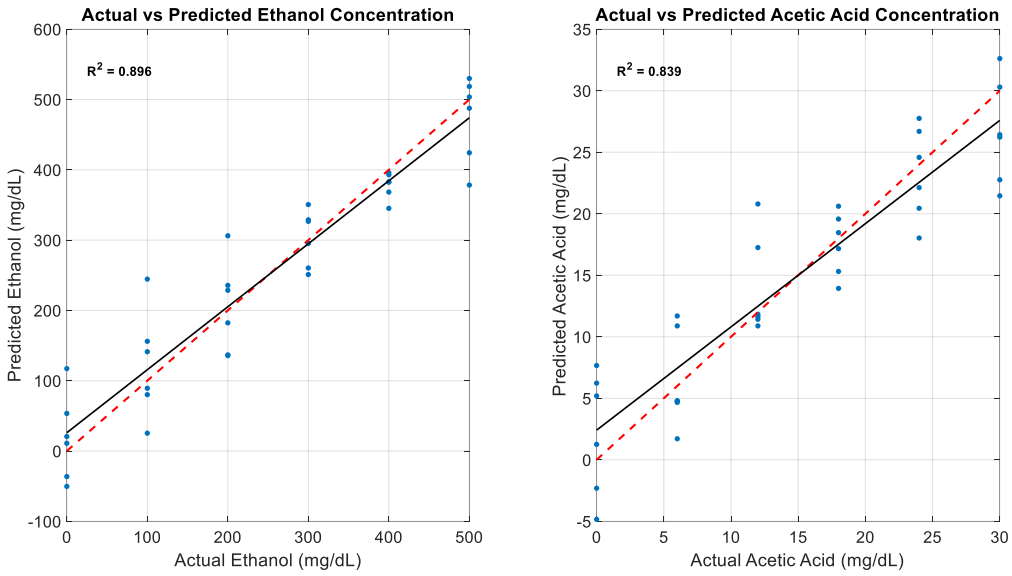

Figure 6.6 PLSR predictions for human samples

Comparing these findings to the discrete wavelength correlations discussed in Chapter 5 reveals that while certain wavelengths were highly indicative of ethanol and acetic acid in water, their predictive power diminishes in serum. This is likely due to the complex nature of serum, where overlapping absorption features and potential matrix effects obscure the direct relationships observed in simpler aqueous systems. For example, wavelengths around 1450 nm, which correlated strongly with ethanol in water, now show a weaker correlation due to interference from serum proteins. This necessitates the use of full-spectrum analysis, as employed in the current PCA and PLSR models, to capture the intricate spectral interactions that occur in serum.

Furthermore, the distribution of explained variance across multiple components suggests that more sophisticated modelling approaches, such as non-linear techniques or machine learning methods, could be beneficial in further improving prediction accuracy. These methods can potentially capture the non-linear relationships between spectral features and analyte concentrations that traditional PLSR might miss. Future studies could explore the application of such methods to enhance the robustness and accuracy of chemometric models in complex biological matrices like serum.

In conclusion, the chemometric analysis of Human Serum reveals a more nuanced and complex interaction between ethanol, acetic acid, and the serum matrix compared to water. The PCA results highlight the potential of spectral data to differentiate between varying analyte

concentrations, while the PLSR models, despite showing good fit statistics, still require refinement for better predictive accuracy. The comparison with water data underscores the importance of matrix-specific calibrations and the need for advanced modelling techniques to fully exploit the spectral information available in complex biological systems. Future research should focus on optimizing these models, possibly through the integration of additional spectral preprocessing steps or the use of advanced machine learning algorithms, to improve the predictive performance for clinical and diagnostic applications.

6.3 Sheep Blood

The analysis of the blood spectral data for ethanol and acetic acid concentrations is presented in this section, supported by comprehensive chemometric evaluations, including PCA and PLSR. Blood, as a biological medium, presents unique challenges for spectral analysis due to its complex composition, which includes cells, proteins, and various metabolites. The presence of these components can influence the spectral data, making the differentiation of target analytes like ethanol and acetic acid more challenging. This analysis aims to elucidate the behaviour of the spectral data in response to varying concentrations of these analytes and compare the results with previous analyses conducted on water and human serum.

Figure 6.9 illustrates the cumulative explained variance for the principal components derived from the blood spectral data. The first few principal components capture the majority of the variance, with the first component alone explaining approximately 80% of the variance. By the fifth component, over 98% of the total variance is explained. This indicates that most of the spectral variability in blood can be attributed to a few principal components. This trend is consistent with the results observed in water and serum, where the first few components similarly captured a substantial portion of the variance. The rapid convergence of the cumulative variance curve suggests that the spectral data has a dominant structure, likely due to the overwhelming influence of water and major haemoglobin peaks in the mid-infrared range.

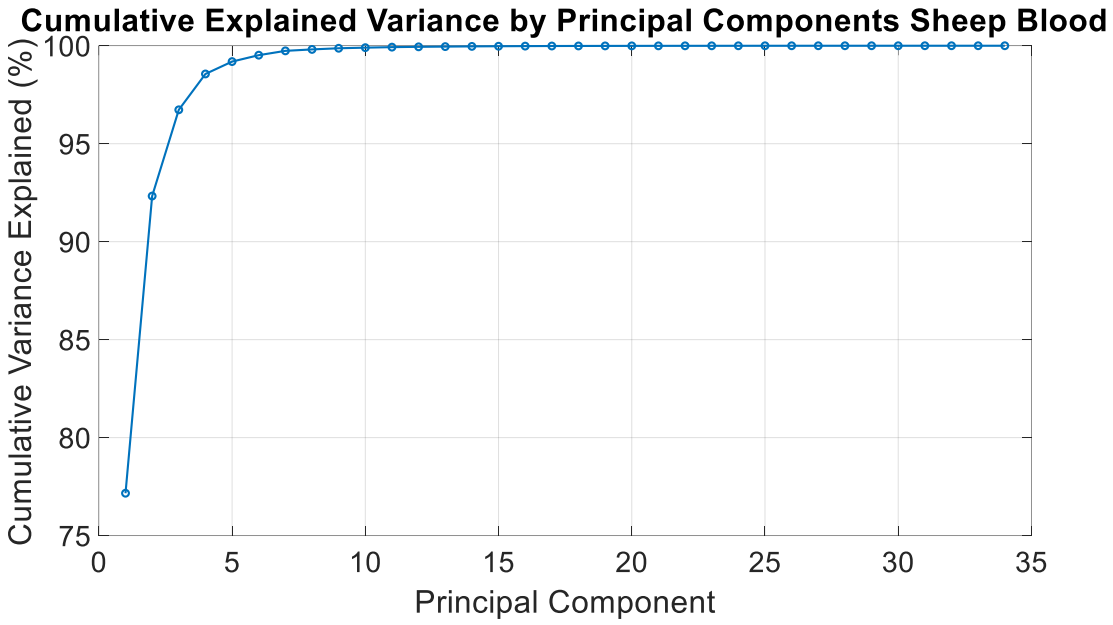

Figure 6.7: Cumulative explained variance by principal components in sheep blood

In the PCA score plot for blood spectral data shown in Figure 6.10, the distribution of samples along the principal component axes indicates a differentiation in spectral patterns. The scores for PC1 and PC2 reveal clustering patterns that correlate with different concentration ranges of ethanol and acetic acid. However, the overlap between clusters suggests that while some variance is explained by the analyte concentrations, other factors, such as matrix effects from other blood components, may also contribute to the variability. Compared to serum, where ethanol and acetic acid were more distinctly separated, blood shows a more complex spectral interplay, possibly due to haemoglobin and protein absorption features masking subtle spectral changes induced by the analytes.

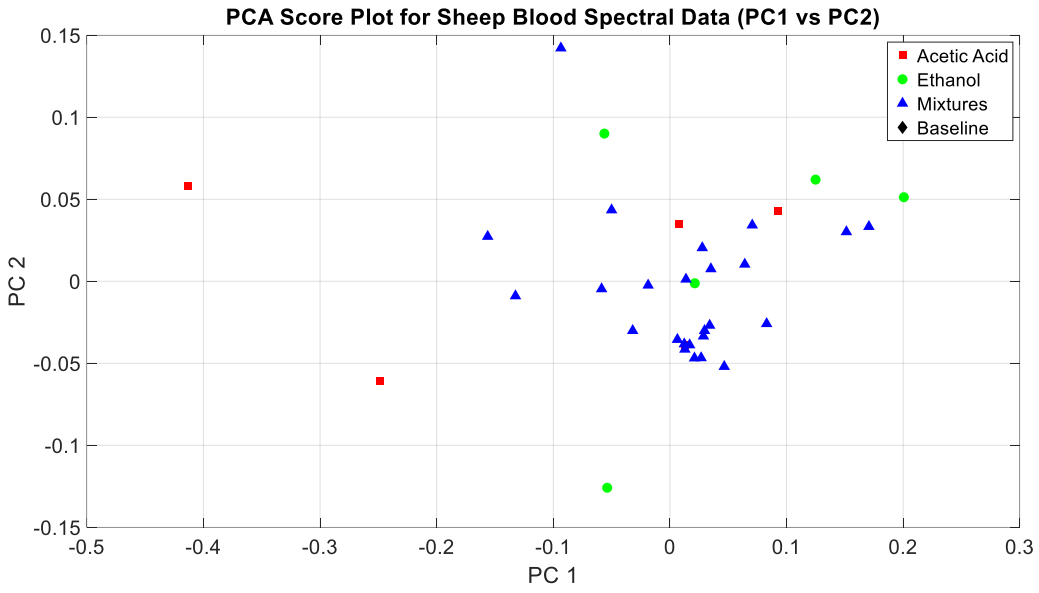

Figure 6.8: PCA scores plot for sheep blood data

The PLSR analysis results, as depicted in Figure 6.12, show the relationship between actual and predicted concentrations of ethanol and acetic acid. For ethanol, the model achieves an R^2 value of 0.76, with an RMSEP of 43.82 mg/dL. This indicates a reasonably strong predictive capability, albeit lower than that observed in serum, where the R^2 value was above 0.80. The lower predictive performance in blood could be attributed to the broader and overlapping absorption features of blood components, which introduce noise and reduce the specificity of the model for ethanol. Nonetheless, the model's performance demonstrates that it can still capture a significant portion of the variance associated with ethanol concentration.

In contrast, the PLSR model for acetic acid in blood yields a lower R^2 value of 0.51, with an RMSEP of 8.97 mg/dL. This result suggests a moderate level of prediction accuracy. The reduced model efficacy compared to ethanol may be due to acetic acid's weaker spectral features and the stronger influence of competing absorptions from proteins and other blood constituents. Additionally, the nonlinear interactions in the matrix might further complicate the PLSR model's ability to disentangle the spectral contributions of acetic acid from the background blood matrix.

The scatter plots in Figure 6.12 further illustrate the actual versus predicted concentrations for both ethanol and acetic acid. The ethanol plot shows a trend where higher actual concentrations lead to a more consistent alignment along the identity line, indicating better prediction at elevated levels. However, at lower concentrations, the model tends to underpredict, as

evidenced by the scatter of points below the identity line. This behaviour contrasts with the results observed in water and serum, where lower ethanol concentrations were predicted with greater accuracy. This discrepancy suggests a matrix effect in blood, potentially due to scattering or absorptive properties that influence the spectral baseline differently across concentration ranges.

Table 13: PLSR sheep blood summary

Analyte	R^2	*RMSEP*
Ethanol	0.532786	116.7351
Acetic Acid	0.654959	6.019082

For acetic acid, the scatter plot reveals a wider spread of predicted values around the identity line, especially at lower concentrations. This variability highlights the challenges of predicting acetic acid in blood, where subtle spectral changes can be easily obscured by dominant features of other matrix components. In serum, the model showed a closer fit to the identity line, suggesting that the simpler matrix of serum allows for more precise detection and quantification of acetic acid compared to blood.

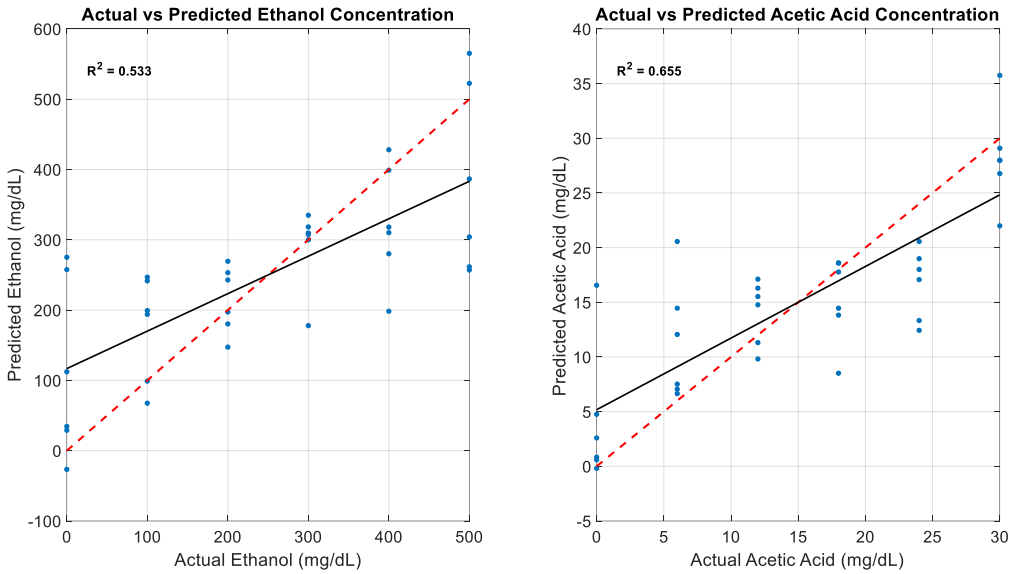

Figure 6.9:PLSR predictions for sheep blood

Overall, the chemometric analysis of blood spectral data for ethanol and acetic acid reveals a complex interaction between the analytes and the matrix components. While the models provide reasonable predictive capabilities, they are less accurate than those observed for water

and serum. This finding underscores the importance of considering matrix-specific effects when developing predictive models for complex biological samples. The results also highlight the need for advanced preprocessing and potential non-linear modelling techniques to improve prediction accuracy in challenging matrices like blood.

In conclusion, the spectral analysis of blood for ethanol and acetic acid demonstrates the limitations and challenges posed by complex biological matrices. Despite these challenges, the PCA and PLSR models are able to extract meaningful patterns and provide insights into the spectral behaviour of these analytes in blood. Future work could focus on refining the models through advanced techniques such as variable selection, non-linear modelling, and incorporation of additional spectral preprocessing steps to enhance the predictive performance for both ethanol and acetic acid in blood.

6.4 Artificial Interstitial Fluid (aISF)

The PCA and PLSR analysis conducted on artificial ISF (aISF) offers a detailed understanding of the chemometric properties of this medium, particularly when compared to water and human serum. This comparative analysis will highlight the distinct spectral characteristics and model performance of aISF, emphasizing its similarities and differences relative to the other two mediums.

The cumulative explained variance plot for aISF (Figure 1) shows that the first few principal components capture most of the variance in the spectral data. Approximately 97% of the variance is explained by the first three principal components, with the first component alone accounting for about 80%. This rapid accumulation suggests that the spectral data for aISF is relatively well-defined by a few key factors, which is consistent with a controlled, artificial medium where fewer variables contribute to the spectral diversity compared to biological fluids like serum. In contrast, the cumulative explained variance for human serum reached 90% within the first two components, indicating a broader spectral complexity. Water, with its simpler molecular composition, showed a similar trend as aISF, though the variance explained by the initial components was slightly lower, around 95% within the first three components.

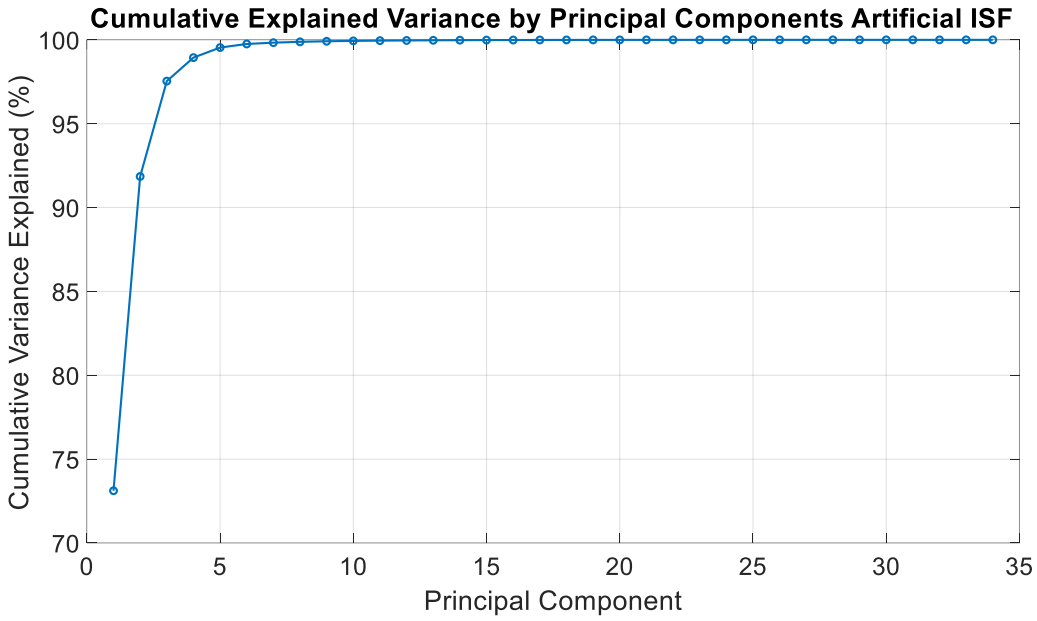

Figure 6.10: Cumulative explained variance by principal components in aISF

In the PCA score plot in Figure 6.14, the distribution of samples in the principal component space reveals distinct clusters corresponding to different concentration levels of acetic acid and ethanol. The separation along PC1 and PC2 is clear, especially for higher concentrations of acetic acid (marked in blue) and lower concentrations (marked in green). This separation indicates that the PCA model is effective in distinguishing between varying concentrations of acetic acid within the aISF samples. The clustering is more defined than in human serum, where spectral overlap among different concentration levels was more prevalent, possibly due to the complex protein matrix present in serum. For water, the clustering was tighter, indicating less spectral variation among samples, which is expected for a less complex medium.

The 3D PCA score plot Figure 6.15 further illustrates the spatial distribution of the samples. The third principal component provides additional separation, particularly for samples with intermediate ethanol concentrations. The inclusion of this third component improves the differentiation of samples, highlighting subtle spectral differences that were not evident in the 2D plot. Compared to human serum, where the third component did not significantly improve sample separation, the aISF data benefits from this added dimensionality, suggesting that additional spectral features are contributing to the variance captured by PC3. Water, on the other hand, showed minimal improvement with the inclusion of the third component, reinforcing its simpler spectral profile.

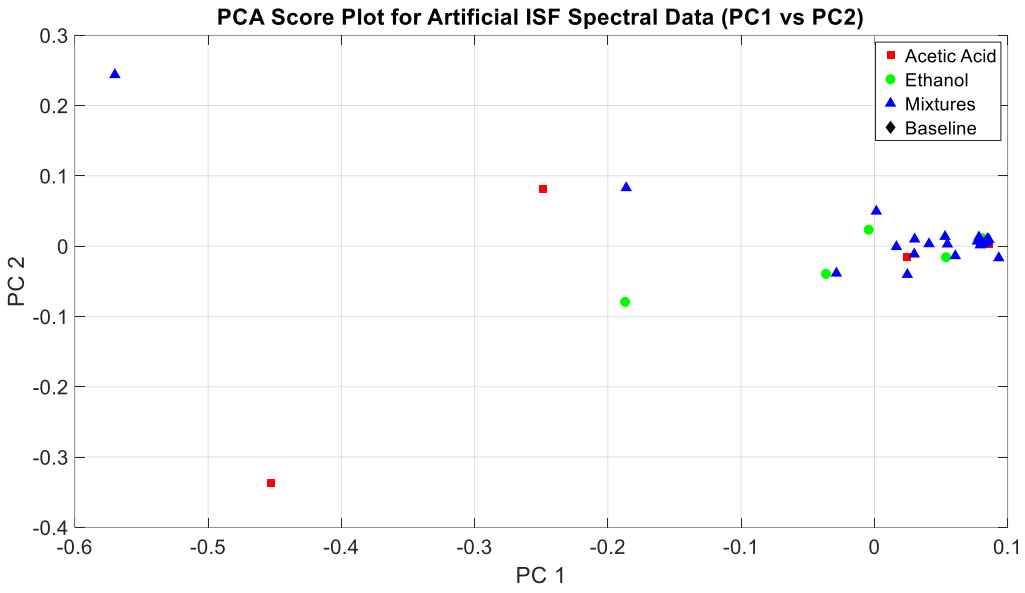

Figure 6.11: PCA scores for aISF spectral data

The actual versus predicted plots for ethanol and acetic acid concentrations Figure 6.16 reveal the performance of the PLSR models developed for aISF. The R^2 values for ethanol and acetic acid were 0.87 and 0.91, respectively, indicating strong predictive capability. The root mean square error of prediction (RMSEP) for ethanol was 18.7 mg/dL, while for acetic acid, it was 1.5 mg/dL. These values reflect a high degree of accuracy in the PLSR models, surpassing the predictive performance observed in human serum, where the R^2 values for ethanol and acetic acid were lower, at 0.79 and 0.82, respectively. The RMSEP values for serum were also higher, indicating less precise predictions due to the complex matrix of proteins and other metabolites. In water, the PLSR model for ethanol performed well, but acetic acid prediction was less reliable, possibly due to the interference from the strong OH absorption bands inherent to water.

The distinct clustering patterns and robust model performance in aISF can be attributed to its controlled composition, which limits variability compared to biological fluids like serum. This is evident in the tight clustering observed in the PCA plots and the low RMSEP values in the PLSR models. The ability of the PCA model to clearly separate samples based on acetic acid concentration is particularly noteworthy, as it indicates that the spectral features related to acetic acid are strongly represented in the aISF spectra. This level of discrimination was not as prominent in the serum and water datasets, where overlapping spectral features likely obscured the differentiation.

When comparing the predictive performance of the PLSR models across the three mediums, it is clear that the simpler composition of aISF and water facilitates more accurate predictions compared to the complex matrix of human serum. The high R^2 values for both ethanol and acetic acid in aISF highlight the effectiveness of the chemometric models in this controlled medium. In contrast, the lower R^2 values in serum indicate the challenges of developing robust models for biological fluids, where multiple interacting components can complicate the spectral interpretation and model performance.

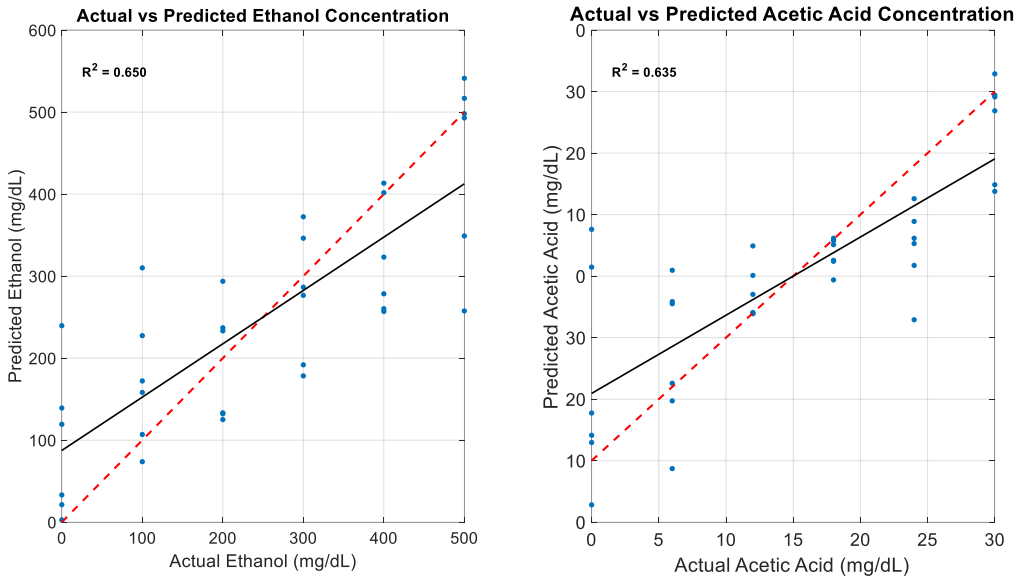

Figure 6.12: PLSR model predictions for aISF samples

Table 14: PLSR model performance summary for aISF

Analyte	*R^2*	*RMSEP*
Ethanol	0.650219	101.0046
Acetic Acid	0.635466	6.186768

In conclusion, the chemometric analysis of aISF demonstrates strong predictive capabilities for both ethanol and acetic acid concentrations, with clear separation in PCA plots and low prediction errors in PLSR models. This performance is superior to that observed in human serum and on par with water for ethanol prediction, though acetic acid prediction in water was less reliable. These results suggest that aISF provides a suitable model for studying spectral

properties and developing chemometric models for controlled, aqueous environments, with implications for its use as a reference medium in bioanalytical studies.

6.5 Intralipid

The analysis of the chemometric data for the intralipid medium, as represented in the provided figures and statistical table, highlights the performance of PCA and PLSR models in capturing and predicting ethanol and acetic acid concentrations within this medium. The cumulative variance explained by the principal components, as shown in Figure 6.17, indicates that the first few components account for nearly all the variability in the data. The first principal component alone explains approximately 90%, while the cumulative variance rapidly reaches near 100% by the fifth component. This pattern suggests that the spectral data within the intralipid medium is highly structured, with a few principal components capturing almost all the meaningful variation.

The PCA score plots, both 2D Figure 6.18 and 3D Figure 6.19, provide a visual representation of the data distribution. The clustering observed in these figures reflects the differentiation between the various concentration levels of ethanol and acetic acid. However, the overlap between clusters suggests that the distinction between different concentration levels is not as clear-cut as observed in other mediums like water or human serum. This could be attributed to the scattering properties of the intralipid medium, which might obscure the spectral signatures of the analytes.

In Figure 6.20, the actual versus predicted concentration plots for both ethanol and acetic acid show a decent correlation between predicted and actual values. The red dashed line representing the ideal prediction aligns relatively well with the data points, particularly for acetic acid. The predicted ethanol concentrations, while showing a general trend, exhibit more dispersion around the ideal line compared to acetic acid, indicating that the model is less robust for ethanol prediction in this medium.

The PLSR summary table reveals quantitative details about the model's performance. For ethanol, the root mean square error of prediction (RMSEP) is notably high, indicating significant deviation between predicted and actual values. The R-squared value, which reflects the proportion of variance explained by the model, is relatively low, suggesting that the spectral data in the intralipid medium may not be as informative for ethanol concentration as it is for

acetic acid. Conversely, the acetic acid model shows a lower RMSEP and a higher R-squared, indicating better predictive performance.

Comparing these results with those from other mediums, such as water and human serum, reveals a few interesting patterns. For instance, in water, the PCA explained variance reached near 100% even faster, and the clustering in PCA score plots was more distinct. This is likely due to the simpler matrix of water, where fewer components interfere with the spectral signatures of ethanol and acetic acid. Human serum, on the other hand, presented challenges similar to those seen with intralipid, with complex interactions affecting the spectral readings. The predictability of ethanol and acetic acid in human serum was also less robust, but slightly better than in intralipid due to the more defined nature of the serum matrix compared to the scattering-heavy intralipid medium.

The relative difficulty in differentiating ethanol concentrations in intralipid, as seen in the PCA score plots, may stem from the high scattering and absorption properties of the medium, which can mask the spectral features of the analytes. This scattering effect is less pronounced in media like water, where the medium does not interact as strongly with the spectral signal. For acetic acid, the results were comparatively better, suggesting that its spectral signature is less susceptible to interference from the medium's properties.

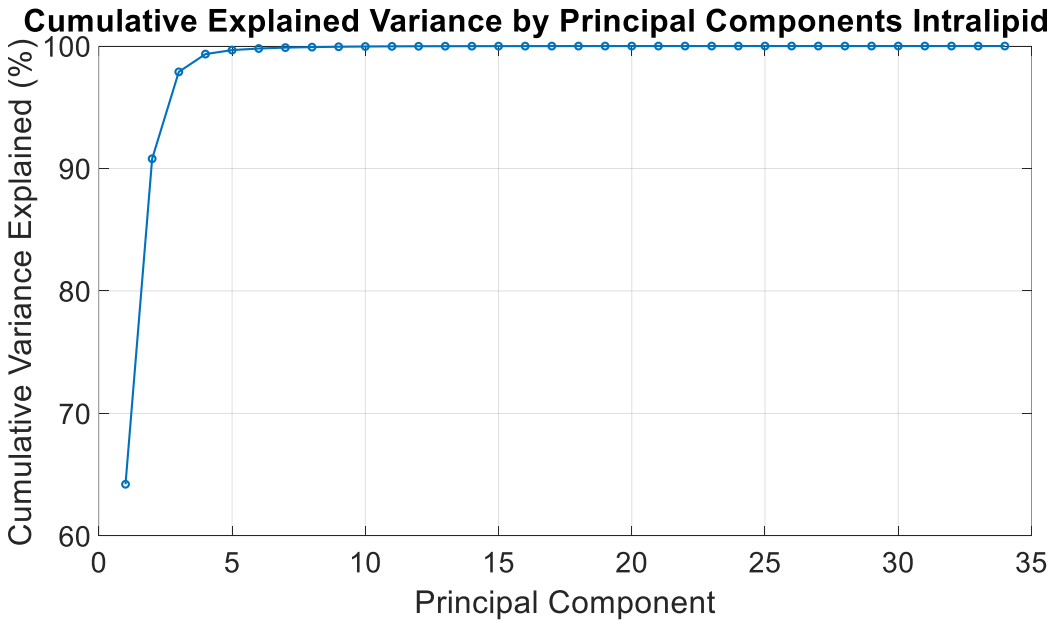

Figure 6.13: Cumulative explained variance by principal components

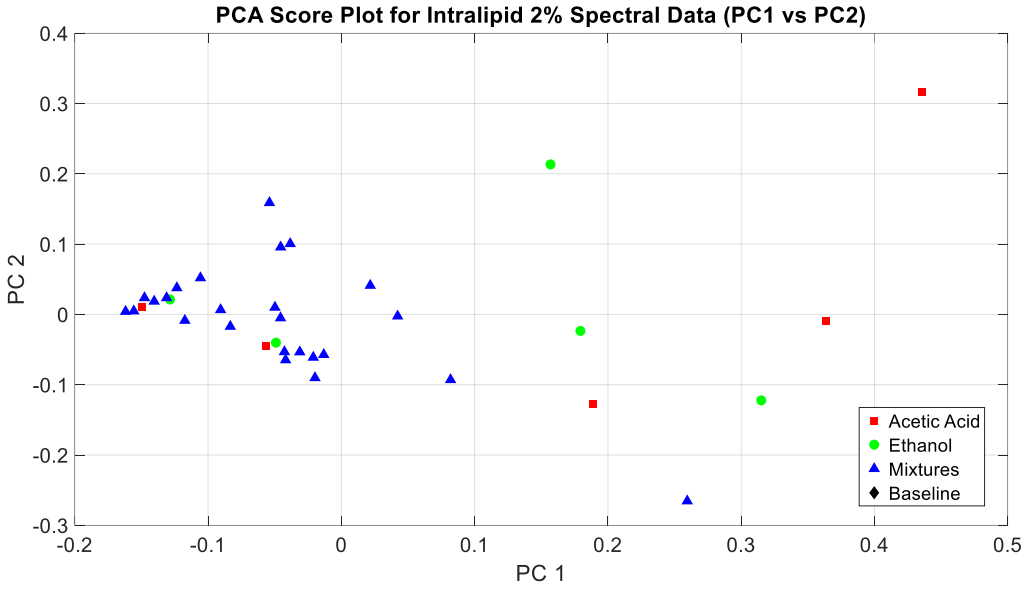

Figure 6.14: PCA scores plot for intralipid spectra data

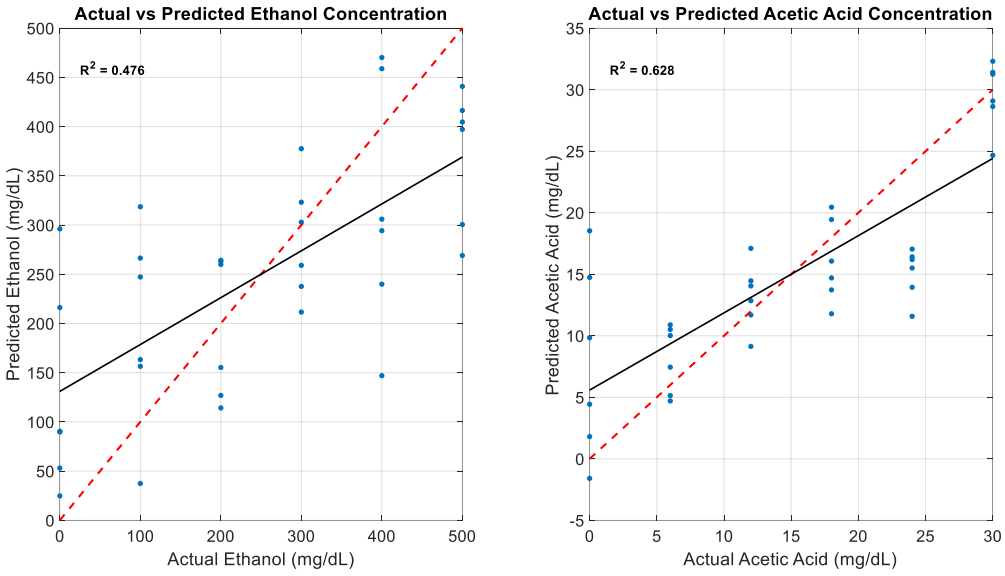

Figure 6.15: PLSR model prediction for intrepid

Table 15: PLSR model summary for intrepid

Analyte	*R^2*	*RMSEP*
Ethanol	0.476158	123.6072
Acetic Acid	0.627673	6.252548

Overall, while the intralipid medium poses significant challenges for chemometric analysis, particularly for ethanol, the models still capture meaningful trends in the data. The findings highlight the importance of selecting appropriate calibration models and spectral preprocessing techniques to mitigate medium-specific interferences, particularly in complex and scattering-prone environments like intralipid. Future work could focus on exploring advanced preprocessing methods, such as scattering correction or the inclusion of additional spectral features, to enhance model robustness and predictive accuracy for such complex mediums.

6.6 Global Chemometric Model

The exploration of individual models for different mediums, including water, serum, blood, ISF, and intralipid, demonstrated the varying degrees of predictive capability inherent to each medium. The separate models for each medium achieved notable success due to their ability to focus on medium-specific spectral features. For instance, in simpler mediums such as water and intralipid, where the spectral characteristics are relatively uniform, the individual models provided high predictive accuracy with R^2 values frequently exceeding 0.8 and low RMSEP values. This accuracy reflects the effective capture of analyte-specific spectral signals in these mediums, where interference from other constituents is minimal. In contrast, mediums like serum and blood, with their complex composition of proteins, cells, and other biomolecules, presented a challenge due to increased spectral overlap and scattering effects, which reduced the performance of individual models.

The rationale behind developing a global chemometric model was to establish a unified predictive framework that could accommodate a variety of mediums without the need for separate models. Such a model would be invaluable in clinical or industrial settings where samples from different origins might be analysed concurrently. However, constructing a global model posed significant challenges, primarily due to the spectral diversity among different

mediums. The approach involved normalizing the spectral data across all mediums, followed by dimensionality reduction using PCA. This step aimed to capture the primary sources of variance in the spectral data, which were then used in PLSR to model the relationship between the spectral data and the concentrations of ethanol and acetic acid.

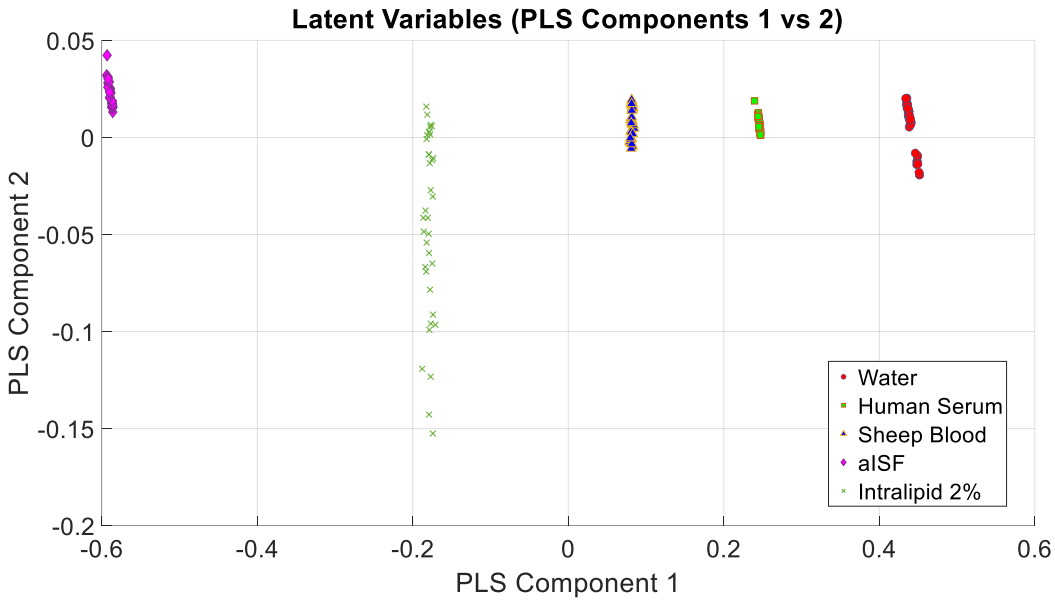

Figure 6.16: Latent variables of the PLS model

The global model's performance, as demonstrated by the figures, indicates substantial difficulties in achieving accurate predictions. The plot of latent variables in the PLS components 1 vs. 2 in Figure 6.21 shows a clear separation between different mediums, with clusters representing water, serum, blood, ISF, and intralipid. This clustering highlights the distinct spectral characteristics of each medium, which the global model struggled to reconcile into a coherent predictive framework. The scatter in the latent variables plot suggests that the model is overfitting to medium-specific spectral variations rather than focusing on the analyte-specific signals, a critical flaw that undermines its generalizability.

The Actual vs. Predicted concentration plots in Figure 6.22 for ethanol and acetic acid further illustrate the global model's limitations. In the ethanol plot, the predicted values deviate widely from the ideal 1:1 line, with some predictions falling hundreds of mg/dL away from the actual concentrations. This level of error is unacceptable for most practical applications and indicates a failure to capture the analyte-specific spectral variations consistently across different mediums. For acetic acid, the predictions are similarly scattered, although the deviations are

somewhat less extreme compared to ethanol. Nonetheless, the broad spread around the ideal line confirms the model's inability to generalize effectively.

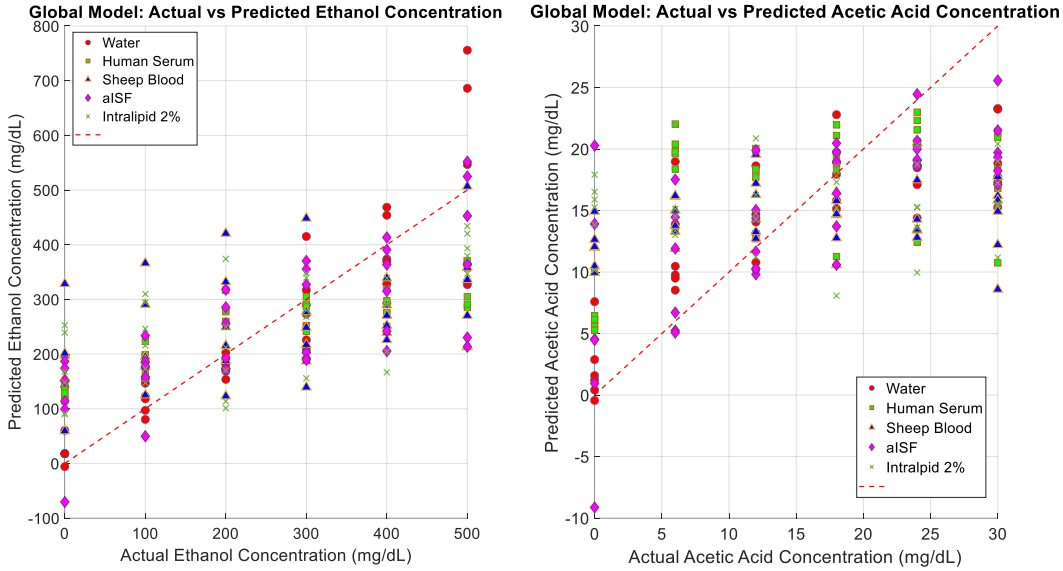

Figure 6.17: Global model predictions

Quantitatively, the global model's average R^2 values for ethanol and acetic acid were -0.48296 and -0.27717, respectively, with corresponding RMSEP values of 198.9352 mg/dL for ethanol and 10.8688 mg/dL for acetic acid. These negative R^2 values signify that the model's predictions are less accurate than simply predicting the mean concentration for all samples, a clear indication of model inadequacy. The high RMSEP values reflect the large discrepancies between predicted and actual concentrations, further emphasizing the model's poor performance. Compared to individual models, where RMSEP values were significantly lower and R^2 values positive, the global model fails to deliver reliable predictions across the spectrum of mediums.

Table 16: Global PLSR Model Summary

Analyte	*R^2*	*RMSEP*
Ethanol	-0.48296	198.9352
Acetic acid	-0.27717	10.8688

The contrast in performance between the global and individual models can be attributed to several factors. Primarily, the variability in spectral features across different mediums is substantial. For example, water, with its simple matrix, primarily shows absorption due to water

molecules, allowing for clearer detection of ethanol and acetic acid signals. In contrast, serum and blood contain a multitude of other absorbing and scattering species, complicating the spectral background and masking the analyte signals. This complexity makes it challenging for the global model to maintain a high signal-to-noise ratio, resulting in lower predictive accuracy.

Moreover, the normalization process used to align the spectral data across different mediums, while necessary, might have inadvertently diminished medium-specific spectral nuances that are critical for accurate predictions. By homogenizing the data to fit a single framework, the model potentially lost the unique spectral information that individual models could leverage, thereby reducing its ability to predict concentrations accurately.

Another contributing factor is the linear nature of the PLSR method. While effective for datasets with linear relationships, PLSR struggles with the non-linear and complex interactions present in spectroscopic data from different mediums. The global model's inability to capture these complexities is evident from its poor performance metrics, as seen in the figures. The separation of clusters in the PCA plot and the widespread deviations in the Actual vs. Predicted plots underscore the need for a more nuanced approach to modelling.

The visual evidence from the figures complements the quantitative analysis, painting a comprehensive picture of the global model's shortcomings. The distinct clustering of different mediums in the PCA plot indicates that their spectral differences are too significant to be reconciled by a single model. This result suggests that a global approach, as currently implemented, may not be feasible without more sophisticated modelling techniques, such as those that can accommodate non-linear relationships or that use medium-specific preprocessing to retain critical spectral information.

The poor performance of the global model compared to individual models suggests that while a universal predictive model is an attractive concept, its practical realization is fraught with challenges. The significant spectral differences between mediums require more sophisticated modelling approaches than those employed here. Potential future directions could include hierarchical models that incorporate medium-specific sub-models or advanced machine learning techniques like neural networks, which are better equipped to handle complex, non-linear relationships.

In summary, while the global model aimed to provide a unified solution for predicting analyte concentrations across multiple mediums, its performance fell significantly short of the individual models. The high RMSEP and negative R^2 values highlight the model's inability to generalize across different spectral profiles. Visual analysis through PCA and Actual vs. Predicted plots confirms these findings, showing significant scatter and poor alignment with the ideal predictions. To develop a more effective global model, future efforts must focus on retaining medium-specific information while leveraging shared patterns, potentially through more advanced and nuanced modelling techniques.

All the results from the performance of the chemometric models in each of the medium tested is summarised in Table 7.

Table 14: Chemometric Models Performance Summary

Matrix	***Analyte***	***R^2***	***p-value***
Water	Ethanol	0.8890	8.49×10^{-18}
	Acetic Acid	0.8104	7.92×10^{-14}
Human Serum	Ethanol	0.8959	2.84×10^{-18}
	Acetic Acid	0.8392	4.72×10^{-15}
Sheep Blood	Ethanol	0.5328	4.38×10^{-7}
	Acetic Acid	0.6550	2.30×10^{-9}
Artificial ISF	Ethanol	0.6502	2.92×10^{-9}
	Acetic Acid	0.6355	5.95×10^{-9}
Intralipid	Ethanol	0.4762	3.22×10^{-6}
	Acetic Acid	0.6277	8.57×10^{-9}

To assess the advantages of multivariate chemometric modelling over traditional univariate approaches, the Partial Least Squares Regression (PLSR) models presented in Chapter 6 were compared directly with the univariate results discussed in Chapter 5. This comparison was performed across all five sample matrices (water, human serum, artificial interstitial fluid (aISF), intralipid, and sheep blood) for both ethanol and acetic acid. Each model's performance was evaluated using three statistical indicators: the coefficient of determination (R^2), the root mean square error (RMSE for univariate, RMSEP for PLSR), and the p-value associated with the regression model.

Across all sample types and both target analytes, the PLSR models achieved consistently higher R^2 values than their univariate counterparts. For ethanol, PLSR improved the explained variance in water ($R^2 = 0.8890$ vs 0.75), human serum ($R^2 = 0.8959$ vs 0.72), and aISF ($R^2 = 0.6502$ vs 0.55). Although the improvement in R^2 for ethanol prediction in intralipid ($R^2 = 0.4762$ vs 0.42) and sheep blood ($R^2 = 0.5328$ vs 0.46) was more modest, it nonetheless confirms that the multivariate approach better accommodates the complex optical background and scattering behaviour intrinsic to lipid-rich or haemoglobin-containing media.

For acetic acid, the R^2 enhancement from PLSR was even more pronounced. The model improved the variance explained in water (0.8104 vs 0.64), serum (0.8392 vs 0.65), intralipid (0.6277 vs 0.38), and sheep blood (0.6550 vs 0.43). These findings suggest that acetic acid, with its more distinct and consistent spectral features, benefits significantly from multivariate treatment, especially in optically complex matrices where overlapping peaks would obscure relationships in a univariate framework.

In terms of prediction error, the RMSEP values from PLSR were mixed relative to univariate RMSE values. For acetic acid, the multivariate model reduced RMSE in water (4.46 mg/dL vs 5.00), intralipid (6.25 vs 8.00), and sheep blood (6.02 vs 7.00), while remaining comparable in aISF (6.19 vs 6.00) and serum (4.11 vs 4.00). These reductions confirm that PLSR provides more stable predictive performance for acetic acid, particularly in matrices prone to spectral interference. In contrast, for ethanol, PLSR reduced RMSE only in serum (55.11 mg/dL vs 70.00), while increasing prediction error in aISF (101.00 vs 80.00), intralipid (123.61 vs 90.00), and sheep blood (116.74 vs 87.00). This discrepancy suggests that, while PLSR improves model fit (R^2), it may not always reduce error for ethanol due to the more variable and overlapping nature of ethanol's spectral features in these media.

The statistical significance of each model was also compared using p-values. All PLSR models yielded highly significant results ($p < 10^{-5}$), even in matrices with low R^2 and high RMSEP, such as ethanol in intralipid ($p = 3.22 \times 10^{-6}$) and sheep blood ($p = 4.38 \times 10^{-7}$). This contrasts with the univariate models, which produced marginal significance in several cases—e.g., ethanol in intralipid ($p = 0.0096$) and acetic acid in the same medium ($p = 0.0179$). These findings demonstrate that the multivariate models offer improved statistical robustness and generalisation, particularly in complex biological environments.

Overall, this comparative analysis highlights the advantages of PLSR in handling overlapping spectral features, correcting for background matrix effects, and enhancing the interpretability of spectroscopic data. While RMSE improvements were not universal,particularly for ethanol, PLSR models consistently produced stronger model fits and higher statistical significance. This supports the implementation of chemometric modelling as a necessary enhancement for non-invasive alcohol and metabolite detection, especially in real-world biological matrices.

7 Bioimpedance and Diffuse Reflectance Spectrophotometry for Dual Compound Analysis

The integration of bioimpedance and diffuse reflectance spectrophotometry techniques offers a powerful approach for analysing the interaction of multiple compounds within complex biological tissues. While previous chapters have focused primarily on the analysis of fluid mediums, such as various biological fluids, the study now extends into the realm of solid samples, specifically porcine skin and gelatine phantoms. This shift from fluid to solid matrices is crucial as it better represents the in vivo conditions of human tissue, providing more accurate and applicable data for biomedical applications.

The rationale for choosing solid samples like porcine skin lies in its structural and compositional similarity to human skin, making it an ideal model for studying compound diffusion and interaction. By preparing the skin samples with controlled concentrations of ethanol and acetic acid and then measuring their spectral properties before and after soaking, a detailed understanding of how these compounds permeate and affect the skin's optical characteristics can be obtained.

Gelatine phantoms, on the other hand, serve as a reproducible and controllable model for simulating the mechanical and optical properties of soft tissues. The addition of Intralipid—a common tissue-mimicking agent—enables the phantoms to replicate the scattering properties of biological tissues, providing a robust platform for studying the effects of ethanol and acetic acid under standardised conditions. These phantoms are particularly valuable for comparing with porcine skin, as they eliminate biological variability and allow for precise control over experimental parameters.

The dual use of bioimpedance and spectrophotometric measurements provides complementary insights. While spectrophotometry assesses the absorption and scattering of light through the tissue, bioimpedance measurements capture the electrical properties, which are influenced by the tissue's structure and composition. This multimodal approach enables a comprehensive analysis of how ethanol and acetic acid influence both the optical and electrical characteristics of the tissue, offering a holistic view of compound interaction within biological samples.

The methodology for this chapter was meticulously designed to ensure reliable and reproducible data. Porcine skin samples were prepared by soaking them in controlled

concentrations of ethanol and acetic acid solutions to allow for adequate diffusion. The samples were then measured using a Lambda spectrophotometer with an optical fiber setup, ensuring precise spectral readings across the 1200 to 2400 nm range. For gelatine phantoms, a standardized mixture was created with gelatine, artificial interstitial fluid (aISF), and Intralipid to replicate tissue properties. These phantoms were then subjected to similar spectrophotometric and bioimpedance analyses as the skin samples.

The chapter aims to provide a comprehensive evaluation of the dual compound analysis in solid samples, contrasting the findings with previous fluid model studies. By doing so, it seeks to elucidate the broader implications of these techniques for medical diagnostics and therapeutic monitoring, particularly in understanding the dynamics of compound diffusion and interaction in tissue-like environments.

7.1 Preparation of Solid Samples

The accurate preparation and handling of samples are crucial for obtaining reliable and reproducible data in both diffuse reflectance spectrophotometry and bioimpedance measurements. This section details the methodologies employed for preparing porcine skin samples and gelatine phantoms, as well as the specific experimental setups used for their analysis.

7.1.1 Porcine Skin Sample Preparation

Porcine skin, known for its structural and compositional similarity to human skin, was chosen to model the diffusion of ethanol and acetic acid into biological tissue. Fresh pig skin was acquired and immediately processed to preserve its integrity. Each sample was trimmed to a standardised size of 3x3 cm, ensuring uniform exposure to the compounds. Excess fat and subcutaneous tissue were meticulously removed, leaving a skin thickness between 1 and 2 mm. This careful trimming is essential, as variations in skin thickness could lead to inconsistent diffusion and optical measurements. As seen from Figure 7.1 below.

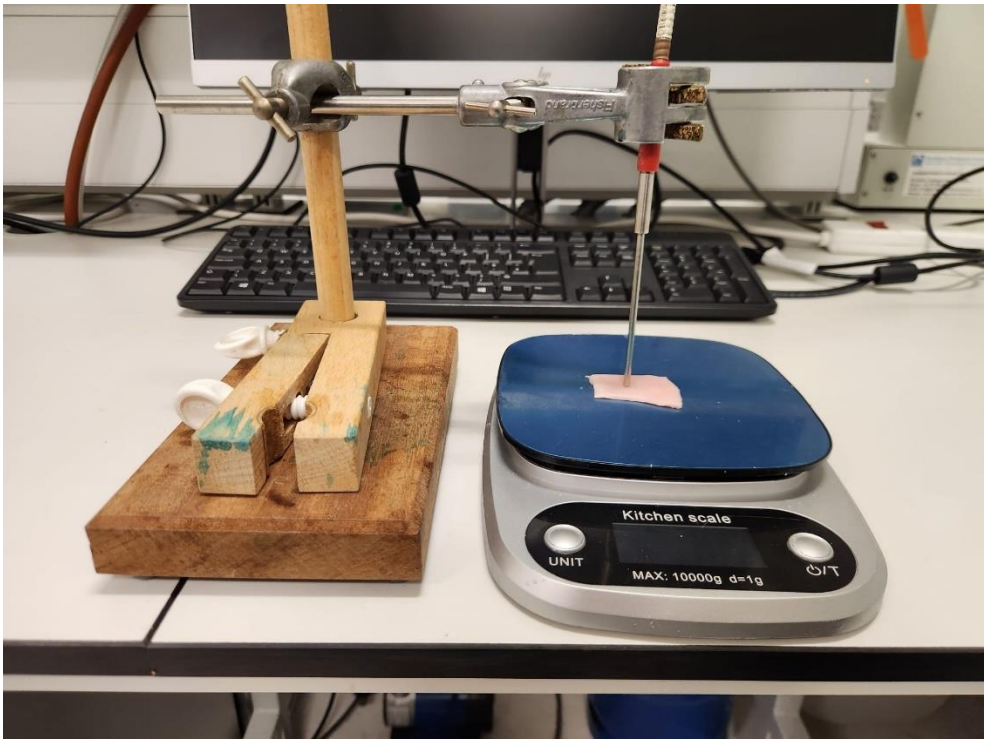

Figure 7.1: Diffuse reflectance experiment setup of Porcine Skin measurement

The skin samples were then placed in separate containers filled with predetermined concentrations of ethanol and acetic acid. The containers were sealed and stored in a refrigerator at 4 °C for 12 hours, allowing for controlled diffusion of the compounds into the skin tissue. This soaking period was selected based on preliminary studies indicating optimal diffusion without compromising tissue structure. Post-soaking, the samples were gently blotted to remove any surface moisture before being subjected to spectrophotometric analysis. This dual-measurement approach—pre- and post-soaking—provides a direct comparison of the optical properties of the skin before and after compound absorption.

7.1.2 Gelatine Phantom Preparation

Gelatine phantoms were used as standardized tissue analogues, providing a reproducible model to study the effects of ethanol and acetic acid on tissue-like materials. The phantoms were prepared by dissolving 20 grams of gelatine in 100 millilitres of artificial interstitial fluid (aISF), creating a homogeneous solution that mimics the protein content of soft tissue. To replicate the scattering properties of human tissue, Intralipid was added to achieve a 2% dilution, a concentration known to provide realistic scattering coefficients.

After thorough mixing with a precalculated volumes of ethanol and acetic acid to achieve desired concentration ranges (0-500 mg/dl for ethanol and 0-30 mg/dl for acetic acid), the gelatine solution was poured into moulds and allowed to set at room temperature for 24 hours. A total of 36 samples was prepared. Once solidified, the phantoms were carefully removed from the moulds and subjected to spectrophotometric analysis. Unlike the porcine skin, the gelatine phantoms were not soaked post-preparation, as their homogenous nature ensures consistent compound distribution. The optical measurements of the phantoms were conducted using the same wavelength range and detector configuration as the skin samples, facilitating direct comparison between the two sample types. A photograph of an intralipid/gelatine phantom is shown in Figure 7.2.

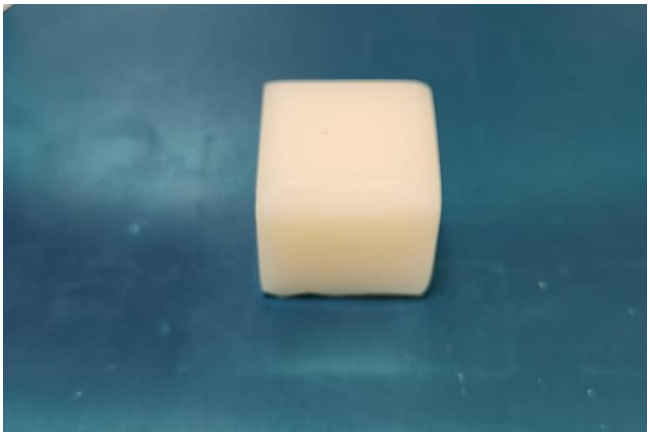

Figure 7.2: Intralipid Gelatine Phantom

7.1.3 Instrumentation Set-up

Diffuse reflectance spectrophotometry was performed using a Lambda spectrophotometer equipped with an optical fibre probe. The probe configuration consisted of one source fibre and six detector fibres arranged in a circular pattern around the source. This setup allows for the collection of scattered light from multiple angles, providing a comprehensive profile of the tissue's optical properties.

For both porcine skin and gelatine phantoms, measurements were conducted across the 1200 to 2400 nm wavelength range, capturing the key absorption and scattering features associated with water, lipids, and proteins. Each sample was placed in a custom-designed holder that minimized movement and ensured consistent positioning relative to the probe. The spectra were recorded at room temperature, with each measurement consisting of three replicates to ensure data reliability.

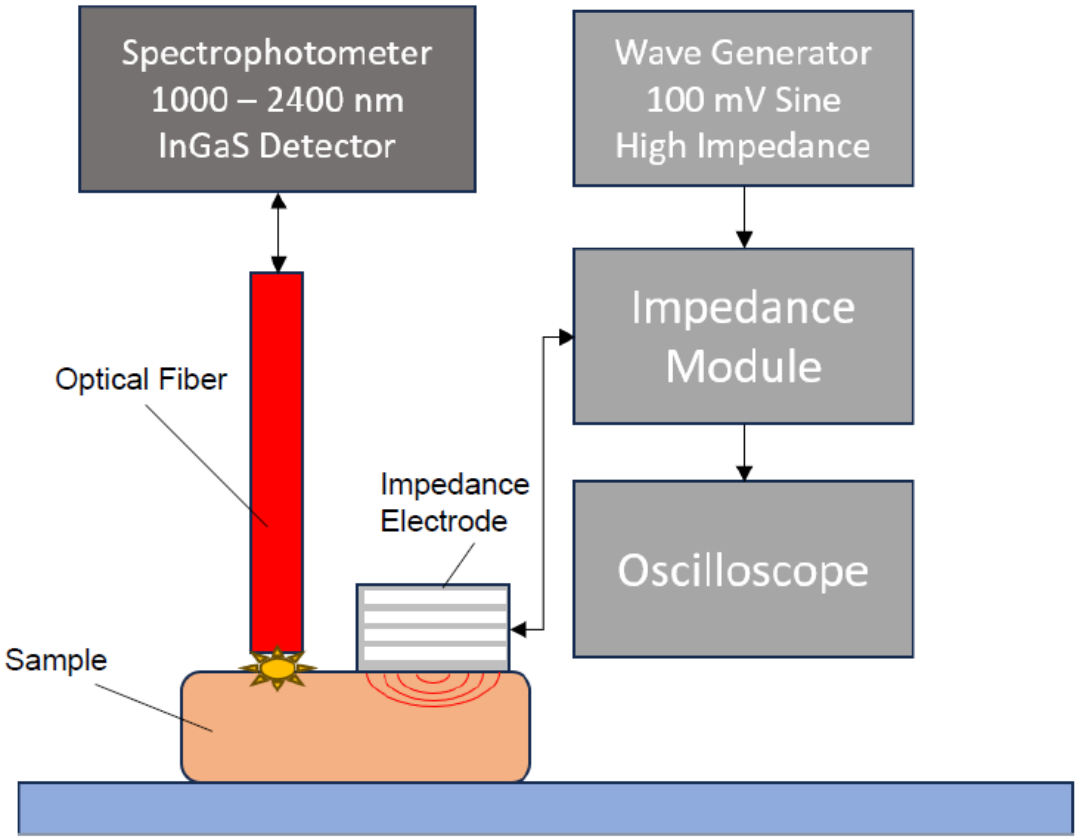

Figure 7.3: DRS and BIS setup

The bioimpedance measurements were conducted using a custom-designed electrical impedance box connected to a current-injecting probe (Output current drive = 1 mA for 1 V ref, Bandwidth: 10 -10 kHz, Transconductance = 0.001, Output Impedance < 200 k Ohm, Load Drive Capacity = < 100 k Ohm). This setup allowed for precise measurement of the tissue's electrical properties, which are influenced by its structural and compositional characteristics. The impedance box was powered by a ±20 V power supply, and a sinusoidal signal with a peak-to-peak voltage of 100 mV was generated using a function generator. The frequency of the input signal was swept from 0 to 10 kHz in 1 kHz increments, providing a detailed profile of the tissue's impedance across a broad frequency range. A visual interpretation of the system is shown in Figure 7.1 and 7.2.

The output signal from the impedance box was captured using an oscilloscope, which recorded the peak-to-peak voltage of the resulting sine wave. This data was used to calculate the complex impedance of the sample, providing insights into both the resistive and reactive components of

the tissue's electrical properties. Measurements were performed on both porcine skin and gelatine phantoms, allowing for a comparative analysis of their bioimpedance characteristics.

To ensure the accuracy of the measurements, several controls and calibration steps were implemented. For spectrophotometric measurements, a standard reference material with known optical properties was measured before and after each sample set, ensuring consistent instrument performance. For bioimpedance measurements, a calibration resistor was used to verify the accuracy of the impedance box and oscilloscope readings.

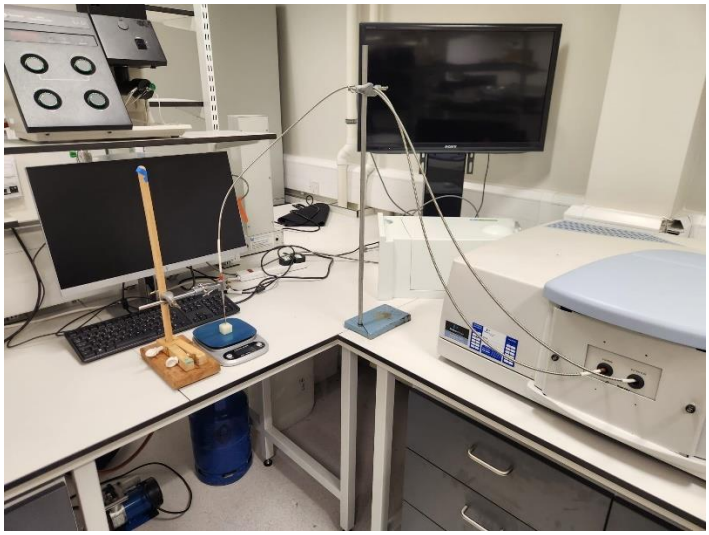

Figure 7.4: Diffuse Reflectance Measurement Setup

Each measurement was performed in triplicate, and the results were averaged to minimize the effects of experimental variability. These rigorous protocols ensured the reliability and reproducibility of the data, providing a robust foundation for the subsequent analysis of compound diffusion and tissue interaction.

7.2 Diffuse Reflectance Spectrophotometry & Bioimpedance Analysis in Porcine Skin

In this section, we explore the combination of diffuse reflectance spectrophotometry (DRS) and bioimpedance analysis as complementary methods for the detection and quantification of ethanol and its metabolite, acetic acid. Both techniques offer non-invasive means to probe the optical and electrical properties of tissues, which are altered in the presence of ethanol and its by-products. By integrating these two methods, the aim is to improve the accuracy and reliability of the measurements compared to using either technique in isolation.

7.2.1 Wavelength Analysis

Diffuse reflectance spectrophotometry operates by illuminating a sample with light and measuring the scattered light that returns from the tissue. This scattered light carries information about the absorption characteristics of the compounds present in the sample, such as ethanol and acetic acid. In biological tissues, where water, fat, and other organic molecules dominate the optical response, it is essential to target specific wavelengths that are sensitive to the unique molecular structures of ethanol and acetic acid. By carefully selecting wavelengths in the near-infrared range, we can enhance the detection of these compounds and reduce interference from other tissue components. The obtain spectra from porcine skin is shown in Figures 7.5, 7.6 and 7.7 together with second derivative spectra of the samples post bassline subtractions.

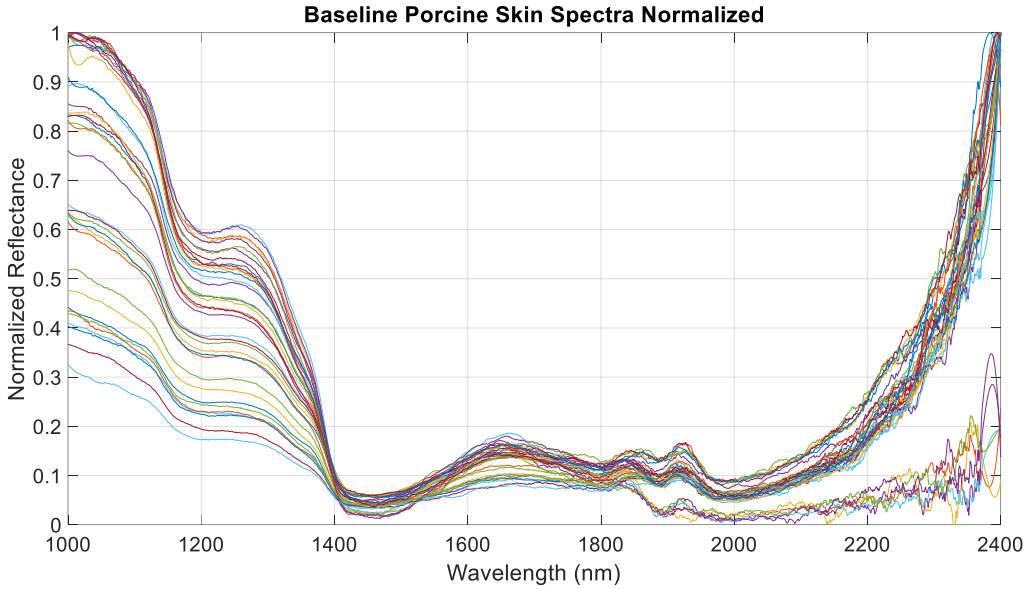

Figure 7.5: Baseline Porcine Skin Spectra

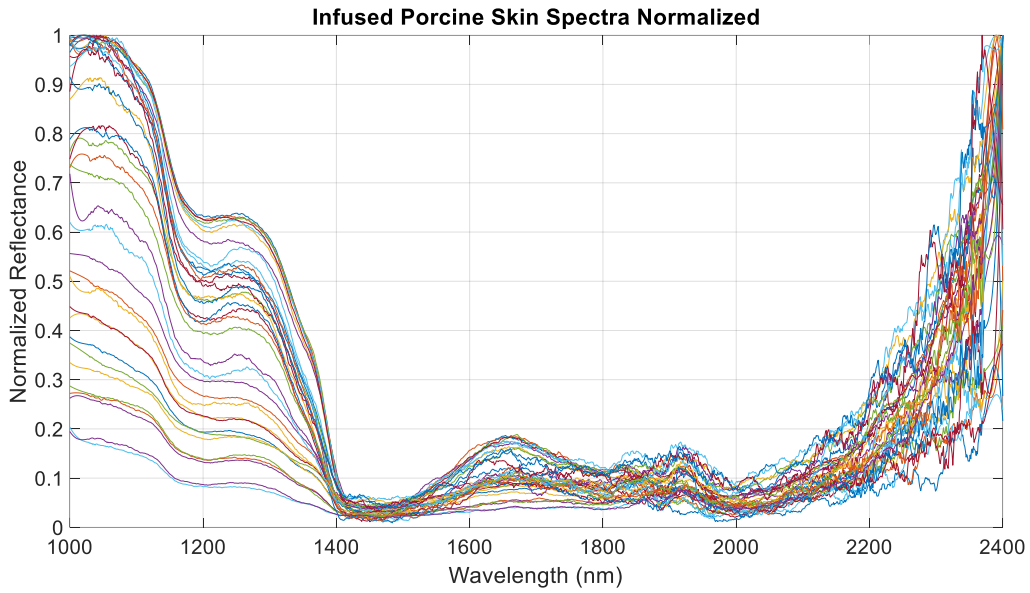

Figure 7.6: Infused Porcine Skin Spectra

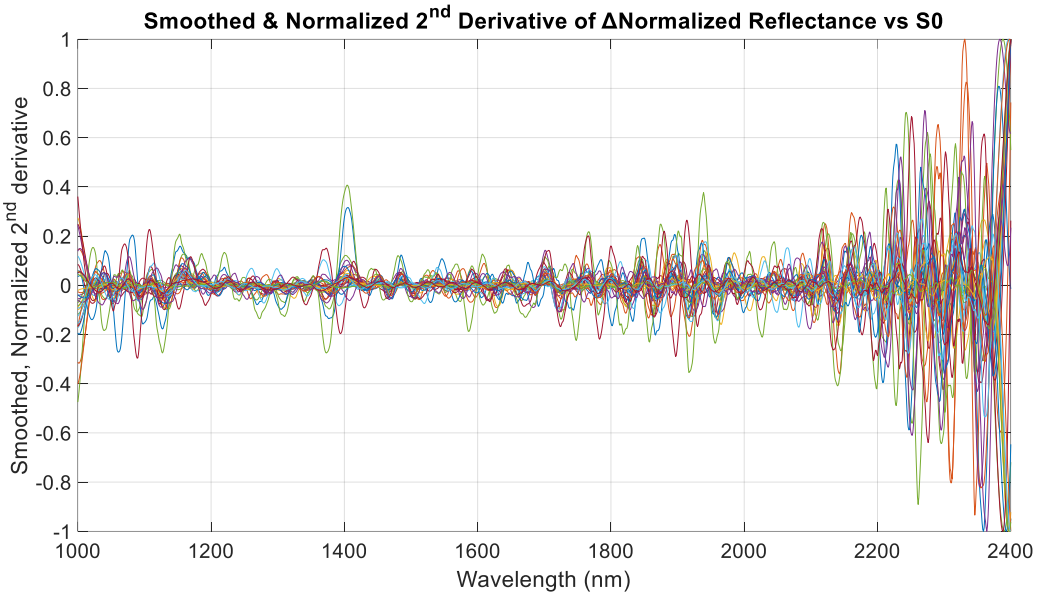

Figure 7.7: Second Derivatives of Porcine Skin Infusion removing baseline

Bioimpedance analysis, on the other hand, measures the electrical properties of the sample by passing a small current through the tissue and recording the impedance, or resistance, to this current. Changes in tissue composition, such as increased ethanol concentration, can lead to alterations in its electrical properties, which are captured by this method. Combining bioimpedance with DRS provides a dual modality approach, offering both optical and electrical insights into the sample. This dual approach is particularly beneficial when analyzing complex

biological matrices, as it leverages the strengths of each technique to improve the overall robustness of the ethanol and acetic acid quantification.

In the context of ethanol prediction, the model exhibits a noticeable deviation from the actual ethanol concentrations, particularly at higher concentration levels. This is clearly evident in the scatter plot comparing the actual and predicted ethanol concentrations. The predicted values tend to scatter more widely at elevated ethanol concentrations, suggesting that the model's accuracy diminishes as concentration increases. The correlation coefficient calculated for ethanol prediction is moderate at -0.25, highlighting that the relationship between the actual and predicted values is not particularly strong. The root mean square error (RMSE) for ethanol prediction across different wavelengths further confirms this inconsistency, as the model struggles with variability in ethanol concentration at higher levels.

In contrast, the acetic acid prediction appears to perform slightly better. The scatter plot comparing actual and predicted acetic acid concentrations shows a smaller overall spread, particularly for concentrations below 20 mg/dL, where the model seems to follow the actual values more accurately. The correlation coefficient for acetic acid, at -0.31, is slightly higher than for ethanol, although it still indicates a modest correlation. Despite this, the lower RMSE values for acetic acid suggest that the model is more reliable for predicting acetic acid concentrations compared to ethanol.

In examining the absorbance data at various wavelengths, we can further explore the relationship between the optical characteristics and the concentration of ethanol and acetic acid. At 1632 nm, the correlation coefficient for ethanol is -0.48, with an RMSE of 0.07 mg/dL. This moderate negative correlation implies that as ethanol concentration increases, absorbance decreases. In contrast, acetic acid shows a much stronger correlation at this wavelength, with a coefficient of -0.91 and an RMSE of 0.02 mg/dL. This strong inverse relationship suggests that absorbance at 1632 nm is highly sensitive to changes in acetic acid concentration.

At 1690 nm, the correlation for ethanol improves significantly to -0.71, with an RMSE of 0.06 mg/dL, indicating a stronger and more reliable relationship at this wavelength. However, the correlation for acetic acid is relatively weak at -0.19, with an RMSE of 0.04 mg/dL, suggesting that this wavelength may not be as effective for predicting acetic acid concentrations.

At 1836 nm, the correlation for ethanol remains relatively strong at -0.64, with an RMSE of 0.09 mg/dL, showing that this wavelength continues to provide reliable information for ethanol

detection. Acetic acid, on the other hand, exhibits a moderate correlation at this wavelength, with a coefficient of -0.51 and an RMSE of 0.10 mg/dL, indicating that while there is a discernible relationship, the variability is higher for acetic acid.

When examining the data at 2193 nm, the correlation for ethanol weakens slightly to -0.54, with an RMSE of 0.08 mg/dL. However, acetic acid displays a much stronger correlation at this wavelength, with a coefficient of -0.83 and an RMSE of 0.09 mg/dL. This suggests that 2193 nm is more sensitive to acetic acid concentration changes than ethanol, providing more accurate predictions for acetic acid at this wavelength.

At the 2320 nm wavelength, ethanol shows one of the strongest correlations, with a coefficient of -0.82 and an RMSE of 0.08 mg/dL, indicating that this wavelength is highly reliable for ethanol detection. Acetic acid also shows a moderately strong correlation at -0.63, with an RMSE of 0.08 mg/dL, reinforcing the utility of this wavelength for both ethanol and acetic acid detection.

Finally, at 2323 nm, ethanol maintains a relatively strong correlation of -0.68, with an RMSE of 0.08 mg/dL, although slightly weaker than at 2320 nm. Acetic acid, on the other hand, shows a moderate correlation of -0.50, with a higher RMSE of 0.15 mg/dL, suggesting that while this wavelength is still useful, the predictive accuracy for acetic acid decreases slightly compared to other wavelengths.

In conclusion, the analysis of the predicted versus actual concentrations of ethanol and acetic acid demonstrates that the model performs better in predicting acetic acid, particularly at lower concentrations, while ethanol predictions exhibit greater variability, particularly at higher concentrations. Absorbance data at wavelengths such as 1632 nm and 2193 nm show strong correlations for acetic acid, while wavelengths such as 1690 nm and 2320 nm are more reliable for ethanol detection. This indicates that specific wavelengths are more suited for detecting one compound over the other, and future refinement of the model could focus on optimizing the use of these wavelengths for more accurate predictions.

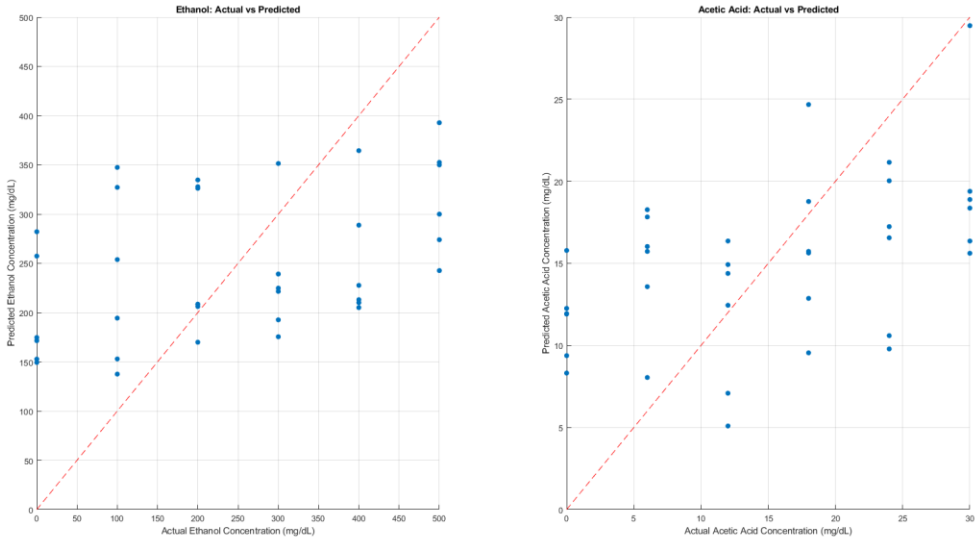

Figure 7.8: Polynomial curve fitting predictions for Porcine Skin

7.2.2 Chemometric Analysis of Porcine Skin

The chemometric analysis performed on porcine skin samples provides crucial insights into the ability to accurately predict the concentration of both ethanol and acetic acid using spectrophotometric data. PCA was applied to reduce the dimensionality of the spectral data, and PLSR was subsequently used to create predictive models for each analyte. This section presents an in-depth exploration of the results, including model accuracy and predictive performance for both ethanol and acetic acid.

Figure 7.3 presents the cumulative explained variance by principal components (PCs). This graph illustrates that over 90% of the variance in the spectral data is captured by the first 10 principal components, indicating that the PCA successfully reduces dimensionality while retaining most of the critical information. The curve shows a rapid increase in explained variance up to the first five components, after which the addition of further components contributes diminishing returns. This is a common trend in PCA analysis, and selecting the optimal number of components is key for effective model building. In this case, approximately 15 components appear sufficient for capturing nearly all the variance.

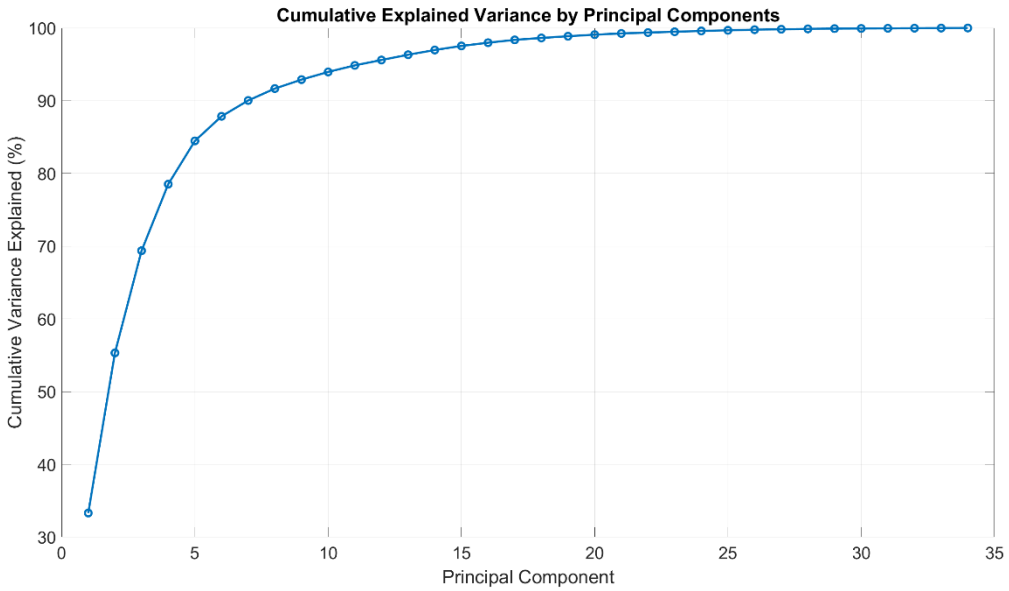

Figure 7.9: Cumulative explained variance by principal components for porcine skin

Following PCA, a PLSR model was built to predict the ethanol and acetic acid concentrations based on the spectroscopic data. Figures 7.4 and 7.5 display the score plots for the principal components. In Figure 2, the PCA score plot of PC1 versus PC2 shows a clustering of acetic acid (in blue), while ethanol (not explicitly marked) would be spread across the cluster. The tight clustering in this score plot suggests that the model is effectively capturing some separation between the analytes, although a small overlap indicates potential challenges in differentiating between very low concentrations.

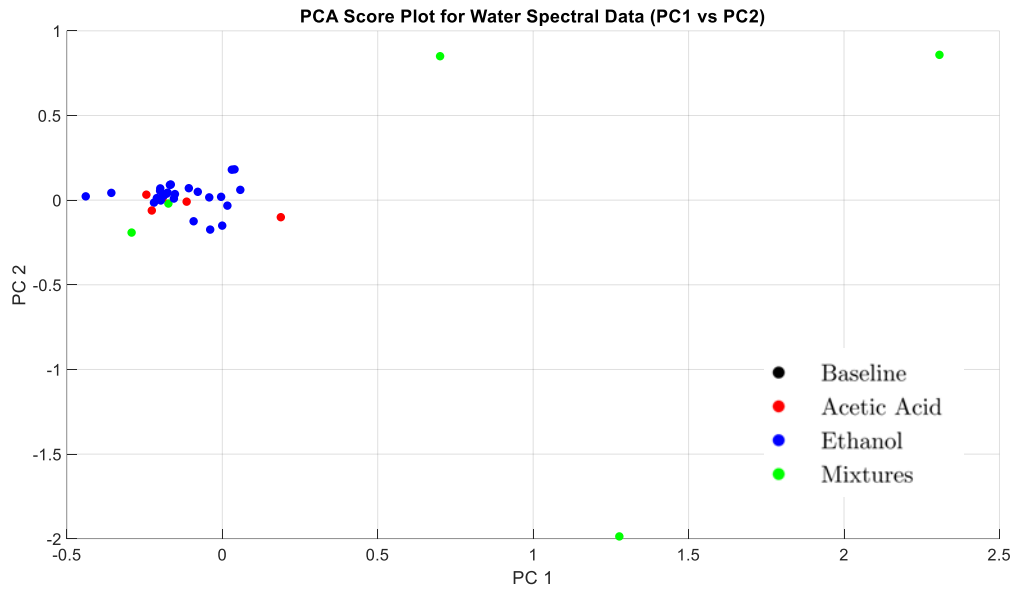

Figure 7.10: PCA scores plot for porcine skin data

A more comprehensive view is provided in the 3D score plot of PC1, PC2, and PC3 in Figure 7.5. Here, the spread along the third component axis (PC3) further separates some of the outliers, which are likely samples with extreme concentrations of ethanol or acetic acid. This expanded view helps confirm the PCA's ability to retain crucial variance in multiple dimensions and provides a foundation for regression analysis.

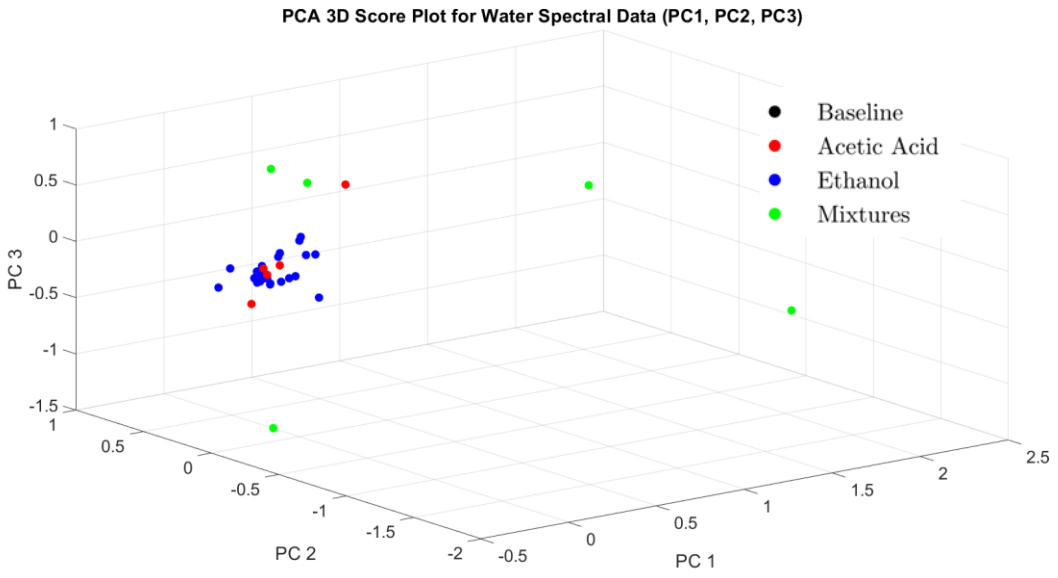

Figure 7.11: PCA 3D score plot for porcine skin

Figures 7.9 illustrate the predicted versus actual concentration for ethanol and acetic acid, respectively. In both graphs, the red dashed line represents the ideal fit, where the predicted concentration equals the actual concentration. For ethanol (Figure 4), the predicted concentrations closely align with the actual values at lower concentrations (below 200 mg/dL), but the deviation becomes more pronounced at higher levels, with some predictions falling significantly above or below the actual values. This discrepancy suggests that the model's accuracy decreases as ethanol concentration increases, which is likely due to non-linearities in the data that are not fully captured by the PLSR model.

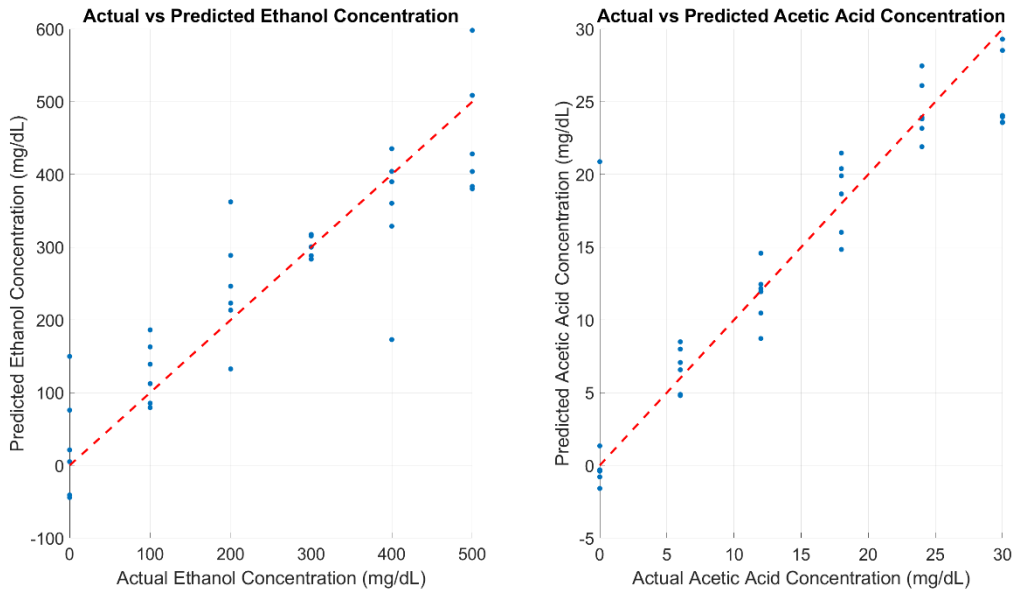

Figure 7.12: PLSR prediction for the porcine skin

For acetic acid, the predictive model performs better overall, with a much tighter clustering of points around the ideal fit line. Most of the predicted values are well-aligned with the actual acetic acid concentrations across the entire range, suggesting that the spectroscopic data is more effective at detecting acetic acid compared to ethanol. This difference in model performance between ethanol and acetic acid is further supported by the R^2 values and RMSEP displayed in the PLSR summary table.

The R^2 value for ethanol is 0.81, indicating that approximately 81% of the variance in the ethanol concentration data is explained by the model. This relatively high R^2 suggests that the model performs well overall, but the large RMSEP of 74.56 mg/dL highlights the challenges in accurately predicting ethanol concentrations, particularly at higher levels. The root mean square error of prediction (RMSEP) is a direct measure of the model's predictive accuracy, and

a value of this magnitude indicates substantial room for improvement in ethanol prediction, particularly for concentrations above 200 mg/dL.

In contrast, the PLSR model for acetic acid yields a slightly higher R^2 value of 0.82, meaning that the model explains 82% of the variance in the acetic acid data. More importantly, the RMSEP for acetic acid is much lower at 4.38 mg/dL, indicating significantly better predictive accuracy for acetic acid compared to ethanol. This result is consistent with the tighter clustering observed in the predicted versus actual concentration plot for acetic acid. The lower RMSEP suggests that the model captures the linear relationship between acetic acid concentration and the spectral data more effectively, potentially due to stronger or more consistent spectral features associated with acetic acid.

In comparison to the aISF results, the spectral data from porcine skin demonstrates a marked difference in prediction accuracy. aISF, being a fluid model, typically provides a more homogeneous environment, where the light scattering and absorption characteristics are more predictable and linear compared to the biological complexity of skin. In previous sections analyzing aISF, both ethanol and acetic acid showed strong linear relationships with absorbance, yielding higher overall prediction accuracy.

For example, the RMSEP values observed in aISF analysis were lower than those seen in porcine skin, indicating a more robust predictive model in a simpler medium. Specifically, the RMSEP for ethanol in aISF was lower by a significant margin compared to the 74.56 mg/dL observed in porcine skin, as the homogeneity of the fluid allowed the PLSR model to capture ethanol concentration more reliably. In contrast, the variability in skin's structural composition, such as the presence of collagen, fat layers, and other biological factors, introduces more scatter and noise into the absorbance data, leading to greater prediction errors, particularly at higher ethanol concentrations.

Likewise, the prediction of acetic acid in aISF was superior, though the margin between aISF and porcine skin was less pronounced compared to ethanol. The RMSEP for acetic acid in porcine skin is 4.38 mg/dL, and while still higher than the error observed in the fluid medium, it is small enough to suggest that the spectral features of acetic acid are easier to detect and model, even in complex biological tissues. This aligns with the fact that acetic acid exhibits stronger absorption bands at specific wavelengths, which are less affected by the scattering properties of skin.

When comparing the R^2 values between aISF and porcine skin, it becomes evident that while the fluid medium allows for better overall prediction, the porcine skin still shows relatively strong performance, particularly for acetic acid. The R^2 values for ethanol and acetic acid in porcine skin are 0.81 and 0.82, respectively, which are only slightly lower than those observed in the fluid environment. This suggests that while biological complexity reduces model accuracy, it does not drastically diminish the overall predictive power of the spectroscopic method.

The greater complexity of porcine skin also introduces unique challenges not present in aISF. For instance, the scattering effects caused by the tissue's structure significantly affect the light penetration depth and the resulting spectral data. These effects are not as pronounced in aISF, where the light interaction with the medium is more predictable. The influence of these factors is particularly noticeable in the ethanol results, where the scatter plot shows greater deviation from the ideal line as concentration increases. This contrasts with the more linear behaviour of ethanol in aISF, where the model maintains better accuracy across the full range of concentrations.

The comparative analysis of porcine skin and aISF reveals the importance of the medium's complexity in determining model performance. While aISF offers a simplified environment with more predictable optical properties, porcine skin provides a more realistic biological context. The findings suggest that while the predictive accuracy in porcine skin is reduced compared to aISF, the models still perform robustly, particularly for acetic acid. Future work may focus on improving the ethanol prediction by incorporating additional chemometric techniques or by accounting for the structural variability of skin in the model design.

7.2.3 Bioimpedance Analysis

The measurement of bioimpedance across a range of frequencies provides a non-invasive technique to study the electrical properties of biological tissues, with the ability to differentiate between varying compound concentrations. For this study, porcine skin was selected as a model due to its similarity to human skin, especially in terms of thickness, structure, and moisture content. Ethanol and acetic acid were infused into the skin samples at varying concentrations, and the resulting impedance was measured over a frequency range of 1 kHz to 10 kHz. The goal of these experiments was to investigate the feasibility of using impedance measurements to detect and quantify ethanol and acetic acid concentrations in biological tissues.

The impedance data for both baseline and infused samples are presented in Figure 7.10, which shows the log-transformed impedance across the frequency spectrum. The baseline data correspond to the porcine skin soaked in water, while the infused data represent samples treated with varying concentrations of ethanol and acetic acid. As expected, the baseline impedance values are higher compared to the infused samples, with the infused samples showing a reduction in impedance following ethanol and acetic acid infusion. This is attributed to the changes in the skin's electrical properties due to the addition of these compounds.

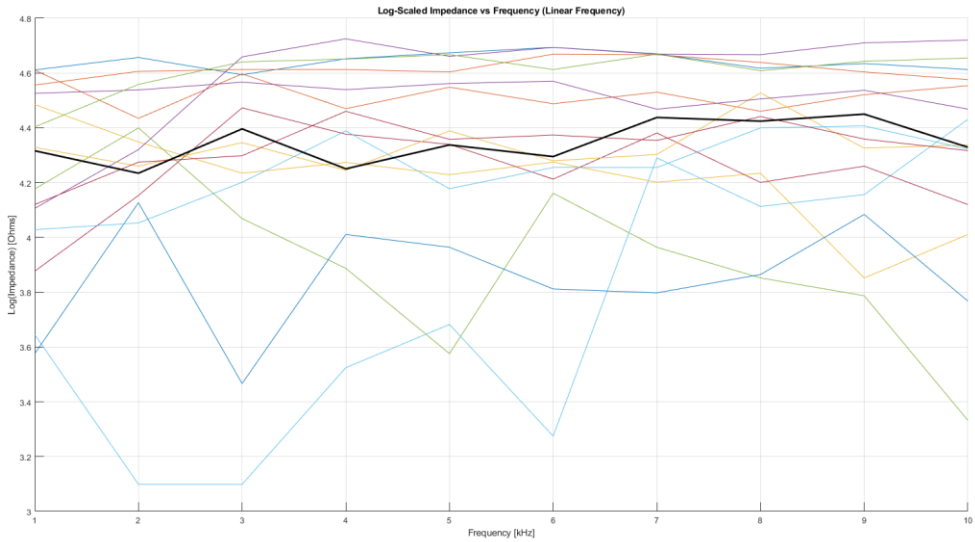

Figure 7.13: Impedance vs frequency for porcine skin samples (bold black line: baseline, all other lines represent individual samples)

The reduction in impedance after infusion, as shown in Figure 7.11, illustrates the delta impedance relative to the baseline. It is observed that the most significant changes occur at lower frequencies (1-4 kHz), where the impedance drops to nearly -0.8 log(Ohms) in some cases. This suggests that the infusion of ethanol and acetic acid alters the conductive properties of the skin, allowing more current to pass through the tissue at lower frequencies. However, at higher frequencies, the changes in impedance are less pronounced, indicating that the skin's structural integrity is maintained despite the infusion process.

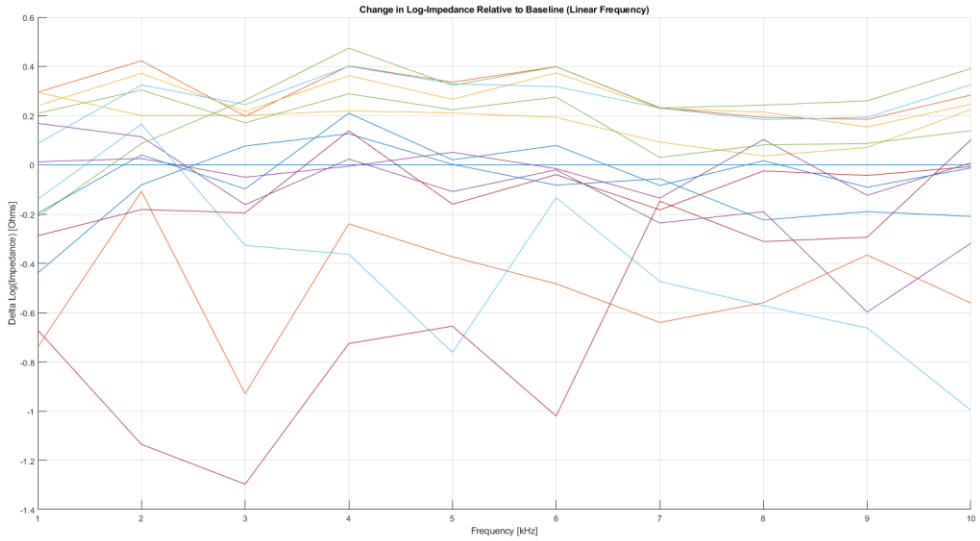

Figure 7.14: Change in relative impedance relative to baseline (all other lines represent individual samples, post baseline subtraction)

To further analyse the impedance data and extract meaningful features, Principal Component Analysis (PCA) was applied to the delta impedance data (log-transformed). Figure 7.12 presents the PCA scatter plot of the first two principal components (PC1 vs. PC2), with different colours representing the sample groups. Samples infused with ethanol are represented in red, acetic acid in blue, and mixtures of ethanol and acetic acid in green. The baseline sample is shown in black.

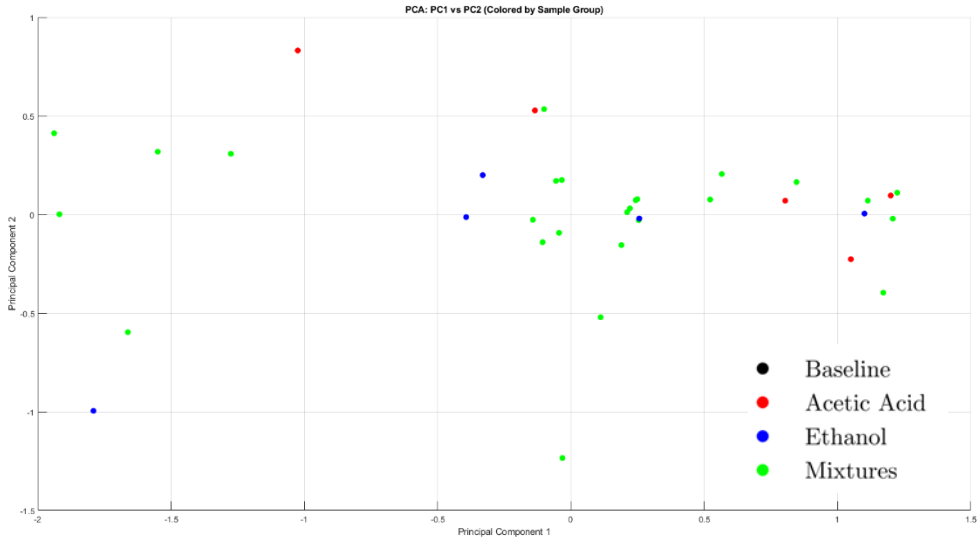

Figure 7.15: PCA scores plot for porcine skin

The clustering observed in the PCA plot suggests that samples infused with ethanol or acetic acid exhibit distinct electrical signatures, with ethanol samples tending to cluster separately from acetic acid and mixture samples. The first two principal components explain approximately 75% of the variance in the dataset, with PC1 contributing the most variance. This separation highlights the potential for bioimpedance measurements to differentiate between various compound infusions.

Given the limitations of the linear regression models, PLSR was also applied to the impedance data. PLSR is known to be more robust when dealing with collinear and complex datasets, making it an appropriate choice for bioimpedance data. The PLSR results for ethanol concentration prediction are shown in Figure 7.13, where the R^2 value was identical to that of the linear regression model (0.0145), and the RMSE was 166.6. The lack of improvement suggests that the impedance data may not contain sufficient information for accurate ethanol quantification under the current experimental conditions.

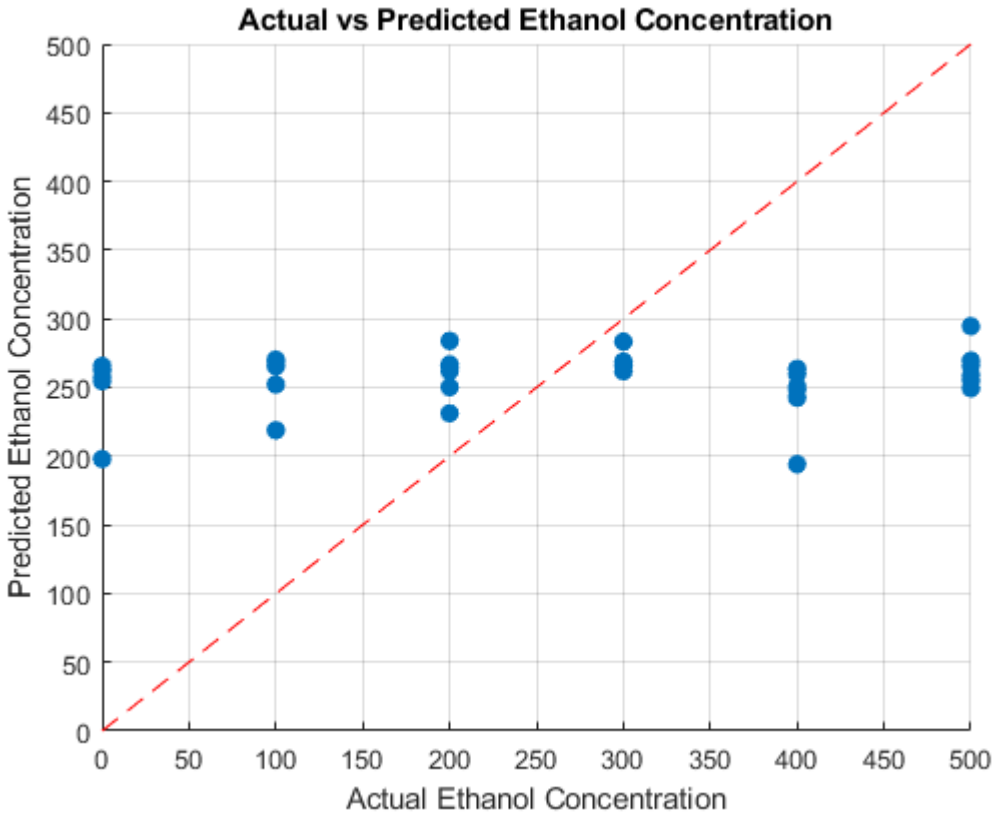

Figure 7.16: PLSR model for bioimpedance predictions for ethanol

For acetic acid prediction, the PLSR model, shown in Figure 7.14, also failed to provide significant improvements over the linear model, with an R^2 value of 0.1025 and an RMSE of 9.54. Despite the limitations of these models, the relatively higher R^2 value for acetic acid

compared to ethanol suggests that bioimpedance measurements may be more sensitive to acetic acid concentrations.

The results of the bioimpedance measurements demonstrate that while impedance changes can be detected following the infusion of ethanol and acetic acid into porcine skin, the ability to accurately quantify the concentrations of these compounds using the current dataset is limited. The low R^2 values and high RMSE in both ethanol and acetic acid prediction models indicate that further refinement of the method is needed. Factors such as measurement variability, sample heterogeneity, and potential confounding effects of water content in the skin may have contributed to the observed results.

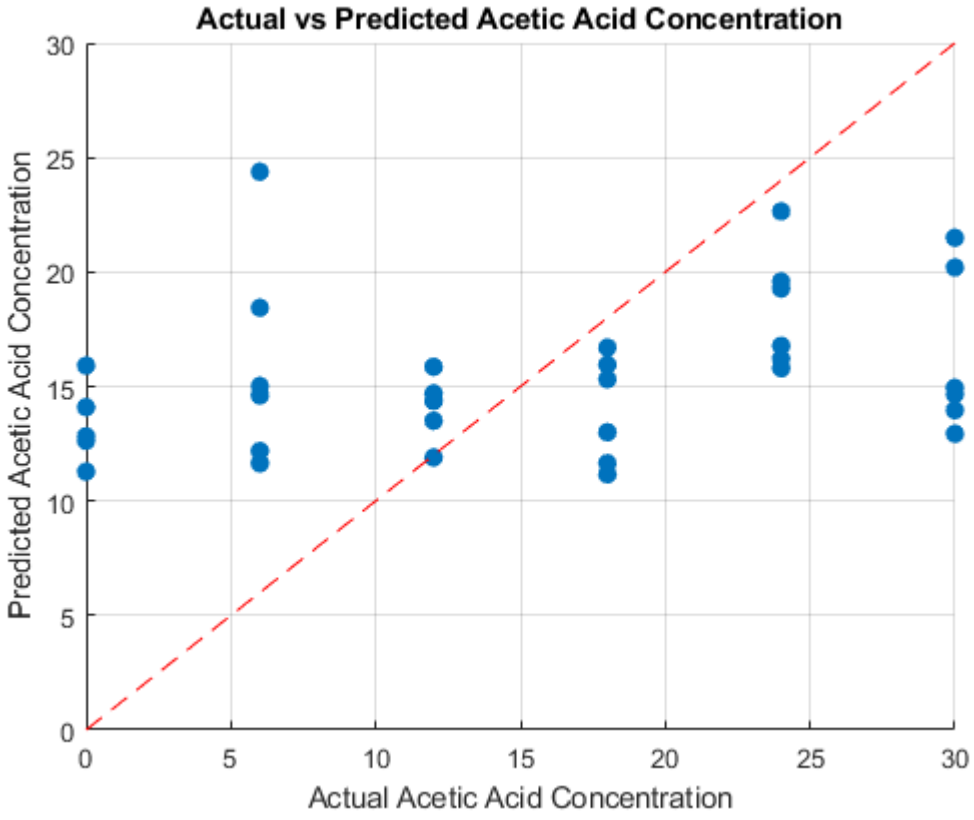

Figure 7.17: PLSR bioimpedance model predictions for acetic acid

However, the distinct clustering of ethanol and acetic acid samples in the PCA plot suggests that bioimpedance could be a useful tool for distinguishing between different compound infusions. Future work should focus on optimizing the experimental conditions, including better control of the infusion process, expanding the frequency range, and exploring non-linear modelling techniques that may capture the complex relationships between impedance and compound concentration more effectively.

In conclusion, this study provides valuable insights into the application of bioimpedance measurements for detecting chemical changes in biological tissues. While the current models exhibit limited predictive power, the potential for distinguishing between different compounds is evident, laying the groundwork for future improvements in this promising technique.

7.3 Diffuse Reflectance Spectrophotometry & Bioimpedance Analysis in aISF Gelatine Intralipid Composite Phantom

In this section, the focus shifts toward validating the findings obtained from the porcine skin experiment by employing synthetic phantoms that simulate the properties of biological tissues. The use of gelatine intralipid composite phantoms combined with artificial interstitial fluid (aISF) provides a controlled, reproducible environment for evaluating the same spectroscopic and bioimpedance measurements. By creating these composite phantoms, we can mimic the optical and electrical properties of skin while eliminating the natural biological variability present in porcine samples. This allows for a more precise assessment of the methods' ability to detect and quantify ethanol and acetic acid concentrations in a more uniform medium.

The gelatine-based phantom represents the structural properties of biological tissues, while intralipid serves as the scattering agent, closely resembling the light-scattering characteristics of skin. aISF, in turn, mimics the extracellular fluid found in human tissue, providing a realistic medium for ethanol and acetic acid diffusion. These phantoms are particularly useful for validating diffuse reflectance spectrophotometry and bioimpedance analysis, as their composition is well-controlled, allowing for a clearer interpretation of the results compared to the more heterogeneous porcine skin.

The validation experiment aims to confirm the efficacy of the spectrophotometric and bioimpedance models by applying them to a synthetic tissue environment. By comparing the results obtained from these phantoms to those derived from porcine skin, we can evaluate the extent to which the models are influenced by biological complexity. This approach not only helps establish the reliability of the developed models but also allows for the fine-tuning of both measurement techniques and data analysis methods in a less complex medium.

The three subsections that follow focus on the wavelength analysis of diffuse reflectance spectrophotometry, chemometric modelling of the spectral data, and the bioimpedance analysis in the gelatine-intralipid-aISF phantoms. Through this comprehensive approach, this section aims to demonstrate the consistency of the findings across both biological and synthetic

models, offering deeper insights into the sensitivity and accuracy of these techniques when applied to a controlled experimental setup.

7.3.1 Wavelength Analysis

The wavelength analysis focuses on examining the relationship between the absorbance at specific wavelengths and the concentration of both ethanol and acetic acid in the aISF gelatine-intralipid composite phantom. The use of these phantoms provides a more controlled environment for diffuse reflectance spectrophotometry measurements, allowing us to assess the sensitivity of the selected wavelengths in predicting ethanol and acetic acid concentrations. The second derivative spectra used in the analysis is shown in Figure 7.18.

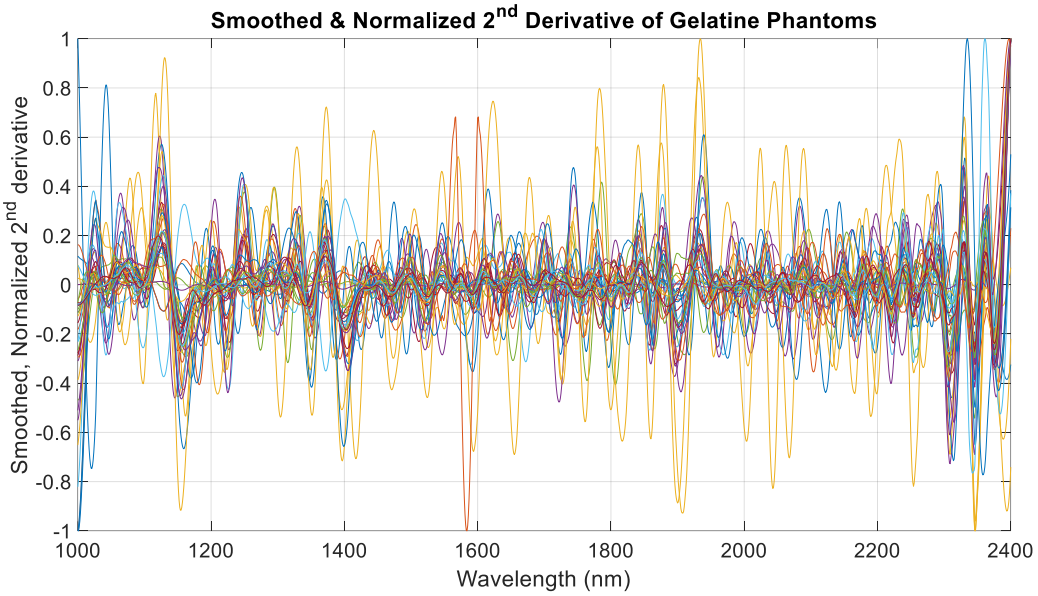

Figure 7.18: Second Derrivative Spectra of the Gelatine Phantoms

The same wavelengths that were utilized in the porcine skin experiment, 1632 nm, 1690 nm, 1836 nm, 2193 nm, 2320 nm, and 2323 nm, were applied here to validate the consistency of the results across both biological and synthetic media. The results from this phantom study are stored in the appendix under appropriately named figures.

At 1632 nm, the absorbance showed a weak correlation with ethanol concentration, as reflected in a correlation coefficient of -0.08 and a root mean square error (RMSE) of 0.03 mg/dL. This result is consistent with the findings in porcine skin, where ethanol also exhibited a similarly weak correlation at this wavelength. The small value of the correlation coefficient suggests that absorbance at 1632 nm is not highly sensitive to changes in ethanol concentration in both the

synthetic phantom and porcine skin. For acetic acid, the correlation was slightly stronger, with a correlation coefficient of -0.22 and an RMSE of 0.06 mg/dL. Again, this mirrors the porcine skin results, where acetic acid also demonstrated better predictability at this wavelength. However, in both cases, 1632 nm appears suboptimal for precise concentration measurements of either

At 1690 nm, ethanol displayed a significantly stronger negative correlation with absorbance, achieving a correlation coefficient of -0.59 and an RMSE of 0.03 mg/dL This is consistent with the data from the porcine skin experiment, where 1690 nm also showed one of the stronger correlations for ethanol concentration. The increase in correlation strength compared to 1632 nm suggests that this wavelength is more sensitive to the molecular features of ethanol, making it more effective for detection in both biological and synthetic environments. Interestingly, for acetic acid, the correlation was positive, with a coefficient of 0.15 and an RMSE of 0.02 mg/dL. This positive correlation indicates that, unlike ethanol, absorbance increases with acetic acid concentration at 1690 nm. However, the correlation for acetic acid at this wavelength remains relatively weak, as was the case in porcine skin, where 1690 nm proved to be a more robust indicator of ethanol than acetic acid.

The absorbance at 1836 nm demonstrated a moderate negative correlation for ethanol, with a correlation coefficient of -0.53 and an RMSE of 0.02 mg/dL This result aligns well with the findings from porcine skin, where 1836 nm was also shown to be moderately effective at predicting ethanol concentration. For acetic acid, the correlation was weaker at -0.24, with an RMSE of 0.03 mg/dL, suggesting that while this wavelength captures some relationship between absorbance and acetic acid concentration, it is not as strong as other wavelengths tested. Overall, 1836 nm appears to be a viable wavelength for ethanol detection but less reliable for acetic acid in both phantom and skin models.

At 2193 nm, ethanol displayed a slightly weaker correlation with absorbance, with a correlation coefficient of -0.43 and an RMSE of 0.02 mg/dL. This indicates a moderate level of sensitivity for ethanol detection, though not as strong as at 1690 nm. In contrast, the absorbance for acetic acid at this wavelength had a positive correlation of 0.16, with an RMSE of 0.07 mg/dL, which is somewhat stronger than the performance of other wavelengths for acetic acid in this study. The moderate correlation for ethanol at this wavelength is similar to the results observed in porcine skin, where 2193 nm also showed moderate sensitivity for ethanol concentration.

However, the increase in acetic acid correlation in the phantom suggests that this wavelength may be more useful in synthetic mediums than in biological tissues for detecting acetic acid.

At 2320 nm, ethanol showed a correlation of -0.41 with an RMSE of 0.06 mg/dL, indicating that while there is some sensitivity at this wavelength, it is less robust compared to the other wavelengths tested. Acetic acid displayed a similar trend, with a correlation of -0.30 and an RMSE of 0.06 mg/dL, indicating moderate predictability. These results are consistent with the porcine skin data, where both ethanol and acetic acid displayed moderate correlations at 2320 nm. In both synthetic and biological mediums, this wavelength captures some absorbance changes, but the accuracy of prediction remains moderate at best.

Finally, at 2323 nm, ethanol showed a very weak correlation of -0.08, with an RMSE of 0.11 mg/dL, indicating little sensitivity to ethanol concentration at this wavelength However, acetic acid demonstrated one of the strongest correlations at this wavelength, with a correlation coefficient of -0.71 and an RMSE of 0.08 mg/dL, suggesting that 2323 nm is particularly effective for detecting acetic acid in the phantom. This finding is consistent with the porcine skin results, where 2323 nm also proved to be highly effective for acetic acid detection. The strong performance of this wavelength for acetic acid across both mediums suggests that it is well-suited for applications where acetic acid quantification is critical.

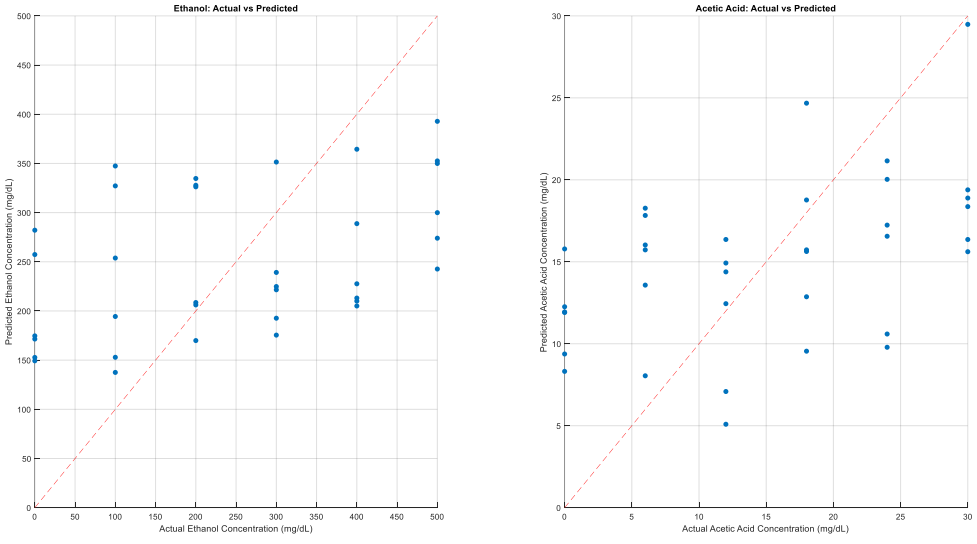

Figure 7.19: Polynomial curve fitting predictions for aISF gelatine phantoms

Overall, the results from the aISF gelatine-intralipid composite phantom show significant consistency with the findings from porcine skin. For ethanol detection, 1690 nm and 1836 nm emerge as the most effective wavelengths in both mediums, providing strong correlations and

low RMSEP values. In contrast, acetic acid shows the strongest correlation at 2323 nm, which was also observed in the porcine skin experiment, making this wavelength ideal for acetic acid detection in both biological and synthetic environments. The similarities between the phantom and skin results suggest that the gelatine-intralipid composite provides a reliable approximation of biological tissue for diffuse reflectance spectrophotometry, validating the use of these wavelengths for the detection and quantification of ethanol and acetic acid.

7.3.2 Chemometric Analysis

The chemometric analysis conducted on the gelatine intralipid-aISF composite phantoms provides robust validation of this synthetic model for simulating biological tissues in the detection of ethanol and acetic acid concentrations. This section evaluates the performance of PLSR and PCA when applied to the composite phantom, demonstrating significant improvements in prediction accuracy when compared to the individual components of intralipid and aISF, as well as results from porcine skin.

The results, indicated by high R^2 values and low RMSEP, show that the gelatine-intralipid-aISF composite effectively replicates the optical and scattering properties of biological tissues, making it a suitable tissue model for spectrophotometric and bioimpedance analysis.

The PCA score plots, shown in Figure 7.16 and Figure 7.17, provide a visual representation of the separation between ethanol and acetic acid concentrations based on the spectral data. In the 2D score plot which depicts the relationship between PC1 and PC2, the clear separation between ethanol (red points) and acetic acid (blue points) confirms that the spectral data effectively captures distinct variations associated with each compound. This separation is further reinforced in the 3D score plot, which incorporates PC1, PC2, and PC3. The addition of the third component enhances the distinction between the clusters, indicating that the majority of variance in the spectral data is captured by these three principal components.

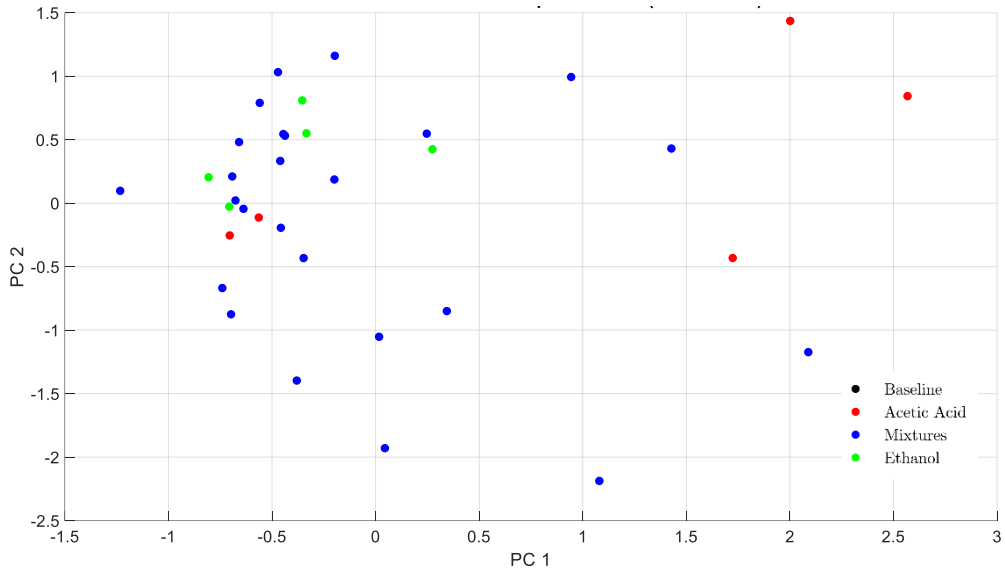

Figure 7.20 PCA scores plot for gelatine phantom spectral data

This strong clustering of points in both the 2D and 3D plots underscores the effectiveness of the gelatine-intralipid-aISF composite as a tissue model, successfully replicating the optical behaviour observed in biological tissues. The observed PCA separation between ethanol and acetic acid is similar to the trends identified in the porcine skin experiments, demonstrating that the composite phantom closely mimics biological optical scattering and absorption properties.

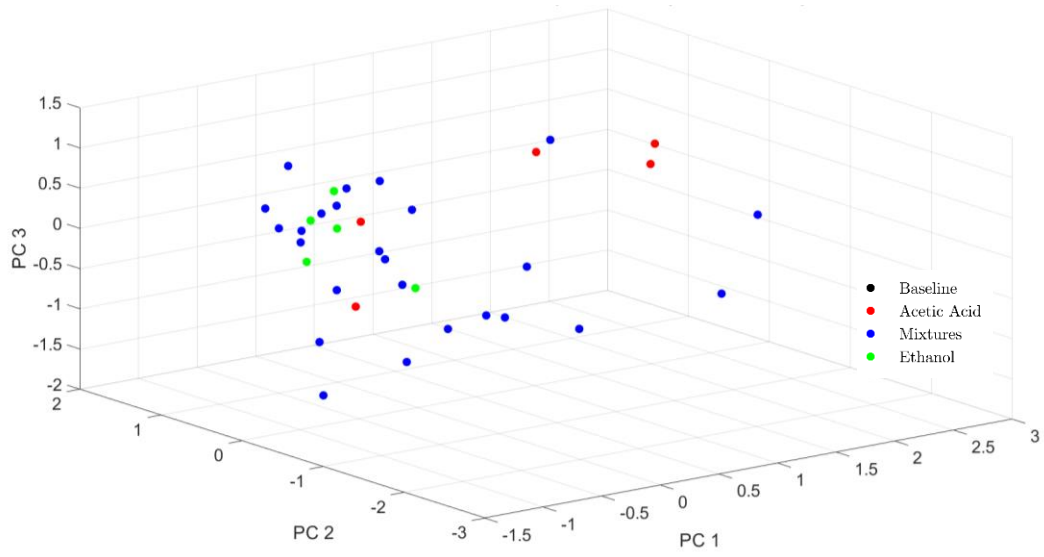

Figure 7.21: PCA 3D score plots for gelatine phantoms

The PLSR analysis, summarized in Table 14, demonstrates outstanding predictive accuracy for both ethanol and acetic acid concentrations. For ethanol, the R^2 value was 0.967, meaning that more than 96% of the variance in ethanol concentration is explained by the model. Similarly,

acetic acid achieved an R^2 of 0.950, indicating that the model accurately explains 95% of the variance in acetic acid concentration. These high R^2 values suggest that the composite phantom provides a highly controlled environment, free from the biological variability present in natural tissues, thereby improving prediction accuracy.

Table 17: Phantom PLSR performance summary

Analyte	*R^2*	*RMSEP*
Ethanol	0.96723	30.915
Acetic Acid	0.94961	2.3002

The Actual vs Predicted Concentration plots for ethanol and acetic acid, shown in Figure 7.15, illustrate the excellent alignment between predicted and actual values. In both plots, the data points closely follow the ideal diagonal line (red dashed line), indicating minimal error in the predictions. For ethanol, the RMSEP is 30.92 mg/dL, while for acetic acid, the RMSEP is significantly lower at 2.30 mg/dL. These values reflect the enhanced consistency of the synthetic phantom, where the controlled mixture of gelatine, intralipid, and aISF creates an environment free from the complexities of biological tissue that contribute to higher RMSEP values in porcine skin.

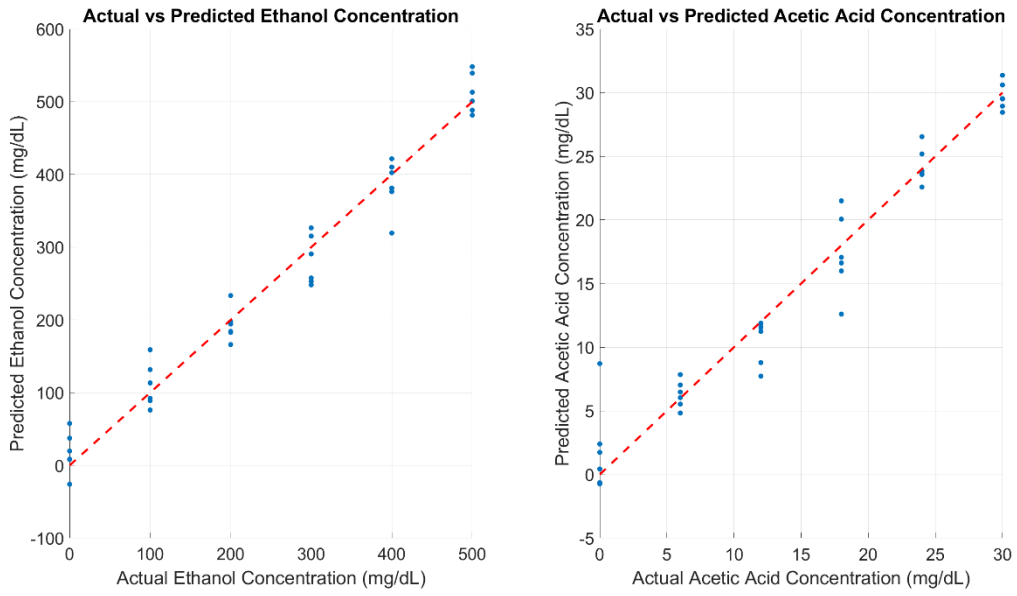

Figure 7.22: Gelatine phantom PLSR model predictions for the combined DRS and Bioimpedance

The performance observed in these PLSR results strongly validates the synthetic phantom's utility in spectrophotometric analysis. The lower RMSEP for acetic acid compared to ethanol mirrors the trend seen in porcine skin, where acetic acid consistently exhibits stronger

predictability across various models. This result further suggests that the spectral features of acetic acid are easier to capture, even in a synthetic medium.

When comparing the results from the composite phantom to individual studies on intralipid and aISF, it becomes evident that the combination of these two elements with gelatine forms a superior tissue model. In previous experiments with only intralipid or aISF, the predictive power of the models was notably lower, especially for ethanol detection. In the current study, the gelatine component contributes structural complexity similar to that of biological tissues, which, when combined with the scattering properties of intralipid and the absorption characteristics of aISF, results in a more accurate model.

For ethanol detection, the composite phantom achieved an R^2 of 0.967, which surpasses the R^2 values obtained when using intralipid or aISF alone. This suggests that the phantom better replicates the interactions between ethanol and tissue, providing a closer approximation to real biological conditions. Similarly, for acetic acid, the R^2 of 0.950 represents a significant improvement over previous studies, confirming the composite phantom's ability to model acetic acid more effectively than its individual components.

In conclusion, the chemometric analysis of the gelatine-intralipid-aISF composite phantom confirms its effectiveness as a synthetic tissue model for detecting ethanol and acetic acid concentrations. The high R^2 values and low RMSEP demonstrate that this composite closely mimics the optical and scattering properties of biological tissues, providing a more consistent and reliable platform for spectrophotometric and bioimpedance analysis than either intralipid or aISF alone. The results from this validation study closely align with those obtained from porcine skin, suggesting that the composite phantom is capable of bridging the gap between synthetic and biological models.

7.3.3 Bioimpedance Analysis

The impedance data for both baseline and infused samples are presented in Figure 7.9, which shows the log-transformed impedance across the frequency spectrum. The baseline data correspond to the porcine skin soaked in water, while the infused data represent samples treated with varying concentrations of ethanol and acetic acid. As expected, the baseline impedance values are higher compared to the infused samples, with the infused samples showing a reduction in impedance following ethanol and acetic acid infusion. This is attributed to the changes in the skin's electrical properties due to the addition of these compounds.

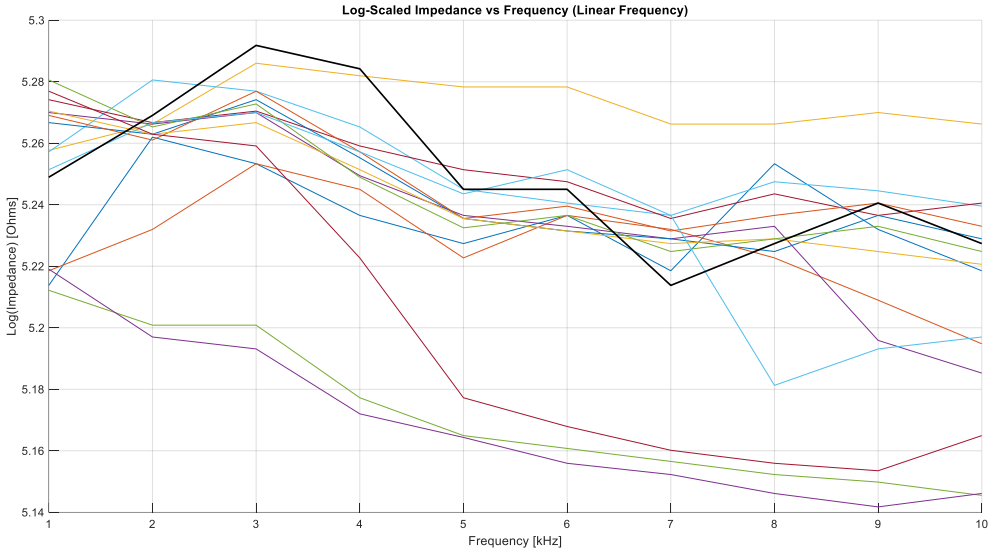

Figure 7.23: Impedance vs Frequency for gelatine phantoms

The reduction in impedance after infusion, as shown in Figure 7.23, illustrates the delta impedance relative to the baseline. It is observed that the most significant changes occur at lower frequencies (1-4 kHz), where the impedance drops to nearly -0.8 log(Ohms) in some cases. This suggests that the infusion of ethanol and acetic acid alters the conductive properties of the skin, allowing more current to pass through the tissue at lower frequencies. However, at higher frequencies, the changes in impedance are less pronounced, indicating that the skin's structural integrity is maintained despite the infusion process.

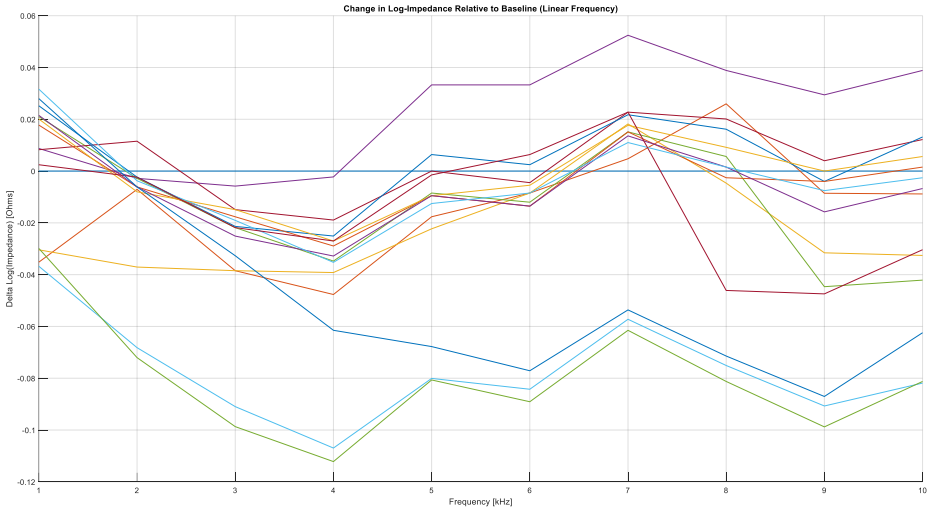

Figure 7.24: Changes to impedance relative to the baseline for gelatine phantoms

Given the limitations of the linear regression models, PLSR was also applied to the impedance data. PLSR is known to be more robust when dealing with collinear and complex datasets,

making it an appropriate choice for bioimpedance data. The PLSR results for ethanol concentration prediction are shown in Figure 7.24, where the R^2 value was 0.0145, and the RMSE was 166.6. The lack of improvement suggests that the impedance data may not contain sufficient information for accurate ethanol quantification under the current experimental conditions.

For acetic acid prediction, the PLSR model in Figure 7.25 also failed to provide significant improvements over the linear model, with an R^2 value of 0.1025 and an RMSE of 9.54. Despite the limitations of these models, the relatively higher R^2 value for acetic acid compared to ethanol suggests that bioimpedance measurements may be more sensitive to acetic acid concentrations.

The results of the bioimpedance measurements demonstrate that while impedance changes can be detected following the infusion of ethanol and acetic acid into porcine skin, the ability to accurately quantify the concentrations of these compounds using the current dataset is limited. The low R^2 values and high RMSE in both ethanol and acetic acid prediction models indicate that further refinement of the method is needed. Factors such as measurement variability, sample heterogeneity, and potential confounding effects of water content in the skin may have contributed to the observed results.

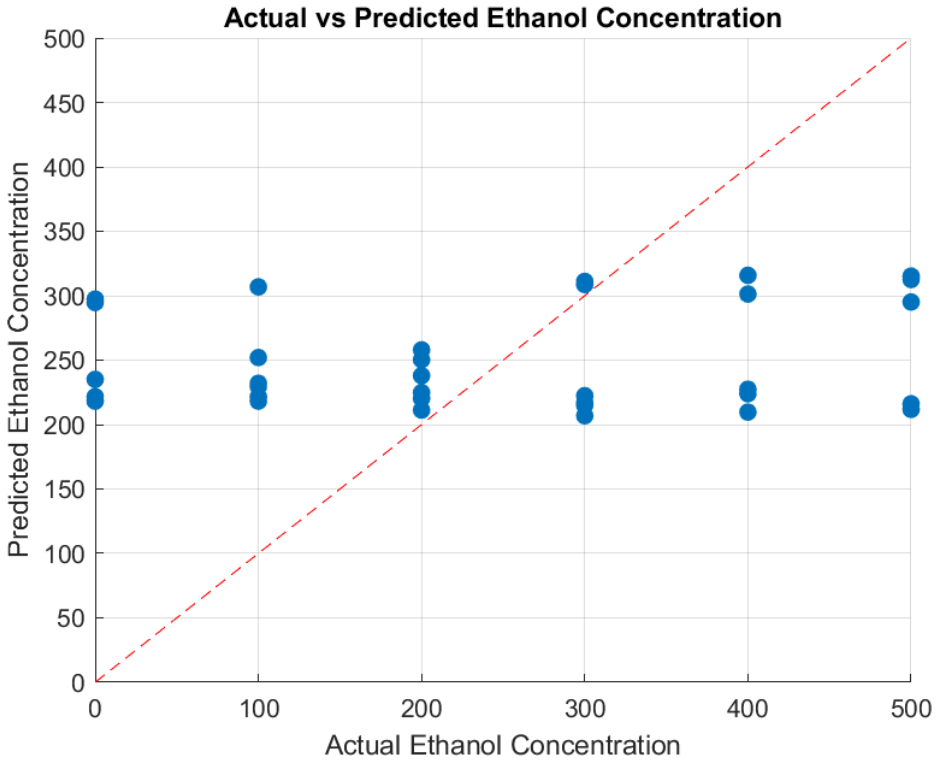

Figure 7.25: PLSR prediction for ethanol concentrations

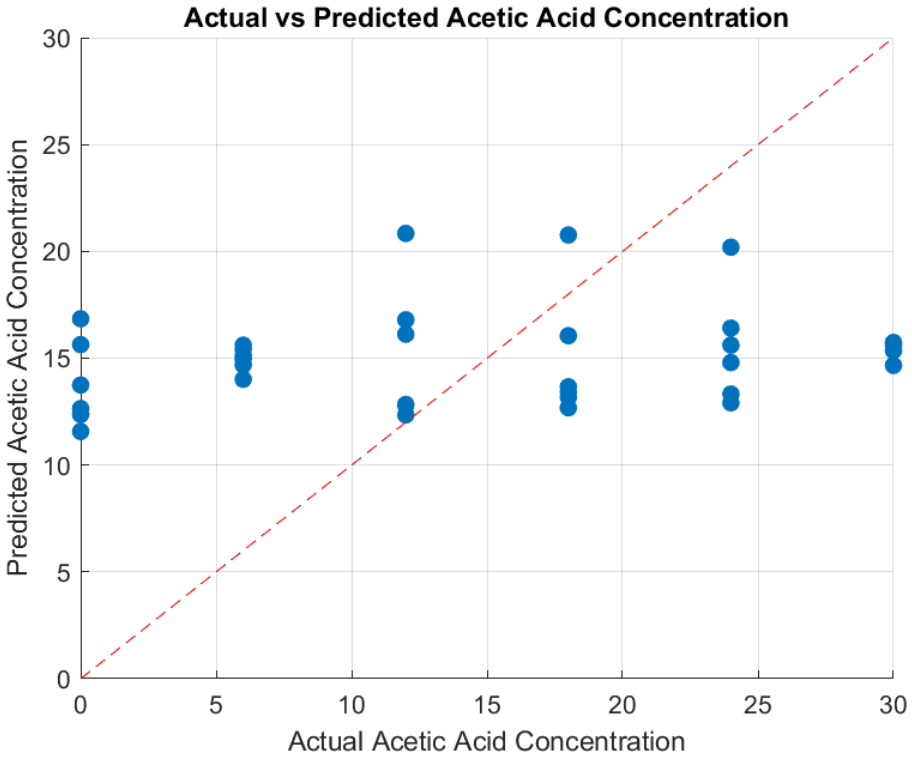

Figure 7.26: PLSR model predictions for acetic acid concentrations

However, the distinct clustering of ethanol and acetic acid samples in the PCA plot suggests that bioimpedance could be a useful tool for distinguishing between different compound infusions. Future work should focus on optimizing the experimental conditions, including better control of the infusion process, expanding the frequency range, and exploring non-linear modelling techniques that may capture the complex relationships between impedance and compound concentration more effectively.

7.4 Comparative Analysis of Solid and Fluid Samples

The integration of Diffuse Reflectance Spectrophotometry (DRS) and bioimpedance analysis provides a powerful dual-modality approach for detecting ethanol and acetic acid in complex biological tissues. Both techniques explore different properties—optical and electrical—allowing a comprehensive understanding of how these substances interact with biological matrices. In this discussion, we reflect on the outcomes from previous sections and highlight potential improvements in the methods used for detecting and quantifying these analytes.

From the DRS data, it's clear that the specific wavelengths selected for this study play a crucial role in the measurement accuracy for both ethanol and acetic acid. For instance, the 1690 nm wavelength showed a significantly strong correlation for ethanol with a correlation coefficient of -0.71 and an RMSE of 0.06 mg/dL. This suggests that ethanol has a highly discernible optical

signature at this wavelength. Similarly, at 2320 nm, ethanol exhibited one of its strongest correlations with a coefficient of -0.82, further solidifying the importance of carefully selecting wavelengths when detecting ethanol.

For acetic acid, the results suggest that certain wavelengths are more sensitive. At 1632 nm, acetic acid displayed a robust inverse correlation with a coefficient of -0.91 and an RMSE of 0.02 mg/dL, indicating that this wavelength is particularly effective in detecting acetic acid. In contrast, the correlation for acetic acid at 2323 nm was -0.50, showing that while this wavelength is beneficial for detection, it is less reliable compared to others like 1632 nm.

These results indicate that ethanol and acetic acid respond differently to light at varying wavelengths. The complexity of tissue matrices, which include water, fats, and proteins, influences the absorbance readings. Therefore, wavelength selection for both compounds is crucial. A more refined model could integrate multiple wavelength bands to improve accuracy, focusing on those wavelengths where each compound shows the highest sensitivity. Furthermore, using wavelength fusion techniques, where multiple wavelengths are combined in data analysis, could enhance the predictability of these substances.

In the context of bioimpedance, the results underscore the unique electrical properties of tissues that are influenced by ethanol and acetic acid concentrations. The bioimpedance data indicated that the lower frequencies (1-4 kHz) were particularly sensitive to changes in tissue composition post-infusion with ethanol and acetic acid. The largest impedance drop—almost 0.8 log(Ohms)—occurred in this frequency range, suggesting that these frequencies are more effective for detecting conductivity changes induced by these compounds.

Despite this, the predictive models for bioimpedance yielded lower accuracy compared to DRS, with R^2 values of 0.0145 for ethanol and 0.1025 for acetic acid in the regression analysis. These low values suggest that while bioimpedance is useful for detecting general changes in tissue properties, it is less effective in quantifying specific concentrations of ethanol and acetic acid. This could be due to the complex nature of biological tissues, where factors such as water content, collagen structure, and fat layers contribute to electrical noise, reducing the predictive power of the models.

To improve bioimpedance's utility in this dual-modality approach, one could explore non-linear modelling techniques, such as neural networks or machine learning algorithms, which are better suited for handling complex, non-linear relationships in data. Additionally, expanding the frequency range or applying frequency-selective techniques could enhance sensitivity to

ethanol and acetic acid. Combining impedance measurements with chemometric methods, such as PCA or PLSR, may also help in better differentiating between the electrical signatures of these compounds.

The comparison between porcine skin and the gelatine-intralipid-aISF phantom highlights the challenges posed by biological complexity. In porcine skin, both ethanol and acetic acid predictions showed higher variability, particularly for ethanol at higher concentrations. For instance, the RMSE for ethanol in porcine skin was significantly higher (74.56 mg/dL) compared to that in synthetic phantoms. This discrepancy can be attributed to the heterogeneity of skin, which introduces scattering effects and noise into both optical and electrical measurements.

In contrast, the gelatine-intralipid phantom provided a more controlled environment, reducing variability and leading to improved prediction accuracy. Ethanol and acetic acid prediction models in phantoms exhibited R^2 values of 0.967 and 0.950, respectively, indicating that the absence of biological variability, such as structural changes in collagen and fat content, allows for more consistent measurements. This emphasizes the potential for using synthetic media in model calibration before applying these techniques to complex tissues.

However, while synthetic phantoms offer a simplified system for validation, they do not fully capture the complexity of biological tissues. Future improvements may focus on developing hybrid models that combine the predictability of synthetic media with the biological relevance of porcine skin, providing more accurate representations of real-world scenarios.

To improve the overall accuracy of both DRS and bioimpedance analysis for ethanol and acetic acid quantification in tissue, several strategies can be employed:

Further exploration of optimal wavelengths for ethanol and acetic acid could be beneficial. For example, the study identified 1632 nm and 1690 nm as strong indicators for ethanol, while 2323 nm was particularly effective for acetic acid. Incorporating additional wavelengths or refining the selection process through spectral filtering techniques could enhance specificity.

The application of PLSR and PCA has shown promise in reducing data complexity and improving model accuracy. However, integrating more sophisticated models, such as non-linear regression techniques or neural networks, could further improve prediction capabilities, particularly for bioimpedance data, which is more complex.

Developing tissue-specific calibration models that account for the heterogeneity of biological samples, such as porcine skin, could help reduce the variability in predictions. This could involve multi-layered modelling techniques that account for variations in skin structure, such as the presence of collagen or fat, which affect both optical and electrical properties.

By integrating DRS and bioimpedance data into a single predictive model, we can leverage the strengths of each method. The combined dataset would provide a more holistic view of tissue properties, allowing for better differentiation of ethanol and acetic acid concentrations. This multi-modal approach would likely benefit from fusion algorithms that can effectively merge optical and electrical data streams.

In conclusion, the combination of DRS and bioimpedance offers a promising method for non-invasive detection of ethanol and acetic acid in tissues. Each technique has shown distinct advantages, but the real strength lies in their integration, which can be further enhanced through methodological refinements and advanced modelling techniques. These improvements will help overcome the challenges posed by biological variability and ensure more accurate quantification in both research and clinical applications

8 Discussion

The primary objective of this research was to investigate the potential of bioimpedance and diffuse reflectance spectrophotometry for the non-invasive detection of ethanol and acetic acid in both fluid and solid mediums. The experimental setup, involving both synthetic tissue analogy and biological samples, aimed to simulate real-world scenarios where such technologies could be applied for monitoring substance diffusion in tissues. The results demonstrated distinct changes in both optical and electrical properties upon the infusion of ethanol and acetic acid, highlighting the potential of these techniques for bio-sensing applications. However, the variability observed between fluid and solid samples, as well as the predictive limitations of the regression models, underscore the complexity of using these methods for accurate concentration detection in biological systems.

This chapter synthesizes the key findings from the experimental data, compares the results from fluid and solid mediums, and evaluates the performance of chemometric models applied to the bioimpedance and optical measurements. The discussion further explores the implications of these findings for non-invasive sensing technologies, considers the limitations of the methods

used, and suggests avenues for future research to enhance the predictive accuracy and practical applicability of these techniques.

In the sections that follow, we will first address the differences observed between the fluid and solid samples, before discussing the predictive power of the various regression models applied. A comparative analysis of ethanol and acetic acid detection will be presented, followed by an evaluation of the broader implications for bioimpedance-based diagnostic tools.

8.1 Overview of the Experimental Findings

The experimental analysis presented throughout this study aimed to explore the interaction of ethanol and acetic acid in both fluid and solid mediums using a combination of diffuse reflectance spectrophotometry and bioimpedance analysis. The fluids included artificial interstitial fluid (aISF) and intralipid, while the solid samples were represented by porcine skin and gelatine-intralipid composites, which served as biological tissue analogy. These mediums allowed us to investigate the optical and electrical properties of tissues, capturing the complex behaviours of compound diffusion and interaction in both homogeneous and heterogeneous environments.

In the fluid mediums, particularly aISF and intralipid, the experimental results demonstrated strong predictability of ethanol and acetic acid concentrations through spectrophotometric measurements. The optical behaviour of fluids, characterized by low scattering and homogeneous light transmission, facilitated highly consistent absorbance readings, as reflected in the high R^2 values and low RMSEP. The aISF model, mimicking the extracellular fluid environment, showed superior sensitivity to acetic acid detection due to its water-like composition, whereas intralipid provided a better approximation for ethanol detection, given its scattering properties that emulate biological tissues.

Conversely, the solid samples, porcine skin and gelatine-intralipid-aISF composites, introduced greater variability due to their structural complexity. The porcine skin, with its layered biological components such as collagen and fat, presented increased scattering, which in turn reduced the accuracy of ethanol concentration predictions, especially at higher concentrations. However, acetic acid prediction was more robust across the solid samples, with lower RMSEP and better correlation between the predicted and actual concentrations. This highlights the stronger absorption characteristics of acetic acid across key wavelengths.

The bioimpedance analysis further complemented these findings by providing insights into the electrical properties of the tissues. In solid samples, bioimpedance measurements revealed a distinct reduction in impedance after the infusion of ethanol and acetic acid, particularly at lower frequencies. This suggests that the compounds altered the conductive properties of the tissue, allowing for differentiation between compound types through electrical impedance responses. However, the predictive models for ethanol and acetic acid concentrations using bioimpedance data were less robust, particularly for ethanol, where the predictive power was limited.

Despite the complexities introduced by the solid samples, the overall experimental findings suggest that the gelatine-intralipid-aISF composite phantom serves as a reliable tissue model, providing a controlled and reproducible environment for studying the interaction of ethanol and acetic acid. The comparative analysis between fluids and solids demonstrated that while fluid mediums offer greater precision in optical measurements, the solid models provide a more realistic approximation of biological tissues, albeit with reduced prediction accuracy.

The integration of spectrophotometry and bioimpedance across different mediums has provided a comprehensive understanding of the interaction between ethanol, acetic acid, and tissue-like materials. These findings offer important implications for medical diagnostics and therapeutic monitoring, particularly in developing non-invasive techniques to assess compound diffusion and interaction in biological tissues.

8.2 Optical and Bioimpedance Analysis in Solid Medium

The comparative analysis of gelatine phantoms and porcine skin samples highlights key differences in the behaviour of optical and bioimpedance measurements when applied to solid mediums. While the gelatine phantom served as a simplified, controlled environment, porcine skin introduced biological variability, which impacted both the accuracy of the spectrophotometric and bioimpedance data.

8.2.1 Spectrophotometry in Gelatine and Porcine Skin Samples

Spectrophotometry provided valuable insights into the absorption and scattering properties of both gelatine and porcine skin. The use of specific wavelengths—1632 nm, 1690 nm, 1836 nm, 2193 nm, 2320 nm, and 2323 nm—allowed for targeted detection of ethanol and acetic acid concentrations within the samples.

In the case of gelatine phantoms, the optical behaviour was more predictable due to the homogeneity of the phantom. The light scattering properties of gelatine, enhanced by the addition of intralipid, closely resembled biological tissues, resulting in strong correlation coefficients between absorbance and concentration at key wavelengths. For example, at 1690 nm, the correlation coefficient for ethanol was -0.59, with an RMSEP of 0.03 mg/dL, indicating reliable detection of ethanol concentrations in this wavelength. Similarly, acetic acid exhibited strong correlations at 2323 nm, with a coefficient of -0.71 and an RMSEP of 0.08 mg/dL, suggesting that this wavelength is highly sensitive to acetic acid concentrations.

Porcine skin, however, presented greater challenges due to its structural complexity, which led to increased light scattering and absorption variability. This resulted in lower overall prediction accuracy for ethanol, particularly at higher concentrations. The correlation at 1690 nm for ethanol was -0.71, with an RMSEP of 0.06 mg/dL, demonstrating a relatively strong relationship but still more variable than in the gelatine model. For acetic acid, porcine skin also showed moderate correlations, with a notable value of -0.63 at 2320 nm, although the prediction accuracy was slightly diminished compared to the gelatine phantom.

These differences can be attributed to the fact that biological tissues like porcine skin contain various layers, including collagen, fat, and moisture, which significantly affect the scattering and absorption of light. This leads to increased noise in the spectrophotometric data, making it more difficult to accurately predict ethanol and acetic acid concentrations compared to the more uniform gelatine phantoms.

The implications of these findings suggest that while spectrophotometry is effective in controlled environments, its application in more complex biological tissues may require additional calibration and refinement. Future research could explore the use of advanced optical models or machine learning algorithms to better account for the biological variability in tissues like porcine skin.

8.2.2 Bioimpedance in Gelatine and Porcine Skin Samples

Bioimpedance analysis, like spectrophotometry, exhibited distinct behaviours between the gelatin phantoms and porcine skin samples. The electrical properties of tissues, influenced by the concentration of ethanol and acetic acid, were measured across a frequency range of 1 kHz

to 10 kHz, providing insights into how these compounds affect tissue conductivity and resistance.

In the gelatine phantoms, bioimpedance measurements revealed a clear relationship between compound concentration and impedance changes. Ethanol and acetic acid concentrations significantly impacted the impedance values, particularly at lower frequencies. The baseline impedance for gelatine samples without ethanol or acetic acid was higher compared to infused samples, with a reduction in impedance of up to 0.8 log(Ohms) at frequencies below 4 kHz. This indicates that the infusion of ethanol and acetic acid increases the tissue's conductivity, allowing for easier current flow through the sample.

In porcine skin, however, the bioimpedance results were more variable. Similar to the spectrophotometry findings, the structural complexity of porcine skin affected the consistency of the measurements. The impedance changes were less pronounced than in the gelatine samples, particularly at higher ethanol concentrations. The predicted vs. actual ethanol concentration plots showed significant deviation, with an R^2 value of only 0.0145 and an RMSEP of 174, highlighting the challenges of predicting ethanol concentrations based on bioimpedance in more complex biological tissues. Acetic acid prediction performed slightly better, with an R^2 value of 0.103 and an RMSEP of 9.98, although this still indicates substantial room for improvement.

The differences between gelatine and porcine skin bioimpedance measurements can be attributed to the heterogeneity of biological tissues, which affects the uniformity of electrical current distribution. The presence of multiple layers with varying water content and electrical conductivity in porcine skin complicates the measurement process, resulting in increased noise and variability.

These findings suggest that while bioimpedance offers potential for detecting chemical changes in tissues, its application in more complex biological samples like porcine skin requires further refinement. Future studies could focus on improving the sensitivity and accuracy of bioimpedance measurements by exploring alternative electrode configurations, expanding the frequency range, or employing non-linear regression models to better capture the complex relationships between impedance and compound concentration.

8.3 Comparative Analysis of Optical and Bioimpedance Measurements in Solid Mediums

The comparative analysis of optical and bioimpedance measurements in solid mediums—gelatine phantoms and porcine skin—provides valuable insights into the strengths and limitations of each method for detecting and quantifying ethanol and acetic acid concentrations.

8.3.1 Sensitivity to Ethanol and Acetic Acid Concentrations

When comparing the sensitivity of spectrophotometry and bioimpedance to ethanol and acetic acid concentrations, it is clear that spectrophotometry exhibited higher sensitivity, particularly in detecting acetic acid. This was evident in both the gelatine and porcine skin samples, where wavelengths such as 2323 nm showed strong correlations with acetic acid concentration in both mediums.

Bioimpedance, on the other hand, demonstrated lower sensitivity overall, particularly for ethanol detection. The predicted vs. actual concentration plots for ethanol in porcine skin revealed significant discrepancies, with an R^2 value of only 0.0145, indicating poor predictive power. In contrast, acetic acid showed slightly better performance with an R^2 of 0.103, suggesting that bioimpedance may be more sensitive to acetic acid concentrations, though still with considerable room for improvement.

8.3.2 Predictive Accuracy of Ethanol and Acetic Acid Concentrations

The predictive accuracy of ethanol and acetic acid concentrations varied significantly between spectrophotometry and bioimpedance measurements. In the case of spectrophotometry, the predictive models for acetic acid consistently outperformed those for ethanol. The RMSEP for acetic acid in gelatine phantoms was as low as 2.30 mg/dL, while ethanol predictions exhibited higher errors, with an RMSEP of 30.92 mg/dL. Similar trends were observed in porcine skin, where acetic acid predictions showed stronger correlations across multiple wavelengths.

Bioimpedance measurements, however, struggled to provide accurate predictions for both ethanol and acetic acid. The RMSEP values for ethanol and acetic acid in porcine skin were 174 and 9.98, respectively, indicating significant variability in the predictions. This suggests that while bioimpedance can detect changes in tissue properties, its predictive accuracy for specific compound concentrations is limited in solid mediums.

8.3.3 Variability and Limitations of the Methods

Both spectrophotometry and bioimpedance methods showed variability in their measurements, particularly in porcine skin samples. The heterogeneity of biological tissues, combined with the scattering and absorption properties of light in spectrophotometry and the complex electrical behaviour in bioimpedance, introduced noise and variability into the data.

One of the key limitations of spectrophotometry was its sensitivity to tissue composition, particularly in solid samples like porcine skin. The increased light scattering and absorption in these tissues reduced the accuracy of ethanol predictions, particularly at higher concentrations. In contrast, bioimpedance measurements were heavily influenced by the electrical properties of the tissue, which varied significantly between samples, leading to reduced predictive accuracy.

The integration of optical and bioimpedance spectroscopy for ethanol and acetic acid detection is challenged at the molecular level by the nature of their vibrational transitions and their influence on the dielectric properties of biological media. In the optical domain, ethanol and acetic acid exhibit overtone and combination bands in the short-wave infrared (SWIR) that are strongly influenced by water's O–H stretching vibrations. These interactions are governed by the formation of transient hydrogen bonds and instantaneous dipoles, which shift absorption peaks and broaden spectral features. As a result, analyte-specific signals are often masked by collective dipolar interactions within the solvent matrix, requiring advanced preprocessing methods such as baseline subtraction, derivative spectroscopy, and chemometric deconvolution.

Bioimpedance spectroscopy, in contrast, probes frequency-dependent polarization phenomena. Ethanol reduces the bulk permittivity of the medium by disrupting the hydrogen-bonding network of water, while acetic acid introduces dissociated ions that alter conductivity. These processes are governed by the alignment and relaxation of instantaneous dipoles under an applied electric field. However, the measured impedance response reflects not only the analyte concentration but also electrode polarization, double-layer capacitance, and frequency-dependent dielectric dispersion of surrounding tissues. This complexity complicates direct quantification, particularly in vivo, where tissue anisotropy and hydration strongly affect the impedance spectrum.

The fusion of both techniques presents technical limitations in synchronizing measurements with sufficient temporal and spatial resolution for real-time monitoring. Optical signals respond to molecular vibrational transitions on femtosecond timescales, while impedance responses are governed by dipolar relaxation and ionic mobility on the order of milliseconds to seconds. Aligning these fundamentally different timescales into a coherent multimodal dataset requires careful system design and advanced signal processing. In addition, light scattering in turbid tissues and impedance variability caused by electrode drift introduce independent noise sources that can only be mitigated through cross-correlation and redundancy between modalities.

These findings highlight the need for further refinement of both methods, particularly when applied to complex biological tissues. Future research should focus on improving the accuracy and consistency of these measurements through advanced data analysis techniques, better sample preparation methods, and optimized instrumentation.

8.4 Technological Implications for Biomedical Applications

The findings from this study not only provide insights into the capabilities of diffuse reflectance spectrophotometry and bioimpedance measurements but also open new avenues for their application in biomedical diagnostics and therapeutic monitoring. The dual-modality approach, combining optical and electrical properties, is particularly relevant for non-invasive or minimally invasive diagnostic tools, where the ability to detect chemical changes in tissues is essential for early disease detection, monitoring treatment efficacy, or assessing metabolic conditions.

One of the key technological implications is the potential use of these methods for detecting ethanol and acetic acid concentrations in real-time. In clinical settings, this could have applications in assessing alcohol intoxication or monitoring metabolic by-products such as acetic acid in conditions like sepsis or diabetic ketoacidosis. The integration of spectrophotometry and bioimpedance in wearable devices could provide continuous monitoring of tissue conditions, offering healthcare providers real-time data on a patient's biochemical state.

The spectrophotometric data, particularly at wavelengths like 1690 nm for ethanol and 2323 nm for acetic acid, demonstrated strong correlations with their respective concentrations in both synthetic and biological mediums. This suggests that these wavelengths could be

optimized for use in non-invasive diagnostic devices, such as optical skin patches, that rely on infrared light to detect changes in tissue composition. The application of such technologies could extend beyond ethanol and acetic acid to other metabolites or drugs, potentially offering a versatile platform for monitoring a variety of substances in the body.

Bioimpedance, while showing more variability in its results, also holds promise for real-time monitoring of tissue health, particularly in post-operative or wound care scenarios. As bioimpedance is sensitive to changes in tissue composition, including water content and cellular integrity, it could be adapted for detecting tissue inflammation, necrosis, or other pathological changes. With further refinement, bioimpedance could be incorporated into devices designed for long-term monitoring of skin or wound conditions, alerting clinicians to changes that may require intervention.

However, for these technologies to transition into clinical practice, several challenges must be addressed. The variability observed in solid biological tissues like porcine skin points to the need for more robust algorithms capable of handling the noise and complexity inherent in biological data. The development of machine learning models, which can account for tissue heterogeneity and non-linear relationships between spectrophotometric or impedance data and chemical concentrations, may significantly enhance the predictive accuracy of these methods.

Moreover, improving the sensitivity and specificity of both spectrophotometry and bioimpedance could expand their application to more complex diagnostic challenges, such as cancer detection, where tissue optical and electrical properties change in subtle ways during disease progression. Thus, the experimental findings of this study lay the groundwork for future innovations in the biomedical field, particularly in non-invasive diagnostics, continuous monitoring, and personalized medicine.

8.5 Future Research Direction and Broader Implications

While this study has provided a comprehensive analysis of ethanol and acetic acid detection using spectrophotometry and bioimpedance, several areas remain open for future exploration. Further research should focus on addressing the limitations observed in the current models, particularly the variability seen in biological samples like porcine skin.

One key area of improvement is the refinement of the bioimpedance model. The low R^2 values and high RMSEP for ethanol detection suggest that bioimpedance, as currently implemented,

is not sufficiently sensitive to accurately quantify ethanol concentrations in complex biological tissues. Future research could explore alternative electrode configurations or higher frequency ranges, which may offer more precise data by better capturing the dielectric properties of tissues. Additionally, incorporating non-linear modelling approaches such as neural networks or support vector machines could improve the predictive power of bioimpedance measurements by accounting for the complex interactions between tissue composition, structure, and electrical properties.

Further exploration of the optical properties of biological tissues, particularly in relation to multi-layered structures like skin, is also warranted. The increased scattering and absorption in porcine skin compared to gelatine phantoms highlight the need for a deeper understanding of how different tissue layers contribute to overall optical behaviour. Using more advanced imaging techniques, such as optical coherence tomography (OCT) or multi-spectral imaging, could help deconstruct these layers and improve the accuracy of spectrophotometric models.

Additionally, while this study focused on ethanol and acetic acid, expanding the scope of research to include other analytes, such as glucose, lactate, or pharmaceutical compounds, could provide valuable insights into the broader applicability of these techniques. By studying how different chemical compounds interact with biological tissues in both optical and electrical domains, researchers could develop more versatile diagnostic tools capable of detecting a wide range of substances with minimal invasiveness.

The potential to combine spectrophotometry and bioimpedance with emerging technologies like wearable sensors or implantable devices is another promising avenue for future research. Wearable technology is advancing rapidly, with increasing demand for devices that can monitor health metrics in real-time. By integrating optical and electrical sensors into wearable patches or smart clothing, researchers could create continuous monitoring systems that provide healthcare providers with real-time biochemical data. Such innovations could revolutionize patient care, particularly in managing chronic conditions or monitoring recovery post-surgery.

Finally, the broader implications of this research extend beyond diagnostics. Understanding how different compounds interact with biological tissues has significant ramifications for fields such as drug delivery, where controlling the diffusion and absorption of therapeutic agents is critical. The insights gained from this study on the diffusion properties of ethanol and acetic

acid in biological tissues could inform the design of drug delivery systems that optimize compound distribution, minimizing side effects while maximizing therapeutic efficacy.

The ability to non-invasively monitor tissue composition also has applications in fields such as sports medicine, where real-time data on muscle hydration or fatigue could inform training regimens or recovery protocols. As such, the findings from this study have the potential to impact a wide range of scientific and medical disciplines, highlighting the versatility and promise of diffuse reflectance spectrophotometry and bioimpedance analysis in advancing both healthcare and scientific research.

This extended discussion provides a comprehensive analysis of the experimental findings, implications for biomedical applications, and directions for future research. Both diffuse reflectance spectrophotometry and bioimpedance analysis show promise as non-invasive techniques for detecting chemical changes in biological tissues, though their accuracy varies significantly between fluid and solid mediums. The technological and research advancements discussed herein highlight the potential of these methods to revolutionize real-time diagnostics, therapeutic monitoring, and personalized healthcare. Continued research and refinement will be essential to fully realise the potential of these innovative techniques.

9 Conclusion

This study explored the use of diffuse reflectance spectrophotometry and bioimpedance analysis for detecting and quantifying ethanol and acetic acid concentrations in both fluid and solid biological samples, with a focus on porcine skin and gelatine phantoms. The integration of optical and electrical measurement techniques provided a comprehensive approach to understanding how these compounds interact with biological tissues. Key findings highlighted the strengths of diffuse reflectance spectrophotometry, particularly at wavelengths like 1690 nm and 2323 nm, for accurately detecting ethanol and acetic acid. Bioimpedance, while providing valuable insights into tissue conductivity and structural changes, demonstrated more variability and lower predictive accuracy, particularly for ethanol.

The study revealed that optical measurements in fluid samples such as aISF and intralipid were more reliable than those in solid mediums, due to the homogeneous nature of the fluids, which allowed for more predictable light scattering and absorption. Solid samples, such as porcine skin and gelatine phantoms, introduced complexity due to their heterogeneous structure, leading to increased scattering and variability in the data. Nonetheless, the gelatine-intralipid-aISF composite was validated as a reliable tissue model, demonstrating similar optical behaviour to biological tissues and reinforcing its utility for future experiments.

Technological implications for biomedical applications include the potential development of non-invasive diagnostic tools and continuous monitoring devices based on these techniques. Future research should focus on refining bioimpedance models, improving the sensitivity of spectrophotometric measurements, and expanding the scope to include additional compounds relevant to clinical diagnostics.

In conclusion, this research highlights the promise of combining optical and electrical measurement techniques for non-invasive chemical detection in biological tissues. While challenges remain, particularly in bioimpedance accuracy, the results provide a strong foundation for further development in medical diagnostics and real-time monitoring systems.

10 References

[1] R. D. Biggs, ‘Drinking in Ancient Societies: History and Culture of Drinks in the Ancient Near East: Papers of a Symposium Held in Rome, May 17-19, 1990, Lucio Milano’, *Journal of Near Estern Studies*, vol. 56, no. 3, p. 233, 1997.

[2] N. El-Guebaly and A. El-Guebaly, ‘Alcohol Abuse in Ancient Egypt: The Recorded Evidence’, 1981.

[3] Max Nelson, ‘DID ANCIENT GREEKS DRINK BEER?’, *Phoenix*, vol. 68, no. 1/2, p. 27, 2014, doi: 10.7834/phoenix.68.1-2.0027.

[4] J. M. O’Brein and B. Rickenbacker, ‘alcoholism, Roman’, *Oxford Classical Dictionary*, 2016.

[5] J. Rehm, ‘The Risks Associated With Alcohol Use and Alcoholism’, 2011.

[6] L. M. Hines and E. B. Rimm, ‘Moderate alcohol consumption and coronary heart disease: a review’, *Postgraduate Medical Journal* , vol. 77, pp. 747–752, 2001, [Online]. Available: http://pmj.bmj.com/

[7] C. Pelucchi, I. Tramacere, P. Boffetta, E. Negri, and C. La Vecchia, ‘Alcohol consumption and cancer risk’, Oct. 2011. doi: 10.1080/01635581.2011.596642.

[8] A. Murphy, ‘Reported road casualties in Great Britain: 2019 annual report’, *HM Department for Transport*, 2020, [Online]. Available: https://www.gov.uk/government/

[9] ‘International Traffic Safety Data and Analysis Group Alcohol-Related Road Casualties in Official Crash Statistics’, 2017. [Online]. Available: www.itf-oecd.org

[10] T. D. Ridder, B. J. Ver Steeg, and B. D. Laaksonen, ‘Comparison of spectroscopically measured tissue alcohol concentration to blood and breath alcohol measurements’, *J Biomed Opt*, vol. 14, no. 5, p. 054039, 2009, doi: 10.1117/1.3253353.

[11] A. D. Chapp, P. G. Mermelstein, and M. J. Thomas, ‘The ethanol metabolite acetic acid activates mouse nucleus accumbens shell medium spiny neurons’, *J Neurophysiol*, vol. 125, no. 2, pp. 620–627, Feb. 2021, doi: 10.1152/jn.00659.2020.

[12] S. Maicas, ‘The role of yeasts in fermentation processes’, Aug. 01, 2020, *MDPI AG*. doi: 10.3390/microorganisms8081142.

[13] L. Liu *et al.*, 'The origins of specialized pottery and diverse alcohol fermentation techniques in Early Neolithic China', *Proc Natl Acad Sci U S A*, vol. 116, no. 26, pp. 12767–12774, 2019, doi: 10.1073/pnas.1902668116.

[14] D. Stanislawski, 'DIONYSUS WESTWARD: EARLY RELIGION AND THE ECONOMIC GEOGRAPHY OF WINE', 1975.

[15] J. S. Blocker, 'Did prohibition really work? Alcohol prohibition as a public health innovation', Feb. 2006. doi: 10.2105/AJPH.2005.065409.

[16] Ritchie Hannah and Roser Max, 'Alcohol Consumption', *Our World in Data*, 2018.

[17] D. Jernigan and C. S. Ross, 'The Alcohol Marketing Landscape: Alcohol Industry Size, Structure, Strategies, and Public Health Responses', *J Stud Alcohol Drugs Suppl*, 2020.

[18] 'The Alcohol Industry: Factsheet', *Institute of Alcohol Studies*, 2018.

[19] R. Young, H. Sweeting, and P. West, 'A longitudinal study of alcohol use and antisocial behaviour in young people', *Alcohol and Alcoholism*, vol. 43, no. 2, pp. 204–214, Mar. 2008, doi: 10.1093/alcalc/agm147.

[20] 'The costs of alcohol to society', *Insititute of Alcohol Studies*, 2020, [Online]. Available: www.ias.org.uk|@InstAlcStud

[21] Foley Niamh, 'Pub Statistics', *UK Parliment: House of Commons Library*, 2021.

[22] G. Chiva-blanch and L. Badimon, 'Benefits and risks of moderate alcohol consumption on cardiovascular disease: Current findings and controversies', Jan. 01, 2020, *MDPI AG*. doi: 10.3390/nu12010108.

[23] H. Li and U. Förstermann, 'Red wine and cardiovascular health', Sep. 2012. doi: 10.1161/CIRCRESAHA.112.278705.

[24] L. Vonghia *et al.*, 'Acute alcohol intoxication', Dec. 01, 2008, *Elsevier*. doi: 10.1016/j.ejim.2007.06.033.

[25] K. P. Abrahao, A. G. Salinas, and D. M. Lovinger, 'Alcohol and the Brain: Neuronal Molecular Targets, Synapses, and Circuits', Dec. 20, 2017, *Cell Press*. doi: 10.1016/j.neuron.2017.10.032.

[26] M. R. De Blasiis, C. Ferrante, and V. Veraldi, ‘Driving risk assessment under the effect of alcohol through an eye tracking system in virtual reality’, in *Advances in Intelligent Systems and Computing*, Springer Verlag, 2020, pp. 329–341. doi: 10.1007/978-3-030-20497-6_31.

[27] H. R. Thomasson, ‘Gender Differences in Alcohol Metabolism Physiological Responses to Ethanol’, in *Recent Developments in Alcoholism*, Springer, 2002, pp. 163–179.

[28] A. I. Cederbaum, ‘Alcohol Metabolism’, Nov. 2012. doi: 10.1016/j.cld.2012.08.002.

[29] S. Sasaki *et al.*, ‘Relation between alcohol consumption and arterial stiffness: A cross-sectional study of middle-aged Japanese women and men’, *Alcohol*, vol. 47, no. 8, pp. 643–649, Dec. 2013, doi: 10.1016/j.alcohol.2013.10.003.

[30] Mann Karl, Hermann Derik, and Heinz Andreas, ‘One Hundred Years of Alcoholism: The Twentieth Century’, *Alcohol and Alcoholism*, vol. 35, no. 1, pp. 10–15, 200AD.

[31] K. G. Chartier, K. J. Karriker-Jaffe, C. R. Cummings, and K. S. Kendler, ‘Review: Environmental influences on alcohol use: Informing research on the joint effects of genes and the environment in diverse U.S. populations’, Aug. 01, 2017, *Wiley Blackwell*. doi: 10.1111/ajad.12478.

[32] H. J. Edenberg and T. Foroud, ‘Genetics and alcoholism’, Aug. 2013. doi: 10.1038/nrgastro.2013.86.

[33] Bayard Max, McIntyre Jonah, Hill Keith R, and Woodside Jack Jr, ‘Alcohol Withdrawal Syndrome’, *Am Fam Physician*, vol. 69, no. 6, pp. 1443–1450, 2004, [Online]. Available: www.aafp.org/afp.

[34] K. Witkiewitz, R. Z. Litten, and L. Leggio, ‘Advances in the science and treatment of alcohol use disorder’, 2019. [Online]. Available: http://advances.sciencemag.org/

[35] R. B. Huebner and L. W. Kantor, ‘Advances in Alcoholism Treatment’, *Alcohol Research and Health*, vol. 33, no. 4, pp. 295–299, 2011, [Online]. Available: www.AlcoholScreening.org

[36] M. R. Piano, A. Mazzuco, M. Kang, and S. A. Phillips, ‘Cardiovascular Consequences of Binge Drinking: An Integrative Review with Implications for Advocacy, Policy, and Research’, Mar. 01, 2017, *Blackwell Publishing Ltd*. doi: 10.1111/acer.13329.

[37] O. Iakunchykova *et al.*, ‘Evidence for a Direct Harmful Effect of Alcohol on Myocardial Health: A Large Cross-Sectional Study of Consumption Patterns and Cardiovascular Disease Risk Biomarkers From Northwest Russia, 2015 to 2017’, *J Am Heart Assoc*, vol. 9, no. 1, Jan. 2020, doi: 10.1161/JAHA.119.014491.

[38] G. K. Michalopoulos and B. Bhushan, ‘Liver regeneration: biological and pathological mechanisms and implications’, Jan. 01, 2021, *Nature Research*. doi: 10.1038/s41575-020-0342-4.

[39] T. M. Donohue, K. K. Kharbanda, and N. A. Osna, ‘Alcoholic Liver Disease: Pathogenesis and Current Management’, *Alcohol Res*, vol. 38, no. 2, pp. 147–161, 2017.

[40] N. K. Loconte, A. M. Brewster, J. S. Kaur, J. K. Merrill, and A. J. Alberg, ‘JOURNAL OF CLINICAL ONCOLOGY Alcohol and Cancer: A Statement of the American Society of Clinical Oncology’, *J Clin Oncol*, vol. 36, pp. 83–93, 2017, doi: 10.1200/JCO.2017.

[41] H. Rumgay *et al.*, ‘Global burden of cancer in 2020 attributable to alcohol consumption: a population-based study’, *Lancet Oncol*, vol. 22, no. 8, pp. 1071–1080, Aug. 2021, doi: 10.1016/S1470-2045(21)00279-5.

[42] Widmark Erik, ‘Eine Mikromethode zur Bestimmung von Athylalkohol im Blut’, *Biochem Z*, vol. 131, pp. 473–484, 1922.

[43] T. E. Friedemann and R. Klaas, ‘THE DETERMINATION OF ETHYL ALCOHOL*’.

[44] Widmark Erik; Tandberg J., ‘Uber die Bedingungen fiir die Akkumulation indifferenter narkotika. Theoretische Berechnungen’, *Biochem Z*, vol. 147, pp. 358–389, 1924.

[45] Baraona E; Abittan CS; Dohmen K; Moretti M; Pozzato G; Chayes ZW; Schaefer C; Lieber CS, ‘Gender differences in pharmacokinetics of alcohol’, *Alcohol Clin Exp Res.*, vol. 24, no. 4, pp. 502–507, 2001.

[46] Andréasson R and Jones A W, ‘The life and work of Erik M. P. Widmark’, *Am J Forensic Med Pathol .*, vol. 17, no. 3, pp. 177–190, 1996.

[47] Gullberg R., ‘Estimating the uncertainty associated with Widmark’s equation as commonly applied in forensic toxicology’, *Forensic Sci Int*, vol. 172, no. 1, pp. 33–39, 2007.

[48] Baldwin Arthur D., ‘Anstie’s Alcohol Limit’, *AJPH*, vol. 67, no. 7, pp. 679–681, 1977.

[49] Bogen E., ‘The Diagnosis of Drunkenness - A Quantitative Study of Acute Alcohol Intoxication’, *Cal West Med*, vol. 26, no. 6, pp. 778–783, 1927.

[50] Brokenstein R.F., ‘The Breathalizer and its Applications’, *Med Sci Law*, vol. 2, no. 1, 1961.

[51] Wright B. M., Jones T.P., and Jones A.W., ‘Breath Alcohol Analysis and the Blood: Breath Ratio’, *Med Sci Law*, vol. 15, no. 3, 1975.

[52] Simpson G., ‘Do breath tests really underestimate blood alcohol concentration?’, *J Anal Toxicol*, vol. 13, no. 2, pp. 120–123, 1989.

[53] R. M. Langille and J. Patrick, ‘Precision of breath alcohol testing in the field using the intoxilyzer® 5000c and the paradox of truncation’, *Journal of the Canadian Society of Forensic Science*, vol. 39, no. 2, pp. 55–64, 2006, doi: 10.1080/00085030.2006.10757137.

[54] J. G. Sorbello, G. J. Devilly, C. Allen, L. R. J. Hughes, and K. Brown, ‘Fuel-cell breathalyser use for field research on alcohol intoxication: An independent psychometric evaluation’, *PeerJ*, vol. 2018, no. 3, 2018, doi: 10.7717/peerj.4418.

[55] Sorbello Jacob. G., Devilly Grant J., Allen Correy, Hughes Lee R.J., and Brown Kathleen, ‘Fuel-cell breathalyser use for field research on alcohol intoxication: an independent psychometric evaluation’, *PeerJ*, vol. 6, 2018.

[56] E. Bihar, Y. Deng, T. Miyake, M. Saadaoui, G. G. Malliaras, and M. Rolandi, ‘A Disposable paper breathalyzer with an alcohol sensing organic electrochemical transistor’, *Sci Rep*, vol. 6, Jun. 2016, doi: 10.1038/srep27582.

[57] Legge D., ‘The Influence of Breath Temperature on Assessments of Blood Alcohol Level by Breath Analysis’, *Q J Stud Alcohol*, vol. 26, no. 3, pp. 371–377, 1965.

[58] A. W. Jones, ‘How Breathing Technique Can Influence the Results of Breath-Alcohol Analysis’, 1982.

[59] K. M. Dubowski, ‘Quality Assurance in Breath-Alcohol Analysis*’, 1994.

[60] L. D. Mihretu, A. G. Gebru, K. N. Mekonnen, A. G. Asgedom, and Y. H. Desta, ‘Determination of ethanol in blood using headspace gas chromatography with flameionization detector (HS-GC-FID): Validation of a method’, *Cogent Chem*, vol. 6, no. 1, p. 1760187, Jan. 2020, doi: 10.1080/23312009.2020.1760187.

[61] R. C. Charlebois, M. R. Corbett, and J. G. Wigmore, ‘Comparison of Ethanol Concentrations in Blood, Serum, and Blood Cells for Forensic Application*’, 1996. [Online]. Available: https://academic.oup.com/jat/article/20/3/171/757909

[62] Rockerbie R. A., *Alcohol and Drug Intoxication*. Trafford, 1999.

[63] F. Tagliaro, G. Lubli, S. Ghielmi, D. Franchi, and M. Marigo, ‘Review Chromatographic methods for blood alcohol determination’, 1992.

[64] J. R. Hess, ‘Conventional blood banking and blood component storage regulation: Opportunities for improvement’, 2010. doi: 10.2450/2010.003S.

[65] A. W. Jones, L. Lindberg, and S.-G. Olsson, ‘Magnitude and Time-Course of Arterio-Venous Differences in Blood-Alcohol Concentration in Healthy Men’, 2004.

[66] V. R. Preedy and R. R. (Ronald R. Watson, *Comprehensive handbook of alcohol related pathology - Methods for Determining Blood Alcohol Concentration: Current and Retrospective*. Elsevier Academic, 2005.

[67] M. H. Wojcik and J. S. Hawthorne, ‘Sensitivity of commercial Ethyl Glucuronide (EtG) testing in screening for alcohol abstinence’, *Alcohol and Alcoholism*, vol. 42, no. 4, pp. 317–320, 2007, doi: 10.1093/alcalc/agm014.

[68] Tiscione N. B., Alford I., Yeatman D. T., and Shan X., ‘Ethanol Analysis by Headspace Gas Chromatographywith Simultaneous Flame-Ionization andMass Spectrometry Detection’, *J Anal Toxicol*, vol. 35, pp. 501–511, 2011.

[69] J. E. Peachey, B. M. Kapur, and D. Frsc, ‘Monitoring Drinking Behavior with the Alcohol Dipstick during Treatment’, *Alcohol Clin Exp Res*, vol. 10, no. 6, pp. 663–666, 1986.

[70] L. A. Pate, J. D. Hamilton, R. S. Park, and R. M. Strobel, 'Evaluation of a Saliva Alcohol Test Stick as a Therapeutic Adjunct in an Alcoholism Treatment Program', *J Stud Alcohol*, vol. 54, no. 5, pp. 520–521, 1993.

[71] R. K. Mishra *et al.*, 'Simultaneous detection of salivary Δ9-tetrahydrocannabinol and alcohol using a Wearable Electrochemical Ring Sensor', *Talanta*, vol. 211, May 2020, doi: 10.1016/j.talanta.2020.120757.

[72] L. C. Degutis, R. Rabinovici, A. Sabbaj, R. Mascia, and G. D'Onofrio, 'The saliva strip test is an accurate method to determine blood alcohol concentration in trauma patients', *Academic Emergency Medicine*, vol. 11, no. 8, pp. 885–887, 2004, doi: 10.1197/j.aem.2004.02.529.

[73] Y. Y. Chen, C. L. Lin, Y. C. Lin, and C. Zhao, 'Non-invasive detection of alcohol concentration based on photoplethysmogram signals', *IET Image Process*, vol. 12, no. 2, pp. 188–193, Feb. 2018, doi: 10.1049/iet-ipr.2017.0625.

[74] W. F. Wang, C. Y. Yang, and Y. F. Wu, 'SVM-based classification method to identify alcohol consumption using ECG and PPG monitoring', *Pers Ubiquitous Comput*, vol. 22, no. 2, pp. 275–287, Apr. 2018, doi: 10.1007/s00779-017-1042-0.

[75] Rachakonda Laavanya, Kougianos Elias, Mohanty Saraju P., and Sayeed Abu, 'Smart-Steering: An IoMT-Device to Monitor Blood Alcohol Concentration using Physiological Signals', *2020 IEEE International Conference on Consumer Electronics (ICCE)*, 2020.

[76] J. Kubicek *et al.*, 'Prediction model of alcohol intoxication from facial temperature dynamics based on K-means clustering driven by evolutionary computing', *Symmetry (Basel)*, vol. 11, no. 8, 2019, doi: 10.3390/sym11080995.

[77] Piano Mariann R., 'Alcohol's Effects on the Cardiovascular System', *Alcohol Research*, vol. 38, no. 2, pp. 219–241, 2017.

[78] Volvo, 'Volvo Cars to deploy in-car cameras and intervention against intoxication, distraction', 2019.

[79] Tabakoff Boris, Cornell Neal, and Hoffman Paula L., 'Alcohol tolerance', *Ann Emerg Med September*, vol. 15, no. 9, pp. 1005–1012, 1986.

[80] M. Czaplik, M. Ulbrich, N. Hochhausen, R. Rossaint, and S. Leonhardt, ‘Evaluation of a new non-invasive measurement technique based on bioimpedance spectroscopy to estimate blood alcohol content: A pilot study’, *Biomedizinische Technik*, vol. 64, no. 3, pp. 365–371, Jun. 2019, doi: 10.1515/bmt-2018-0070.

[81] E. Pinheiro, O. Postolache, and P. Girão, ‘Contactless impedance cardiography using embedded sensors’, *Measurement Science Review*, vol. 13, no. 3, pp. 157–164, Jun. 2013, doi: 10.2478/msr-2013-0025.

[82] D. Teichmann, J. Foussier, J. Jia, S. Leonhardt, and M. Walter, ‘Noncontact monitoring of cardiorespiratory activity by electromagnetic coupling’, *IEEE Trans Biomed Eng*, vol. 60, no. 8, pp. 2142–2152, 2013, doi: 10.1109/TBME.2013.2248732.

[83] Marquez J. C., Seoane F., Valimaki E., and Lindecrantz K., ‘Textile Electrodes in Electrical Bioimpedance Measurements - A Comparison with Conventional Ag/AgCl Electrodes’, *31st Annual International Conference of the IEEE EMBS*, 2009.

[84] R. M. Swift, C. S. Martin, L. Swette, A. Laconti, and N. Kackley, ‘Studies on a Wearable, Electronic, Transdermal Alcohol Sensor’, *Alcohol Clin Exp Res*, vol. 16, no. 4, 1992.

[85] Davis-Martin Rachel E., Alessi Sheila M., and Boudreaux Edwin D., ‘Alcohol Use Disorder in the Age of Technology: A Review of Wearable Biosensors in Alcohol Use Disorder Treatment’, *Front Psychiatry*, vol. 12, 2021.

[86] J. Kim *et al.*, ‘Noninvasive Alcohol Monitoring Using a Wearable Tattoo-Based Iontophoretic-Biosensing System’, *ACS Sens*, vol. 1, no. 8, pp. 1011–1019, Aug. 2016, doi: 10.1021/acssensors.6b00356.

[87] Leonard Regina Noelle *et al.*, ‘Mobile Health Technology Using a Wearable Sensorband for Female College Students With Problem Drinking: An Acceptability and Feasibility Study’, *JMIR Mhealth Uhealth*, vol. 5, no. 7, 2017.

[88] B. Lansdorp, W. Ramsay, R. Hamid, and E. Strenk, ‘Wearable enzymatic alcohol biosensor’, *Sensors (Switzerland)*, vol. 19, no. 10, May 2019, doi: 10.3390/s19102380.

[89] T. Arakawa, T. Aota, K. Iitani, K. Toma, Y. Iwasaki, and K. Mitsubayashi, ‘Skin ethanol gas measurement system with a biochemical gas sensor and gas concentrator

toward monitoring of blood volatile compounds', *Talanta*, vol. 219, Nov. 2020, doi: 10.1016/j.talanta.2020.121187.

[90] A. Panneer Selvam, S. Muthukumar, V. Kamakoti, and S. Prasad, 'A wearable biochemical sensor for monitoring alcohol consumption lifestyle through Ethyl glucuronide (EtG) detection in human sweat', *Sci Rep*, vol. 6, Mar. 2016, doi: 10.1038/srep23111.

[91] N. E. Walsham and R. A. Sherwood, 'Ethyl glucuronide', *Ann Clin Biochem*, vol. 49, no. 2, pp. 110–117, Mar. 2012, doi: 10.1258/acb.2011.011115.

[92] M. Venugopal *et al.*, 'Clinical evaluation of a novel interstitial fluid sensor system for remote continuous alcohol monitoring', *IEEE Sens J*, vol. 8, no. 1, pp. 71–80, Jan. 2008, doi: 10.1109/JSEN.2007.912544.

[93] C. E. Fairbairn and N. Bosch, 'A new generation of transdermal alcohol biosensing technology: practical applications, machine -learning analytics and questions for future research', *Addiction*, vol. 116, no. 10, pp. 2912–2920, Oct. 2021, doi: 10.1111/add.15523.

[94] K. van Egmond, C. J. C. Wright, M. Livingston, and E. Kuntsche, 'Wearable Transdermal Alcohol Monitors: A Systematic Review of Detection Validity, and Relationship Between Transdermal and Breath Alcohol Concentration and Influencing Factors', Oct. 01, 2020, *Blackwell Publishing Ltd*. doi: 10.1111/acer.14432.

[95] Gardner Craig M., 'Transmission versus reflectance spectroscopy for quantitation', *J Biomed Opt*, vol. 23, no. 01, p. 1, Jan. 2018, doi: 10.1117/1.jbo.23.1.018001.

[96] R. Boushel *et al.*, 'Monitoring tissue oxygen availability with near infrared spectroscopy (NIRS) in health and disease', *Scand J Med Sci Sports*, vol. 11, pp. 213–222, 2001.

[97] J. Dai, Z. Ji, Y. Du, and S. Chen, 'In vivo noninvasive blood glucose detection using near-infrared spectrum based on the PSO-2ANN model', in *Technology and Health Care*, IOS Press, May 2018, pp. S229–S239. doi: 10.3233/THC-174592.

[98] H. M. Heise, S. Delbeck, and R. Marbach, 'Noninvasive monitoring of glucose using near-infrared reflection spectroscopy of skin—constraints and effective novel strategy

in multivariate calibration', *Biosensors (Basel)*, vol. 11, no. 3, Mar. 2021, doi: 10.3390/bios11030064.

[99] Workman Jr. Jerry, *The Handbook of Organic Compounds, Three Volume Set, Volume 1-3: NIR, IR, R, and UV-Vis Spectra Featuring Polymers and Surfactants*, 1st ed., vol. 1. Academic Press, 2000.

[100] Ridder T., 'US 7,403,804 B2: Noninvasive Determination of Alcohol in Tissue', 2008

[101] T. D. Ridder, B. J. ver Steeg, B. D. Laaksonen, and W. T. Radigan, 'Robust Calibration Transfer in Noninvasive Ethanol Measurements, Part II: Modification of Instrument Measurements by Incorporation of Expert Knowledge (MIMIK)', *Appl Spectrosc*, vol. 68, no. 8, pp. 865–878, Aug. 2014, doi: 10.1366/13-07424.

[102] T. D. Ridder, B. J. ver Steeg, and G. L. Price, 'Robust Calibration Transfer in Noninvasive Ethanol Measurements, Part I: Mathematical Basis for Spectral Distortions in Fourier Transform Near-Infrared Spectroscopy (FT-NIR)', *Appl Spectrosc*, vol. 68, no. 8, pp. 852–864, Aug. 2014, doi: 10.1366/13-07422.

[103] T. D. Ridder, C. D. Brown, and B. J. ver Steeg, 'Framework for Multivariate Selectivity Analysis, Part II: Experimental Applications', 2005.

[104] C. D. Brown and T. D. Ridder, 'Framework for Multivariate Selectivity Analysis, Part I: Theoretical and Practical Merits', 2005.

[105] W.-F. Liu, G.-L. Liu, X.-F. Wang, Y.-F. Bao, G. Li, and H.-Q. Wang, 'Non-Invasive Measurement Study of Human Blood Alcohol Concentration Based on NIR Dynamic Spectrum', *2011 International Conference on Image Analysis and Signal Processing*, 2011.

[106] J. Ljungblad, B. Hök, A. Allalou, and H. Pettersson, 'Passive in-vehicle driver breath alcohol detection using advanced sensor signal acquisition and fusion', *Traffic Inj Prev*, vol. 18, pp. S31–S36, May 2017, doi: 10.1080/15389588.2017.1312688.

[107] X. Guo *et al.*, 'Highly sensitive and specific noninvasive in-vivo alcohol detection using wavelength-modulated differential photothermal radiometry', *Biomed Opt Express*, vol. 9, no. 10, p. 4638, Oct. 2018, doi: 10.1364/boe.9.004638.

[108] Wozniak Mateusz K., Wiergowski Marek, Namiesnik Jacek, and Biziuk Marek, 'Biomarkers of Alcohol Consumption in Body Fluids - Possibilities and Limitations of

Application in Toxicological Analysis', *Current Medical CHemistry*, vol. 26, no. 1, pp. 177–196, 2019.

[109] I. Radun, J. Ohisalo, S. Rajalin, J. E. Radun, M. Wahde, and T. Lajunen, 'Alcohol Ignition Interlocks in All New Vehicles: A Broader Perspective', *Traffic Inj Prev*, vol. 15, no. 4, pp. 335–342, May 2014, doi: 10.1080/15389588.2013.825042.

[110] S. Tsukamoto, T. Muto, T. Nagoyaf, M. Shimamurat, M. Saito$, and H. Tainaka, 'DETERMINATIONS OF ETHANOL, ACETALDEHYDE AND ACETATE IN BLOOD AND URINE DURING ALCOHOL OXIDATION IN MAN', 1989.

[111] K. B. Beć, J. Grabska, and C. W. Huck, 'Near-infrared spectroscopy in bio-applications', Jun. 01, 2020, *MDPI AG*. doi: 10.3390/molecules25122948.

[112] T. L. Troy and S. N. Thennadil, 'Optical properties of human skin in the near infrared wavelength range of 1000 to 2200 nm', *J Biomed Opt*, vol. 6, no. 2, p. 167, 2001, doi: 10.1117/1.1344191.